SPECTRAL CHARACTERIZATION OF THIOLATE-MEDIATED METALLOPORPHYRIN-PROTEIN INTERACTIONS AND THEIR FUNCTIONAL IMPLICATIONS

by

Aaron T. Smith

A dissertation in partial fulfillment of
the requirements for the degree of

Doctor of Philosophy

(Chemistry)

at the

UNIVERSITY OF WISCONSIN—MADISON

2012

Date of Final Oral Examination: April 26th, 2012

The dissertation is approved by the following members of the Final Oral Committee:
Judith N. Burstyn, Professor, Department of Chemistry
Thomas C. Brunold, Professor, Department of Chemistry
John F. Berry, Associate Professor, Department of Chemistry
Gary P. Roberts, Professor, Department of Bacteriology
Brian G. Fox, Professor, Department of Biochemistry

SPECTRAL CHARACTERIZATION OF THIOLATE-MEDIATED METALLOPORPHYRIN-PROTEIN INTERACTIONS AND THEIR FUNCTIONAL IMPLICATIONS

by

Aaron T. Smith

Under the supervision of Professor Judith N. Burstyn

At the University of Wisconsin—Madison

Several proteins bind a heme *b* (iron protoporphyrin IX) molecule using the thiolate sidechain of the amino acid cysteine. Cys(thiolate)-ligation confers these proteins with distinctive spectral features, which arise from a unique electronic structure at the heme cofactor. In this work, the spectral features of several Cys(thiolate)-ligated metalloporphyrin-containing proteins are interrogated, and their functional implications are discussed.

The regulator of CO metabolism protein (RcoM) from *Burkholderia xenovorans* is a CO-responsive transcription factor that binds heme *b* using a Cys/His ligation motif in the Fe(III) state. In this work, the spectral signatures of three variants (C94S, C127S, and C130S) are studied. Using several spectroscopic techniques, Cys^{94} is identified as the native Cys ligand of the Fe(III) heme in *Bx*RcoM-2 and, by analogy, *Bx*RcoM-1.

The double-stranded RNA-binding protein DiGeorge Critical Region 8 (DGCR8) is a heme *b*-containing protein. Spectral characterization of DGCR8 demonstrates that this protein uses a unique bis(Cys) ligation to bind heme. Reduction of the heme iron center is accompanied by ligand switching and a loss of primary microRNA processing activity of the DGCR8 RNase

partner Drosha. Spectral characterization also demonstrates that the DGCR8 heme is capable of interacting with CO and NO, but the functional implications are unknown. It is speculated that DGCR8 may function as a heme sensor *in vivo*.

Cystathionine β-Synthase is a pyridoxal-5'-phosphate (PLP) dependent enzyme that binds heme *b* (of unknown function) using a Cys/His ligation motif. Maintenance of the Cys(thiolate)-heme interaction is necessary for maximal enzymatic activity. Spectral and enzymatic investigations of a CoPPIX-substituted form of human CBS (Co hCBS) demonstrated that CoPPIX binds in the same manner as heme (FePPIX). Like the native enzyme, maintenance of the Cys(thiolate)-Co bond is necessary for maximal activity in Co hCBS; these findings support a structural role for heme in hCBS. Spectral and enzymatic analyses of a pathogenic variant, R266K hCBS, demonstrate that alterations in the hydrogen-bonding network at the Cys(thiolate) ligand result in a longer Fe-S(Cys) bond, which in turn alters the PLP active site environment. These results suggest that even subtle changes at the heme site may be transmitted to the enzyme active site.

Approved: _____ Date: _____

Judith N. Burstyn
Professor of Chemistry

Acknowledgements

My first and greatest thanks have to go to my advisor, Prof. Judith Burstyn. I have immensely enjoyed working in your lab. If I had to do graduate school over again tomorrow (egad!), I wouldn't hesitate to work for you. Judith, you have guided me creatively and intellectually throughout these five years, and without you I would not be the chemist and scientist that I am today. I sincerely hope that all of my future bosses will be as congenial, nurturing, and as supportive as you have been.

Many thanks to my committee members: Prof. Thomas Brunold, Prof. John Berry, Prof. Gary Roberts, and Prof. Brian Fox. Each of you has been there for me and helped me whenever I have needed it. You have given me an immense amount of guidance, and for that I thank you. I hope that one day I might have a fraction of the intellect that each of you possess!

My deepest thanks go to the Burstyn group members (both current and past) for making every single day a pleasure at work. I'm not sure how many people can honestly say that they are excited to get out of bed and be with their coworkers, but I can. Special thanks go out to Katie and Yang; I have travailed these past five years with them by my side, and I couldn't have asked for better accompaniment. I would also like to thank the Brunold group members (both current and past) for all their expertise and the generous use of their instrumentation. Without their help, I would still be standing in the dark rR lab fiddling with the laser alignment.

Thank you to the entire Chemistry department (both my friends and staff), especially Roger Clausen, Monika Ivancic, Bob Shanks, and Rob McClain and their help with instrumentation and general inquiry. It is the people in this department truly make it special.

I would like to thank my parents for always supporting me in my endeavors. It takes a lot of caring, patience, and money(!) to support someone who has been in school as long as I

have. They have always made me feel special and reiterated that I could do whatever I set my mind to. I owe everything I have and everything that I am to them.

Lastly, I would like to thank Dan for standing by me these years. He has been a beacon of light and joy in any darkness I encountered. At this point, I almost feel as if he deserves an honorary chemistry Ph.D.! Without his support, I would not have succeeded. There have been many great days in the past; there are many great days to come. Here's looking towards the future!

P.S. Thank you to the transition metals for being the most interesting section of the periodic table to study. Your beautifully colored compounds piqued my life-long obsession with the *d*-block. Without elements such as yourselves, life as we know it would not exist. Thanks for being you!

Table of Contents

List of Tables

Chapter 5

List of Figures

Chapter 1

List of Abbreviations

A

AdoHcy, *S*-adenosylhomocysteine

AdoMet, *S*-adenosylmethionine

*Ax*PDEA1, *Acetobacter xylinum* phosphodiesterase A1, a heme-containing oxygen sensor

B

BMAL1, brain and muscle Arnt-like protein-1, a transcription factor

BSA, bovine serum albumin

*Bx*RcoM-1, a CO-sensing heme-containing transcription factor protein homolog from *Burkholderia xenovorans*

*Bx*RcoM-2, a CO-sensing heme-containing transcription factor protein homolog from *Burkholderia xenovorans*

C

CBS, cystathionine β-synthase

CBS424, an inactive form of CBS obtained by heat treatment of Fe(II)CBS

CBS-45, a truncation variant (dimer) of cystathionine β-synthase in which the C-terminal domain (residues 413-551) has been deleted

CBSDH, CBS-deficient homocystinuria

CcO, cytochrome *c* oxidase

CCP, cytochrome *c* peroxidase

*Ch*CooA, a CooA homologue from the thermophilic bacterium *Carboxydothermus hydrogenoformans*

CHES, 2-(*N*-cyclohexylamino)ethanesulfonic acid

cNP, the *Cimex lectularius* nitrophorin

CO, carbon monoxide

Co hCBS, cobalt hCBS

Co $hCBS_{reox}$, cobalt $hCBS_{reox}$

CooA, a CO-sensing transcription regulator heme protein in *Rhodospirillum rubrum*

CoPPIX, cobalt PPIX

CPO, chloroperoxidase

CPO-I, chloroperoxidase Compound I

CPO-II, chloroperoxidase Compound II

cyt *c* M80C, cytochrome *c* in which the native methionine ligand to heme is replaced by cysteine

D

DFT, density functional theory

DGCR8, DiGeorge critical region 8 protein

DHR51, *Drosophila melanogaster* hormone receptor 51

DNR, *Pseudomonas aeruginosa* dissimilative nitrate respiration regulator

*Dm*CBS, *Drosophila melanogaster* CBS

*Dm*E75, the heme-containing nuclear receptor E75 from *Drosophila melanogaster*

DTT, dithiothreitol

E

E75, a heme-containing protein from *Drosophila melanogaster*

*Ec*Dos, heme-containing direct oxygen sensor in *Escherichia coli*

eIF2α, heme-regulated eukaryotic initiation factor 2α kinase

eNOS, endothelial nitric oxide synthase

EPPS, 3-[4-(2-hydroxyethyl)-1-piperazinyl]propanesulfonic acid

EPR, electronic paramagnetic resonance

F

FAD, flavin adenine dinucleotide

FePPIX, iron PPIX (heme)

$\{FeNO\}^6$, a heme-nitrosyl adduct derived from Fe(III) heme

$\{FeNO\}^7$, a heme-nitrosyl adduct derived from Fe(II) heme

FixL, an O_2-sensing heme protein that regulates gene expression associated with N_2 fixation

FMN, flavin mononucleotide

*Fo*NOR, the heme-thiolate nitric oxide reductase from the fungus *Fusarium oxysporum*

G

H

HasA, heme acquisition system protein A

Hb, hemoglobin

H_4B, (6*R*)-5,6,7,8-tetrahydro-L-biopterin

HBD, heme-binding domain

hCBS, human cystathionine β-synthase

$hCBS_{Reox}$, ambiently reoxidized hCBS

Hcy, homocysteine

HemAT, heme-based aerotactic transducer (oxygen sensor) from *Bacillus subtilis*

HEPES, 4-(2-hydroxylethyl)-1-piperazineethanesulfonic acid

HO, heme oxygenase

HRI, heme-regulated eukaryotic initiation factor 2α kinase

HRP, horseradish peroxidase

*Hs*Rev-erbβ, the heme-containing nuclear receptor Rev-erbβ from *Homo sapiens*

I

ICP-OES, inductively-coupled plasma optical-emission spectroscopy

ImH, imidazole

iNOS, inducible nitric oxide synthase

J

K

KatG, a heme-containing catalase-peroxidase

L

LMCT, ligand-to-metal-charge-transfer transition

M

Mb, myoglobin

MCD, magnetic circular dichroism

1-MeIm, 1-methyl imidazole

2-MeImH, 2-methyl imidazole

4-MeImH, 4-methyl imidazole

MES, 2-(*N*-morpholino)ethanesulfonic acid

miRNA, microRNA

MOPS, 3-(*N*-morpholino)propanesulfonic acid

N

NADH, reduced form of nicotinamide adenine dinucleotide

NADPH, reduced form of nicotinamide adenine dinucleotide phosphate

NC1, truncated human DGCR8 AAs 276-751

NC9, truncated human DGCR8 AAs 499-751

nNOS, neuronal nitric oxide synthase

NO, nitric oxide

NOR, nitric oxide reductase

NPAS2, neuronal PAS domain protein 2, a heme CO-sensor eukaryotic transcriptional regulator

O

P

P420, an inactive form of cytochrome P450

P450-II, cytochrome P450 Compound II

$P450_{CAM}$, cytochrome P450 from camphor-hydroxylating *Pseudomonas putida*

$P450_{CAM}$+ImH, cytochrome P450 from camphor-hydroxylating *Pseudomonas putida* with imidazole as an axial ligand to the Fe(III) heme

PAS, a domain structure named for the proteins in which the motif was first identified: Period, aryl hydrocarbon receptor nuclear translocator (ARNT), Simple-minded proteins

PLP, pyridoxal 5'-phosphate

PPIX, protoporphyrin IX

pre-miRNA, precursor miRNA

pri-miRNA, primary miRNA

Q

R

Rev-erbα, a heme-binding nuclear receptor from *Homo sapiens*

Rev-erbβ, a heme-binding nuclear receptor from *Homo sapiens*

rR, resonance Raman

*Rr*CooA, a CO-sensing transcription factor in *Rhodospirillum rubrum*

S

SAM, *S*-adenosylmethionine

SeMet, selenomethionine

sGC, soluble guanylyl cyclase, an NO-sensing heme protein that catalyzes the conversion of GTP to cGMP

T

TD-DFT, time-dependent DFT

TGB, thioglycolate *n*-butyl ester ($C_6H_{11}O_2SH$)

TGE, thioglycolate ethyl ester ($C_4H_7O_2SH$)

TGEH, thioglycolate 2-ethylhexyl ester ($C_{10}H_{19}O_2SH$)

TN, thionalide ($C_{12}H_{10}ONSH$)

Tris, tris(hydroxymethyl)aminomethane

U

V

VTVH-MCD, variable temperature-variable field magnetic circular dichroism

W

WT, wild-type

X,Y,Z

Dedicated to my dear friends and family.

We are all only as strong as the shoulders on which we stand.

Chapter One

Functional Divergence of Heme-Thiolate Proteins: A Classification Based on Spectroscopic Attributes

The original draft of this chapter was developed by Professor Samuel Pazicni (2006) and substantially edited by Dr. Kathy A. Marvin (2008).

Introduction

Heme proteins are some of the most versatile players within the biological milieu; their functions range widely and include electron transfer, catalysis, and small-molecule sensing and transport *(1-3)*. This broad functional diversity can be attributed to the protein environment that constitutes the heme cofactor's binding site, particularly those amino acid residues which serve as axial ligands of the heme iron atom. For example, cytochromes, globins, heme oxygenases, and the majority of peroxidases employ the imidazole moiety of a histidine (His) residue as an axial ligand. Certain cytochromes are also coordinated by the thioether of methionine (Met) or, rarely, the polypeptide N-terminal amino group *(4)*. Catalases *(5)* utilize a tyrosine (Tyr) phenolate. An ever-growing class of heme proteins employs a cysteine (Cys) thiolate as an axial ligand to heme *b* (iron-protoporphyrin IX, Figure 1.1).

Differences in solvent exposure, hydrophobicity, iron atom oxidation and spin state, and the identity of the iron atom axial ligand(s) give rise to a wide variety of spectroscopic characteristics; a combination of these spectroscopic signatures provides useful fingerprinting handles with which to classify hemoproteins. In accordance with nearly fifty years of work on cysteine(thiolate)-ligated heme proteins, coordination of a Cys ligand to heme *b* confers two differing sets of spectroscopic signatures to these proteins. Because the different spectroscopic signatures arise from differences in electronic structure at the heme cofactor, it is unsurprising that the different types of Cys-ligated hemoproteins display distinct types of reactivity. These two types of reactivity allow heme-thiolate proteins to play distinct roles in Nature: catalysts or small molecule sensors/transporters.

Classification of Heme-Thiolate Proteins

Based on differential spectroscopic and functional attributes, we propose that thiolate-ligated heme proteins may be separated into two groups: type-1 and type-2 (Table 1.1). The type-1 heme-thiolates are centers of biological reactions in which small molecules, e.g. O_2, H_2O_2 or NO, are activated for catalysis. The type-1 heme centers are catalytically competent only in a five-coordinate, high-spin state with an available vacant (or labile) sixth iron coordination site. The distinguishing reactivity characteristic of the type-1 centers is a cysteine(thiolate) ligand that is stable to ligand exchange upon reduction (non-labile). Thus, the cysteine(thiolate) residue is retained during the catalytic cycle as well as upon binding exogenous ligands (Figure 1.2A). In contrast, the type-2 heme-thiolates are centers of small molecule sensing or transport. The type-2 cysteine(thiolate) heme ligand is labile, which is fundamental to its function. Upon reduction of the type-2 heme-thiolates, the cysteine(thiolate) ligand may become protonated, and is replaced either by a protein-derived ligand (termed a "ligand switch") or an exogenous ligand. Type-2 heme-thiolates are generally six-coordinate and low-spin, and the cysteine(thiolate) is bound to the iron opposite a neutral donor, most often a histidine imidazole, in the Fe(III) state. Because of the propensity for type-2 heme-thiolates to undergo ligand switches upon reduction, the low spin, six-coordinate state is preserved when converted to the ferrous state (Figure 1.2B).

X-ray crystallographic, spectroscopic, and biochemical studies of native proteins, complemented by computational investigations, studies of protein-based heme-ligand adducts, and transition-metal model complexes have contributed significantly to the understanding of the characteristics that define the two proposed categories of heme-thiolate proteins. First identified in the extensive cytochrome P450 family *(6)*, type-1 heme-thiolate coordination has

now been characterized in chloroperoxidase (CPO) from *Caldariomyces fumago (7, 8)*, the fungal nitric oxide reductases (NORs) (*9*) and the nitric oxide synthases (NOSs) *(10)*. The type-2 heme-thiolates include CooA from *Rhodospirillum rubrum (11, 12)*, human cystathionine β-synthase (hCBS) (*13, 14*), heme-regulated eukaryotic initiation factor 2α (eIF2α) kinase (*15*), neuronal PAS domain protein 2 (NPAS2) *(16)*, the *Cimex lectularius* nitrophorin (cNP) (*17*), the regulators of CO metabolism (RcoM-1 and RcoM-2) from *Burkholderia xenovorans (18)*, the nuclear receptors E75 *(19, 20)* from *Drosophila melanogaster*, human Rev-erbα and Rev-erbβ (*20*), and DHR51 from *Drosophila melanogaster (21)*. This review outlines the distinctive spectroscopic and functional attributes of the two types of heme-thiolate coordination and draws upon both historical knowledge and recent advances in heme-thiolate chemistry to gain insight into how the catalytic and small-molecule sensing/transport functions are supported and distinguished by the heme-thiolate moiety.

First Spectroscopic Evidence of Heme-Thiolate Proteins

Though cysteine(thiolate) coordination is a unifying feature of heme-thiolate proteins, type-1 and type-2 heme centers typically exhibit distinctly different spectral features either in the same oxidation states or in the presence of exogenous ligands. The type-1 and type-2 heme-thiolates are excellent examples of how the protein environment of a heme cofactor influences both the function and spectrosopic characteristics of the heme. The unique spectroscopic signatures of heme-thiolate ligation were first observed over 50 years ago in studies of a CO-binding pigment from liver microsomes that contained iron protoporphyrin IX and exhibited an ‘anomalous’ red-shifted electronic absorption band at 450 nm *(22, 23)*. Stern and Peisach *(24)* later proposed sulfur coordination of this cytochrome “P450” CO adduct

based on their model compound studies; however, the identity of the axial ligands remained in question until the X-ray crystal structure of soluble camphor-hydroxylating cytochrome P450 from *Pseudonomas putida* (cytochrome $P450_{CAM}$) confirmed the presence of a thiolate-bound heme cofactor *(25)*. The spectroscopic "fingerprints" that have been used to identify essentially all other heme-thiolate proteins originate from studies on cytochrome P450, its derivatives, and related model complexes. Here, we review the lines of spectroscopic evidence that separate type-1 and type-2 heme-thiolates.

Ferric Heme-Thiolates

Electronic absorption spectroscopy distinguishes between type-1 and type-2 heme-thiolates.

Electronic absorption spectroscopy provides a straightforward and useful means to identify the difference between type-1 and type-2 Fe(III) heme-thiolates. The visible and near-ultraviolet regions (300-800 nm) of heme absorption spectra are dominated by porphyrin ($\pi \rightarrow \pi^*$) electronic transitions (*26*). In type-2 heme-thiolates, the six-coordinate, low-spin Fe(III) state is common; the P450 cytochromes and NOSs also exhibit six-coordinate, low-spin Fe(III) resting states, in which the sixth axial position is coordinated by water or hydroxide *(27-29)*. A classical Fe(III) low-spin heme absorption spectrum consists of (in order of decreasing energy) the δ (or "n") band, the Soret (γ or "B") band, and the α and β (visible or "Q") bands (*26*). The position of the low-spin heme-thiolate Soret band typically ranges from 415-430 nm, while the α–β bands appear at 535-575 nm and may be resolved (typical for H_2O or the N-terminal amino group *trans* to the thiolate) or consist of a broad absorption envelope (typical for histidine *trans* to thiolate). An intense, well-resolved δ band consistently appears at 355-365 nm. This band is interpreted as being the result of mixing between a cysteine(thiolate)-

associated ligand-to-metal charge transfer (LMCT or CT) (S(p) → Fe(d_{π})) transition and the porphyrin ($\pi \rightarrow \pi^*$) Soret transition (*30, 31*). A second distinctive feature of six-coordinate heme-thiolates is a pair of broad, low-energy (and low intensity) visible absorption LMCT bands (S(p) → Fe(III)), which are observed at approximately 650 nm and 750 nm *(32)* (Figure 1.3).

The five-coordinate, high-spin Fe(III) state with a sole cysteine(thiolate) heme ligand is accessed only by the type-1 heme-thiolates and exhibits spectral features distinct from those of the type-2 heme-thiolates. The resting states of isolated CPO and NOR are predominantly high-spin, while the six-coordinate, low-spin resting states of P450 and NOS are converted to the high-spin state by the binding of substrate *(8, 27-29, 33, 34)*. In contrast to low-spin heme-thiolate spectra, high-spin Fe(III) heme-thiolate absorption spectra are dominated by a broadened, blue-shifted Soret band at 390-400 nm and bear little difference from that of other high-spin hemoproteins. Broad visible bands are observed between 500-600 nm, as well as a characteristic S(p) → Fe(III) LMCT feature at approximately 650 nm.

Magnetic circular dichroism (MCD) spectra of low-spin heme-thiolates possess multiple charge transfer bands.

Magnetic circular dichroism (MCD) spectroscopy is a powerful probe of spin state, oxidation state, and axial ligand identity that readily discriminates between type-1 and type-2 heme-thiolates. This technique has been used quite successfully to compare synthetic heme model complexes to heme proteins of unknown axial ligation, particularly in studies of the P450 cytochromes (*31, 35, 36*). Whereas electronic absorption transitions of numerous heme proteins can be broad and generally non-descript, the MCD transitions of heme proteins are

circularly-polarized transitions that are frequently oppositely-signed; this increase in fine structure gives rise to the detailed fingerprinting capability of MCD spectroscopy *(37-44)*. In most heme proteins that are six-coordinate and low-spin, a characteristic temperature-dependent (*C*-term) peak/trough/peak pattern in the Soret region dominates the Fe(III) MCD spectrum. The peak/trough/peak position, which is typically red-shifted in six-coordinate, low-spin heme-thiolate proteins, is used as a marker for Cys coordination (*45, 46*) (Table 1.2, Figure 1.4). Furthermore, the MCD δ- and Soret-band troughs are typically more intense in low-spin heme-thiolates with cytochrome P450-like coordination. In contrast, high-spin Fe(III) heme-thiolates display an asymmetric MCD spectral pattern that spans the visible and UV regions with an intense negative feature between 390-400 nm *(47)* (Table 1.2, Figure 1.4).

In low-spin heme proteins, the visible and near-IR regions display ligand-sensitive LMCT transitions involving the heme iron that are detectable in MCD spectroscopy *(32, 48-50)*. Unlike the visible region CT bands, the lower energy near-IR bands are difficult to observe in electronic absorption spectra due to overlap with O-H, C-H, and N-H vibrational overtones from water or protein. However, upon deuteration these bands can be detected as two positive temperature-dependent *C*-terms in near-infrared MCD spectra. In low-spin heme proteins, the porphyrin(π) → Fe(III) CT transitions occur between 800-2400 nm and are modulated by the donor ligand strength; in heme-thiolates, these transitions are observed at 1035-1200 nm (*49, 51*) (Figure 1.5). These weak charge transfer bands in the visible and near-IR regions provide strong evidence for the presence of a low-spin Fe(III) heme-thiolate.

A distinctive Fe-S stretching mode is observed in resonance Raman (rR) spectra.

Resonance Raman (rR) spectroscopy is a powerful and selective probe of molecular vibrations in heme proteins that distinguishes between the type-1 and type-2 heme-thiolate coordination states. Excitation at wavelengths near the heme Soret band in rR results in a spectrum that is dominated by bands corresponding to the totally symmetric porphyrin stretching modes *(52)*. The high frequency region (1200-1700 cm^{-1}) of heme Raman spectra exhibits well-resolved porphyrin in-plane modes that are sensitive to the oxidation state (ν_4), or the spin and coordination state (ν_3 and ν_4) of the heme iron *(53, 54)*. Most Fe(III) heme centers exhibit comparable frequencies for ν_4 (~ 1370-1375 cm^{-1}); similarly, ν_3 lies at ~ 1500 cm^{-1} for low-spin, six-coordinate hemes and at ~ 1490 cm^{-1} for high-spin, five-coordinate hemes. The dependence of ν_3 on spin and coordination state was elegantly illustrated by substrate binding to cytochrome $P450_{CAM}$ complexed with putidaredoxin, which converts the low-spin, six-coordinate resting state (ν_3 = 1503 cm^{-1}) to a high-spin, five-coordinate Fe(III) heme-thiolate (ν_3 = 1488 cm^{-1}) *(55)*.

The low frequency rR spectrum of the Fe(III) heme-thiolate is extremely useful in differentiating between type-1 and type-2 heme-thiolates via the iron-sulfur(thiolate) bond stretching vibration. Unlike the high frequency window, the low frequency window of Fe(III) heme Raman spectra (200-700 cm^{-1}) is useful for ligand identification, as metal-ligand vibrations that are coupled to the porphyrin $\pi \rightarrow \pi^*$ totally symmetric mode appear at these frequencies and are sensitive to isotopic substitution. Champion, *et al*. *(56, 57)* directly demonstrated the presence of a heme iron-sulfur bond ($\nu_{Fe\text{-}S}$) in cytochrome P450 using ^{34}S- and ^{57}Fe-enriched, substrate-bound Fe(III) cytochrome $P450_{CAM}$. Selective enhancement using 363.8 nm excitation revealed $\nu_{Fe\text{-}S}$ at 351 cm^{-1} in the Fe(III) enzyme. Several other $\nu_{Fe\text{-}S}$ modes have been identified based on either this comparison or isotopic substitution: 348 cm^{-1} for the

high-spin, five-coordinate H25C variant of heme oxygenase (*58*); 347 cm^{-1} for high-spin, five-coordinate chloroperoxidase (*59*); 333 cm^{-1} for the high-spin, five-coordinate iron response regulator (Irr) (*60*); and 338 cm^{-1} for the high-spin, five-coordinate inducible nitric oxide synthase (iNOS) (*61*) (Table 1.3). Soret excitation at 413.1 nm of the globally ^{34}S substituted type-2 heme-thiolate Fe(III)hCBS, in contrast, identified the ν_{Fe-S} mode in the low-spin protein at 312 cm^{-1} *(62)*. The lower frequency of the ν_{Fe-S} mode in hCBS, as compared to those identified in high-spin heme-thiolates, suggests that the Fe-S bond is weaker in six-coordinate, low-spin hemes than in five-coordinate, high-spin systems. Indeed, support for this argument is garnered by the putative assignments for Fe(III) ν_{Fe-S} modes in the type-2 heme-thiolates Rev-erbβ (312 cm^{-1}) (*20*), E75 (312 cm^{-1}) (*20*), and RcoM-2 (310 cm^{-1}) (*18*) (Table 1.3).

Low- and high-spin Fe(III) heme-thiolates exhibit unique electron paramagnetic resonance (EPR) spectra.

One of the most useful spectroscopic techniques used to characterize and ultimately distinguish between the type-1 and type-2 heme-thiolates is electron paramagnetic resonance (EPR) spectroscopy, which is a technique highly sensitive to the coordination environment of metal ions. EPR was indispensable in the characterization of ligand-globin adducts and model complexes of cytochrome P450 *(63-68)*. Subsequent studies using synthetic model complexes with low-spin P450-like heme centers demonstrated EPR features that were unique among low-spin heme systems. The majority of low-spin hemes, including heme-thiolates, exhibit a rhombic signal centered about $g \sim 2$, due to their low symmetry. However, the narrow separation between g_x, g_y, and g_z in heme-thiolate EPR spectra easily distinguishes this group from other low-spin heme centers *(69)* (Table 1.4). The extent of *g*-value separation in low-

spin Fe(III) heme spectra was described by Blumberg and Peisach in terms of V/Δ, also termed "rhombicity." This ratio relates the crystal field parameters to the heme plane ligand field (V) and the axial ligand field (Δ) strengths. Low-spin heme-thiolates typically exhibit a low value of V/Δ, due to their strong ligand field. This effect is illustrated graphically in crystal field diagrams, which plot rhombicity against tetragonality (Δ/λ), which is a function of electrostatic charge (Figure 1.6). Blumberg and Peisach *(69)* defined five regions in the crystal field diagram: C, B, H, O, and P, which correspond to His/Met, His/His(N^-), His/His, His/OH^-, and Cys(S^-)/X ligation, respectively. The heme-thiolates fall into the P region, whose members exhibit a combination of the largest values of Δ/λ and the smallest values of V/Δ. The large variability in tetragonal field of the P region suggests that heme-thiolates experience widely varying electrostatic charge, which may be a function of hydrogen bonding at the thiolate anion.

In addition to a narrow g anisotropy, low-spin heme-thiolates also frequently exhibit two (or more) overlapping rhombic signals in their EPR spectra *(63)* (Table 1.4). Originally observed in thiol adducts of hemoglobin and myoglobin, this phenomenon has been documented in the type-2 heme-thiolates CooA *(12),* hCBS *(14),* RcoM-2 (*18*), E75 (*19, 20*), and Rev-erbβ *(20).* Dual EPR signals have only also been observed for the tyrosinate-ligated hemophore HasA, which has a strongly hydrogen-bonded His residue at the phenolate moiety (*70*). These findings suggest that the protein environment may induce inhomogeneity in the heme-anion environment. Our studies on heme-thiolate proteins and model complexes indicate that multiple signals are related to the extent of hydrogen bonding to the cysteine (*71*). Evidence for this assertion comes from many angles. First, the EPR signals in CooA (*11*), CBS (*72*) and Rev-erbβ (*20*) exhibit high sensitivity to pH. Second, a mutation of a histidine near the

thiolate heme ligand in CooA abolishes the presence of the second EPR signal, possibly by elimination of an important hydrogen-bonding interaction with the axial cysteine (*11*). Third, the disease-associated R266K hCBS variant, which alters the hydrogen-bonding partner at the cysteine(thiolate), changes the EPR *g* value spread and the relation of the dual signals; this observation is also correlated with a weaker $\nu_{Fe\text{-}S}$ mode in rR spectroscopy (*73*). Fourth, the dual signal in hCBS may be converted to a single signal in the presence of glycerol, which is frequently used as a glassing agent in EPR samples and has a different hydrogen-bonding capacity than water (*71*).

The high-spin Fe(III) type-1 heme-thiolates exhibit EPR spectra distinct from low-spin heme-thiolates as well as other high-spin heme systems. High-spin Fe(III) heme-thiolates possess a spin sextet ground state ($S = 5/2$); however, because the energy of axial zero field splitting in high-spin heme centers (typically D = 5-10 cm^{-1}) is larger than that of the microwave quantum responsible for inducing the EPR transition (~0.3 cm^{-1} for a 9 GHz X-band instrument), observed EPR activity is limited to the lowest-energy Kramers doublet ($m_S = \pm 1/2$) of the ground state sextet (Figure 1.7). Thus, the observed EPR signal is similar in nature to that of low-spin heme-thiolates, but the degree of rhombic splitting in the EPR spectra of high-spin heme-thiolates is generally much greater than that of other high-spin heme centers *(74-76)*. EPR *g*-values are typically observed at $g = 6$ and $g = 2$ for purely five-coordinate, axial species; the *g* values are similar for six-coordinate, rhombic species, although a third *g*-value is rarely noted. When evaluated by the method of Peisach *(77)*, the iron atom of high-spin heme-thiolates experiences the most rhombic environment observed for a high-spin heme system.

Ferrous Heme-Thiolates

Low-spin Fe(II) heme-thiolates exhibit coordination-dependent spectral characteristics.

Reduction of type-2 heme-thiolates induces dramatic changes in the heme coordination upon replacement of the labile cysteine(thiolate) ligand by a neutral protein ligand, which eliminates the distinctive spectral characteristics of cysteine(thiolate) ligation. The Soret band transition of a low-spin Fe(II) (*S*=0) heme center coordinated by two neutral donors normally occurs in the range of 420-430 nm, accompanied by intense, well-resolved, assymmetric visible region peaks (usually $\varepsilon_\alpha > \varepsilon_\beta$). The Fe(II) type-2 heme-thiolates (except Fe(II) hCBS; see Figure 1.8) display these spectral characteristics, due to their propensity to have the Cys(thiolate) ligand replaced by a neutral donor ligand upon reduction (Figure 1.8). The type-1 Fe(II) heme-thiolates, which retain their thiolate ligand upon reduction, are usually encountered as the five-coordinate, high-spin (*S*=2) state. The low-spin (*S*=0) Fe(II) type-1 heme-thiolates are usually accessed by adding exogenous ligands, such as carbon monoxide *(78, 79)*, nitric oxide *(80-82)*, nitrosoalkanes *(83, 84)*, thiols and thioethers *(85)* and amines (*64, 86*). The various low-spin ligand adducts of cytochrome $P450_{CAM}$ universally exhibit an extremely red-shifted Soret absorption maximum. The ~450 nm Soret, first observed in CO-bound Fe(II)P450 cytochromes, is now a hallmark diagnostic of low-spin, Fe(II) type-1 heme-thiolate centers.

Elegant absorption and MCD characterization of Fe(II) $P450_{CAM}$ ligand adducts by Dawson and coworkers (*87*) divide the low-spin Fe(II) heme-thiolates into two groups: 1) hyperporphyrins (*26, 88*), which exhibit a prominent extra absorption band in the $320 < \lambda < 400$ nm region (called the "split Soret" or "blue Soret") of nearly equivalent intensity to the Soret (called the "red Soret") and a single, broad α-β absorption envelope at ~ 550 nm; and 2) regular heme-thiolates, which exhibit one, red-shifted Soret band with discrete α and β bands at ~ 560

and ~540 nm, respectively. Fe(II) hyperporphyrin spectral features arise only in low-spin heme-thiolates with a sixth strong π-acceptor ligand, e.g. CO or nitrosoalkanes, which enables orbital mixing of the Soret and charge transfer transitions between the iron and axial ligand π orbitals *(89, 90)*. In contrast, "regular" low-spin Fe(II) heme-thiolate centers are observed with pure σ–donors, e.g. dimethylsulfide, *n*-phenylimidazole, and metyrapone (*87*).

MCD spectroscopy distinguishes among low-spin hyperporphyrin Fe(II) type-1, regular Fe(II) type-1, and type-2 heme-thiolates. Hyperporphyrin MCD spectra are dominated by transitions in the Soret region. A strong negative δ band and an intense, derivative-shaped temperature-independent *A*-term in the Soret region are hallmarks of hyperporphyrin Fe(II) low-spin type-1 heme-thiolates ($S = 0$). In contrast, the most prominent feature of regular low-spin Fe(II) type-1 and type-2 heme-thiolate MCD spectra is an intense *A*-term ('α-band') in the visible region. The α-band feature is present in most low-spin Fe(II) heme MCD spectra, and its position is indicative of the identity of the axial heme ligands. An α-band crossover position between 562-576 nm is typical for low-spin Fe(II) type-1 heme-thiolates; an α-band position between 550-560 nm is typical for low-spin Fe(II) type-2 heme-thiolates (*87*) (Figure 1.9).

High-spin Fe(II) heme-thiolates exhibit atypical optical and rR spectra.

A high-spin, thiolate-coordinated Fe(II) state is only accessed by the type-1 heme-thiolates, which present spectral features distinct from both low-spin type-1 and type-2 heme-thiolate systems. Biologically, this spin and ligation state is most relevant to the catalytic cycle of the P450 (and P450-like) enzymes. Five-coordinate, high-spin Fe(II) heme-thiolates typically exhibit Soret and unresolved visible absorption maxima at 410 nm and 540 nm, respectively *(91)*. High-spin Fe(II) heme-thiolates ($S = 2$) are also characterized by a

temperature-dependent MCD *C*-term similar in the Soret region (Figure 1.10). The red-shifted Soret region MCD term bears a strong negative band at 420 nm with a plateau of positive intensity and a weak negative feature at 570 nm in the visible region *(92, 93)*. However, an equilibrium mixture of high and low spin states is commonly encountered in the MCD spectra.

Resonance Raman spectroscopy reveals further disparities between the type-1 high-spin and type-1 and type-2 low-spin heme-thiolate centers. The oxidation state marker bands (ν_4) of Fe(II) P450 cytochromes *(94, 95)*, CPO *(94, 96, 97)* and NOS *(98)* occur at unusually low energies as compared to other Fe(II) high-spin heme centers. High-spin Fe(II) heme-thiolates exhibit ν_4 in the range of 1341-1348 cm^{-1}; the analogous band for high-spin Fe(II) heme centers with a lone histidine ligand as well as low-spin Fe(II) heme centers with two neutral ligands occurs between 1355-1360 cm^{-1}. Similarly, the spin and coordination state marker band ν_3 consistently appears near 1466 cm^{-1} for high-spin Fe(II) heme-thiolates; ν_3 occurs at 1470-1475 cm^{-1} for histidine-coordinated high-spin Fe(II) heme proteins and at 1485-1490 cm^{-1} for low-spin Fe(II) heme proteins. These anomalously low frequencies are attributed to the strong π-donor influence of the cysteine(thiolate) ligand, which is sensed by the Raman-active porphyrin π^* orbitals via back-donation from the d_π orbitals of the Fe(II) atom *(99, 100)*.

Ferrous Dioxygen Adducts

Two distinct dioxgen adducts appear to be a function of the oxyheme-thiolate environment.

The most relevant reaction of the type-1 heme-thiolate oxygenases involves interaction with dioxygen at the Fe(II) high-spin heme center to form a reversible complex with triplet O_2. This diamagnetic, low-spin adduct is generally described as a Fe(II)-dioxygen (Fe(II)-O_2) complex, a Fe(III)-superoxo (Fe(III)-$O_2^{\bullet-}$) complex, or a resonance hybrid of the two *(101)*.

Ishimura, *et al*. *(102)* reported the first dioxygen complex of cytochrome $P450_{CAM}$, which exhibits an absorbance spectrum with two prominent maxima at 355 nm and 418 nm. While the absorption features are very similar to those of oxymyoglobin (*103*), the MCD spectrum of oxy-cytochrome $P450_{CAM}$ is distinct from that of oxymyoglobin, suggesting a different electronic structure *(104, 105)*. The $\nu_{O\text{-}O}$ stretch observed (1140 cm^{-1}) in the rR spectrum of oxy-cytochrome $P450_{CAM}$ *(106)* is of nearly identical frequency (1140 cm^{-1}) to that of the oxy-thiolate-bound "picket fence" porphyrin complex *(107)* and an elaborate cytochrome P450 model (1137 cm^{-1}) containing a hydrogen-bonded dioxygen ligand *(108)*. The relatively low $\nu_{O–O}$ of oxyheme-thiolate centers suggests there is a weaker O-O bond than in oxyhemoglobin, where a multiplet of bands are detected at higher average energy *(109)*. This decrease in $\nu_{O–O}$ for heme-thiolates relative to imidazole-ligated heme centers likely originates from greater π back-bonding from the iron into the π^* orbitals of oxygen, weakening the O–O bond and facilitating its cleavage *(44)*.

The variability in the spectral features of oxy-heme-thiolates, including the sensitivity of the Soret band position to solvent polarity, has been well-documented for synthetic model complexes *(110, 111)*. Furthermore, several crystal structures exist that reveal differences in hydrogen-bonding at the Cys(thiolate) ligand among the P450s and CPOs; these secondary interactions may differentially attenuate the donor capability of the thiolate ion, and thus modify the electronics at the oxy-heme center (*112-116*). This difference may be one way of controlling the reactivity of P450 vs. CPO towards O_2. These observations likely explain why the absorption and MCD spectra of oxy-CPO are distinct from those of oxy-cytochrome $P450_{CAM}$ despite the extensive spectroscopic similarities between other adducts of the P450 cytochromes and CPO *(117)*. Interestingly, the transitory oxo-adducts of the NOSs, which

have been observed with stopped-flow techniques, exhibit distinct temperature-dependent species termed heme-oxy I and heme-oxy II, which parallel the respective dioxygen adducts of CPO and cytochrome P450 *(118, 119)*.

Heme-thiolate Compound I is likely a ferryl-oxo species with a porphyrin-based radical.

Reactive oxygen intermediates are responsible for the biological transformations inherent to the type-1 heme-thiolate oxygenases. By analogy to intermediates formed in other heme-containing oxidases, the putative heme-thiolate-based oxidants are thought to be an Fe(IV)-oxo porphyrin radical cation species (Compound I) and an Fe(IV)-oxo porphyrin species (Compound II) *(120, 121)* (Figure 1.11). Compound I is doubly oxidized above the Fe(III) resting state, one equivalent being associated with a ferryl center $[Fe(IV)=O]^{2+}$, and the other with the porphyrin-based radical that is delocalized onto the Cys(thiolate) ligand. It functions as a two-electron oxidant in cytochrome P450 and a one-electron oxidant in the peroxidase mode of CPO. Compound II, produced by one-electron reduction of Compound I, is inherent to the peroxidase cycle of CPO, and can also be formed in the P450 cytochromes via reaction with peroxynitrate *(122, 123)*. However, recent work has questioned the nature of the protonation state of Compound II (*124, 125*).

Compound I of CPO (CPO-I) is the most fully characterized heme-thiolate Compound I and has been spectroscopically characterized by absorption *(126, 127)*, resonance Raman *(126, 128, 129),* EPR and Mössbauer *(130)* as well as X-ray absorption spectroscopies *(131)*. The CPO-I absorption spectrum exhibits an extremely blue-shifted asymmetric Soret band (364 nm) and a distinct feature in the visible region (689 nm), which are comparable to peak positions calculated by DFT *(132)* for a model complex. The EPR properties (g^{eff} 1.61, 1.72, 2.00) are

interpreted as arising from the lowest-energy Kramers doublet of a strongly antiferromagnetically-coupled spin $S = 1$ ferryl and a spin $S' = ½$ porphyrin radical *(130, 133)*. Egawa, *et al*. *(129)* identified a ν_4 band for CPO-I which is downshifted and weak compared to other species in the CPO catalytic cycle, compatible with ν_4 observed in model systems upon porphyrin π cation radical formation *(128, 134, 135)*. The presence of a ferryl-oxo core was later verified by X-ray absorption spectroscopy *(131)*.

Recent studies have identified and characterized the spectroscopic and kinetic properties of Compound 1 generated from reaction of *m*-chloroperbenzoic acid with P450 from the thermophilic bacterium *Sulfolobus acidocaladarius* (CYP119-I) (*133, 136*). Despite being superficially similar, CYP119-I is substantially more reactive than CPO-I and is capable of reacting with unactivated C-H bonds, whereas CPO-I will not; it is suggested that this difference is attributable to electronics, not substrate access (*133, 137*). Indeed, while electronic absorption (Figure 1.12) and Mössbauer spectroscopies suggest a similarity between CPO-I and CYP119-I, their EPR spectra are different. The fitted *g* values reported for CYP119-I are g^{eff} 1.86, 1.96, and 2.00, slightly shifted from those of CPO-I; furthermore, fitted values of $|J|/D$, a measure of the ratio of the antiferromagnetic coupling to that of the axial ZFS, suggest that there is stronger coupling for CYP119-I (*133*). This stronger coupling is thought to arise from the shorter Fe-S bond in CYP119-I compared to CPO-I (*133*).

Fe(II) type-2 heme-thiolates reoxidize in the presence of dioxygen.

In contrast to the type-1 heme-thiolates, which form dioxygen adducts as part of their catalytic cycle, the type-2 heme-thiolates react with oxygen in an outer-sphere mechanism (i.e. via autoxidation). To date, no oxygenated adducts of type-2 heme-thiolates have been

identified. Oxygen reactivity has been investigated for *Rr*CooA (*11*), *Bx*RcoM-2 (*18*) , eIF2α kinase (*15*), E75 and Rev-erbβ *(20),* and hCBS (*138, 139*). Thiolate coordination is retained in Fe(II)hCBS at high pH (Figure X), and exposure of the protein to air results in oxidation to Fe(III)CBS without changes in heme iron coordination (*138, 139*). The redox-mediated ligand switch of *Rr*CooA (*vide infra*) is reversed when exposed to air. A reasonable explanation for this behavior is that type-2 Fe(II) heme-thiolates exist as low-spin, spin singlet species, and the reaction of triplet O_2 with singlet heme iron to yield a singlet oxyheme adduct is a spin-forbidden process. The high-spin, quintet ground state of Fe(II) type-1 heme-thiolates, however, bind O_2 quite readily (*vide supra*). DFT calculations have suggested that binding of O_2 to high-spin Fe(II) heme arises from the near degeneracy (within 10 kJ/mol) of the triplet (O_2) and quintet (Fe) states of these species *(140).* This near degeneracy facilitates spin-crossover in the transition state, allowing the spin-forbidden reaction to occur. Low-lying quintet states likely do not exist for low-spin Fe(II) heme-thiolates, thereby eliminating any potential reactivity with O_2 beyond the observed autoxidation chemistry.

Ferrous Carbonyl Adducts

Heme-thiolate CO adducts exhibit distinctive optical spectra and rR frequencies.

Though only relevant to the functions of certain type-2 heme-thiolates, the differences in the spectroscopic attributes of carbon monoxide (CO) adducts of the type-1 and type-2 heme-thiolates provide further evidence for the separation of the two sub-classes. Now a common probe of heme centers, $CO_{(g)}$ was first reacted with the Fe(II) heme-thiolate cytochrome P450 to reveal the anomalous Soret absorption maximum at ~ 450 nm; this strongly red-shifted Soret maximum is now commonly attributed to CO binding *trans* to

cysteine(thiolate) in type-1 heme-thiolates (*88*). Because the type-2 cysteine(thiolate) is displaced either by a redox-mediated ligand switch or by the CO molecule itself, the type-2 heme-thiolate CO adducts display a Soret band at 420 nm and equivalent α–β peaks at approximately 560 and 540 nm, respectively. In further contrast to type-1 heme-thiolate CO adducts (*vide supra*), MCD spectra for the type-2 CO adducts are dominated by symmetric, derivative-shaped temperature-independent *A*-terms in the Soret and visible regions (*18, 20, 87, 141, 142*).

Resonance Raman spectroscopy further distinguishes the CO adducts derived from type-1 and type-2 heme-thiolates. Heme-CO adducts exhibit two characteristic stretching modes attributed to Fe-CO ($\nu_{Fe\text{-}CO}$) and C-O ($\nu_{C\text{-}O}$) vibrations in the 460-540 cm^{-1} and 1900-2000 cm^{-1} regions, respectively. An inverse linear correlation exists between the frequencies of the $\nu_{C\text{-}O}$ and $\nu_{Fe\text{-}CO}$ stretching modes of heme proteins and model compounds *(143, 144)* (Figure 1.13). This correlation arises from the degree of back-bonding of the Fe(II) heme atom to the CO molecule, the extent of which is sensitive to the ligand (or lack thereof) *trans* to CO. Strong donor ligands, such as cysteine(thiolate), cause two different phenomena: 1) an inherently weaker Fe-C bond, due to stronger polarization of the d_z^2 orbital towards the mercaptide moiety, and 2) a strong inverse correlation due to π back-bonding from the Fe atom to the π* CO molecular orbital *(145)*. These phenomena result in a consistent deviation by type-1 heme-thiolate CO adducts from the neutral *trans* ligand $\nu_{C\text{-}O}/\nu_{Fe\text{-}CO}$ correlation for the type-2 CO-adducts. Thus, type-1 and type-2 heme-thiolates can be distinguished by which $\nu_{C\text{-}O}/\nu_{Fe\text{-}CO}$ correlation their respective CO-adducts obey.

Ferric/Ferrous Nitrosyl Adducts

Three distinct nitrosyl adducts are observed in heme-thiolate proteins.

The type-1 and type-2 heme-thiolates exhibit quite different reactivity and spectral features when coordinated by nitric oxide (NO˙). Unlike other exogenous heme ligands, such as CO and O_2, NO is able to bind to both Fe(III) and Fe(II) heme centers. These species have been termed in the nomenclature of Feltham and Enemark as $\{FeNO\}^6$ and $\{FeNO\}^7$, respectively *(146, 147)*. Addition of NO to Fe(III) type-1 heme-thiolates, regardless of heme iron spin state, results in a six-coordinate thiolate-ligated $\{FeNO\}^6$ species characterized by absorption maxima at approximately 430-440 nm (Soret), 540 nm (β) and 570 nm (α) (*148, 149*). The $\{FeNO\}^7$ type-1 heme-thiolate adduct is characterized by a hyperporphyrin absorption spectrum with a split Soret band (370, 440 nm) and a broad visible absorption at approximately 560 nm. Under certain conditions, such as denaturation, type-1 heme-thiolates convert to a second, distinct five-coordinate $\{FeNO\}^7$ species, in which both protein-derived axial ligands have been lost *(82)*. This five-coordinate $\{FeNO\}^7$ species is characterized by a broad, low-intensity Soret band at 400 nm and visible bands at 540 nm (β) and 570 nm (α).

The type-2 heme-thiolates typically form a five-coordinate $\{FeNO\}^7$ adduct, though recently characterized type-2 hemes have exhibited a six-coordinate $\{FeNO\}^7$ species. In all published accounts involving addition of NO to Fe(III) type-2 heme-thiolates, auto-reduction of the heme center occurs with loss of both endogenous ligands. Thus, reaction of NO with both Fe(III) and Fe(II) CooA yields the five coordinate $\{FeNO\}^7$ species *(150)*. Both hCBS (*151*) and eIF2α kinase (*15*) form five-coordinate NO adducts, although reaction with NO has only been investigated in the Fe(II) state of these two enzymes. Reaction of Fe(II) *Bx*RcoM-2 (*18*) and *Hs*Rev-erbβ (*20*) with NO forms six-coordinate adducts, while reaction of Fe(II) *Dm*E75

with NO (*20*) forms a five-coordinate NO adduct. Similar to globin proteins with NO bound opposite a neutral donor ligand, the six-coordinate NO adducts exhibit a sharp Soret band in the 415-425 nm range with a broad α–β absorption envelope centered about 560 nm (*103*).

EPR spectroscopy, which is capable of detecting nuclear-electronic spin-coupling of a coordinated NO˙ radical with a *trans* ligand, readily distinguishes between the five- and six-coordinate $\{FeNO\}^6$ and $\{FeNO\}^7$ type-1 and type-2 heme-thiolate adducts. In Fe(III) type-1 heme-thiolate $\{FeNO\}^6$ species, the binding of NO forces a spin-state crossover; the only unpaired electron on the Fe(III) atom then couples to the unpaired electron on the bound NO, resulting in a spin-paired, EPR-silent species *(152)*. In contrast, the type-1 heme-thiolate $\{FeNO\}^7$ adducts exhibit a rhombic EPR signal whose central resonance (g_2) displays a well-resolved triplet hyperfine structure due to coupling of the unpaired electron of NO to the nuclear spin of ^{14}N ($I = 1$) *(31)* (Figure 1.14, left panel). The analogous type-2 $\{FeNO\}^7$ adducts typically display classic nine-line rhombic EPR spectra in which g_2 is split into hyperfine and superhyperfine signals that arise from coupling of the NO electron with the nuclear spin of the *trans* nitrogen-atom of the coordinated residue (usually His) *(153)* (Figure 1.14, left panel). The five-coordinate $\{FeNO\}^7$ adducts that are observed in the heme-thiolates exhibit only axially symmetric three-line EPR spectra *(154)* (Figure 1.14, right panel).

Significant differences among the five- and six-coordinate $\{FeNO\}^6$ and $\{FeNO\}^7$ adducts in type-1 and type-2 heme-thiolates are also observed in their corresponding rR spectra. Type-1 heme-thiolate $\{FeNO\}^6$ adducts exhibit vibrational Fe-NO (ν_{Fe-NO}) and N-O (ν_{N-O}) stretching frequencies in the 520-540 cm^{-1} and 1800-1880 cm^{-1} ranges, respectively (*155, 156*). While the $\nu_{Fe–NO}$ frequency of the six-coordinate thiolate-bound $\{FeNO\}^7$ adduct (approximately 560 cm^{-1}) is only modestly elevated from that of the $\{FeNO\}^6$ species, the ν_{N-O}

frequency upshifts considerably to about 1600 cm^{-1} in the type-1 $\{FeNO\}^7$ adducts (*156*). The $\nu_{Fe\text{-}NO}$ Raman frequencies of the type-2 six-coordinate $\{FeNO\}^7$ adducts with a *trans* neutral ligand are shifted to higher frequencies in the 560-570 cm^{-1} range, while $\nu_{N\text{-}O}$ frequencies upshift from about 1600 cm^{-1} to 1630-1640 cm^{-1} (*18, 20, 157, 158*). Type-1 and type-2 rR spectra of five-coordinate $\{FeNO\}^7$ systems typically show shifts of $\nu_{Fe\text{-}NO}$ and $\nu_{N\text{-}O}$ in the 520-525 cm^{-1} and 1660-1680 cm^{-1} ranges, respectively. Similar to the Fe(II)CO $\nu_{Fe\text{-}CO}/\nu_{C\text{-}O}$ correlation, type-1 and type-2 heme-thiolates that form six-coordinate $\{FeNO\}^7$ adducts also follow a roughly linear inverse correlation of $\nu_{Fe\text{-}NO}/\nu_{N\text{-}O}$ *(159)*.

The Nature of the Type-1 Heme-Thiolates

The type-1 heme-thiolates form high-valent intermediates during catalytic cycles.

As catalytic centers for biological reactions, the type-1 heme-thiolate centers generally activate small molecules for substrate transformations. This chemistry is accomplished via reaction of O_2 or H_2O_2 directly with the heme-thiolate center to form highly reactive oxo adducts of [(P)Fe(IV)=O)] species, known generally as "ferryls" (Figure 1.11). The heme-thiolate ferryl species are very similar in nature to those employed by the histidine-ligated oxygenases, as demonstrated by the peroxidase function of CPO.

The cytochromes P450 are a ubiquitous family of type-1 heme-thiolate enzymes that perform a variety of reactions including the activation of carbon centers for catabolism, steroid metabolism, and detoxification of xenobiotics *(160, 161)*. These monooxygenase reactions (Equation 1.1) are performed with a remarkable degree of stereo- and regioselectivity.

$$XH + {}^*O_2 + AH_2 \longrightarrow X(^*O)H + H_2{}^*O + A \qquad (1.1)$$

The catalytic cycle of the P450 cytochromes is presumed to involve a high-valent iron-oxo intermediate (Figure 1.15) *(3)*. Substrate binding to a nearby cavity in the low-spin resting state expels a heme-bound water/hydroxide molecule to generate the five-coordinate high-spin Fe(III) state. This spin-state crossover causes a significant positive increase in the redox potential of the heme center, which is then reduced by electron transfer from NADH or NADPH via a redox partner protein. To activate O_2, the P450 cytochromes utilize the high-spin Fe(II) state of the heme-thiolate. The rate-limiting addition of a second electron to the oxy-Fe(II) complex is proposed to initiate a cascade, yielding the putative oxy-ferryl porphyrin π-cation radical species (Compound I) that serves as the reactive oxygenating species. Compound I of cytochrome P450 is predicted to undergo oxygen-atom transfer by an "oxygen

rebound" mechanism in which hydrogen atom abstraction from substrate by Compound I is followed by radical recombination to form the hydroxylated product *(162-164)*.

Chloroperoxidase (CPO) from the marine fungus *Cimex fumago* is a versatile type-1 heme-thiolate enzyme that possesses typical peroxidase (Equation 1.2) and catalase (Equation 1.3) functions, as well as the unique ability to catalyze the halogenation (chloride, bromide, and iodide) of organic substrates using H_2O_2 as the oxidant (Equation 1.4) *(165, 166)*. CPO is regarded as a "hybrid" of the cytochromes P450 and heme peroxidases, as it contains a polar, peroxidase-like heme pocket housing a thiolate-ligated cytochrome P450-like heme center *(7)*.

$$2\ RH\ +\ H_2O_2 \longrightarrow R\text{-}R\ +\ 2\ H_2O \qquad (1.2)$$

$$2\ H_2O_2 \longrightarrow O_2 + 2\ H_2O \qquad (1.3)$$

$$RH + H_2O_2 + Cl^- + H^+ \longrightarrow R\text{-}Cl + 2\ H_2O \qquad (1.4)$$

The enzymatic cycles of CPO (Figure 1.16) involve both transient Compound I and II intermediates (*141*). High-spin Fe(III) CPO reacts with hydrogen peroxide to form the oxo-ferryl porphyrin π-cation radical Compound I (Equations 1.1 – 1.3). In the peroxidase reaction cycle, Compound I serves as a one-electron oxidant that converts organic substrates (RH) into radical products (R·) with reduction of Compound I to Compound II, a ferryl heme with an unoxidized porphyrin macrocycle.

The nitric oxide synthases (NOSs) catalyze the oxidation of L-arginine into L-citrulline and NO using a high valent oxo-intermediate equivalent to other Compounds I (Figure 1.11). Three mammalian isoforms of NOS have been identified: 1) endothelial (eNOS), 2) inducible, (iNOS, expressed in stimulated macrophages), and 3) neuronal (nNOS, from brain) *(167-169)*. All isoforms have essentially identical crystallographic structures and chemistry *(170, 171)*. The homodimeric NOSs contain a reductase and an N-terminal catalytic oxygenase domain

(NOSoxy) in each subunit. Each NOSoxy domain binds a type-1 heme-thiolate moiety and (6*R*)-5,6,7,8-tetrahydro-L-biopterin (H_4B), which is adjacent to the heme and provides reduction equivalents *(10, 170, 172)*. Electrons from NADPH are provided by the flanking C-terminal reductase domains, which also bind flavin mononucleotide (FMN) and flavin adenine dinucleotide (FAD). The substrate, L-arginine, binds directly above the heme-thiolate center, and oxidation of L-arginine to L-citrulline and NO occurs via two consecutive oxygenase reactions using an activated oxo-ferryl porphyrin π-cation radical species *(173)*. Insertion of oxygen into one of the terminal guanidine N-H bonds of L-arginine produces N^{ω}-hydroxy- L-arginine (NOHA, Figure 1.17) with conversion of the heme back to the Fe(III) state. In the second step, a heme-hydroperoxide adduct acts as the reactive oxygen species, initiating a nucleophilic attack on the guanidino carbon to form a heme-bound peroxy-substrate that breaks down to form L-citrulline (Figure 1.17) and $NO_{(g)}$.

The nitric oxide reductase (NOR) from *Fusarium oxysporum* was the first isolated heme-thiolate NOR and remains the most thoroughly characterized NOR *(174-177)*. Genomic analyses show that NOR enzymes occur frequently in fungi and are employed in denitrification processes *(178)*. The NORs catalyze the reduction of NO to N_2O according to Equation 1.5 and are the only known type-1 heme-thiolates which function outside the realm of oxygen activation *(179, 180)*.

$$2\ NO + NADH + H^+ \longrightarrow N_2O + NAD^+ + H_2O \qquad (1.5)$$

The electrons required for NO reduction by the fungal NORs are directly transferred from NADH. A 1.0 Å X-ray crystal structure of *Fo*NOR revealed the solvent-exposed distal heme pocket, which is consistent with the much more negative reduction potential than the P450 cytochromes *(179-181)*. The chemistry of *Fo*NOR has been nicely reviewed by Daiber,

et al. (*9*) and evidence for the catalytic mechanism, involving the Fe(II)NOR-HNO intermediate (I) after hydride transfer from NADH, has been documented (Figure 1.18) (*155, 179, 182-186*).

The type-1 heme-thiolates use a "thiolate-push" mechanism.

Though the nature of the highly reactive species inherent to the chemistry of type-1 heme-thiolates is a subject of ongoing investigation, a long-standing hypothesis (the "thiolate-push" formalism) concerning the ability of the heme-thiolate moiety to stabilize these intermediates remains widely accepted. This formalism, first proposed by Dawson in 1976 (*35*), suggests that the cysteine(thiolate) ligand serves as a strong internal electron donor that facilitates O-O bond cleavage by pushing electron density onto the *trans* position via the heme iron atom as a conduit, weakening the O-O bond and stabilizing the resulting high-valent oxo-ferryl species. Early comparative experiments of P450 and myoglobin revealed the greater acidity (a measure of electron deficiency) of ligands bound *trans* to histidine in myoglobin than to the cysteine(thiolate) in cytochrome P450 *(187-189)*. Ohno, *et al. (190)* investigated model systems that demonstrated enhanced reactivity promoted by thiolate coordination to iron, which stabilizes the transition state during hydroxylation and lowers the activation energy for homolytic C–H bond cleavage. In 2002, Ogliaro and co-workers *(191)* used density functional theory (DFT) calculations that placed the "thiolate push" in a transition state at about 29 kcal/mol relative to the ground state. A more recent comparative computational study by Kamachi, *et al. (192)* further elucidated how the anionic thiolate ligand influences reactivity; their calculations suggested that strong donor–acceptor interactions occur between the axial ligand and the Fe-O bond, and the strong electron donation from the thiolate ligand is essential

in the transition state to weaken and activate the Fe-O bond. Recent work by Green and coworkers has demonstrated the ability of the thiolate ligand to influence the pK_a of the ferryl species, thus creating an extremely potent and basic oxidant that facilitates H-atom abstraction (*125, 193, 194*).

The protein environment, via hydrogen bonding interactions with the cysteine(thiolate) ligand, also influences the reactivity of the resulting intermediate species. This effect has been elegantly demonstrated by work on $P450_{CAM}$ and NOS variants that alter the hydrogen-bonding capabilities at the thiolate ligand, both *in vitro* and *in silico* (*195-201*). While a definitive consensus on the role of secondary interactions at the type-1 heme-thiolate mercaptide moiety is still not achieved, several groups have suggested that hydrogen bonding at the Cys(thiolate) ligand modulates the electron density at the iron center by controlling the electron-donating capability of the sulfur atom, thus attenuating the thiolate "push" effect. This regulation of the "push" effect may alter the rate of ferryl formation (*197*), the overall rate of reaction (*200*), or even enzymatic coupling (*195, 199*).

Does the thiolate ligand facilitate multiple reaction pathways?

The existence of type-1 heme-thiolate complexes in non-monooxygenase enzymes such as CPO, NOSs and NOR suggests an additional role(s) of the thiolate ligand in catalysis. Based on studies of the P450 cytochromes, CPO, NOR and related enzymes in combination with DFT calculations, Ullrich *(202)* suggested that the thiolate may perform different functions in the pure monooxygenases versus non-monoxygenases. In this proposal, the monooxygenase enzymes utilize the thiolate ligand's electron density to restrict π donation of oxygen to the iron, which maintains the "active oxygen" complex in the transition state. The ferryl

(Compound I, Fe^{IV}=O) ground state exists with an electron hole delocalized about the porphyrin and the thiolate (thiyl). As part of the differentiated function utilized in non-monoxygenases, Compound II acts as a very rapid electron acceptor to assist in the facile oxidation of the substrate radical and subsequent reaction with the poised nucleophile. In this proposal, the "oxygen rebound" is abandoned as a final step in the reaction mechanism, and Compound II is an atypical ferryl-oxo in which the thiolate interaction may also be invoked to assist in electron transfer.

The heme-thiolate affects the basicity of Compounds II.

Type-1 heme-thiolate Compounds II are quite dissimilar from those of the analogous Compounds II in histidine-ligated oxygenases *(126, 203)*. Chloroperoxidase Compound II (CPO-II) was the only example of a high-valent heme peroxidase intermediate for which a ν_{Fe-O} stretching frequency had not yet been reported, and this was originally attributed to an abnormally weak iron(IV)-oxo bond *(126, 129)*. X-ray absorption measurements of CPO-II by Green, *et al. (204)* yielded an Fe-O bond length of 1.82 Å, a value much longer than typical ferryl iron-oxo distances (1.65 Å), suggesting that the oxo moiety is protonated ($pK_a \geq 8.2$) (Figure 1.19). Green, *et al*. *(205)* combined DFT and Mössbauer spectroscopy to detect a protonated ferryl moiety in CPO-II, and Stone, *et al*. *(206)* reported two ferryl species in a sample of CPO-II which were assigned as iron(IV)(porphyrinato)(oxo) and iron(IV)(porphyrinato)(hydroxo) species. The ν_{Fe-O} for CPO-II was then identified at 565 cm^{-1}, which is consistent with the presence of an Fe^{IV}-OH species (*207*). DFT and Mössbauer spectroscopies of cytochrome P450 by Behan, *et al*. *(125)*, have also detected a protonated ferryl species for P450-II at physiological pH. Several studies by Mayer and coworkers *(208-*

210) have established that the strength of the O-H bond formed during H-atom abstraction scales with the ability of the metal-oxo species to abstract hydrogen, and its formation is controlled by the one-electron reduction potential of Compound I and the pK_a of Compound II *(125, 206)*. The ability of cysteine(thiolate) to promote hydrogen abstraction in this situation could be essential. The π-donating ability of the thiolate ligand imparts a partial negative charge upon the oxo unit to facilitate protonation of the oxygen atom. This proposal assumes that the rebound mechanism *is* operative in P450 hydroxylations and that basic ferryls are a general and unique feature of cysteine(thiolate)-coordinated hemes.

The Nature of the Type-2 Heme-Thiolates

Type-2 heme-thiolates are (frequently) part of signaling pathways.

The labile nature of the cysteine(thiolate) ligand in type-2 heme-thiolates makes these heme centers ideally suited for functions in small molecule sensing and transport. A role for the type-2 heme-thiolates in redox sensing stems from the almost universal replacement of the cysteine(thiolate) ligand upon reduction of the Fe(III) heme-thiolate complex. The positioning of another protein residue as a sixth ligand in the Fe(II) heme complex results in local movement of the protein structure. In the type-2 heme-thiolates, gas binding requires replacement of at least one of the heme protein ligands; similar to the ferric/ferrous ligand-switch, gas-induced ligand replacement may result in additional changes in the protein structure, as gas binding alters protein-protein interactions and forms new ligand-protein contacts. In the type-2 heme-thiolates, mounting evidence links local changes in heme coordination to global conformational and dynamical changes, especially that of the protein functional domains.

The CO oxidation activator (CooA) from the purple photosynthetic bacterium *Rhodospirillum rubrum* represents the paradigm for gas-sensing type-2 heme-thiolate proteins *(211)*. The *coo* regulon contains two transcriptional operons, including *cooA*, whose products are required for *R. rubrum* to anaerobically oxidize CO to CO_2 *(212)*. Like other members of the cAMP receptor protein (CRP) and fumarate and nitrate reductase (FNR) superfamily of transcriptional regulators, *Rr*CooA is arranged into distinct regulatory and DNA-binding domains. In the Fe(III) state, the regulatory domain heme is coordinated by Cys^{75} and the N-terminal Pro^{2} of the opposing monomer; reduction replaces Cys^{75} with His^{77} while CO binding replaces Pro^{2} on the opposing side (Figure 1.20) *(11, 12, 142, 213-215)*. Coordination of NO results in a five-coordinate NO adduct, which is inactive for DNA binding *(216)*. A 2.6 Å X-ray crystal structure of Fe(II)CooA by Lanzilotta *et al. (217)* verified that Cys^{75} is replaced by His^{77} via a redox-mediated ligand switch. Biochemical and spectroscopic studies have demonstrated that it is a CO-specific ligand replacement that initiates the global conformational change that activates *Rr*CooA to bind DNA (Figure 1.21) *(211, 218)*. The allosteric signal from the effector (CO)-binding domain to the DNA-binding domain is thought to be transmitted via two α-helices at the dimer interface of the protein that form a leucine-zipper motif *(219)*.

The transcription factor neuronal PAS domain protein 2 (NPAS2) was the first CO-responsive type-2 heme-thiolate protein to be identified in mammals *(220)*. NPAS2 forms a heterodimeric complex with BMAL1 to activate the expression of *per* and *cry* genes, which are negative regulatory components of the circadian clock. NPAS2 is a member of the basic helix-

loop-helix (bHLH)-PAS[‡] family of transcription activators; the N-terminal bHLH DNA binding domain is coupled to two PAS domains, termed PAS-A and PAS-B, which bind heme (*220-222*). Formation of the DNA complex with the NPAS2/BMAL1 heterodimer is directly coupled to the levels of heme present, and a study on the PAS-A and bHLH domains (bHLH-PAS-A) found specific binding to the E-box DNA sequence occurs only in the presence of heme *(223)*. Independent characterization of the NPAS2 PAS-A domain revealed Cys^{170} coordination to the Fe(III) PAS-A heme, which is replaced by a His^{171} upon reduction *(16, 224)*. rR data suggest that CO binds opposite a neutral nitrogen donor at the Fe(II)NPAS2 heme, which is characteristic of type-2 heme-thiolates; formation of this CO adduct inhibits heterodimerization of NPAS2 with BMAL1 *(220)*. Binding of NO results in a five-coordinate nitrosyl adduct, but no functional aspects of this complex have been reported *(223)*. However, recent studies on the PAS-A domain expressed with its bHLH domain intact have suggested the Fe(III) ligation scheme shifts from Cys/His ligation to His/His ligation, which is speculated to aid in signal transduction in NPAS2 (*225*). The spectral features exhibited by the PAS-B domain are consistent with thiolate coordination in the Fe(III) state, but not in the Fe(II) state, suggesting the presence of a second type-2 heme-thiolate *(226)*. Though CO is a likely candidate for the native signal of NPAS2, putative sensing of other small molecules has not been conclusively ruled out.

The aerobic PCB-degrading bacterium *Burkholderia xenovorans* has been shown to express at least two transcriptional proteins named the regulators of CO metabolism, *Bx*RcoM-1 and *Bx*RcoM-2, which were recently characterized as type-2 heme-thiolate proteins (*18, 227*).

[‡] PAS is an acronym formed from the names of the proteins in which imperfect repeat sequences were initially recognized: PER (the *Drosophila* period clock protein), ARNT (vertebrate aryl hydrocarbon receptor nuclear translocator), and SIM (*Drosophila* single-minded protein).

Aerobic CO-dependent transcriptional activation *in vivo* has been observed *(227)*. The *Bx*RcoM proteins couple an N-terminal PAS-fold heme domain to a C-terminal LytTR DNA-binding domain, of which little is known. Structural modeling and mutagenic analyses implicate His^{74} and Met^{104} as heme iron ligands in the Fe(II) state. Recent spectroscopic data for *Bx*RcoM-2 revealed that, similar to *Rr*CooA, the Fe(III) state is low-spin, coordinated by a cysteine(thiolate) (Cys^{94}) and a sixth neutral ligand, likely His^{74} (*18, 227, 228*). In RcoM-2, a redox-mediated ligand switch occurs in which the Fe(III) heme ligand Cys^{94} is replaced with a neutral donor ligand, likely Met^{104}, in the Fe(II) state. Binding of CO and NO in *Bx*RcoM-2 occurs via replacement by the gas molecule of one of the axial ligands of the Fe(II) heme; resonance Raman and EPR spectral features are indicative of a histidine *trans* to both the CO and NO ligand, consistent with displacement of the weakly-coordinated Met^{104} (Figure 1.22) (*18*).

The nuclear receptors (NRs) *Drosophila melanogaster* E75, *Drosophila melanogaster* DHR51, and *Homo sapiens* Rev-erbβ are transcriptional silencers that are now known to possess type-2 heme-thiolate centers (*19, 20, 229*). The NRs comprise a superfamily of eukaryotic transcription factors that coordinate inter- and intracellular signaling processes and regulate development, growth and reproduction, cell proliferation and death, and overall homeostasis *(230)*. NRs are modular proteins with a highly conserved DNA binding domain (DBD) coupled to a ligand binding domain (LBD) via a flexible hinge region *(231)* (Figure 1.14). NRs may function as transcriptional activators or repressors, and binding of a small, lipophilic ligand within the LBD typically acts as a signaling event for these functions; while several NRs have been cloned, overexpressed, and purified, their native ligands are not known. E75, Rev-erbα and Rev-erbβ are NR homologues that belong to the NR1D subfamily of

transcriptional silencers, which regulate growth and development, energy metabolism and the circadian clock through complicated feedback mechanisms (*232-235*). In 2005, Reinking, *et al*. *(236)* reported that *Drosophila* E75 bound a redox- and gas-sensitive heme cofactor within the LBD, which also regulated proper folding and association with its heterodimeric partner protein DHR3; they also identified two conserved histidines (His^{574} and His^{364}) as potential heme ligands. De Rosny and coworkers *(19)* verified that the Fe(III) heme iron was coordinated by histidine and cysteine(thiolate) using EPR. The human Rev-erbα and Rev-erbβ NRs were also reported to bind heme reversibly, which mediated co-repressor binding; spectroscopic characterization of Rev-erbβ revealed a six-coordinate heme environment with cysteine(thiolate) bound opposite a neutral donor, likely histidine (*20, 237, 238*). Under reducing conditions, spectroscopic evidence for E75 and Rev-erbβ strongly suggest that thiolate coordination is lost or replaced by a neutral donor ligand (*20*). Reinking, *et al*. *(236)* demonstrated that binding of CO and NO, which form six- and five-coordinate heme complexes, respectively, results in inhibition of E75 repressor activity. Current published reports for similar redox- or CO- and NO-binding dependence for the Rev-erb NRs are inconclusive *(236, 237)*. De Rosny and coworkers have also identified the *Drosophila* homologue of the human photoreceptor and cell-specific nuclear receptor DHR51 as a heme-thiolate protein. Using UV-Vis and EPR data, they showed that the DHR51-LBD binds heme in a six-coordinate fashion and utilizes a Cys(thiolate)/neutral donor (likely His) motif, nearly identical to E75; furthermore, they demonstrated that DHR51 binds CO and NO to form six- and five-coordinate species, respectively, and speculate that DHR51 may be involved in gas-sensing (*229*). Similar to NPAS2, spectroscopic and biochemical studies on these proteins have only been performed on fragmentary LBD constructs; thus, the functional implications of

the observed heme coordination states are unknown. In at least one case, the binding of heme to a nuclear receptor has been deemed adventitious (*239*), which emphasizes that caution must be taken to avoid over-interpretation of *in vitro* studies on isolated, fragmentary domains.

The heme-regulated eIF2α kinase (HRI) is a multidomain heme-protein with two distinct heme-binding sites, one of which is a type-2 heme-thiolate that functions as an NO sensor *(240, 241)*. HRI is a member of a family of kinases that regulate initiation of protein synthesis in eukarotic cells *(242, 243)*. The eIF2α kinases catalyze phosphorylation of eIF2α, which then binds eIF2β and inhibits the guanine nucleotide exchange activity required for protein synthesis. HRI specifically regulates globin synthesis in reticulocytes in response to available heme levels *(244)*. Several environmental and chemical stimuli, including NO binding to heme, activate HRI. Metal cations, including Hg^{2+}, Fe^{2+}, Cu^{2+}, Zn^{2+} and Pb^{2+}, have been reported to inhibit HRI function; the strong inhibition by Hg^{2+} (and only Hg^{2+}) is fully reversed by NO *(241, 243, 245)*. The heme-binding domains of HRI consist of a kinase insertion domain, which binds heme reversibly and regulates HRI activity in response to heme concentration, and an N-terminal domain, which binds a type-2 heme-thiolate complex (*241, 246, 247*). Site-directed mutagenesis on only the HRI N-terminal heme domain (HRI-NTD) suggested coordination of the heme by two histidine residues *(248)*. Subsequent examination of full-length HRI by absorption, EPR, and rR spectroscopies revealed a thiolate-bound heme center (*15*). Interrogation via mutagenesis and spectroscopic studies on the full-length HR implicated Cys^{385} of the kinase insertion domain and a histidine of the N-terminal domain as axial ligands *(249, 250)*. Upon reduction, the spectral characteristics of cysteine(thiolate) coordination are lost, suggesting either a ligand switch or protonation to cysteine(thiol) occurs. NO binds to the type-2 heme-thiolate center with loss of both endogenous ligands and a

concomitant upregulation of kinase activity. Studies have also demonstrated that the activation of HRI kinase activity is specific for NO, as CO suppresses activity in HRI (*251*). These findings suggested that the N-terminal heme domain adopts a conformation that inhibits HRI kinase activity; NO binding may induce the correct conformational change to release heme domain inhibition of HRI kinase activity.

Human cystathionine β-synthase (hCBS) is a pyridoxal 5′-phosphate (PLP)-dependent enzyme, which also binds a type-2 heme-thiolate cofactor of unknown function. Human CBS catalyzes the condensation of serine and homocysteine to yield cystathionine via a β-replacement reaction performed by the PLP cofactor. A member of the fold type-II family of PLP-dependent enzymes, hCBS is unique in that it also binds a heme cofactor, which is non-covalently bound within a N-terminal hydrophobic pocket (*13, 252-254*). The thiolate of Cys^{52} and the $N_{\varepsilon 2}$ atom of His^{65}, both located on the N-terminal loop, axially coordinate the heme (Figure 1.22). This N-terminal heme-binding region in hCBS is absent in CBS isolated from *Saccharomyces cerevisiae* and *Trypanosoma cruzi*, suggesting that heme is an evolutionarily recent acquisition *(255-257)*. Studies have demonstrated that the hCBS heme serves no direct catalytic role; the β-replacement reaction catalyzed by CBS follows a typical PLP-based mechanism, and the heme-free enzyme is catalytically competent, albeit with lowered activity, and heme-domain deletion variants have substantially decreased activity (*258-262*). Furthermore, CBS expressed in heme-free systems results in inactive enzyme; activity may be rescued by expression of CBS in the presence of chemical chaperones or exogenous metalloporphyrins (*263*). In at least one example, expression of hCBS in the presence of $CoCl_2$ resulted in the incorporation of CoPPIX in place of heme. Not only did the CoPPIX maintain the native type-2 thiolate ligation motif, but the enzyme was fully active; these results have

suggested heme may play a structural role by stabilizing the N-terminus (*264, 265*). Other studies have suggested that the hCBS heme behaves in a regulatory fashion as seen in other type-2 heme-thiolates; this proposal is very attractive, as it would connect the redox activity of CBS to supplies of Cys (produced in a downstream pathway), which is necessary for glutathione production. Binding of NO, CO or cyanide, as well as thiolate-bond disruption by $HgCl_2$ (both Fe and Co hCBS), have a strong negative effect on hCBS activity, alluding to communication between the heme and active site *(151, 265-267)*. Studies from our lab have shown that the CBS heme reduction destabilizes thiolate coordination at near-physiological temperature and pH, ultimately resulting in a redox-mediated ligand switch similar to other type-2 heme-thiolates (*138*) (Figure 1.8). However, at lower temperatures and pH, the Fe(II) state forms only transiently before reoxidizing to the native Fe(III) heme-thiolate environment *(72)*. Because hCBS activity was observed to decrease two-fold upon reduction of the heme, Taoka, *et al. (268)* proposed that the hCBS heme is a redox sensor. However, we have shown that formation of the ligand-switched species (CBS424, Figure 1.7) under assay conditions causes the observed decrease in activity; the enzyme is deactivated by conversion to CBS424, not by heme reduction alone *(269)*. Recent results have suggested that displacement of the Cys(thiolate) ligand by CO, formed under physiological conditions, may function to control CBS activity (*270*); however, the lengthy amount of time (2 h) required to form the inactive PLP tautomer suggests that this mode of regulation is unlikely (at least as studied *in vitro*). The molecule or environment that is putatively sensed by the hCBS heme remains elusive, as does the physiological significance of the unusual redox behavior of the heme.

Cimex lectularius (the bedbug) makes use of a salivary heme-thiolate protein, termed a nitrophorin, to ensure a robust blood meal (*17*). Nitrophorins are a class of heme proteins from

blood-sucking insects that bind and transport NO; dilution and pH changes inside the host lead to release of NO, which results in vasodilation *(271-275)*. The nitrophorin of *C. lectularius* (cNP) is unique in that Cys^{60} serves as a ligand to the heme; all other nitrophorin hemes are coordinated by a histidine imidazole (*17*). The heme-thiolate of the cNP also exhibits characteristics of both type-1 and type-2 heme-thiolates. A 1.75 Å X-ray crystal structure of Fe(III) cNP shows a solvent-exposed heme pocket with a weakly-associated water molecule *trans* to thiolate, though EPR spectroscopy revealed a predominantly high-spin, five-coordinate Fe(III)cNP species (*17*). Unlike the type-1 heme-thiolates, the cNP heme is unable to form a stable complex with imidazole but does form stable NO and CO adducts *(276)*. As in other type-1 heme-thiolates, NO binds opposite the thiolate moiety of Fe(III)cNP to form a six-coordinate NO adduct. Consistent with its role as an NO transporter, however, cNP reversibly binds *two* molecules of NO. The second NO equivalent binds via heme-assisted *S*-nitrosylation of the thiolate (Cys^{60}), generating an Fe(II) heme-NO and a cysteine(thiyl) radical. This novel mechanism of binding and transporting NO is consistent with the labile nature of cysteine(thiolate) in type-2 heme-thiolates. The cNP CO adduct also exhibits a Soret maximum at ~420 nm, though this result conflicts with a 1.45 Å x-ray crystal structure, which places CO opposite the cysteine ligand *(277)*. Elegant work by Perera *(278)* has demonstrated that neutral cysteine(thiol) coordination to a heme center yields spectroscopic features very similar to neutral nitrogen coordination. A reasonable, if unverified, explanation for this apparent conflict may be that CO is bound opposite a neutral cysteine(thiol) in cNP. We have thus placed cNP with the type-2 heme-thiolates due to greater apparent spectroscopic and functional similarities to this class of heme-thiolates.

Type-2 heme-thiolates destabilize thiolate coordination in the ferrous state.

Unlike type-1 heme-thiolates, which function as high-spin, five-coordinate species, type-2 heme-thiolates generally exist as low-spin, six-coordinate species in the Fe(III) state, which may be central to their predilection toward ligand-switching when reduced. The presence of the sixth ligand in the Fe(III) type-2 centers may promote the lability of the cysteine(thiolate), a characteristic of these heme centers. The negative charge on the cysteine(thiolate) ligand, coupled with strong electron donation from the sixth ligand (most often a neutral nitrogen donor), are expected to stabilize the Fe(III) state of the heme. Upon reduction, however, the type-2 heme-thiolates may be intrinsically unstable unless the heme center compensates by decreasing the large amount of charge density donated by the cysteine(thiolate). This compensation may take the form of a weakened Fe-S interaction, and thus, a labile cysteine(thiolate) ligand, which is susceptible to replacement by a nearby residue. The low-spin resting states of the P450 cytochromes and NORs need no such compensation when reduced because the *trans* ligand (H_2O) is a very weak donor in comparison to the neutral nitrogen donors *trans* to the type-2 cysteine(thiolate). The discriminating factor between type-1 and type-2 heme-thiolates may therefore simply be effects of *trans* coordination to the heme-thiolate. This argument, however, does not include cNP, which contains a high-spin type-2 heme-thiolate that nonetheless becomes labile upon NO coordination/heme reduction. The unusual temperature- and pH-dependent effects on the coordination of hCBS also deviate from expected behavior. These discrepancies may be rationalized by invoking second-sphere interactions. The type-1 cysteine(thiolate) ligands have been shown crystallographically to engage in a number of hydrogen-bonding interactions with surrounding residues (*113-115, 279-281*). These interactions stabilize the heme iron upon reduction by drawing thiolate electron

density away from the heme iron, resulting in a non-labile heme-thiolate moiety. Unfortunately, relatively few crystal structures of the less classical type-2 heme-thiolates (hCBS, *Dm*CBS and cNP) exist with which to make comparisons (*13, 17, 254*). While the cNP heme-thiolate engages in few hydrogen-bonding interactions, the hCBS heme-thiolate engages in several hydrogen bonds (Figure 1.23). This observation is not wholly inconsistent with the observed labile behavior of these two type-2 heme-thiolates, as hCBS undergoes a ligand switch at elevated temperatures. Furthermore, recent studies on the R266K variant of hCBS, which modifies one of the heme Cys(thiolate) hydrogen-bonding partners, have shown that the thiolate ligand is more labile in the reduced form, and becomes more like a "classical" type-2 heme-thiolate by ligand-switching almost instantaneously at physiological temperature (*73*). Thus, we propose that a combination of second-sphere hydrogen bonding interactions and ligand *trans* effects accounts for the functionally and behaviorally distinct type-2 heme-thiolates.

Conversion of type-1 heme-thiolates to type-2 heme-thiolates results in loss of activity and unique spectral characteristics.

The type-1 heme-thiolates cytochrome P450 and CPO can be converted to an inactive, type-2 heme-thiolate species. The cytochromes P450 undergo a universal transition to a stable but inactive species known as cytochrome P420. The term "P420" is derived from the 420 nm Soret absorption maximum exhibited by the ferrous-CO adduct of cytochrome P420. Numerous chemical and physical techniques (*282-285*), including increased temperature, increased pressures, the addition of salts, denaturants, or even organic solvents, convert cytochrome P450 to cytochrome P420 (*141, 286, 287*). Conversion to P420, a six-coordinate,

low-spin heme-thiolate, is also accompanied by an increase in cysteine(thiolate) lability, as CO is able to displace the thiolate ligand in Fe(II) cytochrome P420 (*286, 288*). Similarly, a change in CPO heme coordination at alkaline pH converts the CPO heme to a type-2 heme-thiolate, rendering the enzyme inactive. This species was also termed C420 for the CO adduct Soret absorption maximum at 420 nm *(288)*. Moreover, unlike native CPO, the heme-thiolate of C420 is susceptible to thiol-specific modifying agents, such as *p*-mercuribenzoate (*289*). The C420 Fe(III) heme appears to be coordinated by the native cysteine(thiolate) (Cys^{29}) and an additional neutral donor. When reduced, C420 loses its cysteine(thiolate) ligand via replacement by a neutral donor ligand. Thus, according to the classification scheme presented in this work, P420 and C420 are type-2 heme-thiolates. Formation of low-spin, six-coordinate heme-thiolate centers in CPO and cytochrome P450 explains the lack of catalytic activity, as an open coordination site at the heme no longer exists in the Fe(III) or Fe(II) forms to bind and activate peroxide or oxygen.

An Emergent Type-3 Heme-Thiolate?

Recent spectral work in our lab has been used to identify a heretofore unseen native bis(cysteine) ligation motif. The homodimeric double-stranded RNA-binding protein Di George Critical Region 8 (DGCR8) (also called Pasha in worms and flies) is a part of the Microprocessor complex; together with its RNase Drosha, the two proteins are responsible for the first step in micro RNA (miRNA) processing: the cleavage of primary miRNAs (pri-miRNAs) to form precursor miRNAs (pre-miRNAs) (*290-292*). The absorbance spectrum of the purified, overexpressed DGCR8 displayed a hyperporphyrin spectrum with a red-shifted Soret at approximately 450 nm (Figure 1.24); this spectrum was originally attributed to either

an Fe(II)-thiolate or CO-Fe(II)-thiolate ligated heme (*293*). Using electronic absorption, MCD, rR, and EPR spectroscopies, we have shown that this unique spectrum arises from an Fe(III) heme *b* that is ligated by Cys^{352} from each DGCR8 monomer (*294*). While several forms of Fe(III) P450 and Fe(III) CPO are known to bind exogenous thiols and display strongly-split hyperporphyrin spectra (*141, 295-297*), DGCR8 is the first known protein to bind heme using two endogenous Cys ligands. To generate this hyperporphyrin spectrum, at least one of the Cys ligands must be a thiolate and not a protonated thiol; the protonation state of the second Cys ligand, however, is unknown (*298*). That the Fe(III) form of DGCR8 does not bear spectral similarities to native forms of Fe(III) type-1 or type-2 heme-thiolates places it in a category of its own; thus, DGCR8 represent the first member of the putative type-3 heme-thiolates.

Similar to type-2 heme-thiolates, Fe(II) DGCR8 loses thiolate-coordination upon reduction. The spectral similarities of Fe(II) DGCR8 are most similar to Fe(II) heme proteins that have two neutral donors. Furthermore, the electronic absorption and MCD spectral changes that occur upon pH titration of the Fe(II) form of DGCR8 are inconsistent with a protonated thiol that is retained upon reduction (*299*). Therefore, we propose that DGCR8 undergoes a dual ligand-switch in which both Cys^{352} ligands are lost upon heme reduction. Intriguingly, DGCR8 loses its ability to upregulate pri-miRNA processing once reduced to the Fe(II) state due to a lowered RNA binding cooperativity; the functional activity may be rescued by reconstitution of apoDGCR8 with Fe(III) heme (restoring the characteristic hyperporphyrin spectrum), but not Fe(II) heme (*299*). Thus, it is clear that the Fe(III) DGCR8-heme complex is necessary for full activity; however, the exact nature of how this interaction upregulates pri-miRNA processing is unknown. Fe(II) DGCR8 will interact with CO and NO to form six- and

five-coordinate species, respectively, but the implications for processing activity are also unknown.

Although only one protein has been identified that bears a bis(Cys) ligation motif at the heme iron center, the type-3 heme-thiolates are likely functionally distinct from type-1 or type-2. In DGCR8, there is clearly no need to invoke a catalytic argument for the heme macrocycle. While the functional aspects of gas-binding have yet to be explored in Fe(II) DGCR8, the slow (and likely unfavorable) reduction process may implicate that the Fe(II) state is physiologically irrelevant for DGCR8, ruling out possible regulation by CO or NO. We currently favor the theory that DGCR8 may use its unusual ligation motif in a specific manner to function as a heme sensor (*294, 299*). DGCR8 may be the first of many novel hemoproteins yet to be discovered in the type-3 category that use the specificity of a bis(Cys) ligation motif to respond to the presence of heme as a metabolic signal *in vivo*.

Conclusion

This review has presented a new classification scheme for cysteine(thiolate)-coordinated heme proteins. Nearly all known heme-thiolate centers can be described as having a non-labile or labile thiolate ligand, type-1 and type-2, respectively, according to the nomenclature introduced in this work. The type-1 heme-thiolates are catalytic centers that engage in diverse reactions with common themes. The electron-donating ability of the cysteine(thiolate) ligand is fundamental in the formation and stabilization of very reactive, high-valent catalytic intermediates in these systems. In contrast, the type-2 heme-thiolates are generally small molecule sensors and transporters. The labile nature of the cysteine(thiolate) is exploited by the sensor heme to ensure that a signal cascade is transmitted from the heme to the region of activity. Thus, two distinct chemical characteristics of the heme-thiolate—excellent electron-donating ability and lability in the reduced state—are distinguished and employed independently of each other in type-1 and type-2 heme-thiolate centers. This review has also postulated the existence of a type-3 heme-thiolate center in which an unusual bis(Cys) ligation motif is utilized to recognize heme with high degree of specificity; we speculate that this category may grow as more hemoproteins with this unconventional ligation motif are discovered.

Acknowledgements

This review was made possible by the work of Prof. Samuel L. Pazicni, who conceived the initial classification of heme-thiolate proteins and compiled spectroscopic and biological data. This review was also made possible by the efforts of Dr. Kathy Marvin, who edited and

updated the initial classification. Without their efforts, the current version of this review would not have been possible.

References

1. Bertini, I., Gray, H. B., Lippard, S. J., and Valentine, J. S. (1994) *Bioinorganic Chemistry*, University Science Books, Mill Valley, CA.
2. Gilles-Gonzalez, M.-A., and Gonzalez, G. (2005) Heme-based sensors: definining characteristics, recent developments, and regulatory hypotheses, *J. Inorg. Biochem. 99*, 1-22.
3. Sono, M., Roach, M. P., Coulter, E. D., and Dawson, J. H. (1996) Heme-containing oxygenases, *Chem. Rev. 96*, 2841-2887.
4. Martinez, S. E., Huang, D., Szczepaniak, A., Cramer, W. A., and Smith, J. L. (1994) Crystal structure of chloroplast cytochrome *f* reveals a novel cytochrome fold and unexpected heme ligation, *Structure 2*, 95-105.
5. Murthy, M. R. N., Reid, T. J., Sicignaro, A., Tanaka, N., and Rossmann, M. G. (1981) Structure of beef liver catalase, *J. Mol. Biol. 152*, 465-499.
6. Poulos, T. L., and Johnson, E. F. (2005) Structures of cytochrome P450 enzymes, in *Cytochrome P450: Structure, Mechanism, and Biochemistry* (Ortiz de Montellano, P. R., Ed.) 3rd ed., Plenum Publishers, New York.
7. Sundaramoorthy, M., Terner, J., and Poulos, T. L. (1995) The crystal structure of chloroperoxidase: a heme peroxidase-cytochrome P450 functional hybrid, *Structure 3*.
8. Dawson, J. H., Trudell, J. R., Barth, G., Linder, R. E., Bunnenberg, E., Djerassi, C., Chiang, R., and Hager, L. P. (1976) Chloroperoxidase. Evidence for P-450 type heme enviroment from magnetic circular dichroism spectroscopy, *J. Am. Chem. Soc. 98*, 3709-3710.

9. Daiber, A., Shoun, H., and Ullrich, V. (2005) Nitric oxide reductase ($P450_{nor}$) from *Fusarium oxysporum*, *J. Inorg. Biochem. 99*, 185-193.

10. Li, H., and Poulos, T. L. (2005) Structure-function studies on nitric oxide synthases, *J. Inorg. Biochem. 99*, 293-305.

11. Shelver, D., Thorsteinsson, M. V., Kerby, R. L., Chung, S.-Y., Roberts, G. P., Reynolds, M. F., Parks, R. B., and Burstyn, J. N. (1999) Identification of two important heme site residues (Cysteine 75 and Histidine 77) in CooA, the CO-sensing transcription factor of *Rhodospirillum rubrum*, *Biochemistry 38*, 2669-2678.

12. Reynolds, M. F., Shelver, D., Kerby, R. L., Parks, R. B., Roberts, G. P., and Burstyn, J. N. (1998) EPR and electronic absorption spectroscopies of the CO-sensing CooA protein reveal a cysteine-ligated low-spin ferric heme, *J. Am. Chem. Soc. 120*, 9080-9081.

13. Meier, M., Janosik, M., Kery, V., Kraus, J. P., and Burkhard, P. (2001) Structure of human cystathionine β-synthase: A unique pyridoxal 5'-phosphate dependent heme protein, *EMBO J. 20*, 3910-3916.

14. Omura, T., Sadano, H., Hasegawa, T., Yoshida, Y., and Kominami, S. (1984) Hemoprotein H-450 identified as a form of cytochrome P-450 having an endogenous ligand at the 6th coordination position of the heme, *J. Biochem. 96*, 1491-1500.

15. Igarashi, J., Sato, A., Kitagawa, T., Yoshimura, T., Yamauchi, S., Sagami, I., and Shimizu, T. (2004) Activation of heme-regulated eukaryotic initiation factor 2a kinase by nitric oxide is induced by the formation of a five-coordinate NO-heme complex, *J. Biol. Chem. 279*, 15752-15762.

16. Uchida, T., Sato, E., Sato, A., Sagami, I., Shimizu, T., and Kitagawa, T. (2005) CO-dependent activity-controlling mechanism of heme-containing CO-sensor protein, neuronal PAS domain protein 2, *J. Biol. Chem. 280*, 21358-21368.

17. Weichsel, A., Maes, E. M., Andersen, J. F., Valenzuela, J. G., Shokhireva, T. K., Walker, F. A., and Montfort, W. R. (2005) Heme-assisted S-nitrosation of a poximal thiolate in a nitric oxide transport protein, *Proc. Natl. Acad. Sci. USA 102*, 594-599.

18. Marvin, K. A., Kerby, R. L., Youn, H., Roberts, G. P., and Burstyn, J. N. (2008) The Transcription Regulator RcoM-2 from *Burkholderia xenovorans* Is a Cysteine-Ligated Hemoprotein That Undergoes a Redox-Mediated Ligand Switch, *Biochemistry 47*, 9016-9028.

19. de Rosny, E., Groot, A. d., Jullian-Binard, C., Gaillard, J., Borel, F., Pebay-Peyroula, E., Fontecilla-Camps, J. C., and Jouve, H. l. n. M. (2006) *Drosophila* nuclear receptor E75 is a thiolate hemoprotein, *Biochemistry 45*, 9727-9734.

20. Marvin, K. A., Reinking, J. L., Lee, A. J., Pardee, K., Krause, H. M., and Burstyn, J. N. (2009) Nuclear Receptors *Homo sapiens* Rev-erbβ and *Drosophila melanogaster* E75 Are Thiolate-Ligated Heme Proteins Which Undergo Redox-Mediated Ligand Switching and Bind CO and NO, *Biochemistry 48*, 7056-7071.

21. de Rosny, E., Groot, A. d., Jullian-Binard, C., Borel, F., Suarez, C., Le Pape, L., Fontecilla-Camps, J. C., and Jouve, H. M. (2008) DHR51, the *Drosophila melanogaster* Homologue of the Human Photoreceptor Cell-Specific Nuclear Receptor, Is a Thiolate Heme-Binding Protein, *Biochemistry 47*, 13252-13260.

22. Klingenberg, M. (1958) Pigments of Rat Liver Microsomes, *Arch. Biochem. Biophys. 75*, 376-386.

23. Omura, T., and Sato, R. (1962) A new cytochrome in liver microsomes, *J. Biol. Chem. 237*, 2370-2371.

24. Stern, J. O., and Peisach, J. (1974) A model compound study of the CO-adduct of cytochrome P-450, *J. Biol. Chem. 249*, 7495-7498.

25. Poulos, T. L., Finzel, B. C., Gunsalus, I. C., Wagner, G. C., and Kraut, J. (1985) The 2.6-Å crystal structure of *Pseudonomas putida* cytochrome P-450, *J. Biol. Chem. 260*, 16122-16130.

26. Gouterman, M. (1978) Optical spectra and electronic stucture of porphyrins and related rings, in *The Porphyrins* (Dolphin, D., Ed.), pp 1-165, Academic Press, New York.

27. Silgar, S. G. (1976) Coupling of spin, substrate, and redox equilibria in cytochrome P450, *Biochemistry 15*, 5399-5406.

28. Raag, R., and Poulos, T. L. (1989) The structural basis for substrate-induced changes in redox potential and spin equilibrium in cytochrome P-450$_{CAM}$, *Biochemistry 28*, 917-922.

29. Haines, D. C., Tomchick, D. R., Machius, M., and Peterson, J. A. (2001) Pivotal role of water in the mechanism of P450BM-3, *Biochemistry 40*, 13456-13465.

30. Galinato, M. G. I., Spolitak, T., Ballou, D. P., and Lehnert, N. (2011) Elucidating the Role of the Proximal Cysteine Hydrogen-Bonding Network in Ferric Cytochrome P450cam and Corresponding Mutants Using Magnetic Circular Dichroism Spectroscopy, *Biochemistry 50*, 1053-1069.

31. Sono, M., Andersson, L. A., and Dawson, J. H. (1982) Sulfur Donor Ligand Binding to Ferric Cytochrome P-450-CAM and Myoglobin, *J. Biol. Chem. 257*, 8308-8320.

32. McKnight, J., Cheeseman, M. R., Thomson, A. J., Miles, J. S., and Munro, A. W. (1993) Identification of charge-transfer transitions in the optical spectrum of low-spin ferric cytochrome P-450 Bacillus megaterium, *Eur. J. Biochem. 213*, 683-687.

33. Sono, M., Stuehr, D. J., Ikeda-Saito, M., and Dawson, J. H. (1995) Identification of nitric oxide synthase as a thiolate-ligated heme protein using magnetic circular dichroism, *J. Biol. Chem. 270*, 19943-19948.

34. Stuehr, D. J., and Ikeda-Saito, M. (1992) Spectral characterization of brain and macrophage nitric oxide synthases, *J. Biol. Chem. 267*, 20547-20550.

35. Dawson, J. H., Holm, R. H., Trudell, J. R., Barth, G., Linder, R. E., Bunnenberg, E., Djerassi, C., and Tang, C. S. (1976) Oxidized cytochrome P-450. Magnetic circular dichroism evidence for thiolate ligation in the substrate bound form. Implications for the catalytic mechanism, *J. Am. Chem. Soc. 98*, 3707-3709.

36. Collman, J. P., Sorrell, T. N., Dawson, J. H., Trudell, J. R., Bunnenberg, E., and Djerassi, C. (1976) Magnetic circular dichroism of ferrous carbonyl adducrs of cytochromes P-450 and P-420 and their synthetic models: further evidence for mercaptide as the fifth ligand to iron, *Proc. Nat. Acad. Sci. USA 73*, 6-10.

37. Cheek, J., and Dawson, J. H. (2000) Magnetic circular dichroism spectroscopy of heme proteins and model systems, in *The Porphyrin Handbook* (Kadish, K. M., Smith, K. M., and Guilard, R., Eds.), pp 339-369, Academic Press, San Diego.

38. Sutherland, J. C. (1995) Magnetic circular dichroism, *Method. Enzymol. 246*, 110-131.

39. Thomson, A. J., Cheesman, M. R., and George, S. J. (1993) Variable temperature magnetic circular dichroism, *Method. Enzymol. 226*, 199-232.

40. Cheesman, M. R., Greenwood, C., and Thomson, A. J. (1991) Magnetic circular dichroism of hemoproteins, *Adv. Inorg. Chem. 36*, 201-255.

41. Piepho, S. B., and Schatz, P. N. (1983) *Group Theory in Spectroscopy with Applications to Magnetic Circular Dichroism*, Wiley & Sons, New York.

42. Holmquist, B. (1978) The Magnetic Optical Activity of Hemoproteins, in *The Porphyrins* (Dolphin, D., Ed.), pp 249-270, Academic Press, New York.

43. Stephens, P. J. (1976) Magnetic Circular Dichroism, *Adv. Chem. Phys. 35*, 197-264.

44. Anzenbacher, P., Dawson, J. H., and Kitagawa, T. (1989) Towards a unified concept of oxygen acivation by heme enzymes: the role of the proximal ligand, *J. Mol. Struct. 214*, 149-158.

45. Dawson, J. H., and Dooley, D. M. (1989) Magnetic circular dichroism spectroscopy of iron porphyrins and heme proteins, in *Iron Porphyrins* (Lever, A. B. P., and Gray, H. B., Eds.), pp 1-136, VCH Publishers, New York.

46. Walker, F. A. (1999) Magnetic spectroscopic (EPR, ESEEM, Mössbauer, MCD and NMR) studies of low-spin ferriheme centers and their corresponding heme proteins, *Coord. Chem. Rev. 185-186*, 471-534.

47. Andersson, L. A., Johnson, A. K., and Peterson, J. A. (1997) Active site analysis of P450 enzymes: comparative magnetic circular dichroism spectroscopy, *Arch. Biochem. Biophys. 345*, 79-87.

48. Thomson, A. J., and Gadsby, P. M. A. (1990) A theoretical model of the intensity of the near-infrared porphyrin-to-iron charge transfer transitions in low-spin iron (III) haemproteins. A correlation between the intensity of the magnetic circular dichroism bands and the rhombic distortion parameter of iron, *J. Chem. Soc. Dalton*, 1921-1928.

49. Gadsby, P. M. A., and Thomson, A. J. (1990) Assignment of the axial ligands of ferric ion in low-spin hemoproteins by near-infrared magnetic circular dichroism and electron paramagnetic resonance spectroscopy, *J. Am. Chem. Soc. 112*, 5003-5001.

50. Cheesman, M. R., Watmough, N. J., Pires, C. A., Turner, R., Brittain, T., Gennis, R. B., Greenwood, C., and Thomson, A. J. (1993) Cytochrome *bo* from *Escherichia coli*: identification of haem ligands and reaction of the reduced enzyme with carbon monoxide, *Biochem. J. 289*, 709-718.

51. Simpkin, D., Palmer, G., Devlin, F. J., McKenna, M. C., Jensen, G. M., and Stephens, P. J. (1989) The Axial Ligands of Heme in Cytochromes: A Near-Infrared Magnetic Circular Dichroism Study of Yeast Cytochromes *c*, *c*1, and *b* and Spinach Cytochrome *f*, *Biochemistry 28*, 8033-8039.

52. Spiro, T. G. (1983) The resonance Raman spectropscopy of metalloporphyrins and heme proteins, in *Iron Porphyrins* (Lever, A. B. P., and Gray, H. B., Eds.), pp 89-159, Addison-Wesley Publishing Company, Reading, MA.

53. Abe, M., Kitagawa, T., and Kyogoku, Y. (1978) Resonance Raman spectra of octaethylporpyrinato-Ni(II) and *meso*-substituted and ^{15}N substituted derivatives. II. A normal coordinate analysis, *J. Chem. Phys. 69*, 4526-4534.

54. Spiro, T. G., Stong, J. D., and Stein, P. (1979) Porphyrin core expansion and doming in heme proteins. New evidence from resonance Raman spectra of six-coordinate high-spin iron(III) hemes, *J. Am. Chem. Soc. 101*, 2648-2655.

55. Unno, M., Christian, J. F., Benson, D. E., Gerber, N. C., Silgar, S. G., and Champion, P. M. (1997) Resonance Raman investigations of cytochrome $P450_{CAM}$ complexed with putidaredoxin, *J. Am. Chem. Soc. 119*, 6614-6620.

56. Champion, P. M., Stallard, B. R., Wagner, G. C., and Gunsalus, I. C. (1982) Resonance Raman detection of an Fe-S bond in cytochrome $P450_{CAM}$, *J. Am. Chem. Soc. 104*, 5469-5472.

57. Champion, P. M., Gunsalus, I. C., and Wagner, G. C. (1978) Resonance Raman investigations of cytochrome $P450_{CAM}$ from *Pseudomonas putida*, *J. Am. Chem. Soc. 100*, 3743-3751.

58. Liu, Y., Loccoz-Moënne, P., Hildebrand, D. P., Wilks, A., Loehr, T. M., Mauk, A. G., and de Montellano, P. R. O. (1999) Replacement of the Proximal Histidine Iron Ligand by a Cysteine or Tyrosine Converts Heme Oxygenase to an Oxidase, *Biochemistry 38*, 3733-3743.

59. Bangcharoenpaurpong, O., Champion, P. M., Hall, K. S., and Hager, L. P. (1986) Resonance Raman Studies of Isotopically Labeled Chloroperoxidase, *Biochemistry 25*, 2374-2378.

60. Ishikawa, H., Nakagaki, M., Bamba, A., Uchida, T., Hori, H., O'Brian, M. R., Iwai, K., and Ishimori, K. (2011) Unusual Heme Binding in the Bacterial Iron Response Regulator Protein: Spectral Characterization of Heme Binding to the Heme Regulatory Motif, *Biochemistry 50*, 1016-1022.

61. Giroud, C., Moreau, M., Mattioli, T. A., Balland, V., Boucher, J.-L., Xu-Li, Y., Stuehr, D. J., and Santolini, J. (2010) Role of Arginine Guanidinium Moiety in Nitric-oxide Synthase Mechanism of Oxygen Activation, *J. Biol. Chem. 285*, 7233-7245.

62. Green, E. L., Taoka, S., Banerjee, R., and Loehr, T. M. (2001) Resonance Raman characterization of the heme cofactor in cystathionine β-synthase. Identification of the Fe-S(Cys) vibration in the six-coordinate low-spin heme, *Biochemistry 40*, 459-463.

63. Bayer, E., Hill, H. A. O., Röder, A., and Williams, R. J. P. (1969) The interaction between haem-iron and thiols, *J. Chem. Soc. D 3*, 109.

64. Jefcoate, C. R. E., and Gaylor, J. L. (1969) Ligand interactions with hemoprotein P-450. II. Influence of phenobarbital and methylcholanthrene induction processes on P-450 spectra, *Biochemistry 8*, 3464-3472.

65. Tang, S. C., Koch, S., Papaefthymiou, G. C., Foner, S., Frankel, R. B., Ibers, J. A., and Holm, R. H. (1976) Axial ligation modes in iron(III) porphyrins. Models for the oxidized reaction states of cytochrome P-450 enzymes and the molecular structure of iron(III) protoporphyrin IX dimethyl ester *p*-nitrobenzenethiolate, *J. Am. Chem. Soc. 98*, 2413-2434.

66. Collman, J. P., Sorrell, T. N., and Hoffman, B. M. (1975) Models for cytochrome P-450, *J. Am. Chem. Soc. 97*, 913-914.

67. Koch, S., Tang, S. C., Holm, R. H., Frankel, R. B., and Ibers, J. A. (1975) Ferric porphyrin thiolates. Possible relationship to cytochrome P-450 enzymes and the structure of (p-nitrobenzenethiolato)iron(III) protoporphyrin IX dimethyl ester, *J. Am. Chem. Soc. 97*, 916-918.

68. Röder, A., and Bayer, E. (1969) Elektronenspinresonanz-untersuchungen an Hämin-mercaptan-komplexen, *Eur. J. Biochem. 11*, 89-92.

69. Blumberg, W. E., and Peisach, J. (1971) Low-spin compounds of heme proteins, *Adv. Chem. Ser. 100*, 271-291.

70. Caillet-Saguy, C., Turano, P., Piccioli, M., Lukat-Rodgers, G. S., Czjzek, M., Guigliarelli, B., Izadi-Pruneyre, N., Rodgers, K. R., Delepierre, M., and Lecroisey, A.

(2008) Deciphering the Structural Role of Histidine 83 for Heme Binding in Hemophore HasA, *J. Biol. Chem. 283*, 5960-5970.

71. Pazicni, S. (2006) Towards Understanding the Role of the Heme Cofactor in Cystathionine β-Synthase, in *Department of Chemistry*, University of Wisconsin-Madison, Madison, WI.

72. Pazicni, S., Lukat-Rodgers, G. S., Oliveriusova, J., Rees, K. A., Parks, R. B., Clark, R. W., Rodgers, K. R., Kraus, J. P., and Burstyn, J. N. (2004) The redox behavior of the heme is cystathionine β-synthase is sensitive to pH, *Biochemistry 43*, 14684-14695.

73. Smith, A. T., Majtan, T., Su, Y., Stevens, D. J., Kraus, J. P., and Burstyn, J. N. (2012) The Effect of the Disease-Causing R266K Mutation on the Heme and PLP Environments of the Human Enzyme Cystathionine ß-Synthase, *Submitted*.

74. Hollenberg, P. F., Hager, L. P., Blumberg, W. E., and Peisach, J. (1980) An electron paramagnetic resonance study of the high and low spin forms of chloroperoxidase, *J. Biol. Chem. 255*, 4801-4807.

75. Tsai, R., Yu, C. A., Gunsalus, I. C., Peisach, J., Blumberg, W., Orme-Johnson, W. H., and Beinert, H. (1970) Spin-state changes in cytochrome P-450_{cam} on binding of specific substrates, *Proc. Nat. Acad. Sci. USA 66*, 1157-1163.

76. Peisach, J., and Blumberg, W. E. (1970) Electron paramagnetic resonance study of the high- and low-spin forms of cytochrome P-450 in liver and in liver microsomes from a methylcholanthrene-treated rabbit, *Proc. Nat. Acad. Sci. USA 67*, 172-179.

77. Peisach, J., Blumberg, W. E., Ogawa, S., Rachmilewitz, E. A., and Oltzik, R. (1971) The effects of protein conformation on the heme symmetry in high spin ferric heme proteins as studied by electron paramagnetic resonance, *J. Biol. Chem. 246*, 3342-3355.

78. Omura, T., and Sato, R. (1964) The carbon monoxide-binding pigment of liver microsomes. I. Evidence for its hemoprotein nature, *J. Biol. Chem. 239*, 2370-2378.

79. Peterson, J. A., and Griffin, B. W. (1972) Carbon monoxide binding by *Pseudonomas putida* cytochrome P-450, *Arch. Biochem. Biophys. 151*, 427-433.

80. Ebel, R. E., O'Keeffe, D. H., and Peterson, J. A. (1975) Nitric oxide complexes of cytochrome P-450, *FEBS Lett. 55*, 198-201.

81. Stern, J. O., and Peisach, J. (1976) A model compound for the nitrosyl cytochrome *P*-450; futher evidence for mercaptide sulfur ligation to heme, *FEBS Lett. 62*, 364-368.

82. O'Keeffe, D. H., Ebel, R. E., and Peterson, J. A. (1978) Studies of the oxygen binding site of cytochrome P-450, *J. Biol. Chem. 253*, 3509-3516.

83. Mansuy, D., Beaune, P., Chottard, J. C., Bartoli, J. F., and Gans, P. (1976) The nature of the "455 nm absorbing complex" formed during the cytochrome P450 depdendent oxidative metabolism of amphetamine, *Biochem. Pharmacol. 25*, 609-612.

84. Mansuy, D., Gans, P., Chottard, J.-C., and Bartoli, J.-F. (1977) Nitrosoalkanes as Fe(II) ligands in the 455-nm-absorbing cytochrome *P*-450 complexes formed from nitroalkanes in reducing conditions, *Eur. J. Biochem. 76*, 607-615.

85. Ullrich, V., Nastainczyk, W., and Ruf, H. H. (1975) Ligand reactions of cytochrome *P*-450, *Biochem. Soc. Trans. 3*, 803-807.

86. Werringloer, J., and Estabrook, R. W. (1975) Heterogeneity of liver microsomal cytochrome P-450: the special characterization of reactants with reduced cytochrome P-450, *Arch. Biochem. Biophys. 167*, 270-286.

87. Dawson, J. H., Andersson, L. A., and Sono, M. (1983) The Diverse Spectroscopic Properties of Ferrous Cytochrome P-450-CAM Ligand Complexes, *J. Biol. Chem. 258*, 13637-13645.

88. Hanson, L. K., Eaton, W. A., Sligar, S. G., Gunsalus, I. C., Gouterman, M., and Connell, C. R. (1976) Origin of the anomalous Soret spectra of carboxycytochrome P-450, *J. Am. Chem. Soc. 98*, 2672-2674.

89. Jung, C., and Ristau, O. (1977) Quantum-mechanical interpretation of the unusual absorption spectrum of the cytochrome P-450-CO complex, *Chem. Phys. Lett. 49*, 103-108.

90. Jung, C. (1985) Quantum chemical explanation of the "hyper" spectrum of the carbon monoxide complex of cytochrome P-450, *Chem. Phys. Lett. 113*, 589-596.

91. Vickery, L., Salmon, A., and Sauer, K. (1975) Magnetic circular dichroism studies on microsomal aryl hydrocarbon hydroxylase: comparison with cytochrome b_5 and cytochrome P-450_{cam}, *Biochim. Biophys. Acta 386*, 87-98.

92. Greschner, S., Sharonov, Y. A., and Jung, C. (1993) Substrate induced changes of the active site electronic states in reduced cytochrome P450cam and the photolysis product of its CO complex, *FEBS Letters 315*, 153-158.

93. Yarmola, E. G., and Sharonov, Y. A. (1994) Low-temperature magnetic circular dichroism investigation of the active site of chloroperoxidase, *FEBS Letters 355*, 279-281.

94. Champion, P. M., Gunsalus, I. C., and Wagner, G. C. (1978) Resonance Raman investigations of cytochrome $P450_{CAM}$ from *Pseudomonas putida*, *J. Am. Chem. Soc. 100*, 3743-3751.

95. Ozaki, Y., Kitagawa, T., Kyogoku, Y., Shimada, H., Iizuka, T., and Ishimura, Y. (1976) An anomaly in the resonance Raman spectra of cytochrome P-450$_{cam}$ in the ferrous high spin state, *J. Biochem. 80*, 1447-1451.

96. Remba, R. D., Champion, P. M., Fitchen, D. B., Chiang, R., and Hager, L. P. (1979) Resonance Raman investigations of chloroperoxidase, horseradish peroxidase, and cytochrome *c* using Soret band laser excitation, *Biochemistry 18*, 2280-2290.

97. Champion, P. M., Remba, R. D., Chiang, R., Fitchen, D. B., and Hager, L. P. (1976) Resonance Raman spectra of chloroperoxidase, *Biochim. Biophys. Acta 446*, 486-492.

98. Wang, J., Stuehr, D. J., Ikeda-Saito, M., and Rousseau, D. L. (1993) Heme coordination and structure of the catalytic site of nitric oxide synthase, *J. Biol. Chem. 268*, 22255-22258.

99. Champion, P. M. (1988) Cytochrome P450 and the transform analysis of heme proein Raman spectra, in *Biological Applications of Raman Spectroscopy* (Spiro, T. G., Ed.), pp 249-292, Wiley, New York.

100. Anzenbacher, P., Evangelista-Kirkup, R., Schenkman, J., and Spiro, T. G. (1989) Influence of thiolate ligation on the heme electronic structure in microsomal cytochrome P-450 and model compounds: resonance Raman spectroscopic evidence, *Inorg. Chem. 28*, 4491-4495.

101. Momenteau, M., and Reed, C. A. (1994) Synthetic heme dioxygen complexes, *Chem. Rev. 94*, 659-698.

102. Ishimura, Y., Ullrich, V., and Peterson, J. A. (1971) Oxygenated cytochrome P-450 and its possible role in enzymic hydroxylation, *Biochem. Biophys. Res. Comm. 42*, 140-146.

103. Antonini, E., and Brunori, M. (1971) *Hemoglobin and Myoglobin in Their Reactions with Ligands*, Vol. 21, North-Holland Publishing Co., Amsterdam.

104. Dawson, J. H., and Cramer, S. P. (1978) Oxygenated cytochrome P-450$_{cam}$: evidence against axial histidine ligation of iron, *FEBS Letters 88*, 127-130.

105. Vickery, L., Nozawa, T., and Sauer, K. (1976) Magnetic circular dichroism studies of myoglobin complexes. Correlations with heme spin state and axial ligation, *J. Am. Chem. Soc. 98*, 343-350.

106. Bangcharoenpaurpong, O., Rizos, A. K., Champion, P. M., Jollie, D., and Sligar, S. G. (1986) Resonance Raman detection of bound dixoygen in cytochrome P-450$_{cam}$, *J. Biol. Chem. 261*, 8089-8092.

107. Chottard, G., Schappacher, M., Ricard, L., and Weiss, R. (1984) Resonance Raman spectra of iron(II) cytochrome P_{450} model complexes: influence of the thiolate ligand, *Inorg. Chem. 23*, 4557-4561.

108. Matsu-ura, M., Tani, F., Nakayama, S., Nakamura, N., and Naruta, Y. (2000) Hydrogen-bonded dioxygen adduct of an iron porphyrin with an alkanethiolate ligand: an elaborate model of cytochrome P450, *Angew. Chem. Int. Ed. 39*, 1989-1991.

109. Alben, J. O. (1978) Infrared Spectroscopy of Porphyrins, in *The Porphyrins* (Dolphin, D., Ed.), pp 323-345, Academic Press, New York.

110. Okubo, S., Nozawa, T., and Hatano, M. (1981) Magnetic circular dichroism spectra of models for the reduced cytochrome P-450 and its oxygenated form, *Chem. Lett.*, 1625-1628.

111. Budyka, M. F., Khenkin, A. M., and Shteinman, A. A. (1981) Mercaptide-anion as a trans-ligand in oxycytochrome P450, *Biochem. Biophys. Res. Comm. 101*, 615-622.

112. Kühnel, K., Blankenfeldt, W., Terner, J., and Schlichting, I. (2006) Crystal structures of chloroperoxidase with its bound substrates and complexed with formate, acetate, and nitrate, *J. Biol. Chem. 281*, 23990-23998.

113. Cupp-Vickery, J., and Poulos, T. L. (1995) Structure of cytochrome P450 eryF: an enzyme involved in erythromycin biosynthesis, *Nat. Struct. Biol. 2*, 144-153.

114. Ravichandran, K. G., Boddupalli, S. S., Hasemann, C. A., Peterson, J., and Deisenhofer, J. (1993) Crystal structure of hemoprotein domain of P450BM-3, a prototype for microsomal P450's, *Science 261*, 731-736.

115. Hasemann, C. A., Ravichandran, K. G., Boddupalli, S. S., Peterson, J., and Deisenhofer, J. (1995) Structure and function of cytochromes P450: a comparative analysis of three crystal structures, *Structure 3*, 41-62.

116. Sundaramoorthy, M., Terner, J., and Poulos, T. L. (1995) The crystal structure of chloroperoxidase: a heme peroxidase-cytochrome P450 functional hybrid, *Structure 3*, 1367-1377.

117. Sono, M., Eble, K. S., Dawson, J. H., and Hager, L. P. (1985) Preparation and properties of ferrous chloroperoxidase complexes with dioxygen, nitric oxide, and an alkyl isocyanide, *J. Biol. Chem. 260*, 15530-15535.

118. Marchal, S., Gorren, A. C. F., Sørlie, M., Andersson, K. K., Mayer, B., and Lange, R. (2004) Evidence of two distinct oxygen complexes of reduced endothelial nitric oxide synthase, *J. Biol. Chem. 279*, 19824-19831.

119. Ledbetter, A. P., McMillan, K., Roman, L. J., Masters, B. S. S., Dawson, J. H., and Sono, M. (1999) Low-temperature stabilization and spectroscopic characterizaion of the

dioxygen complex of the ferrous neuronal nitric oxide synthase oxygenase domain, *Biochemistry 38*, 8014-8021.

120. Hiner, A. N. P., Raven, E. L., Thorneley, R. N. F., García-Cánovas, F., and Rodríguez-López, J. N. (2002) Mechanisms of compound I formation in heme peroxidases, *J. Inorg. Biochem. 91*, 27-34.

121. Dawson, J. H. (1988) Probing structure-function relations in heme-containing oxygenases and peroxidases, *Science 240*, 433-439.

122. Newcomb, M., Zhang, R., Chandrasena, R. E. P., Halgrimson, J. A., Horner, J. H., Makris, T. M., and Sligar, S. G. (2006) Cytochrome P450 compound 1, *J. Am. Chem. Soc. 128*, 4580-4581.

123. Daiber, A., Herold, S., Schöneich, C., Mangaladze, D., Peterson, J. A., and Ullrich, V. (2000) Nitration and inactivation of cytochrome P450BM-3 by peroxynitrite, *Eur. J. Biochem. 267*, 6729-6739.

124. Behan, R. K., and Green, M. T. (2006) On the status of ferryl protonation, *J. Inorg. Biochem. 100*, 448-459.

125. Behan, R. K., Hoffart, L. M., Stone, K. L., Krebs, C., and Green, M. T. (2006) Evidence for Basic Ferryls in Cytochromes P450 *J. Am. Chem. Soc. 128*, 11471-11474

126. Egawa, T., Proshlyakov, D. A., Miki, H., Makino, R., Ogura, T., Kitagawa, T., and Ishimura, Y. (2001) Effects of a thiolate axial ligand on the $\pi \rightarrow \pi^*$ electronic states of oxoferryl porphyrins: a study of the optical and resonance Raman spectra of compounds I and II or chloroperoxidase, *J. Biol. Inorg. Chem. 6*, 46-54.

127. Palcic, M. M., Rutter, R., Araiso, T., Hager, L. P., and Dunford, H. B. (1980) Spectrum of chloroperoxidase compound I, *Biochem. Biophys. Res. Comm. 94*, 1123-1127.

128. Hosten, C. M., Sullivan, A. M., Palaniappan, V., Fitzgerald, M. M., and Terner, J. (1994) Resonance Raman spectroscopy of the catalytic intermediates and derivatives of chloroperoxidase from *Caldariomyces fumago*, *J. Biol. Chem. 269*, 13966-13978.

129. Egawa, T., Miki, H., Ogura, T., Makino, R., Ishimura, Y., and Kitagawa, T. (1992) Observation of the Fe^{IV}=O stretching Raman band for a thiolate-ligated heme protein, *FEBS Letters 305*, 206-208.

130. Rutter, R., Hager, L. P., Dhonau, H., Hendrich, M., Valentine, M., and Debrunner, P. (1984) Chloroperoxidase compound I: electron paramagnetic resonance and Mössbauer studies, *Biochemistry 23*, 6809-6816.

131. Stone, K. L., Behan, R. K., and Green, M. T. (2005) X-ray absorption spectroscopy of chloroperoxidase compound 1: insight into the reactive intermediate of P450 chemistry, *Proc. Nat. Acad. Sci. USA 102*, 16563-16565.

132. Harris, D., Loew, G., and Waskell, L. (2001) Calculation of the electronic structure and spectra of model cytochrome P450 compound I, *J. Inorg. Biochem. 83*.

133. Rittle, J., and Green, M. T. (2010) Cytochrome P450 Compound I: Capture, Characterization, and C-H Bond Activation Kinetics, *Science 330*, 933-937.

134. Czarnecki, K., Kincaid, J. R., and Fujii, H. (1999) Resonance Raman spectra of legitimate models for the ubiquitous compound I inermediates of oxidative heme enzymes, *J. Am. Chem. Soc. 121*.

135. Kitagawa, T., and Mizutani, Y. (1994) Resonance Raman spectra of highly oxidized metalloporphyrins and heme proteins, *Coord. Chem. Rev. 135/136*, 685-735.

136. Rittle, J., Younker, J. M., and Green, M. T. (2010) Cytochrome P450: The Active Oxidant and Its Spectrum, *Inorg. Chem. 49*, 3610-3617.

137. Zaks, A., and Dodds, D. R. (1995) Chloroperoxidase-Catalyzed Asymmetric Oxidations: Substrate Specificity and Mechanistic Study, *J. Am. Chem. Soc. 117*, 10419-10424.

138. Pazicni, S., Cherney, M. M., Lukat-Rogers, G. S., Oliveriusová, J., Rodgers, K. R., Kraus, J. P., and Burstyn, J. N. (2005) The Heme of Cystathionine β-synthase Likely Undergoes a Thermally Induced Redox-Mediated Ligand Switch, *Biochemistry 44*, 16785-16795.

139. Kim, I.-C., and Deal, W. C. (1976) Isolation and properties of a new, soluble, hemoprotein (H-450) from pig liver, *Biochemistry 15*, 4925-4930.

140. Jensen, K. P., and Ryde, U. (2004) How O_2 binds to heme, *J. Biol. Chem. 279*, 14561-14569.

141. Dawson, J. H., and Sono, M. (1987) Cytochrome P-450 and chloroperoxidase: Thiolate-ligated heme enzymes. Spectroscopic determination of their active site structures and mechanistic implications of thiolate ligation *Chem. Rev. 87*, 1255-1276

142. Dhawan, I. K., Shelver, D., Thorsteinsson, M. V., Roberts, G. P., and Johnson, M. K. (1999) Probing the heme axial ligation in the CO-sensing CooA protein with magnetic circular dichroism spectroscopy, *Biochemistry 38*, 12805-12813.

143. Yu, N.-T., and Kerr, E. A. (1988) Vibrational models of coordinated CO, CN^-, O_2, and NO, in *Biological Applications of Raman Spectroscopy* (Spiro, T. G., Ed.), pp 39-95, John Wiley & Sons, New York.

144. Ray, G. B., Li, X.-Y., Ibers, J. A., Sessler, J. L., and Spiro, T. G. (1994) How far can proteins bend the FeCO unit? Distal polar and steric effects in heme proteins and models, *J. Am. Chem. Soc. 116*, 162-176.

145. Li, X.-Y., and Spiro, T. G. (1988) Is bound CO linear or bent in heme proteins? Evidence from resonance Raman and infrared spectroscopic data, *J. Am. Chem. Soc. 110*, 6024-6033.

146. Traylor, T. G., and Sharma, V. S. (1992) Why NO?, *Biochemistry 31*, 2847-2849.

147. Enemark, J. H., and Feltham, R. D. (1974) Principles of sructure, bonding, and reactivity for metal nitrosyl complexes, *Coord. Chem. Rev. 12*, 339-406.

148. Quaroni, L. G., Seward, H. E., McLean, K. J., Girvan, H. M., Ost, T. W. B., Noble, M. A., Kelly, S. M., Price, N. C., Cheesman, M. R., Smith, W. E., and Munro, A. W. (2004) Interaction of Nitric Oxide with Cytochrome P450 BM3, *Biochemistry 43*, 16416-16431.

149. Sono, M., Eble, K. S., Dawson, J. H., and Hager, L. P. (1985) Preparation and properties of ferrous chloroperoxidase complexes with dioxygen, nitric oxide, and an alkyl isocyanide, *J. Biol. Chem. 260*, 15530-15535.

150. Reynolds, M. F., Parks, R. B., Burstyn, J. N., Shelver, D., Thorsteinsson, M. V., Kerby, R. L., Roberts, G. P., Vogel, K. M., and Spiro, T. G. (2000) Electronic absorption, EPR, and resonance Raman spectroscopy of CooA, a CO-sensing transcription activator from *R. rubrum*, reveals a five-coordinate NO-heme., *Biochemistry 39*, 388-396.

151. Taoka, S., and Banerjee, R. (2001) Characterization of NO binding to human cystathionine β-synthase: Possible implications of the effects of CO and NO binding to the human enzyme, *J. Inorg. Biochem. 87*, 245-251.

152. Yonetani, T., Yamamoto, H., Erman, J. E., Leigh, J. S., and Reed, G. H. (1972) Electromagnetic properties of hemoproteins, *J. Biol. Chem. 247*, 2447-2455.

153. Palmer, G. (1983) Electron paramagnetic resonance of hemoproteins, in *Iron Porphyrins* (Lever, A. B. P., and Gray, H. B., Eds.), pp 43-88, Addison-Wesley, Reading, Massachusetts.

154. Kon, H. (1975) An interpretation of the three line EPR spectrum of nitric oxide hemeproteins and related model systems: the effect of the heme environment, *Biochim. Biophys. Acta 379*, 103-113.

155. Obayashi, E., Tsukamoto, K., Adachi, S.-i., Takahashi, S., Nomura, M., Iizuka, T., Shoun, H., and Shiro, Y. (1997) Unique binding of nitric oxide to ferric nitric oxide reductase from *Fusiarium oxysporum* elucidated with infrared, resonance Raman, and X-ray absorption spectroscopies, *J. Am. Chem. Soc. 119*, 7807-7816.

156. Hu, S., and Kincaid, J. R. (1991) Resonance Raman Spectra of the Nitric Oxide Adducts of Ferrous Cytochrome P450cam in the Presence of Various Substrates, *J. Am. Chem. Soc. 113*, 9760-9766.

157. Maes, E. M., Walker, F. A., Montfort, W. R., and Czernuszewicz, R. S. (2001) Resonance Raman spectroscopic study of nitrophorin 1, a nitric oxide-binding heme protein from *Rhodnius prolixus*, and its nitrosyl and cyano adducts, *J. Am. Chem. Soc. 123*, 11664-11672.

158. Reynolds, M. F., Parks, R. B., Burstyn, J. N., Shelver, D., Thorsteinsson, M. V., Kerby, R. L., Roberts, G. P., Vogel, K. M., and Spiro, T. G. (2000) Electronic absorption, EPR, and resonance Raman spectroscopy of CooA, a CO-sensing transcription activator from *R. rubrum*, reveals a five-coordinate NO-heme, *Biochemistry 39*, 388-396.

159. Vogel, K. M., Kozlowski, P. M., Zgierski, M. Z., and Spiro, T. G. (1999) Determinants of the FeXO [X=C,N,O] vibrational frequencies in heme adducts from experiment and density functional theory, *J. Am. Chem. Soc. 121*, 9915-9921.

160. Guengrich, F. P. (2001) Common and uncommon cytochrome P450 reactions related to metabolism and chemical toxicity, *Chem. Res. Toxicol. 14*, 611-650.

161. Guengrich, F. P. (2005) Human cytochrome P450 enyzmes, in *Cytochrome P450: Structure, Mechanism, and Biochemistry* (Ortiz de Montellano, P. R., Ed.), pp 377-463, Kluwer Academic/Plenum, New York.

162. White, R. E. (1991) The involvement of free radicals in the mechanisms of monooxygenases, *Pharmacol. Therapeut. 49*, 21-42.

163. Groves, J. T. (1985) Key elements of the chemistry of cytochrome P-450. The oxygen rebound mechanism, *J. Chem. Ed. 62*, 928-931.

164. Groves, J. T., Haushalter, R. C., Nakamura, M., Nemo, T. E., and Evans, B. J. (1981) High-valent iron-porphyrin complexes related to peroxidase and cytochrome P-450, *J. Am. Chem. Soc. 103*, 2884-2886.

165. Frew, J. E., and Jones, P. (1984) in *Advances in Inorganic and Bioinorganic Mechanisms* (Sykes, A. G., Ed.), Academic Press, Orlano.

166. Neidleman, S. L., and Geigert, J. (1986) *Biohalogenation: Principles, Basic Roles and Applications*, Halsted Press, New Yorrk.

167. MacMicking, J., Xie, Q.-w., and Nathan, C. (1997) Nitric oxide and macrophage function, *Annu. Rev. Immunol. 15*, 323-350.

168. Lincoln, J., Hoyle, C. H. V., and Burnstock, G. (1997) *Nitric Oxide in Health and Disease*, Cambridge University Press, Cambridge, U. K.

169. Cooke, J. P., and Dzau, V. J. (1997) Nitric oxide synthase: role in the genesis of vascular disease, *Annu. Rev. Med. 48*, 489-509.

170. Alderton, W. K., Cooper, C. E., and Knowles, R. G. (2001) Nitric oxide synthases: structure, function, and inhibition, *Biochem. J. 357*, 593-615.

171. Fischmann, T. O., Hruza, A., Niu, X. D., Fossetta, J. D., Lunn, C. A., Dolphin, E., Prongay, A. J., Reichert, P., Lundell, D. J., Narula, S. K., and Weber, P. (1999) Structural characterization of nirtic oxide synthase isoforms reveals striking acive-site conservation, *Nat. Struct. Biol. 6*, 233-242.

172. Raman, C. S., Martasek, P., and Masters, B. S. S. (2000) Structural Themes Determining Function in Nitric Oxide Synthases, in *The Porphyrin Handbook* (Kadish, K. M., Smith, K. M., and Guilard, R., Eds.), pp 293-339, Academic Press, New York.

173. Rousseau, D. L., Li, D., Couture, M., and Yeh, S.-R. (2005) Ligand-protein interactions in nitric oxide synthase, *J. Inorg. Biochem. 99*, 306-323.

174. Kudo, T., Tomura, D., Liu, D. L., Dai, X. Q., and Shoun, H. (1996) Two isozymes of P450nor of *Cylindrocarpon tonkinense*: molecular cloning of the cDNAs and genes, expressions in the yeast, and the putative NAD(P)H-binding site, *Biochimie 78*, 792-799.

175. Usuda, K., Toritsuka, N., Matsuo, Y., Kim, D. H., and Shoun, H. (1995) Denitrification by the fungus *Cylindrocarpon tonkinense*: anaerobic cell growth and two isozyme forms of cytochrome P-450nor, *Appl. Environ. Microb. 61*, 883-889.

176. Zhang, L., Takaya, N., Kitazume, T., Kondo, T., and Shoun, H. (2001) Purification and cDNA cloning of nitric oxide reductase cytochrome P450nor (CYP55A4) from *Trichosporon cutaneum*, *Eur. J. Biochem. 268*, 3198-3204.

177. Tsuruta, S., Takaya, N., Zhang, L., Shoun, H., Kimura, K., Hamamoto, M., and Nakase, T. (1998) Denitrification by yeasts and occurrence of cytochrome P450nor in *Trichosporon cutaneum*, *FEMS Microbiology Letters 168*, 105-110.

178. Shoun, H., Kano, M., Baba, I., Takaya, N., and Matsuo, M. (1998) Denitrification by actinomycetes and purification of dissimilatory nitrite reductase and azurin from *Streptomyces thioluteus*, *J. Bacteriol. 180*, 4413-4415.

179. Shiro, Y., Fujii, M., Iizuka, T., Adachi, S.-i., Tsukamoto, K., Nakahara, K., and Shoun, H. (1995) Spectroscopic and kinetic studies on reaction of cytochrome P450nor with nitric oxide, *J. Biol. Chem. 270*, 1617-1623.

180. Nakahara, K., Tanimoto, T., Hatano, K.-i., Usuda, K., and Shoun, H. (1993) Cytochrome P-450 55AI (P-450dNIR) acts as nitric oxide reductase employing NADH as the direct electron donor, *J. Biol. Chem. 268*, 8350-8355.

181. Shimizu, H., Park, S.-Y., Shiro, Y., and Adachi, S.-i. (2002) X-ray structure of nitric oxide reductase (cytochrome P450nor) at atomic resolution, *Acta Crystallogr. D. D58*, 81-89.

182. Silaghi-Dumitrescu, R. (2003) Nitric oxide reduction by heme-thiolate enzymes (P450nor): a reevaluation of the mechanism, *Eur. J. Inorg. Chem. 6*, 1048-1052.

183. Harris, D. L. (2002) Cytochrome P450nor: a nitric oxide reductase - structure, spectra, and mechanism, *Int. J. Quant. Chem. 88*, 183-200.

184. Shimizu, H., Obayashi, E., Gomi, Y., Arakawa, H., Park, S.-Y., Nakamura, H., Adachi, S.-i., Shoun, H., and Shiro, Y. (2000) Proton delivery in NO reduction by fungal nitric-oxide reducase, *J. Am. Chem. Soc. 275*, 4816-4826.

185. Kudo, T., Takaya, N., Park, S.-Y., Shiro, Y., and Shoun, H. (2000) A positively charged cluster formed in the heme-distal pocket of cytochrome P450nor is essential for interaction with NADH, *J. Am. Chem. Soc. 276*, 5020-5026.

186. Obayashi, E., Takahashi, S., and Shiro, Y. (1998) Electronic stucture of reaction intermediate of cytochrome P450nor in its nitric oxide reduction, *J. Am. Chem. Soc. 120*, 12964-12965.

187. Sono, M., Andersson, L. A., and Dawson, J. H. (1982) Sulfur donor ligand binding to ferric cytochrome P-450-CAM and myoglobin. Ultraviolet-visible absorption, magnetic circular dichroism, and electron paramagnetic resonance spectroscopic investigation of the complexes, *J. Biol. Chem. 257*, 8308-8320.

188. Sono, M., and Dawson, J. H. (1982) Formation of low spin complexes of ferric cytochrome P-450-CAM with anionic ligands. Spin state and ligand affinity comparison to myoglobin, *J. Biol. Chem. 257*, 5496-5502.

189. LoBrutto, R., Scholes, C. P., Wagner, G. C., Gunsalus, I. C., and Debrunner, P. G. (1980) Electron nuclear double resonance of ferric cytochrome P450CAM, *J. Am. Chem. Soc. 102*, 1167-1170.

190. Ohno, N., Suzuki, T., Dokoh, Y., Urano, H., Kikuchi, M., Hirobe, T., Higuchi, T., and Nagano, S. (2000) Remarkable axial thiolate ligand effect on the oxidation of hydrocarbons by active intermediate of iron porphyrin and cytochrome P450, *J. Inorg. Biochem. 82* 123–125.

191. Ogliaro, F., Visser, S. P. d., and Shaik, S. (2002) The 'push' effect of the thiolate ligand in cytochrome P450: a theoretical gauging, *J. Inorg. Biochem. 91*, 554– 567.

192. Kamachi, T., Kouno, T., Nam, W., and Yoshizawa, K. (2006) How axial ligands control the reactivity of high-valent iron(IV)–oxo porphyrin p-cation radicals in alkane hydroxylation: A computational study *J. Inorg. Biochem. 100*, 751–754

193. Green, M. T. (2009) C-H bond activation in heme proteins: the role of thiolate ligation in cytochrome P450, *Curr. Op. Chem. Biol. 13*, 84-88.

194. Green, M. T., Dawson, J. H., and Gray, H. B. (2004) Chloroperoxidase compound II is basic: Implications for P450 chemistry, *Science 304*, 1653-1656.

195. Brunel, A., Wilson, A., Henry, L., Dorlet, P., and Santolini, J. (2011) The Proximal Hydrogen Bond Network Modulates *Bacillus subtilis* Nitric-oxide Synthase Electronic and Structural Properties, *J. Biol. Chem. 286*, 11997-12005.

196. Yoshioka, S., Takahashi, S., Ishimori, K., and Morishima, I. (2000) Roles of the axial push effect in cytochrome P450cam studied with site-directed mutagenesis at the heme proximal site, *J. Inorg. Biochem. 81*, 141-151.

197. Yoshioka, S., Tosha, T., Takahashi, S., Ishimori, K., Hori, H., and Morishima, I. (2002) Roles of the Proximal Hydrogen Bonding Network in Cytochrome P450cam-Catalyzed Oxidation, *J. Am. Chem. Soc. 124*, 14571-14579.

198. Lang, J., Driscoll, D., Gélinas, S., Rafferty, S. P., and Couture, M. (2009) Trp180 of endothelial NOS and Trp56 of bacterial saNOS modulate sigma bonding of the axial cysteine to the heme, *J. Inorg. Biochem. 103*, 1102-1112.

199. Hannibal, L., Somasundaram, R., Tejero, J., Wilson, A., and Stuehr, D. J. (2011) Influence of Heme-Thiolate in Shaping the Catalytic Properties of a Bacterial Nitric-Oxide Synthase, *J. Biol. Chem. 286*, 39224-39235.

200. Couture, M., Adak, S., Stuehr, D. J., and Rousseau, D. L. (2001) Regulation of the Properties of the Heme-NO Complexes in Nitric-oxide Synthase by Hyrogen Bonding to the Proximal Cysteine, *J. Biol. Chem. 276*, 38280-38288.

201. Usharani, D., Zazza, C., Lai, W., Chourasia, M., Waskell, L., and Shaik, S. (2012) A Single-Site Mutation (F429H) Converts the Enzyme CYP 2B4 into a Heme Oxygenase: A QM/MM Study, *J. Am. Chem. Soc. dx.doi.org/10.1021/ja211905e*.

202. Ullrich, V. (2003) Thoughts on thiolate tethering. Tribute and thanks to a teacher *Arch. Biochem. Biophys. 409*, 45–51.

203. Nakajima, R., Yamazaki, I., and Griffin, B. W. (1985) Spectra of chloroperoxidase compounds II and III, *Biochem. Biophys. Res. Comm. 128*, 1-6.

204. Green, M. T., Dawson, J. H., and Gray, H. B. (2004) Oxoiron(IV) in chloroperoxidase compound II is basic: implications for P450 chemistry, *Science 304*, 1563-1656.

205. Green, M. T. (2006) Application of Badger's Rule to heme and non-heme iron-oxygen bonds: an examination of ferryl protonation states, *J. Am. Chem. Soc. 128*, 1902-1906.

206. Stone, K. L., Hoffart, L. M., Behan, R. K., Krebs, C., and Green, M. T. (2006) Evidence for two ferryl species in chloroperoxidase compound II, *J. Am. Chem. Soc. 128*, 6147-6153.

207. Stone, K. L., Behan, R. K., and Green, M. T. (2006) Resonance Raman spectroscopy of chloroperoxidase compound II provides direct evidence for the existence of an iron(IV)–hydroxide *Proc. Natl. Acad. Sci. USA 103*, 12307–12310

208. Gardner, K. A., Kuehnert, L., and Mayer, J. M. (1997) Hydrogen Atom Abstraction by Permanganate: Oxidations of Arylalkanes in Organic Solvents, *Inorg. Chem. 36*, 2069-2078.

209. Gardner, K. A., and Mayer, J. M. (1995) Understanding C-H bond oxidations: H. and H- transfer in the oxidation of toluene by permanganate, *Science 269*, 1849.

210. Mayer, J. M. (1998) Hydrogen Atom Abstraction by Metal-Oxo Complexes: Understanding the Analogy with Organic Radical Reactions, *Acc. Chem. Res. 31*, 441.

211. Roberts, G. P., Kerby, R. L., Youn, H., and Conrad, M. (2005) CooA, a paradigm for gas sensing regulatory proteins, *J. Inorg. Biochem. 99*, 280-292.

212. Kerby, R. L., Ludden, P. W., and Roberts, G. P. (1995) Carbon monoxide-dependent growth of *Rhodospirillum rubrum*, *J. Bacteriol. 177*, 2241-2244.

213. Aono, S., Ohkubo, K., Matsuo, T., and Nakajima, H. (1998) Redox-controlled ligand exchange of the heme in the CO-sensing transcriptional activator CooA, *J. Biol. Chem. 273*, 25757-25764.

214. Clark, R. W., Youn, H., Parks, R. B., Cherney, M. M., Roberts, G. P., and Burstyn, J. N. (2004) Investigation of the role of the N-terminal proline, the distal ligand in the CO sensor CooA, *Biochemistry 43*, 14149-14160.

215. Yamamoto, K., Ishikawa, H., Takahashi, S., Ishimori, K., Morishima, I., Nakajima, H., and Aono, S. (2001) Binding of CO at the Pro^2 side is crucial for the activation of CO-sensing transcriptional activator CooA*, J. Biol. Chem. 276*, 11473-11476.

216. Reynolds, M. F., Parks, R. B., Burstyn, J. N., Shelver, D., Thorsteinsson, M. V., Kerby, R. L., Roberts, G. P., Vogel, K. M., and Spiro, T. G. (2000) Electronic absorption, EPR and resonance Raman spectroscopies of CooA, a CO-sensing transcription factor from *R. rubrum*, reveals a five-coordinate NO-heme, *Biochemistry 39*, 388-396.

217. Lanzilotta, W. N., Schuller, D. J., Thorsteinsson, M. V., Kerby, R. L., Roberts, G. P., and Poulos, T. L. (2000) Structure of the CO sensing transcription activator CooA, *Nat. Struct. Biol. 7*, 876-880.

218. He, Y., Shelver, D., Kerby, R. L., and Roberts, G. P. (1996) Characterization of a CO-responsive transcriptional activator from *Rhodospirillum rubrum*, *J. Biol. Chem. 271*, 120-123.

219. Kerby, R. L., Youn, H., Thorsteinsson, M. V., and Roberts, G. P. (2003) Repositioning about the dimer interface of the transcription regulator CooA: a major signal transduction pathway between the effector and DNA-binding domains, *J. Mol. Biol. 325*, 809-823.

220. Dioum, E. M., Rutter, J., Tuckerman, J. R., Gonzalez, G., Gilles-Gonzalez, M.-A., and McKnight, S. L. (2002) NPAS2: a gas-responsive transcription factor, *Science 298*, 2385-2387.

221. Reick, M., Garcia, J. A., Dudley, C., and McKnight, S. L. (2001) NPAS2: an analog of clock operative in the mammalian forebrain, *Science 293*, 506-509.

222. Zhou, Y.-D., Barnard, M., Tian, H., Li, X., Ring, H. Z., Francke, U., Shelton, J., Richardson, J., Russelldagger, D. W., and McKnight, S. L. (1997) Molecular characterization of two mammalian bHLH-PAS domain proteins selectively expressed in the central nervous system, *Proc. Nat. Acad. Sci. USA 94*, 713-718.

223. Mukaiyama, Y., Uchida, T., Sato, E., Sasaki, A., Sato, Y., Igarashi, J., Kurokawa, H., Sagami, I., Kitagawa, T., and Shimizu, T. (2006) Spectroscopic and DNA-binding characterization of the isolated heme-bound basic helix–loop–helix-PAS-A domain of

neuronal PAS protein 2 (NPAS2), a transcription activator protein associated with circadian rhythms *FEBS J. 273*, 2528-2539.

224. Koudo, R., Kurokawa, H., Sato, E., Igarashi, J., Uchida, T., Sagami, I., Kitagawa, T., and Shimizu, T. (2005) Spectroscopic characterization of the isolated heme-bound PAS-B domain of neuronal PAS domain protein 2 associated with circadian rhythms, *FEBS J. 272*, 4153-4162.

225. Uchida, T., Sagami, I., Shimizu, T., Ishimori, K., and Kitagawa, T. (2012) Effects of the bHLH Domain on Axial Coordination of Heme in the PAS-A Domain of Neuronal PAS Domain Protein 2 (NPAS2): Conversion from His119/Cys170 Coordination to His119/His171 Coordination *J. Inorg. Biochem. 108*, 188-195.

226. Koudo, R., Kurokawa, H., Sato, E., Igarashi, J., Uchida, T., Sagami, I., Kitagawa, T., and Shimizu, T. (2005) Spectroscopic characterization of the isolated heme-bound PAS-B domain of neuronal PAS domain protein 2 associated with circadian rhythms *FEBS J. 272*, 4153-4162.

227. Kerby, R. L., Youn, H., and Roberts, G. P. (2008) RcoM: A new single-component transcriptional regulator of CO metabolism in bacteria, *J. Bacteriol. 190*, 3336-3343.

228. Smith, A. T., Marvin, K. A., Freeman, K. M., Kerby, R. L., Roberts, G. P., and Burstyn, J. N. (2012) Identification of Cys94 as the distal ligand to the Fe(III) heme in the transcriptional regulator RcoM-2 from *Burkholderia xenovorans*, *Submitted.*

229. de Rosny, E., de Groot, A., Jullian-Binard, C., Borel, F., Suarez, C., Le Pape, L., Fontecilla-Camps, J. C., and Jouve, H. M. (2008) DHR51, the *Drosophila melanogaster* Homologue of the Human Photoreceptor Cell-Specific Nuclear Receptor, Is a Thiolate Heme-Binding Protein, *Biochemistry 47*, 13252-13260.

230. Gronemeyer, H., and Laudet, V. (1995) Nuclear receptors, *Protein Profile 2*, 1173–1308

231. Renaud, J. P., and Moras, D. (2000) Structural studies on nuclear receptors, *Cell. Mol. Life Sci. 57*, 1748-1769.

232. Triqueneaux, G., Thenot, S., Kakizawa, T., Antoch, M. P., Safi, R., Takahashi, J. S., Delaunay, F., and Laudet, V. (2004) The orphan receptor Rev-erbalpha gene is a target of the circadian clock pacemaker, *J. Mol. Endocrinol. 33*, 585–608.

233. Woo, E.-J., Jeong, D. G., Lim, M.-Y., Kim, S. J., Kim, K.-J., Yoon, S.-M., Park, B.-C., and Ryu, S. E. (2007) Structural insight into the constitutive repression function of the nuclear receptor Rev-erbβ, *J. Mol. Biol. 373*, 735-744.

234. Preitner, N., Damiola, F., Lopez-Molina, L., Zakany, J., Duboule, D., Albrecht, U., and Schibler, U. (2002) The orphan nuclear receptor REV-ERBalpha controls circadian transcription within the positive limb of the mammalian circadian oscillator, *Cell 110*, 251–260.

235. Torra, I. P., Tsibulsky, V., Delaunay, F., Saladin, R., Laudet, V., and Fruchart, J. C. (2000) Circadian and glucocorticoid regulation of Rev-erbalpha expression in liver, *Endocrinology 141*, 3799–3806.

236. Reinking, J., Lam, M. M., Pardee, K., Sampson, H. M., Liu, S., Yang, P., Williams, S., White, W., Lajoie, G., Edwards, A., and Krause, H. M. (2005) The *Drosophila* Nuclear Receptor E75 Contains Heme and Is Gas Responsive, *Cell 122*, 195–207.

237. Raghuram, S., Stayrook, K. R., Huang, P., Rogers, P. M., Nosie, A. K., McClure, D. B., Burris, L. L., Khorasanizadeh, S., Burris, T. P., and Rastinejad, F. (2007) Identification

of heme as the ligand for the orphan nuclear receptors REV-ERBα and REV-ERBβ, *Nat. Struct. Mol. Biol. 14*, 1207-1213.

238. Yin, L., Wu, N., Curtin, J. C., Qatanani, M., Szwergold, N. R., Reid, R. A., Waitt, G. M., Parks, D. J., Pearce, K. H., Wisely, G. B., and Lazar, M. A. (2007) Rev-Erbα, a heme sensor that coordinates metabolic and circadian pathways, *Science 318*, 1786-1789.

239. Airola, M. V., Du, J., Dawson, J. H., and Crane, B. R. (2010) Heme Binding to the Mammalian Circadian Clock Protein Period 2 Is Nonspecific, *Biochemistry 49*, 4327-4338.

240. Chefalo, P. J., Oh, J., Rafie-Kolpin, M., Kan, B., and Chen, J.-J. (1998) Heme-regulated eIF-2α kinase purifies as a hemoprotein, *Eur. J. Biochem. 258*, 820-830.

241. Ishikawa, H., Yun, B.-G., Takahashi, S., Hori, H., Matts, R. L., Ishimori, K., and Morishima, I. (2002) NO-induced activation mechanism of the heme-regulated eIF2α kinase, *J. Am. Chem. Soc. 124*, 13696-13697.

242. Denver, T. E. (1999) Translation initiation: adept at adapting, *Trends Biochem. Sci. 24*, 398-403.

243. Chen, J.-J., and London, I. M. (1995) Regulation of protein synthesis by heme-regulated eIF-2α kinase, *Trends Biochem. Sci 20*, 105-108.

244. Chen, J.-J. (2000) in *Translational Control of Gene Expression* (Soneberg, N., Hershey, J. W. B., and Matthews, M. B., Eds.), pp 529-546, Cold Spring Harbor Laboratory, Cold Spring Harbor, NY.

245. Martinkova, M., Igarashi, J., and Shimizu, T. (2007) Eukaryotic initiation factor 2α kinase is a nitric oxide-responsive mercury sensor enzyme: Potent inhibition of catalysis by the mercury cation and reversal by nitric oxide *FEBS Lett. 581*, 4109–4114.

246. Rafie-Kolpin, M., Chefalo, P. J., Hussain, Z., Hahn, J., Uma, S., Matts, R. L., and Chen, J.-J. (2000) Two heme-binding domains of heme-regulated eukaryotic inititation factor-2α kinase. N terminus and kinase insertion, *J. Biol. Chem. 275*, 5171-5178.

247. Uma, S., Matts, R. L., Guo, Y., White, S., and Chen, J.-J. (2000) The N-terminal region of the heme-regulated eIF2α kinase is an autonomous heme binding domain, *Eur. J. Biochem. 267*, 498-506.

248. Inuzuka, T., Yun, B.-G., Ishikawa, H., Takahashi, S., Hori, H., Matts, R. L., Ishimori, K., and Morishima, I. (2004) Identification of crucial histidines for heme binding in the N-terminal domain of the heme-regulated eIF2α kinase, *J. Biol. Chem. 279*, 6778-6782.

249. Miksanova, M., Igarashi, J., Minami, M., Sagami, I., Yamauchi, S., Kurokawa, H., and Shimizu, T. (2006) Characterization of heme-regulated eIF2α kinase: Roles of the N-terminal domain in the oligomeric state, heme binding, catalysis, and inhibition, *Biochemistry 45*, 9894-9905

250. Hirai, K., Martinkova, M., Igarashi, J., Saiful, I., Yamauchi, S., El-Mashtoly, S., Kitagawa, T., and Shimizu, T. (2007) Identification of Cys385 in the isolated kinase insertion domain of heme-regulated eIF2α kinase (HRI) as the heme axial ligand by site-directed mutagenesis and spectral characterization, *J. Inorg. Biochem. 101*, 1172-1179.

251. Yun, B.-G., Matts, J. A. B., and Matts, R. L. (2005) Interdomain interactions regulate the activation of the heme-regulated eIF2α kinase, *Biochim. Biophys. Acta 1725*, 174-181.

252. Kery, V., Bukovska, G., and Kraus, J. P. (1994) Transsulfuration depends on heme in addition to pyridoxal 5'-phosphate. Cystathionine β-synthase is a heme protein, *J. Biol. Chem. 269*, 25283-25288.

253. Taoka, S., Lepore, B. W., Kabil, O., Ojha, S., Ringe, D., and Banerjee, R. (2002) Human cystathionine β-Synthase is a heme sensor protein. Evidence that the redox sensor is heme and not the vicinal cysteines in the CXXC motif seen in the crystal structure of the truncated enzyme, *Biochemistry 41*, 10454-10461.

254. Koutmos, M., Kabil, O., Smith, J. L., and Banerjee, R. (2010) Structural basis for substrated activation and regulation by cystathionine beta-synthase (CBS) domains in cystathionine β-synthase, *Proc. Natl. Acad. Sci. USA 107*, 20958-20963.

255. Maclean, K. N., Janosik, M., Oliveriusova, J., Kery, V., and Kraus, J. P. (2000) Transsulfuration in *Saccharomyces cerevisiae* is not dependent on heme: purification and characterization of recombinant yeast cystathionine β-synthase, *J. Inorg. Biochem. 81*, 161-171.

256. Jhee, K.-H., McPhie, P., and Miles, E. W. (2000) Yeast cystathionine β-synthase is a pyridoxal phosphate enzyme but, unlike the human enzyme, is not a heme protein, *J. Biol. Chem. 275*, 11541-11544.

257. Nozaki, T., Shigeta, Y., Saito-Nakano, Y., Imada, M., and Kruger, W. D. (2001) Characterization of transsulfuration and cysteine biosynthetic pathways in the protozoan hemoflagellate, *Trypanosoma cruzi*. Isolation and molecular characterization of

cystathionine β-synthase and serine acetyltransferase from *Trypanosoma*, *J. Biol. Chem. 276*, 6516-6523.

258. Kery, V., Poneleit, L., and Kraus, J. P. (1998) Trypsin cleavage of human cystathionine β-synthase into an evolutionarily conserved active core: structural and functional consequences, *Arch. Biochem. Biophys. 355*, 222-232.

259. Evande, R., Ojha, S., and Banerjee, R. (2004) Visualization of PLP-bound intermediates in hemeless variants of human cystathionine β-synthase: evidence that lysine 119 is a general base, *Arch. Biochem. Biophys. 427*, 188-196.

260. Oliveriusova, J., Kery, V., Maclean, K. N., and Kraus, J. P. (2002) Deletion mutagenesis of human cystathionine β-synthase. Impact on activity, oligomeric status, and S-adenosylmethionine regulation, *J. Biol. Chem. 277*, 48386-48394.

261. Bruno, S., Schiaretti, F., Burkhard, P., Kraus, J. P., Janosik, M., and Mozzarelli, A. (2001) Functional properties of the active core of human cystathionine β-synthase crystals, *J. Biol. Chem. 276*, 16-19.

262. Kery, V., Elleder, D., and Kraus, J. P. (1995) δ-Aminolevulinate increases heme saturation and yield of human cystathionine β-synthase expressed in *Escherichia coli*, *Arch. Biochem. Biophys. 316*, 24-29.

263. Majtan, T., Singh, L. R., Wang, L., Kruger, W. D., and Kraus, J. P. (2008) Active Cystathionine β-Synthase Can Be Expressed in Heme-free Systems in the Presence of Metal-substituted Porphyrins or a Chemical Chaperone, *J. Biol. Chem. 283*, 34588-34595.

264. Majtan, T., Freeman, K. M., Smith, A. T., Burstyn, J. N., and Kraus, J. P. (2011) Purification and Characterization of Cystathionine β-Synthase Bearing a Cobalt Protoporphyrin, *Arch. Biochem. Biophys. 508*, 25-30.

265. Smith, A. T., Majtan, T., Freeman, K. M., Su, Y., Kraus, J. P., and Burstyn, J. N. (2011) Cobalt Cystathionine β-Synthase: A Cobalt-Substituted Heme Protein with a Unique Thiolate Ligation Motif, *Inorg. Chem. 50*, 4417-4427.

266. Taoka, S., West, M., and Banerjee, R. (1999) Characterization of the heme and pyridoxal phosphate cofactors of human cystathionine β-synthase reveals nonequivalent active sites, *Biochemistry 38*, 2738-2744.

267. Taoka, S., Green, E. L., Loehr, T. M., and Banerjee, R. (2001) Mercuric chloride-induced spin or ligation state changes in ferric or ferrous human cystathionine β-synthase inhibit enzyme activity, *J. Inorg. Biochem. 87*, 253-259.

268. Taoka, S., Ohja, S., Shan, X., Kruger, W. D., and Banerjee, R. (1998) Evidence for heme-mediated redox regulation of human cystathionine β-synthase activity, *J. Biol. Chem. 273*, 25179-25184.

269. Cherney, M. M., Pazicni, S., Frank, N., Marvin, K. A., Kraus, J. P., and Burstyn, J. N. (2007) Ferrous human cystathionine β-synthase loses activity during enzyme assay due to a ligand switch process *Biochemistry 46*, 13199-13210.

270. Kabil, O., Weeks, C. L., Carballal, S., Gherasim, C., Alvarez, B., Spiro, T. G., and Banerjee, R. (2011) Reversible Heme-Dependent Regulation of Human Cystathionine β-Synthase by a Flavoprotein Oxidoreductase, *Biochemistry 50*, 8261-8263.

271. Valenzuela, J. G., Walker, F. A., and Ribeiro, J. M. (1995) A salivary nitrophorin (nitric-oxide-carrying hemoprotein) in the bedbug *Cimex lectularius*, *J. Exp. Biol. 198*, 1519-1526.

272. Champagne, D. E., Nussenzveig, R. H., and Ribeiro, J. M. C. (1995) Purification, partial characterization, and cloning of nitric oxide-carrying heme proteins (nitrophorins) from salivary glands of the blood-sucking insect *Rhodnius prolixus*, *J. Biol. Chem. 270*, 8691-8695.

273. Ribeiro, J. M., and Walker, F. A. (1994) High affinity histamine-binding and antihistaminic activity of the salivary nitric oxide-carrying heme protein (nitrophorin) of *Rhodnius prolixus*, *J. Exp. Med. 180*, 2251-2257.

274. Valenzuela, J. G., and Ribeiro, J. M. (1998) Purification and cloning of the salivary nitrophorin from the hemipteran *Cimex lectularius*, *J. Exp. Biol. 201*, 2659-2664.

275. Ribeiro, J. M., Hazzard, J. M., Nussenzveig, R. H., Champagne, D. E., and Walker, F. A. (1993) Reversible binding of nitric oxide by a salivary heme protein from a bloodsucking insect, *Science 260*, 539-541.

276. Walker, F. A. (2005) Nitric oxide interaction with insect nitrophorins and thoughts on the electron configuration of the $\{FeNO\}^6$ complex, *J. Inorg. Biochem. 99*, 216-236.

277. Walker, F. A. (2006) personal communication.

278. Perera, R., Sono, M., Sigman, J. A., Pfister, T. D., Lu, Y., and Dawson, J. H. (2004) Neutral thiol as a proximal ligand to ferrous heme iron: implications for heme proteins that lose cysteine thiolate ligation on reduction, *Proc. Nat. Acad. Sci. USA 100*, 3641-3646.

279. Bird, L. E., Ren, J., Zhang, J., Foxwell, N., Hawkins, A. R., Charles, I. G., and Stammers, D. K. (2002) Crystal Structure of SANOS, a Bacterial Nitric Oxide Synthase Oxygenase Protein from *Staphylococcus aureus*, *Structure 10*, 1687-1696.

280. Crane, B. R., Arvai, A. S., Ghosh, D. K., Wu, C., Getzoff, E. D., Stuehr, D. J., and Tainer, J. A. (1998) Structure of Nitric Oxide Synthase Oxygenase Dimer with Pterin and Substrate, *Science 279*, 2121-2126.

281. Pant, K., Bilwes, A. M., Adak, S., Stuehr, D. J., and Crane, B. R. (2002) Structure of a Nitric Oxide Synthase Heme Protein from *Bacillus subtilis*, *Biochemistry 41*, 11071-11079.

282. Hui Bon Hoa, G., Di Primo, C., Dondaine, I., Sligar, S. G., Gunsalus, I. C., and Douzou, P. (1989) Conformational changes of cytochromes P-450cam and P-450lin induced by high pressure *Biochemistry 28*, 651-656.

283. Fisher, M. T., Scarlata, S. F., and Sligar, S. G. (1985) High-pressure investigations of cytochrome P-450 spin and substrate binding equilibria, *Arch. Biochem. Biophys. 240*, 456-463.

284. Yu, C. A., and Gunsalus, I. C. (1974) Cytochrome P-450cam. II. Interconversion with P-420, *J. Biol. Chem. 249*, 102-106.

285. Imai, Y., and Sato, R. (1967) Anomalous spectral interactions of reduced P-450 with ethyl isocyanide and some other lipophillic ligands, *J. Biochem. 62*, 464-473.

286. Martinis, S. A., Blanke, S. R., Hager, L. P., Sligar, S. G., Hui Bon Hoa, G., Rux, J. J., and Dawson, J. H. (1996) Probing the heme iron coordination structure of pressure-induced cytochrome P450cam, *Biochemistry 35*, 14530-14536.

287. Collman, J. P., Sorrell, T. N., Dawson, J. H., Trudell, J. R., Bunnenberg, E., and Djerassi, C. (1976) Magnetic circular dichroism of ferrous carbonyl adducts of cytochromes P-450 and P-420 and their synthetic models: Further evidence for mercaptide as the fifth ligand to iron, *Proc. Natl. Acad. Sci. USA 73*, 6-10.

288. Hollenberg, P. F., and Hager, L. P. (1973) The P-450 nature of the carbon monoxide complex of ferrous chloroperoxidase, *J. Biol. Chem. 248*, 2630-2633.

289. Blanke, S. R., Martinis, S. A., Sligar, S. G., Hager, L. P., Rux, J. J., and Dawson, J. H. (1996) Probing the heme iron coordination structure of alkaline chloroperoxidase, *Biochemistry 35*, 14537-14543.

290. Kim, V. N., Han, J., and Siomi, M. C. (2009) Biogenesis of small RNAs in animals, *Nat. Rev. Mol. Cel. Bio. 10*, 126-139.

291. Denli, A. M., Tops, B. B. J., Plasterk, R. H. A., Ketting, R. F., and Hannon, G. J. (2004) Processing of primary microRNAs by the Microprocessor complex, *Nature 432*, 231-235.

292. Gregory, R. I., Yan, K.-p., Amuthan, G., Chendrimada, T., Doratotaj, B., Cooch, N., and Shiekhattar, R. (2004) The Microprocessor complex mediates the genesis of microRNAs, *Nature 432*, 235-240.

293. Faller, M., Matsunaga, M., Yin, S., Loo, J. A., and Guo, F. (2007) Heme is involved in microRNA processing, *Nat. Struct. Mol. Biol. 14*, 23-29.

294. Barr, I., Smith, A. T., Senturia, R., Chen, Y., Scheidemantle, B. D., Burstyn, J. N., and Guo, F. (2011) DiGeorge Critical Region 8 (DGCR8) Is a Double-cysteine-ligated Heme Protein, *J. Biol. Chem. 286*, 16716-16725.

295. Sono, M., and Dawson, J. H. (1982) Formation of Low Spin Complexes of Ferric Cytochrome P-450-CAM with Anionic Ligands. Spin State and Ligand Affinity Comparison to Myoglobin., *J. Biol. Chem. 257*, 5496-5502.

296. Sono, M., Dawson, J. H., and Hager, L. P. (1984) The Generation of a Hyperporphyrin Spectrum upon Thiol Binding to Ferric Chloroperoxidase, *J. Biol. Chem. 259*, 13209-13216.

297. Sono, M., Hager, L. P., and Dawson, J. H. (1991) Electron paramagnetic resonance investigations of exogenous ligand complexes of low-spin ferric chloroperoxidase: further support for endogenous thiolate ligation to the heme iron, *Biochim. Biophys. Acta 1078*, 351-359.

298. Perera, R., Sono, M., Sigman, J. A., Pfister, T. D., Lu, Y., and Dawson, J. H. (2004) Neutral thiol as a proximal ligand to ferrous heme iron: implications for heme proteins that lose cysteine thiolate ligation on reduction, *Proc. Natl. Acad. Sci. USA 100*, 3641-3646.

299. Barr, I., Smith, A. T., Chen, Y., Senturia, R., Burstyn, J. N., and Guo, F. (2012) Ferric, not ferrous, heme activates RNA-binding protein DGCR8 for primary microRNA processing, *Proc. Natl. Acad. Sci. USA 109*, 1919-1924.

300. Vetter, S. W., Terentis, A. C., Osborne, R. L., Dawson, J. H., and Goodin, D. B. (2009) Replacement of the axial histidine heme ligand with cysteine in nitrophorin 1: spectroscopic and crystallographic characterization, *J. Biol. Inorg. Chem. 14*, 179-191.

301. Salerno, J. C., Frey, C., McMillan, K., Williams, R. F., Masters, B. S. S., and Griffith, O. W. (1995) Characterization by Electron Paramagnetic Resonance of the Interactions

of L-Arginine and L-Thiocitrulline with the Heme Cofactor Region of Nitric Oxide Synthase, *J. Biol. Chem. 270*, 27423-27428.

302. Kitanishi, K., Igarashi, J., Hayasaka, K., Hikage, N., Saiful, I., Yamauchi, S., Uchida, T., Ishimori, K., and Shimizu, T. (2008) Heme-Binding Characteristics of the Isolated PAS-A Domain of Mouse Per2, a Transcriptional Regulatory Factor Associated with Circadian Rhythms, *Biochemistry 47*, 6157-6168.

303. Svastits, E. W., Alberta, J. A., Kim, I.-C., and Dawson, J. H. (1989) Magnetic Circular Dichroism Studies of the Active Site Structure of Hemoprotein H-450: Comparison to Cytochrome P-450 and Sensitiviy to pH Effects, *Biochem. Biophys. Res. Commun. 165*, 1170-1176.

304. Chiang, R., Makino, R., Spomer, W. E., and Hager, L. P. (1975) Chloroperoxidase: P-450 type absorption in the absence of sulfhydryl groups, *Biochemistry 14*, 4166-4171.

Table 1.1. Coordination states and functions of the heme-thiolate proteins.

Type-1 Heme-Thiolate	*Fe(III)*	*Fe(II)*	*Fe(II)-CO*	*heme function*
chloroperoxidase (*C. fumago*)	Cys(S^-)	Cys(S^-)	Cys(S^-)/CO	peroxidation
cytochromes P450	Cys(S^-)/H_2O	Cys(S^-)	Cys(S^-)/CO	oxygen activation
nitric oxide reductase	Cys(S^-)/H_2O	Cys(S^-)	Cys(S^-)/CO	NO activation
nitric oxide synthase	Cys(S^-)	Cys(S^-)	Cys(S^-)/CO	oxygen activation
Type-2 Heme-Thiolate	*Fe(III)*	*Fe(II)*	*Fe(II)-CO*	*heme function*
CooA (*R. rubrum*)	Cys(S^-)/Pro(N)	His/Pro(N)	His/CO	CO sensing
human cystathionine β-synthase	Cys(S^-)/His	Cys(S^-)/His[a]	His/CO	unknown
heme-regulated eIF2α kinase	Cys(S^-)/His	His/His	His/CO	NO sensing
nitrophorin (*C. lectularius*)	Cys(S^-)	NR[b]	Cys(SH)/CO[c]	NO storage/transport
NPAS2	Cys(S^-)/His	His/His	His/CO	CO sensing
RcoM-1,-2 (*B. xenovorans*)	Cys(S^-)/His	Met/His	His/CO	CO sensing
E75 (*D. melanogaster*)	Cys(S^-)/His	His/His	His/CO	CO & NO sensing
Rev-erbβ (*H. sapiens*)	Cys(S^-)/His	His/His	His/CO	unknown
DHR51 (*D. melanogaster*)	Cys(S^-)/His	L[d]/His	L[d]/CO	unknown
Type-3 Heme-Thiolate	*Fe(III)*	*Fe(II)*	*Fe(II)-CO*	
DGCR8	Cys(S^-)/Cys[e]	Lys[f]/L[d]	L[d]/CO	unknown

[a]Fe(II) CBS was found to retain its Fe(III) coordination only upon reduction at low temperatures [b]Not reported [c]An x-ray crystal structure of the *C. lectulatius* nitrophorin revealed a cysteine residue opposite CO. However, the CO adduct of this protein exhibits a Soret band at λ = 420 nm. Therefore, we tentatively assign coordination as a cysteine(thiol). [d]Unknown [e]Exact protonation state unknown [f]Putative

Table 1.2. MCD Soret (γ) peak-crossover-trough positions (nm) and LMCT transitions (nm) for select heme-thiolate proteins.

Type-1 Heme-Thiolate	**Peak**	**Crossover**	**Trough**	**LMCT**	**Ref**
CPO	370[a]	380[a]	395	660	(*8*)
$P450_{CAM}$ (CAM free)	406	416	425		(*35*)
(+ CAM)	378	390[a]	397	657	(*91*)
NOS (L-Arg free)	N/A[b]	N/A	395	643	(*33*)
Type-2 Heme-Thiolate	**Peak**	**Crossover**	**Trough**	**LMCT**	**Ref**
CooA	413[a]	420	427[a]		(*142*)
hCBS	419	425	433		(*72*)
Nitrophorin[c]	365[a]	380[a]	395	675[a]	(*300*)
RcoM-2	413	419	427		(*18*)
E75 (LBD)[d]	414	421	429		(*20*)
Rev-erbβ (LBD)[e]	404	412	427		(*20*)
Type-3 Heme-Thiolate	**Peak**	**Crossover**	**Trough**	**LMCT**	**Ref**
DGCR8	430	445	448	671, 694	(*294*)

[a] Not reported but determined from examination of the data [b] No peak or crossover position available [c] Data obtained for the H60C nitrophorin-1 variant [d] 262 amino acid construct of the E75 ligand-binding domain (LBD) studied by Marvin *et al*. [e] 256 amino acid ligand-binding domain of Rev-erbβ studied by Marvin *et al*.

Table 1.3. Resonance Raman ν(Fe-S) vibrational frequencies of various Cys(thiolate)-ligated Fe(III) heme proteins.

	Fe(III) Protein	ν(Fe-S) (cm^{-1})	Ref
Type-1 Coordination	$P450_{CAM}$	351	(*56, 57*)
	H25C Heme Oxygenase[a]	348	(*58*)
	CPO	347	(*59*)
	Irr[a]	333	(*60*)
	iNOS	338	(*61*)
Type-2 Coordination	hCBS	312	(*62*)
	RcoM-2[b]	310	(*18*)
	E75 (LBD)[b,c]	312	(*20*)
	Rev-erbβ (LBD)[b,d]	312	(*20*)
	R266K hCBS	307	(*73*)

[a] Ligation motif similar to that of type-1 heme thiolates [b] Putative [c] 262 amino acid construct of the E75 ligand-binding domain (LBD) studied by Marvin *et al*. [d] 256 amino acid ligand-binding domain of Rev-erbβ studied by Marvin *et al*.

Table 1.4. X-band EPR *g* values of the Fe(III) heme-thiolate proteins.

Type-1 Heme-Thiolate	g_z	g_y	g_x	**Ref**
CPO	2.54	2.28	1.85	(*297*)
$P450_{CAM}$	2.44	2.25	1.91	(*187*)
NOR	2.44	2.26	1.91	(*9*)
	[a][7.97	4.12	1.75]	(*9*)
NOS	7.64	4.3[b]	4.04	(*301*)
	[2.43	2.28	1.89]	(*301*)
Type-2 Heme-Thiolate	g_z	g_y	g_x	**Ref**
CooA	2.46	2.25	1.89	(*12*)
	[2.58	2.25	1.84]	(*12*)
hCBS	2.49	2.31	1.87	(*72*)
	[2.43	2.31	1.90]	(*72*)
HRI	2.49	2.28	1.87	(*15*)
Nitrophorin	7.25	4.75	1.90	(*17*)
	[2.37	2.25	1.94]	(*17*)
NPAS2	2.44	2.27	1.90	(*302*)
RcoM-2	2.52	2.28	1.88	(*18*)
E75(LBD)[c]	[d]2.46	2.26	1.90	(*20*)
	[d]2.56	2.26	1.88	(*20*)
E75(261)[e]	2.54	2.26	1.87	(*19*)
	2.45	2.27	1.90	(*19*)
	2.39	2.26	1.92	(*19*)
Rev-erbβ(LBD)[f]	2.50	2.29	1.99	(*20*)
	2.35	2.29	2.03	(*20*)
	2.60	2.29	1.88	(*20*)
DHR51	2.41	2.27	1.91	(*19*)
Type-3 Heme-Thiolate	g_z	g_y	g_x	**Ref**
DGCR8	2.60	2.27	1.84	(*294*)

[a] Brackets indicate the visual presence of a minor signal, although in most cases quantification is absent [b] Only two digits were given [c] 262 amino acid construct of the E75 ligand-binding domain (LBD) studied by Marvin *et al*. [d] The presence of multiple *g* values without brackets indicates multiple signals of nearly equivalent intensity [e] 261 amino acid construct of the E75 LBD studied by de Rosny *et al*. [f] 256 amino acid ligand-binding domain of Rev-erbβ studied by Marvin *et al*.

Figure 1.1. A) Iron protoporphyrin IX (heme *b*) consists of one iron atom coordinated by the tetradentate protoporhyrin IX dianion. B) Two additional ligands may coordinate the heme iron, at positions above (X) and below (Y) the plane of the porphryin macrocycle (represented as a paralellogram with nitrogen atoms at the corners).

A)

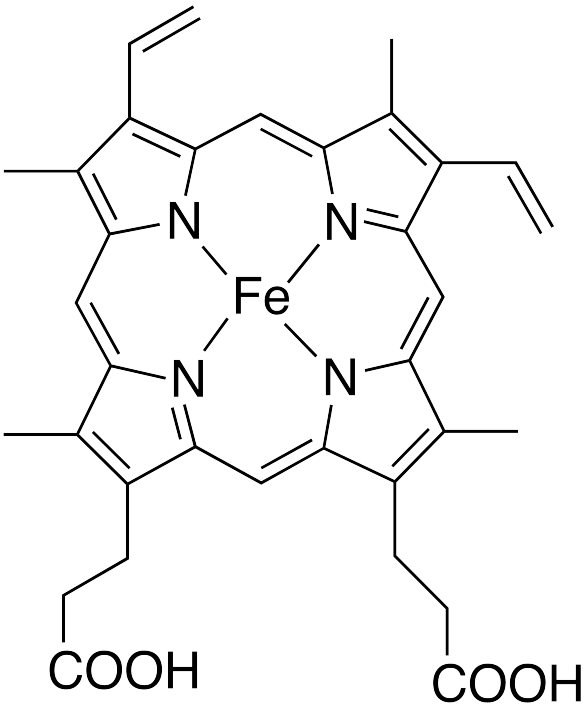

B)

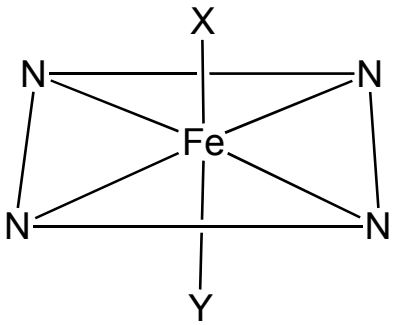

Figure 1.2. Substrate-, redox-, and effector-dependent coordination changes in the type-1 and type-2 heme-thiolates. A) In the resting state of the type-1 heme-thiolates, the Fe(III) heme is ligated by a cysteine(thiolate) ligand and (commonly) a water ligand. The cysteine(thiolate) ligand is retained during substrate (sub) binding and heme iron reduction; during any gas-binding event, the gas molecule (CO in this example) binds *trans* to the cysteine(thiolate) ligand. B) In the resting state of the type-2 heme-thiolates, the Fe(III) heme is ligated by a cysteine(thiolate) ligand and another neutral donor ligand (L), commonly a His residue. Heme reduction is accompanied by a ligand-switching event in which the cysteine(thiolate) is replaced by another neutral donor (L'); during any gas-binding event, the gas molecule (CO in this example) binds *trans* to a neutral donor ligand that is *not* the cysteine(thiolate) ligand.

A) Type-1 Heme-Thiolate

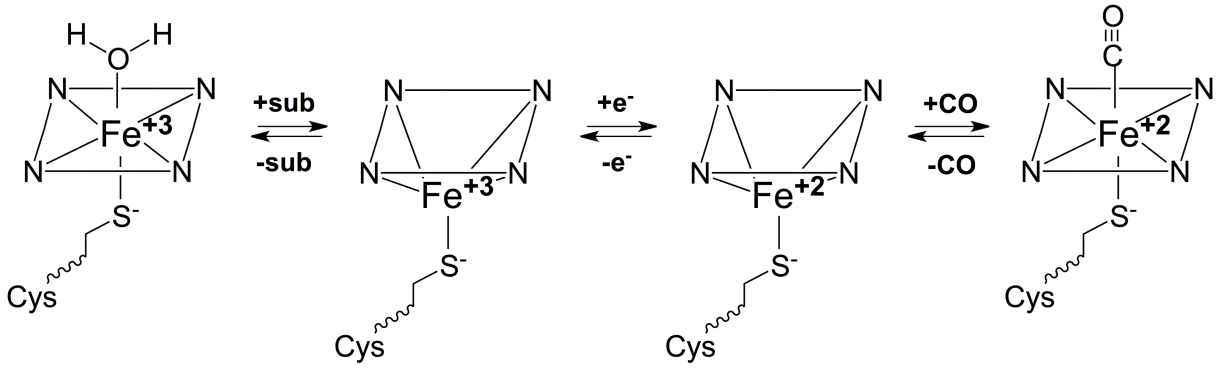

B) Type-2 Heme-Thiolate

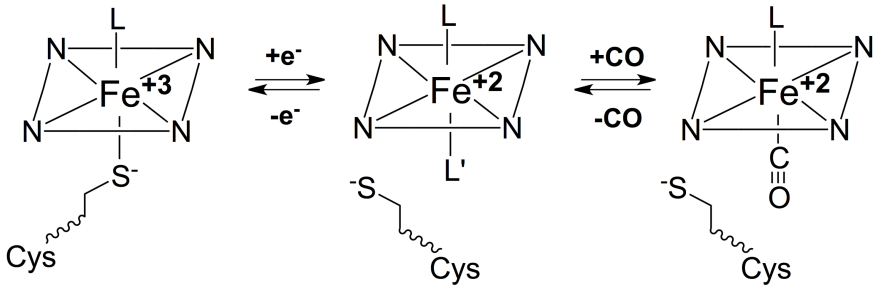

Figure 1.3. Electronic absorption spectrum of Fe(III) *Bx*RcoM-2, a typical type-2 heme-thiolate. Fe(III) RcoM-2 displays a well-resolved δ band (354 nm), a sharp Soret (γ) band (423 nm), a broad α-β absorption envelope (500-600 nm), and two low-energy visible LMCT transitions (640 nm, 730 nm). Figure taken from (*18*).

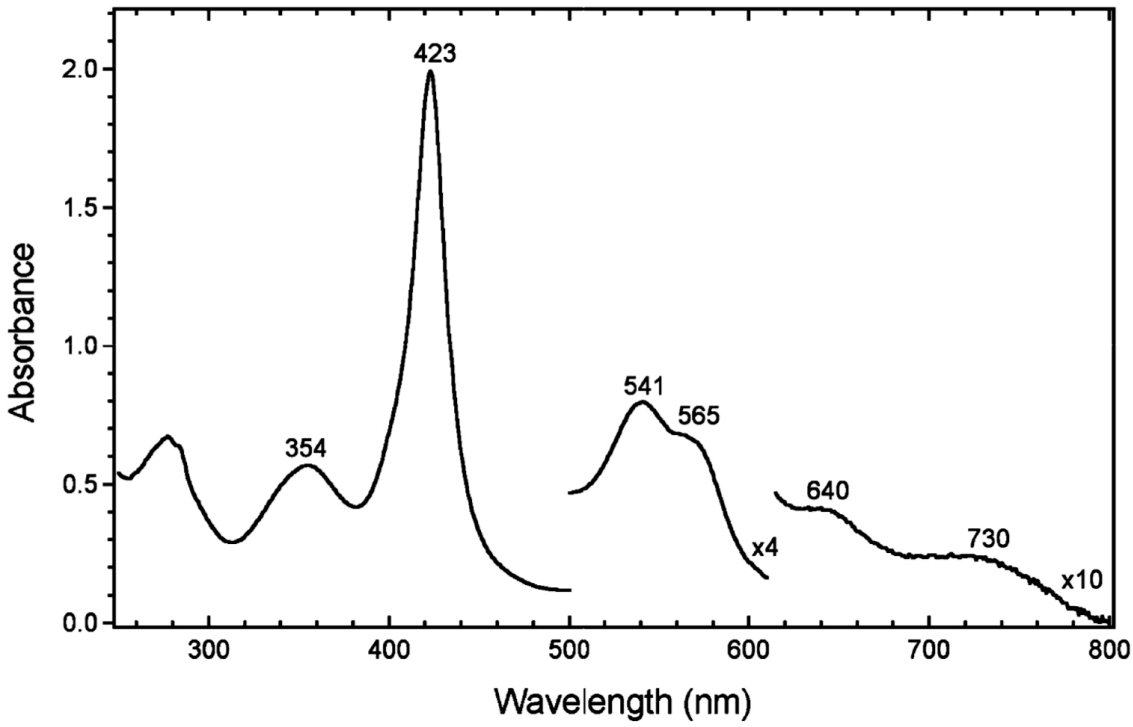

Figure 1.4. Prototypical MCD spectra of type-1 and type-2 heme-thiolates. Left panel: MCD spectral overlays of high-spin Fe(III) cytochrome P450 in the presence of DL-camphor (solid) and chloroperoxidase (dotted), both type-1 heme-thiolates. Figure taken from (*141*). Right panel: MCD spectral overlays of Fe(III) CBS (formerly protein H-450) (solid), imidazole-bound $P450_{CAM}$ (dotted, top), and dimethylsulfide-bound $P450_{CAM}$ (dotted, bottom), all bearing type-2 heme-thiolate coordination. Figure taken from (*303*)

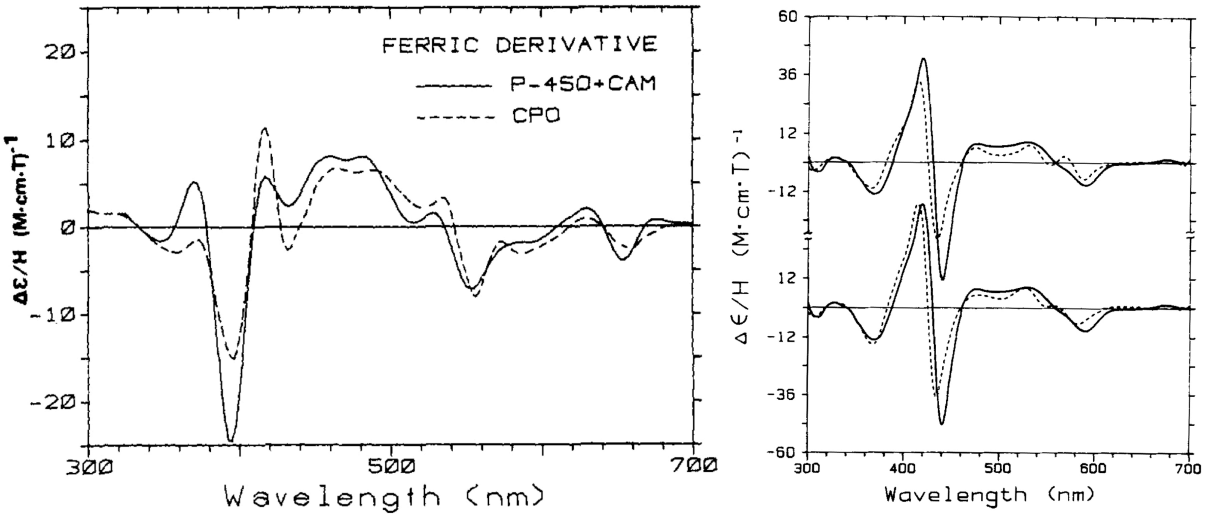

Figure 1.5. Variable-temperature MCD spectra of Fe(III) *Rr*CooA. The presence of the porphyrin(π) → Fe(III) LMCT transition at 1120 nm (E_{CT} 8930 cm^{-1}) is strongly indicative of a low-spin Fe(III) heme center with Cys(thiolate) ligation. Figure taken from (*142*).

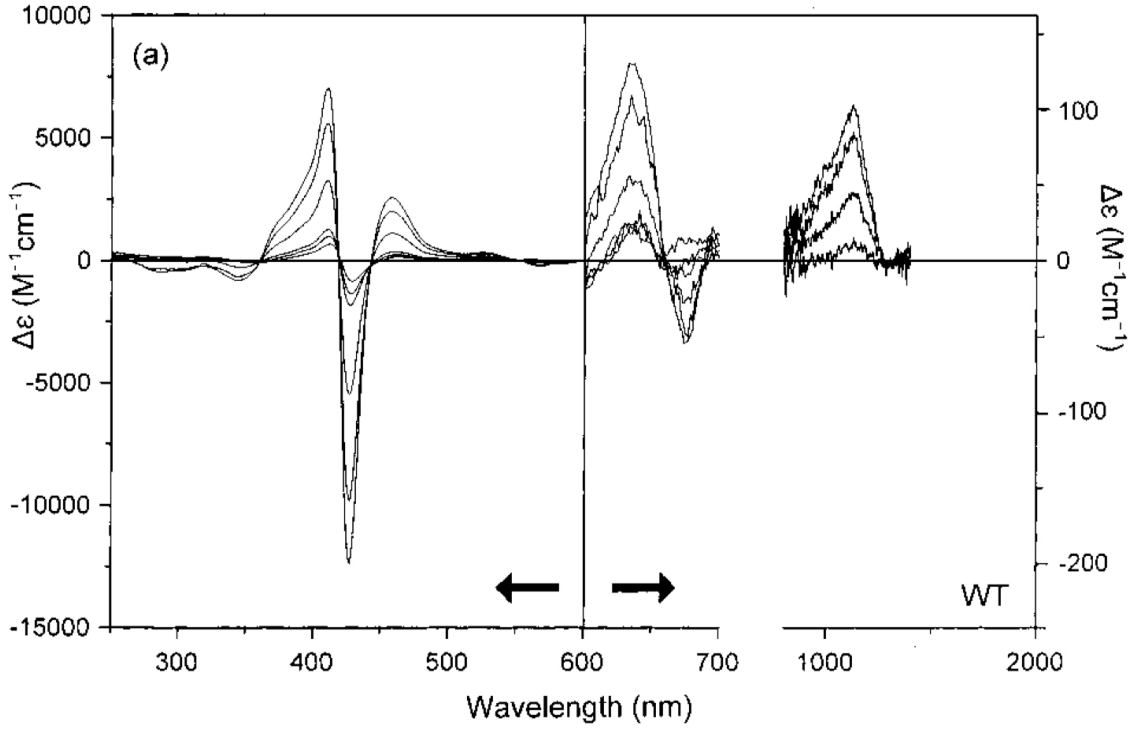

Figure 1.6. Blumberg-Peisach correlation diagram for low-spin heme centers. The regions C, B, H, O, and P are designated for His/Met, His/His(N^-), His/His, His/OH^-, and Cys(S^-)/X heme coordinations, respectively. The abscissa measures the strength of the axial field in units of the spin-orbit coupling constant λ, while the ordinate measures the ratio of the rhombic and axial crystal field parameters.

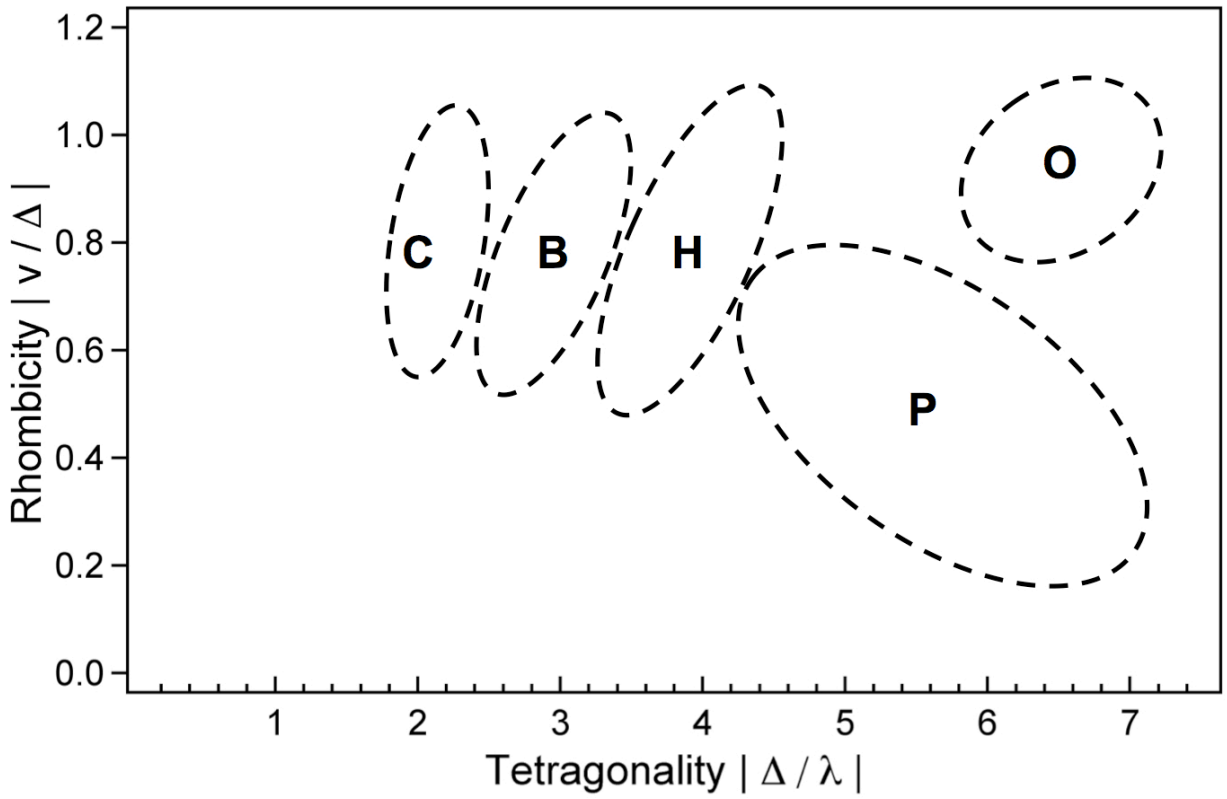

Figure 1.7. Depiction of the effect of large zero-field splitting (D>>hν) on the spin microstates of a high-spin, Fe(III) ($S=^5/_2$) heme system. Only the transitions between $m_s \pm ½$ states are of the appropriate energy to be accessed by a conventional X-band EPR spectrometer ($E_{Zeeman} \sim 0.3\ cm^{-1}$).

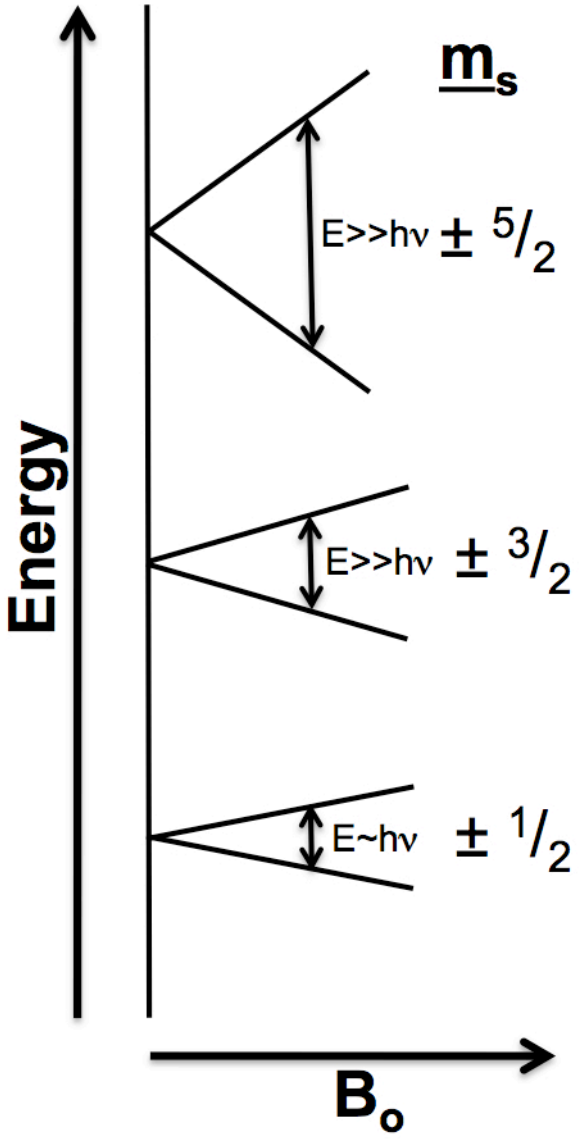

Figure 1.8. Thermally induced ligand switching occurs at the Fe(II) heme in CBS. Upon reduction of the heme in CBS, the Cys(thiolate) ligand is retained, as evidenced by the red-shifted Soret band at 450 nm (solid line). Upon heat treatment, a ligand-switching event occurs in which the Fe(II) Cys(thiolate) ligand is replaced by an unknown neutral donor ligand; the final species has a Soret band at 424 nm (dashed line). Figure taken from (*138*).

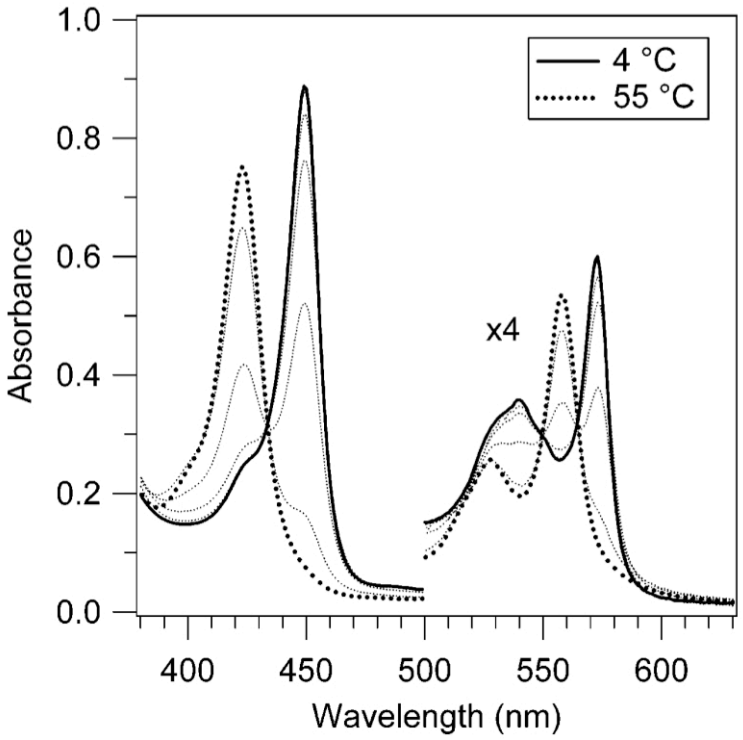

Figure 1.9. Electronic absorption and MCD spectra of Fe(II) *Bx*RcoM-2. RcoM-2 exhibits prototypical behavior of a type-2 heme-thiolate in which Cys(thiolate) ligation is lost upon heme reduction; the Cys(thiolate) ligand is replaced by another neutral donor (Met^{104}), maintaining a six-coordinate, low-spin heme iron center. Figure adapted from (*18*).

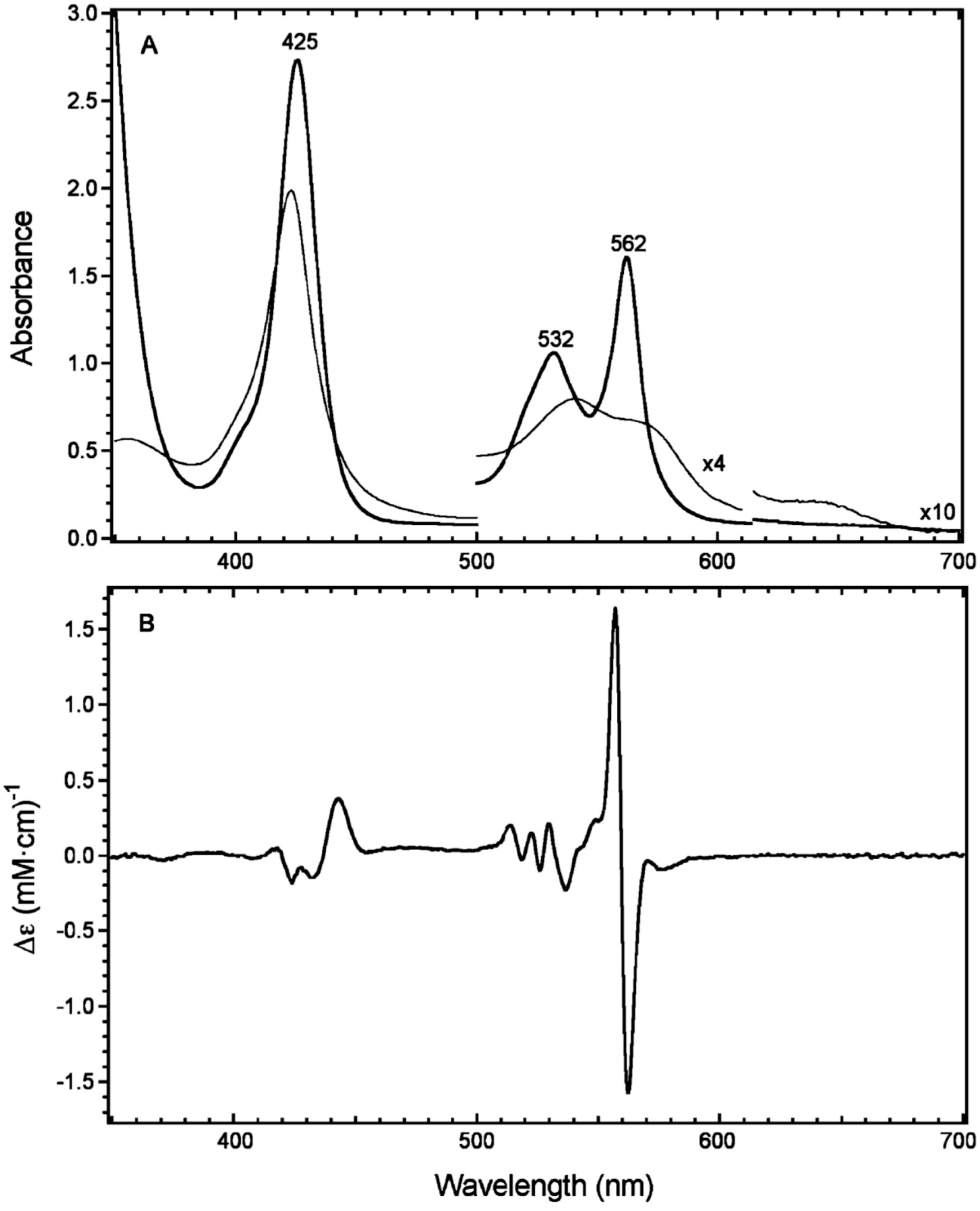

Figure 1.10. MCD spectra of five-coordinate Fe(II) high-spin thiolate-ligated heme complexes. Fe(II) P450-LM2 (top, solid), Fe(II) protoheme-thiolate model complex in dimethylacetamide (top, dotted), and Fe(II) CPO (bottom, solid) all display similar MCD spectra. Figure taken from (*141*).

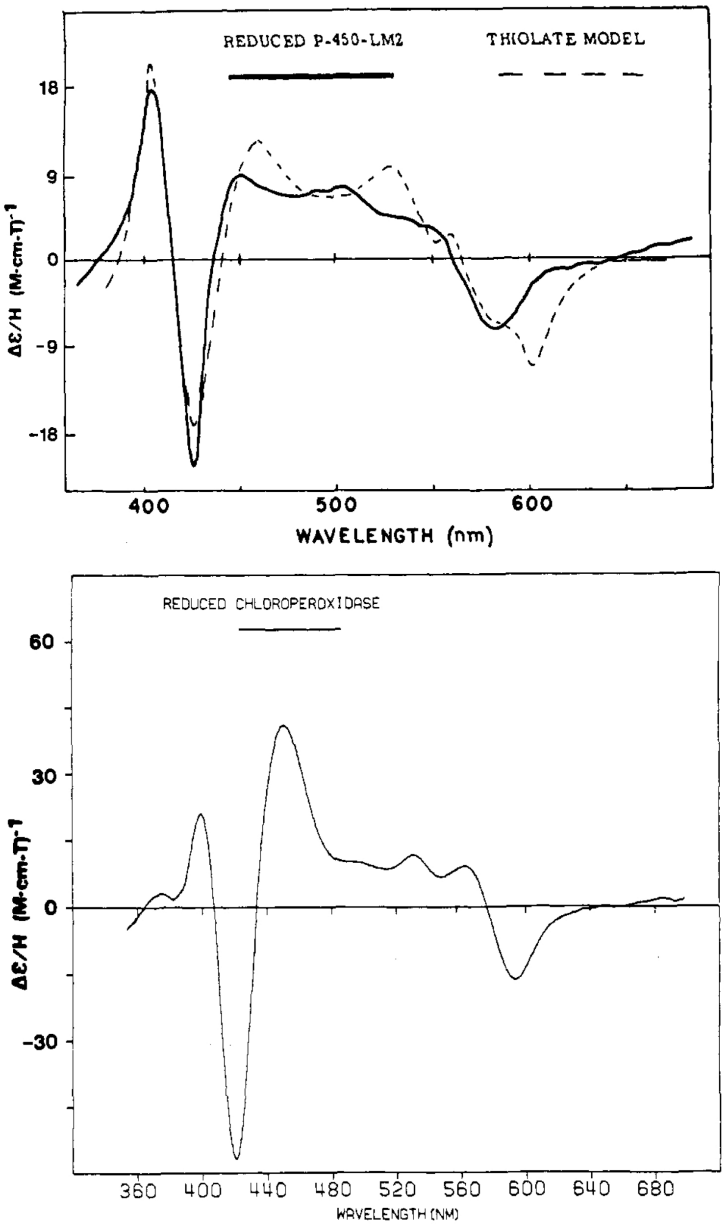

Figure 1.11. Fe(IV), or "ferryl" species attained in the catalytic cycles of the type-1 heme-thiolates. A) The oxy-ferryl porphyrin π-cation radical complex known as Compound I. B) The oxy-ferryl complex known as Compound II, which is one electron reduced from Compound I.

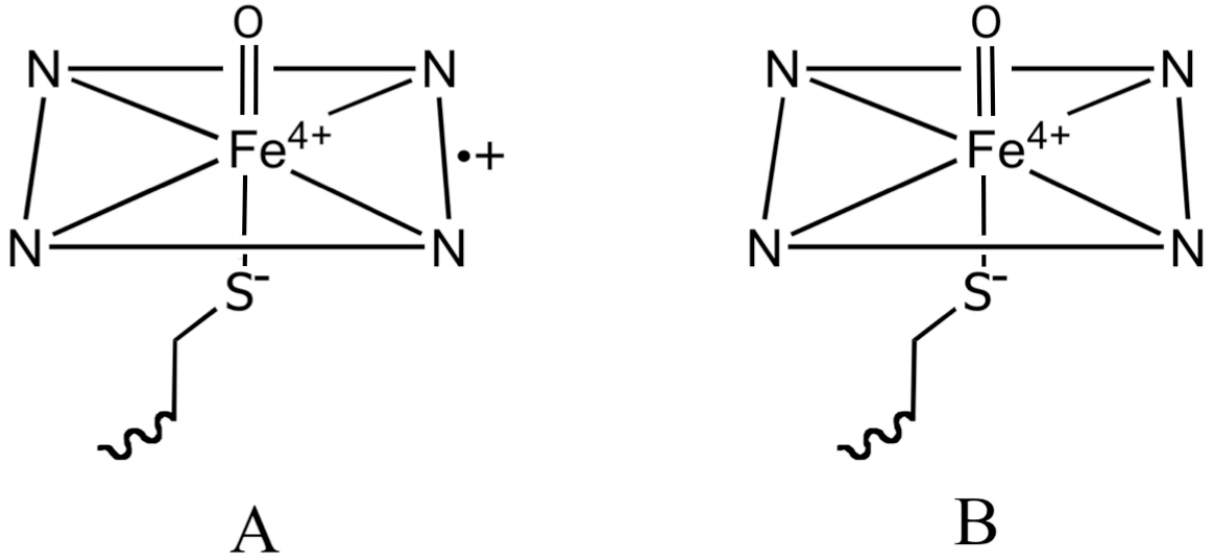

Figure 1.12. Electronic absorption spectrum of *Sulfolobus acidocaladarius* cytochrome P450 (CYP119) Compound 1 (dashed) generated by mixing equal molar amounts Fe(III) CYP119 and *m*-chloroperbenzoic acid (*m*-CPBA). Figure taken from (*133*).

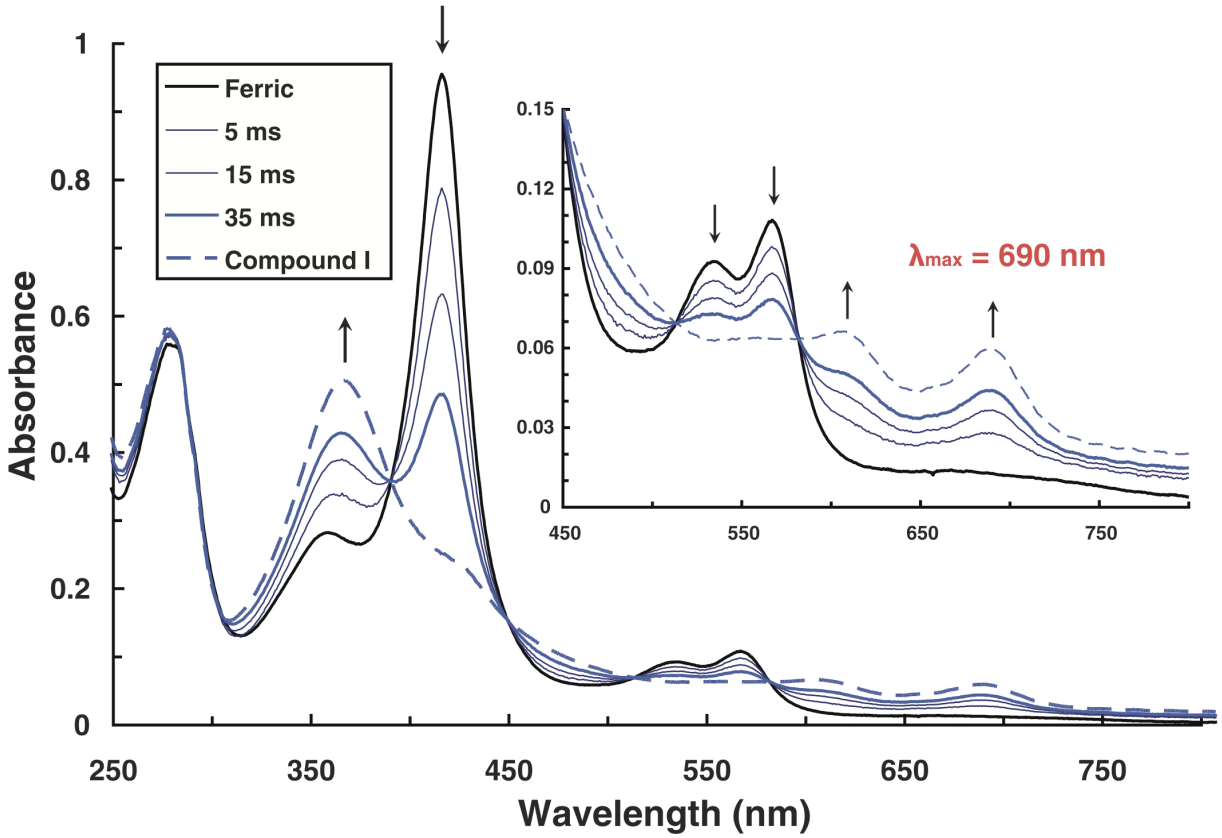

Figure 1.13. Back-bonding correlation diagram for Fe(II)-CO adducts derived from type-1 and type-2 heme-thiolates. CO adducts of type-1 heme-thiolates, which retain the cysteine(thiolate) ligand, obey the ν_{C-O}/ν_{Fe-CO} correlation indicated by the dashed (- - - - -) line. CO adducts of type-2 thiolates, in which CO is bound opposite a neutral donor, obey the ν_{C-O}/ν_{Fe-CO} correlation indicated by the solid (———) line. Figure adapted from (*15*).

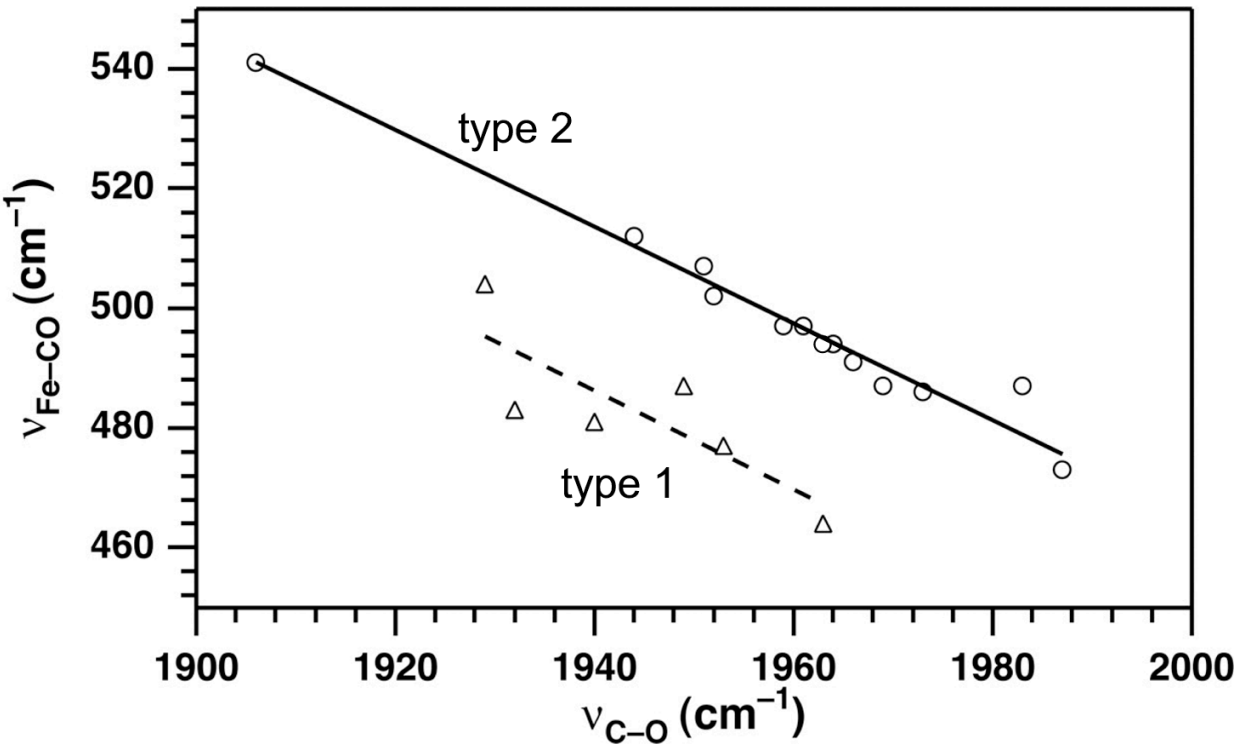

Figure 1.14. Characteristic X-band EPR spectra of several ferrous nitrosyl adducts. The EPR spectrum of the ferrous ^{14}NO adduct of horseradish peroxidase (left panel, top) displays a characteristic 9-line g_2 splitting pattern indicative of a His ligand bound trans to the NO molecule, whereas the EPR spectrum of the ferrous ^{14}NO chloroperoxidase (left panel, bottom) displays only a 3-line g_2 splitting pattern, consistent with retention of the Cys(thiolate) ligand at the ferrous heme of chloroperoxidase. Figure taken from (*304*). The EPR spectrum of the ferrous ^{14}NO adduct of *Rr*CooA (right panel, top) displays a characteristic 3-line g_3 splitting pattern that collapses to a 2-line splitting pattern upon ^{15}NO substitution (right panel, bottom), indicative of a ferrous five-coordinate nitrosyl adduct without endogenous ligation. Figure taken from (*216*).

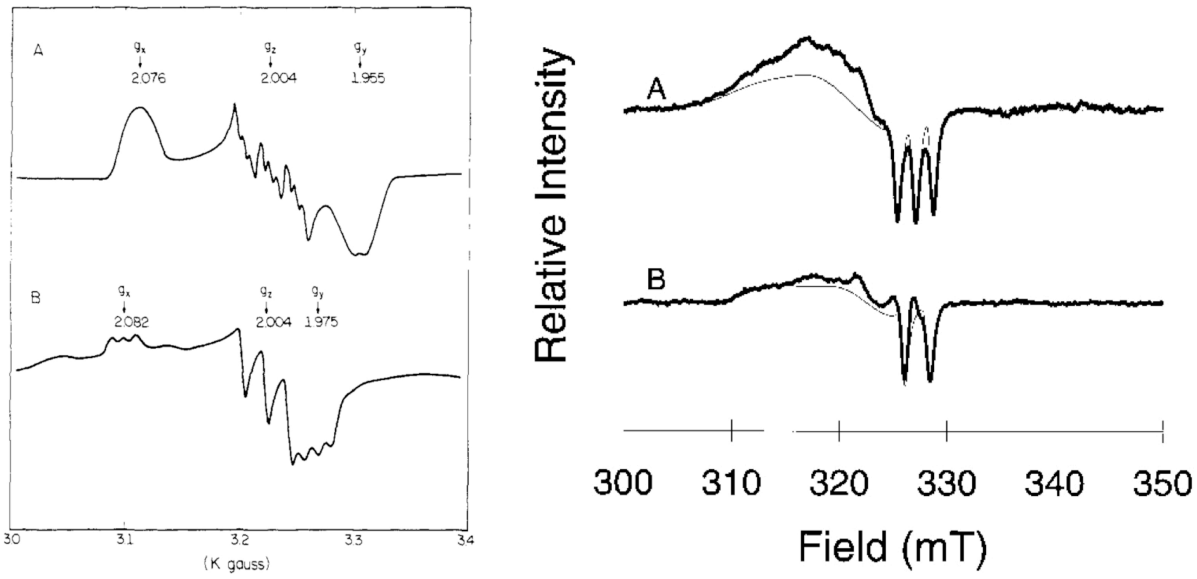

Figure 1.15. Catalytic cycles of the P450 cytochromes. Proposed structures of putative intermediates, including Compound I, are indicated in brackets. The substrate is represented by RH and the product is represented by R(O)H. Figure adapted from (*141*).

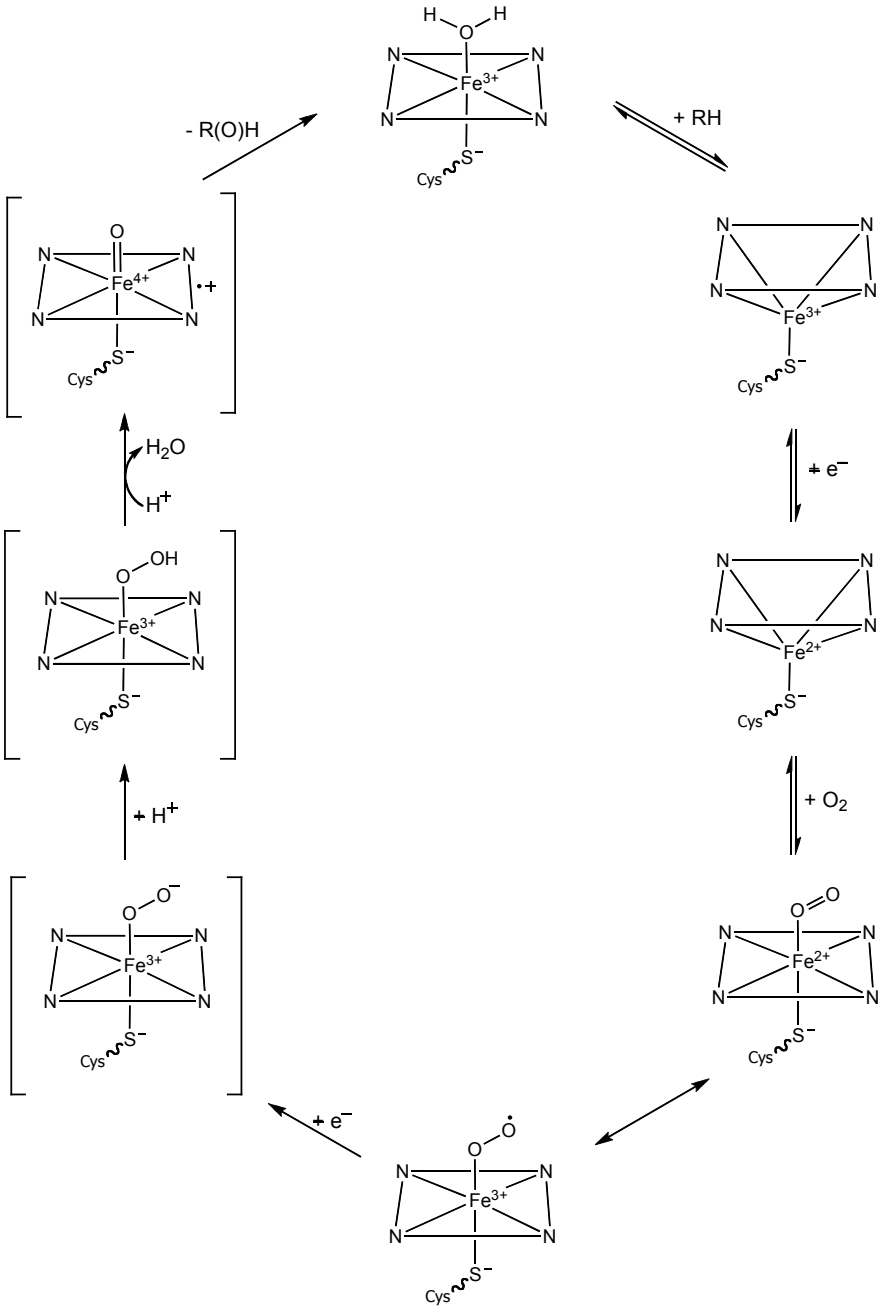

Figure 1.16. The catalytic cycles of chloroperoxidase and the postulated structures of intermediates. Reaction of the high-spin resting form of CPO (blue) with H_2O_2 generates the highly reactive Compound I (green). From CPO-I, the peroxidase function (top) converts two molecules of substrate (AH) to radical products; halogenation (bottom) is performed; or the catalase function (middle) catalyzes the disproportionation of H_2O_2. Figure adapted from (*141*).

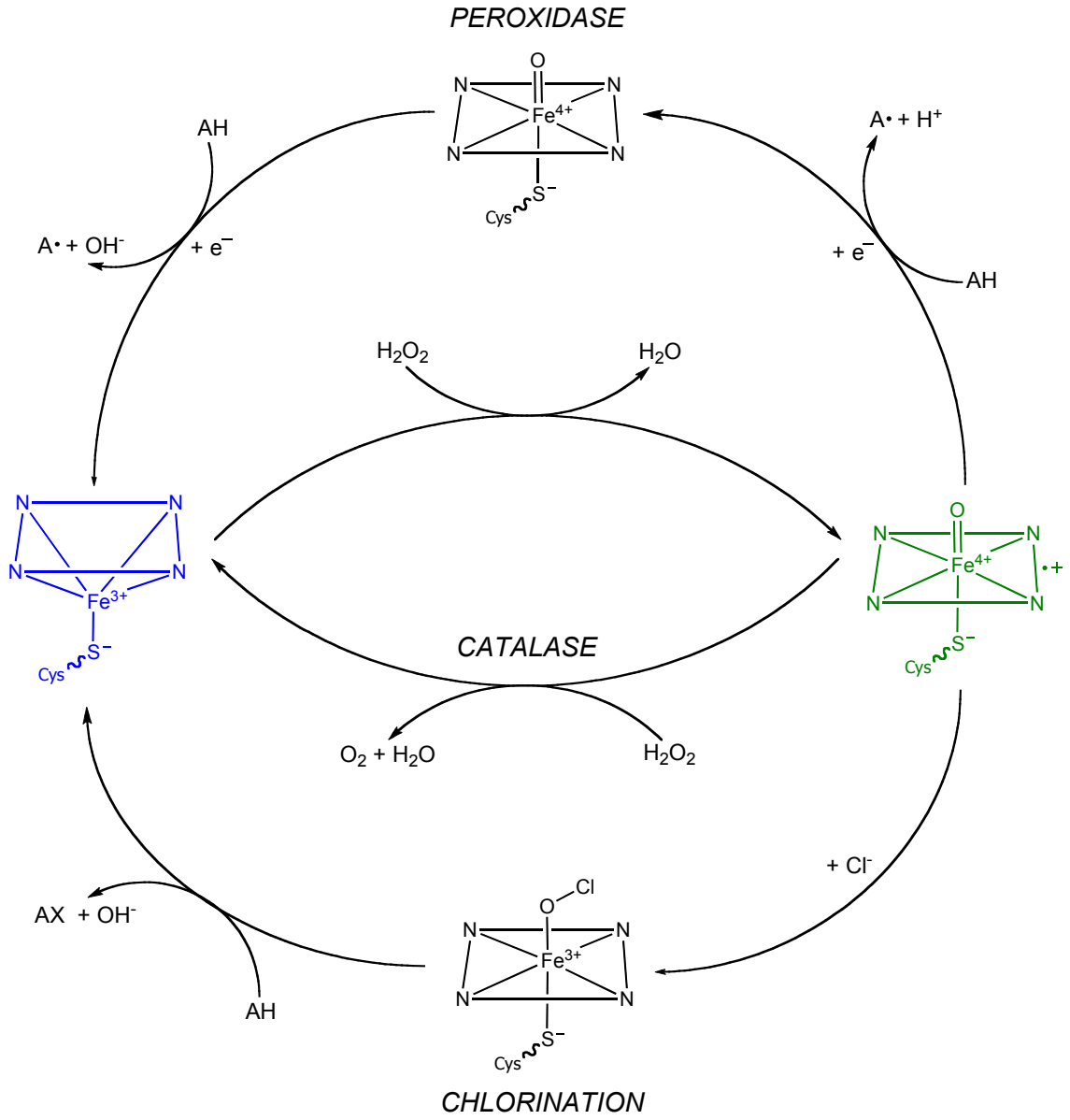

Figure 1.17. The two-step reaction catalyzed by the nitric oxide synthases. In the first step, L-arginine is hydroxylated to form N^{ω}-hydroxy-L-arginine (NOHA), utilizing one molecule of O_2 and two electrons from NADPH. In the second step, NOHA is converted to L-citrulline and nitric oxide, using another molecule of O_2 and one electron from NADPH.

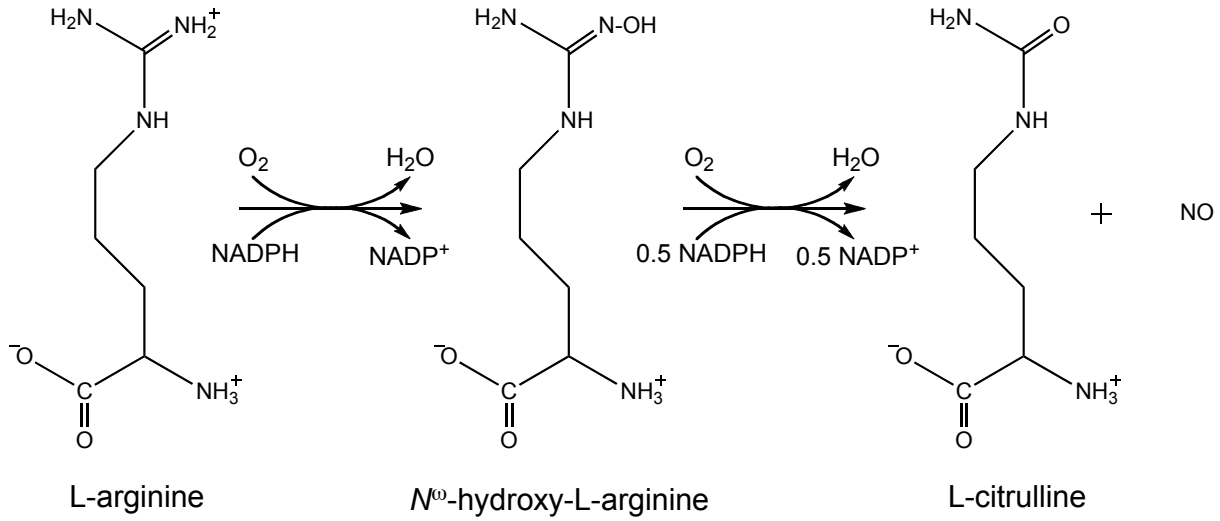

Figure 1.18. Proposed reaction mechanism for the catalytic cycle of the reduction of NO by the fungal NORs. The resonance structures describe the delocalization of electron density over the Fe—N—O unit and thus more realistic electron configurations for the Fe(III)-NO complex and the Intermediate *I*. Figure adapted from (*9*).

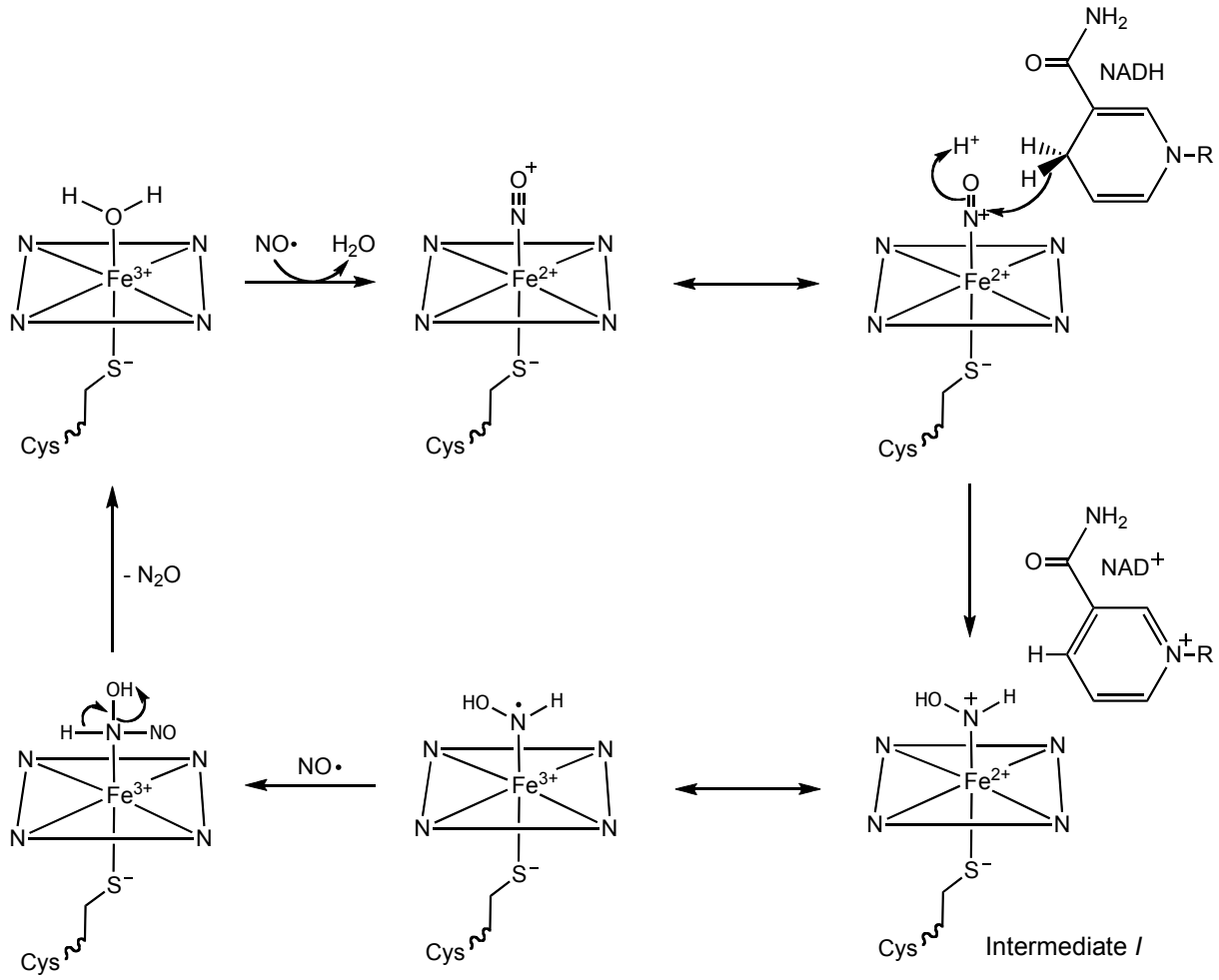

Figure 1.19. Proposed structures of Compounds I and II based on EXAFS and DFT calculations that predict bond lengths and a protonated rebound intermediate (Compound II). Figure taken from (*125*).

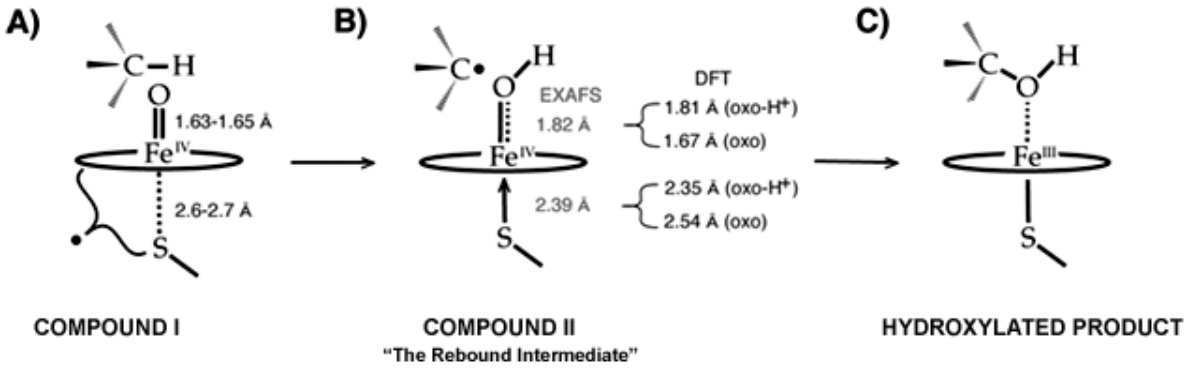

Figure 1.20. The heme coordination states of Fe(III), Fe(II), and Fe(II)CO *Rr*CooA. The cysteine(thiolate) ligand is replaced by a histidine upon reduction of the Fe(III) heme-thiolate. CO binding then replaces the distal proline ligand to yield the type-2 CO adduct. Similar behavior is hypothesized for the other type-2 heme-thiolates such as hCBS, eIF2α kinase, NPAS2, the *Bx*RcoMs and *Drosophila* E75.

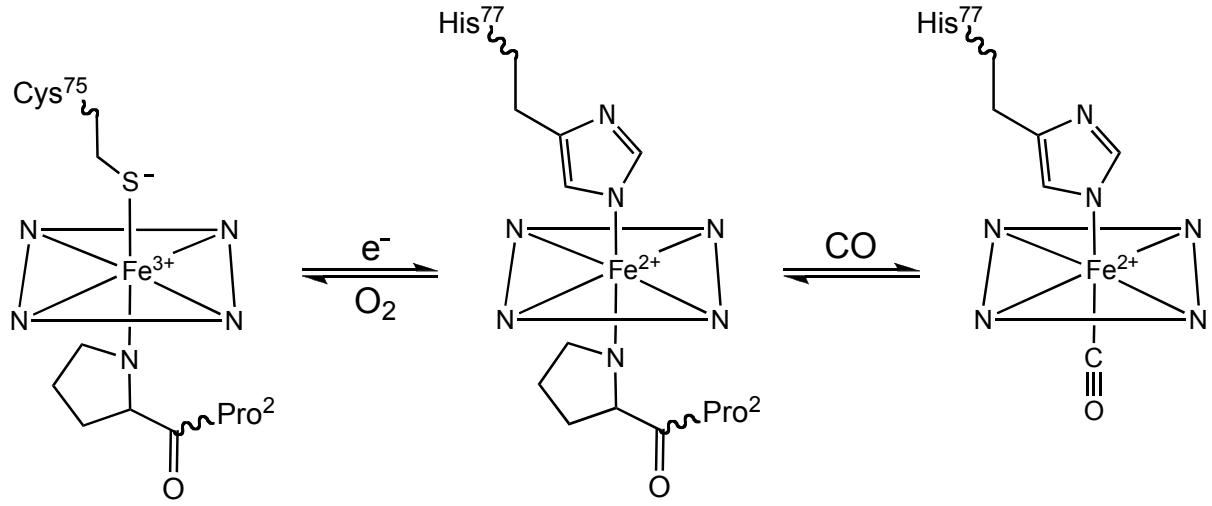

Figure 1.21. Representation of the putative conformational changes induced by reduction and CO binding in *Rr*CooA, which activates the protein for DNA binding. The inactive, "resting state" Fe(III)CooA structure is unknown. The inactive, "ready off" Fe(II)CooA structure (left) was modeled from PDB file 1FT9. The active, "Fe(II)CO CooA" structure is represented by cAMP-bound CRP (right), a close relative of CooA, and was modeled from PDB file 1I5Z.

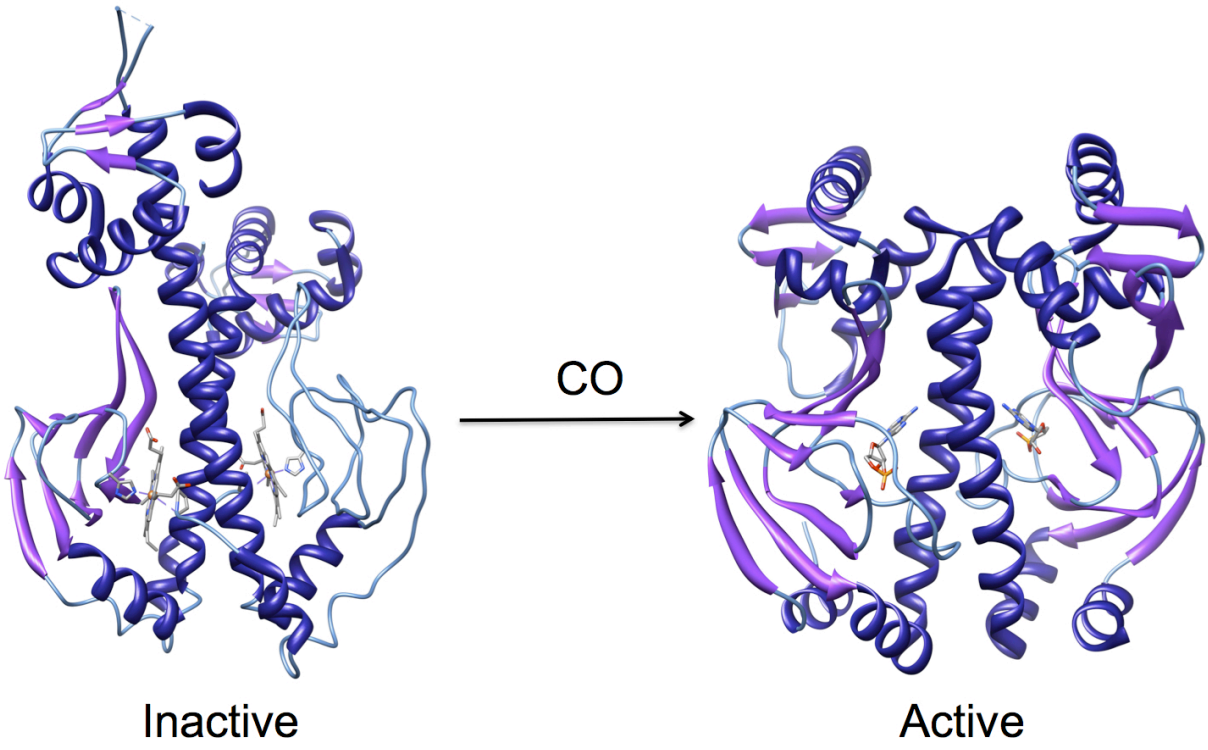

Figure 1.22. Proposed coordination states of Fe(III), Fe(II), and Fe(II)CO *Bx*RcoM-2. The cysteine(thiolate) ligand is replaced by a methionine upon reduction of the Fe(III) heme-thiolate. CO binding then replaces the proximal methionine ligand to yield the type-2 CO adduct. Figure taken from (*228*).

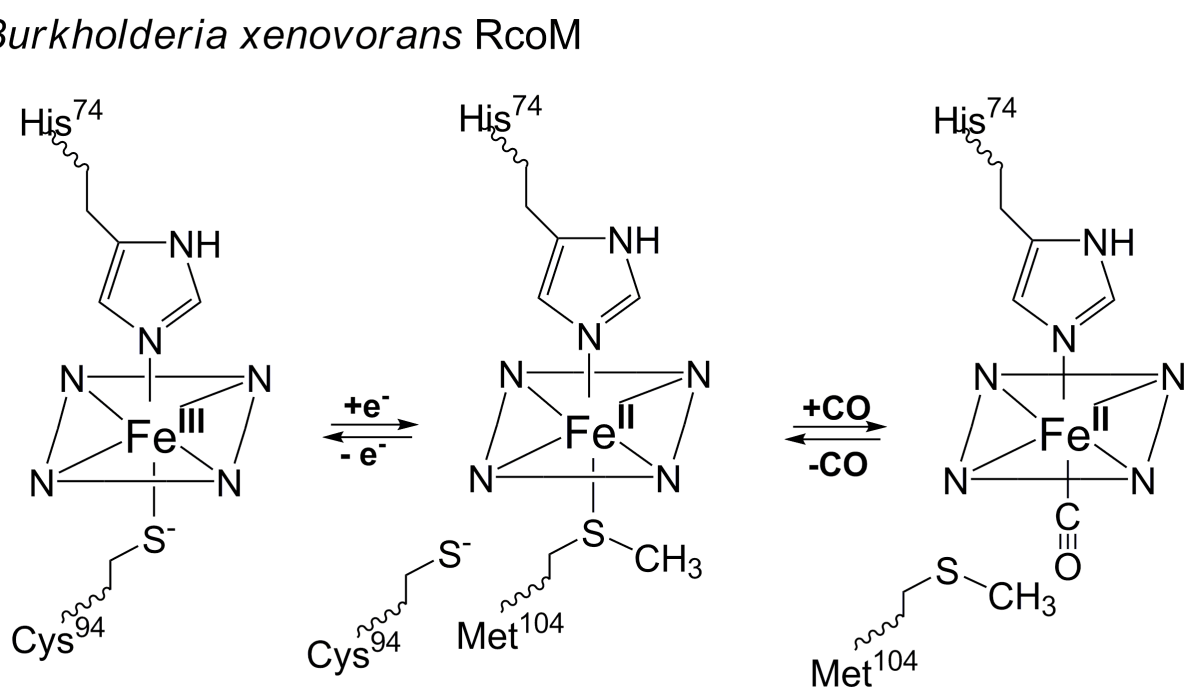

Figure 1.23. Location of key residues that interact with the heme and PLP in hCBS. Highlighted are: the Fe(III) heme ligands Cys^{52} and His^{65}; the cysteine(thiolate) hydrogen bonding partners Arg^{266} and the amide backbone of Trp^{54}; the PLP phosphate hydrogen bonding partners Thr^{257} and Thr^{260}; and Lys^{119} that forms the PLP internal aldimine. Structure modeled from PDB file 1JBQ. Figure taken from (*73*).

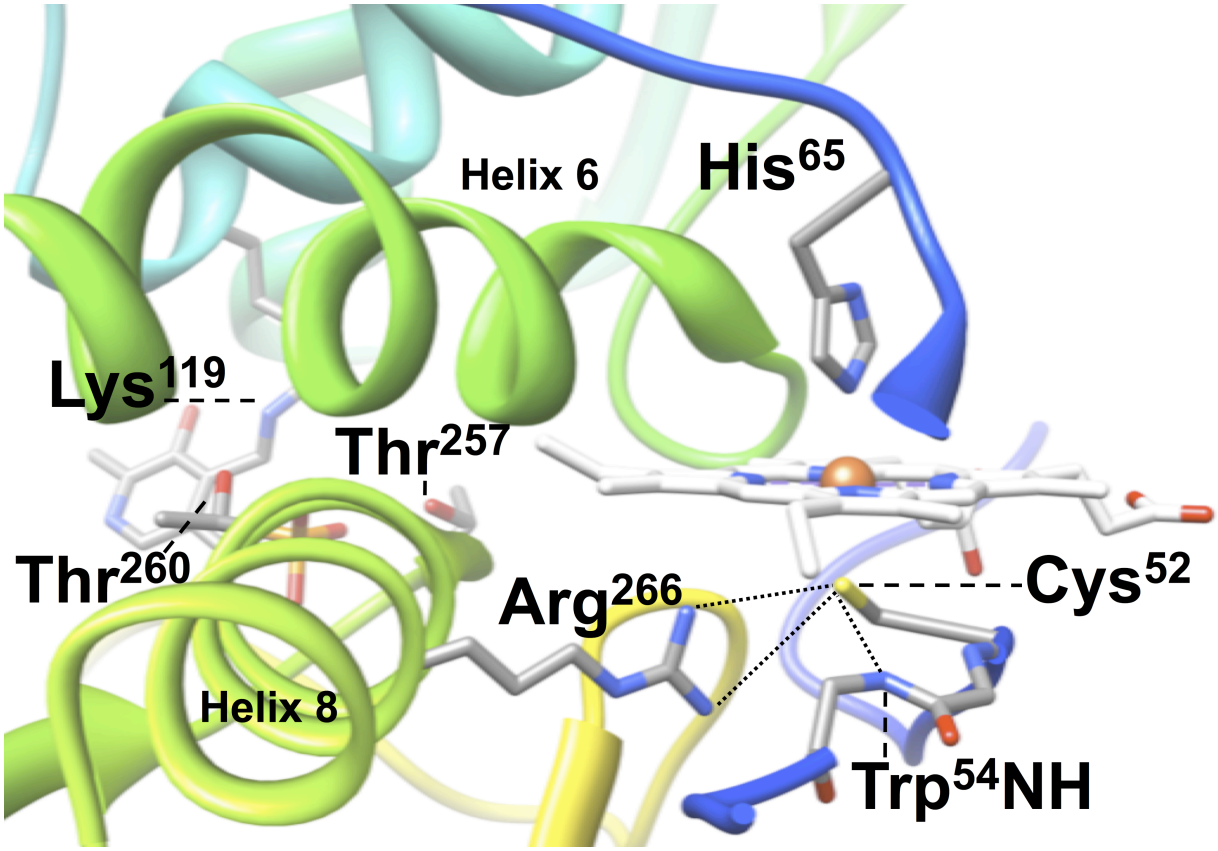

Figure 1.24. Electronic absorption spectrum of Fe(III) DGCR8. The Fe(III) heme in DGCR8, which is ligated by a unique bis(Cys) ligation motif, displays a highly-split hyperporphyrin spectrum. Figure adapted from (*294*).

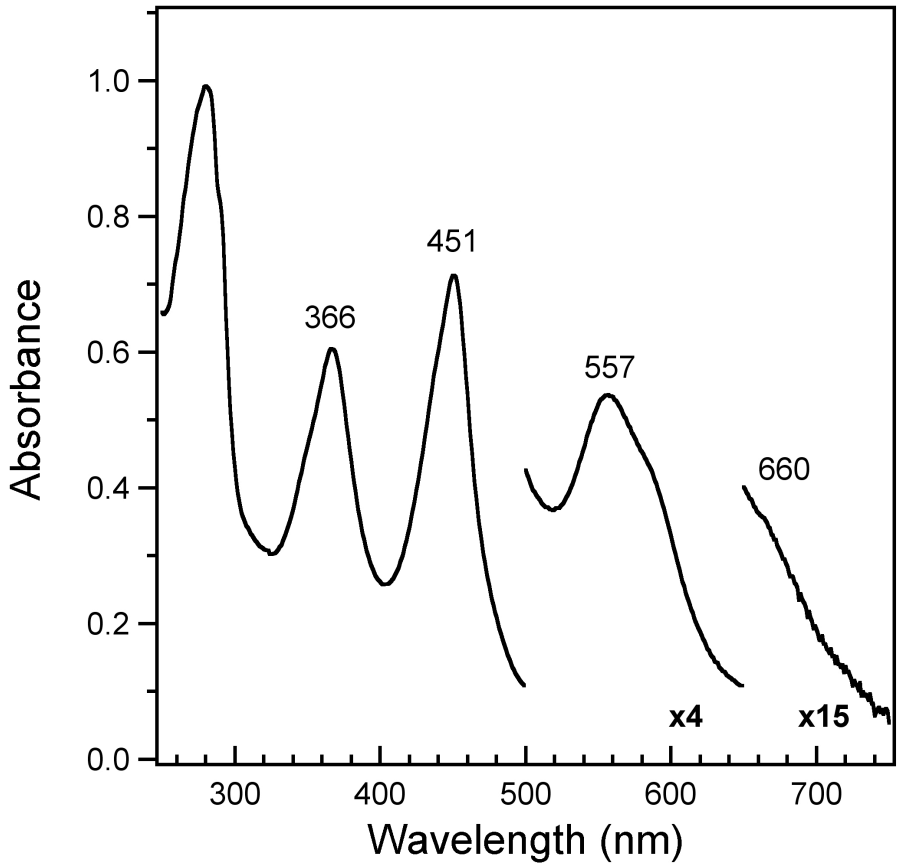

Chapter Two

Identification of Cys^{94} as the distal ligand to the Fe(III) heme in the transcriptional regulator RcoM-2 from *Burkholderia xenovorans*

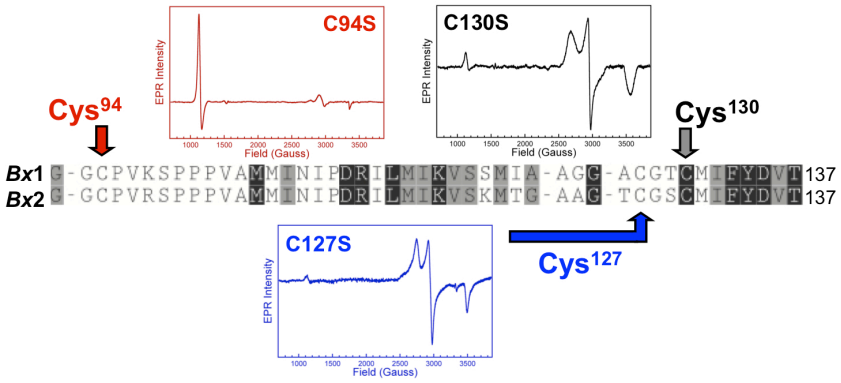

A version of this chapter has been submitted as:

Smith, A. T.; Marvin, K. A.; Freeman, K. M.; Kerby, R. L.; Roberts, G. P.; Burstyn, J. N. *J. Biol. Inorg. Chem*. **2012**.

All mutagenic work was performed by Dr. Robert L. Kerby in the laboratory of Professor Gary P. Roberts at the University of Wisconsin—Madison. RcoM-2 expression and purification was performed by Dr. Robert L. Kerby and Katherine M. Freeman.

Introduction

Small, gaseous diatomic molecules, such as O_2, NO and CO, are important signaling agents in biological systems; one method nature has employed to sense these gaseous signaling agents is the interaction of the diatomic molecule with the heme cofactor (*1-6*). Dioxygen binding to heme in Mb and Hb is a well-known paradigm. Examples of heme-based O_2 sensor proteins, in which the dioxygen-binding heme domain regulates function, include *Rhizobium meliloti* FixL (*7*), *Bacillus subtilis* HemAT (*8*) and *Escherichia coli* DOS (*9*). NO is produced endogenously by nitric oxide synthase; at physiological levels, NO plays a role in both neurotransmission as well as vascular regulation (*10*). Examples of heme-containing NO sensors include the bacterial H-NOX proteins (*11*), mammalian sGC (*12*), heme-regulated eIF2α kinase (*13*), and the putative NO-sensors *Drosophila melanogaster* DHR51 (*14*), *D. melanogaster* E75 (*15*), and *Pseudomonas aeruginosa* DNR (*16*). CO is also believed to function as a neurotransmitter in mammals, where it is endogenously produced by heme oxygenase (*17*). Examples of CO sensors include mammalian NPAS2 (*18*) and bacterial *Rhodospirillum rubrum* CooA (*19, 20*) as well as the putative CO sensors *D. melanogaster* E75 (*15*) and *D. melanogaster* DHR51 (*14*).

CooA is the first-known and best-characterized CO gas sensor (*21*). CooA functions as a transcriptional activator that enables the freshwater bacterium *R. rubrum* to grow anaerobically using CO as an energy source (*22*). The homodimeric protein binds a heme *b* cofactor within each monomer (*20*). The Fe(III) heme in *Rr*CooA is low-spin and six-coordinate; the axial ligands to the Fe(III) heme are a cysteine(thiolate) (Cys^{75}) and the N-terminal proline (Pro^{2}) from the other monomer of the dimer (*23-25*). When Fe(III) is reduced to Fe(II), Cys^{75} is replaced by the neighboring His^{77} while the N-terminal proline is retained

(*25, 26*). The more weakly bound Pro ligand is replaced by CO, and CO binding is proposed to initiate global protein conformational changes that are propagated along the leucine zipper motif at the dimer interface, ultimately resulting in DNA binding (*24, 27-30*). Thus, CooA presents a paradigm in which redox-mediated ligand switching and CO binding at the heme iron center are utilized to trigger DNA binding.

Recently, a new prokaryotic transcriptional regulator of CO metabolism (RcoM) was isolated from the aerobic, polychlorinated biphenyl (PCB)-degrading bacterium *Burkholderia xenovorans* (LB400) (*31, 32*). Two homologous proteins, *Bx*RcoM-1 and *Bx*RcoM-2, were identified in this bacterium and share 93% sequence similarity. These proteins contain a N-terminal PAS domain and a C-terminal LytTR domain. PAS domains frequently function as sensors of environmental signals through the binding of small molecules and may bind various cofactors (*33*). LytTR domains are DNA-binding domains that commonly function within transcriptional regulators and may be found in conjunction with PAS sensor domains (*34*). In *Bx*RcoM-1 and *Bx*RcoM-2, the N-terminal PAS domain binds a *b*-type heme cofactor that controls CO-dependent DNA binding (Kerby *et al*, unpublished).

Studies of *Bx*RcoM-1 and *Bx*RcoM-2 revealed the ligation and oxidation state changes that occur at the RcoM heme. The *Bx*RcoM-1 and *Bx*RcoM-2 homologues were first isolated under aerobic conditions, yet they each contained a six-coordinate Fe(II)CO-bound heme (*31*). Aerobic photolysis of the Fe(II)CO species resulted in conversion to a six-coordinate, low-spin Fe(III) heme. Site-directed mutagenesis of *Bx*RcoM-1 identified His^{74} as the proximal ligand to the Fe(III) heme, and spectral characterization of Fe(III) *Bx*RcoM-2 definitively demonstrated that the protein bears a neutral axial ligand, presumably His^{74}, opposite a cysteine(thiolate) ligand. Furthermore, *Bx*RcoM-2 was shown to undergo a redox-mediated ligand switch,

analogous to that observed in *Rr*CooA, in which the cysteine(thiolate) ligand is lost upon heme reduction. The spectral signatures of the Fe(II) *Bx*RcoM-2 species were consistent with the presence of a methionine *trans* to a neutral proximal ligand; mutagenesis data suggested that the distal Fe(II) ligand for *Bx*RcoM-1, and by analogy *Bx*RcoM-2, is Met^{104} (*31, 35*). Methionine, a weaker ligand than histidine, may easily be replaced by CO, analogous to the replacement of the distal proline ligand by CO in Fe(II)CooA. Consistent with this understanding, resonance Raman data of the heme-CO adduct in *Bx*RcoM-2 was indicative of CO binding *trans* to the proximal histidine (His^{74}) (*35*). Thus, the proximal histidine remains constant during redox- and ligand-binding events, while the distal ligand is exchanged in order to allosterically modulate *Bx*RcoM DNA-binding behavior to initiate transcription. Although the mutagenesis studies were on *Bx*RcoM-1 and the spectroscopic studies were on *Bx*RcoM-2, the presence of His^{74} and Met^{104} in the sequences of the N-terminal PAS domains of both proteins implies that these amino acids are the Fe(II) ligands in these two closely related homologues.

Herein, we present identification of the cysteine(thiolate) distal ligand to the Fe(III) heme in *Bx*RcoM-2. Three cysteine residues are found in *Bx*RcoM-1 and *Bx*RcoM-2, and all three cysteine residues were identified as potential Fe(III) heme ligands based on their proximity to the heme in a structural homology model based on the O_2-sensor, *Ec*Dos (*36*). The spectroscopic signatures of three variants—C94S, C127S, and C130S—were studied using the techniques of electronic absorption, resonance Raman (rR) and electron paramagnetic resonance (EPR) spectroscopies. The C94S variant exhibits differences in its spectroscopic features from those of WT *Bx*RcoM-2 and the other variants, and the spectral signatures of C94S are inconsistent with coordination of a cysteine(thiolate) ligand to the heme. These data

identify Cys^{94} as the distal ligand to the Fe(III) heme in *Bx*RcoM-2, and a comparative sequence alignment implicates Cys^{94} as the most plausible candidate for the distal ligand to the Fe(III) heme in *Bx*RcoM-1.

Materials and Methods

Materials. Glycerol and all chemicals used in buffer preparation were purchased from Sigma-Aldrich and used as received. Potassium ferricyanide ($K_3[Fe(CN)_6]$) was purchased from Sigma-Aldrich and used as received. Sodium dithionite ($Na_2S_2O_4$) was purchased from Fluka and stored under $Ar_{(g)}$ at -20 °C until used. A CO gas (99.5%) cylinder was obtained from AGA.

Mutagenesis, Isolation, and Purification of Bx*RcoM-2 Variants*. Variant proteins were generated by mutagenesis of the cloned *Bx*RcoM-2 (*31*) according to the QuikChange protocol (Agilent Technologies [Stratagene], Santa Clara, CA). Sequences of all constructs were verified using BigDye v. 3.1 reaction chemistry (Life Technologies [Applied Biosystems], Carlsbad, CA) with subsequent analysis by the University of Wisconsin—Madison Biotechnology Center DNA sequencing facility.

Isolation and purification of the *Bx*RcoM-2 variants was similar to our previous reports (*31, 35*). Briefly, *E. coli* bearing the expression vector for the appropriate variant was cultivated at 28-30 °C in rich medium supplemented with ferric citrate. Protein expression was induced at $A_{550} \sim 0.35$ (1:20 v:v dilution) by the addition of isopropyl β-D-thiogalactopyranoside (IPTG) to a final concentration of 7 μM. Cells were further incubated 18-20 h after addition of IPTG at 28°C. Cells were pelleted by centrifugation (10,000 x *g*, 10 min) and then resuspended in lysis buffer (50 mM MOPS, pH 7.5, 500 mM KCl and 0.5 mM DTT) and lysed by passage through a French press. Prior to applying the His-tagged *Bx*RcoM-2 extract supernatant (25 mL) to approximately 8 mL Ni-NTA column (Qiagen), 10 mM imidazole was added. A gradient of imidazole (10 mM, 50 mM, and 220 mM) was used to elute protein. Protein was precipitated

by the addition of a saturated $(NH_4)_2SO_4$ solution to a final concentration of 55% (v/v) and allowed to sit on ice for 30 minutes prior to brief centrifugation to pellet protein. After all liquid was removed, the protein pellet was dissolved in 500 μL of buffer (25 mM MOPS, pH 7.4 and 500 mM KCl), applied to a buffer-equilibrated Sephadex G-25 column, and eluted in the same buffer. The desalted protein was fractioned into aliquots and stored at -80 °C. Protein concentrations were determined using the BCA method (Pierce, Rockford, IL); SDS-PAGE verified protein purity was >90%; heme content was determined using the pyridine hemochromogen assay (*37*).

Electronic Absorption Spectroscopy. Electronic absorption (EA) spectra were recorded on a double-beam Varian Cary 4 Bio spectrophotometer set to a spectral bandwidth of 0.5 nm. Spectra were acquired at room temperature for samples of protein prepared, as indicated in the figure legends, in either 25 mM MOPS buffer, pH 7.4, or 25 mM EPPS buffer, pH 8.0, with 500 mM KCl. Oxygen was removed from anaerobic samples by flowing $Ar_{(g)}$ through the headspace of a septum-sealed cuvette for at least 10 minutes. Reduction of Fe(III) protein samples was accomplished either by adding an anaerobically prepared stock solution of sodium dithionite to achieve a final sample concentration of 1-5 mM or by adding a few solid crystals of sodium dithionite to the protein sample solution with $Ar_{(g)}$ flowing in the cuvette headspace. The Fe(II)CO adducts were prepared by the injection of $CO_{(g)}$ via gas-tight syringe into the headspace of a septum-sealed cuvette containing the Fe(III) or as-isolated protein, followed by gentle agitation of the sample and addition of the dithionite reductant. Final protein and heme concentrations ranged from 7-10 μM, and 100-200 μL of CO gas was injected, as appropriate, to give complete conversion to the Fe(II)CO adduct.

Reoxidation of the Fe(II) Bx*RcoM-2 variants.* Protein that was present in the Fe(II) state to a significant extent after purification was reoxidized using potassium ferricyanide, $K_3[Fe(CN)_6]$. Briefly, a stock solution of potassium ferricyanide (500 µL, 25 mM) was prepared by dissolving 4-5 mg of solid $K_3[Fe(CN)_6]$ in 500 µL of 25 mM MOPS buffer with 500 mM KCl, pH 7.4. The stock solution of $K_3[Fe(CN)_6]$ was added to the protein sample to a final concentration of 1-2 mM. The mixture was allowed to react for 20-30 minutes. The protein solution, containing excess $K_3[Fe(CN)_6]_2$, was loaded onto a YM-30 Amicon Ultra spin concentrator (Millipore) and washed 4 times by concentration and dilution into fresh MOPS buffer (25 mM, 500 mM KCl, pH 7.4) using a table-top centrifuge (RCF 15,000 x *g*). Final heme and protein concentrations were determined using the pyridine hemochromogen and BCA assays, respectively.

EPR Spectroscopy. X-band electron paramagnetic resonance (EPR) spectra were collected on a Bruker ELEXSYS E500 equipped with an Oxford ESR 900 continuous flow liquid helium cryostat and an Oxford ITC4 temperature controller maintained at 10 K. The microwave frequency was monitored using an EIP model 625A CW microwave frequency counter. Protein samples were prepared, as indicated in the figure legends, in either 50 mM borate, pH 8.0, or in 25 mM MOPS, pH 7.4, with 500 mM KCl. Samples were transferred to a quartz EPR tube via small-bore tubing (connected to a gas-tight syringe) and frozen in $N_{2(l)}$. Samples of approximately 150 µL had a final concentration range of 80-250 µM. For all samples, scans of 0 - 10,000 Gauss revealed no signals other than those reported.

Resonance Raman Spectroscopy. Resonance Raman (rR) spectra were obtained with an excitation wavelength of 413.1 nm from a Coherent I-302C Kr^+ laser in a backscattering 135° geometry. An Acton Research triple monochromator was used with gratings of 2400 grooves/mm. Low incident laser powers of <20 mW were focused with a cylindrical lens onto the sample. A Princeton Instruments Spex 1877 triple spectrograph outfitted with a cooled, intensified diode array detector was operated under computer control using Spectrasense software. The frozen protein samples, prepared as described for EPR (*vide supra*), were placed in a quartz dewar and maintained at 77 K in $N_{2(l)}$ to reduce local heating. Peak positions were calibrated relative to the ice peak at 228 cm^{-1} or a Na_2SO_4 peak at 981 cm^{-1}. Windows centered at 650, 1250 and 1850 cm^{-1} were overlaid for a total frequency range of 150-2250 cm^{-1}. IGOR Pro software v. 6.0 (Wavemetrics, Inc.) was used to import and process all spectral data. Major vibrational modes are assigned based on comparison with those of other heme proteins and the work of Kitagawa and Spiro (*38-42*).

Results

Characterization of C127S and C130S Bx*RcoM-2*. The electronic absorption spectra of both purified C127S and C130S *Bx*RcoM-2 are most consistent with a low-spin, six-coordinate Fe(III) heme ligated by a cysteine(thiolate) and a neutral ligand, likely a histidine, in the axial positions. The spectrum for C127S (Figure 2.1c) displays a well-resolved delta (δ) band at 354 nm; a sharp, intense Soret (γ) peak at 422 nm; a broad, asymmetric absorption envelope consisting of α and β bands at 562 and 537 nm, respectively; and a pair of weak ligand-to-metal charge transfer (LMCT) transition bands at 648 and 728 nm. Peak positions for C130S were similar (Figure 2.1b): a well-resolved δ band at 356 nm; a sharp Soret band at 422 nm; a broad, asymmetric absorption envelope consisting of α and β bands at 561 and 539 nm, respectively, and LMCT transition bands at 640 and 720 nm. Peak positions for these variants differ only marginally from those of WT Fe(III) *Bx*RcoM-2 (Table 2.1) (*35*). Reduction (via addition of sodium dithionite) and $CO_{(g)}$ binding to either C127S and C130S *Bx*RcoM-2 results in spectral changes nearly identical to those observed in WT *Bx*RcoM-2 (Figures 2.2 and 2.3; Table 1), suggesting that the reduction and $CO_{(g)}$ binding behaviors of these variants are similar to those of WT.

Resonance Raman analyses of C127S and C130S *Bx*RcoM-2 and their comparisons to WT Fe(III)*Bx*RcoM-2 (Figures 2.4 and 2.5) support the presence of a low-spin, six-coordinate Fe(III) heme with a cysteine(thiolate) ligand in each variant. The mid-frequency window (1300-1700 cm^{-1}) is dominated by in-plane, totally symmetric stretching modes of the porphyrin; as such, the spectra are sensitive to the oxidation state of the heme iron (ν_4) as well as its spin and coordination (ν_3, ν_2, ν_{10}) states (*40, 41*). The assignments for these bands in WT Fe(III)*Bx*RcoM-2 have been reported previously (*35*), and the C127S variant bears a striking

resemblance to that of WT (Figures 2.5c and 2.5a, respectively). The as-isolated C130S *Bx*RcoM-2 rR spectrum is shown in Figure 2.4b. The marker bands present in the spectrum of the as-isolated C130S protein overlap closely with those in the Fe(III) spectrum of *Bx*RcoM-2 (Figures 2.4b and 2.4a, respectively); however, additional bands are present that indicate a mixture of both Fe(II) and Fe(III) is present in the as-isolated sample. Upon oxidation with potassium ferricyanide, the rR profile of C130S (Figure 2.5b) is almost identical to that of WT Fe(III)*Bx*RcoM-2 and is most consistent with a six-coordinate, low-spin Fe(III) heme in C130S variant, although a small shoulder persists in the oxidation-state marker band, ν_4, as well as $\nu_{c=c}$ indicative of residual Fe(II). A putative iron-sulfur stretching mode, $\nu_{Fe\text{-}S}$, was tentatively identified in the low-frequency region of the WT Fe(III)*Bx*RcoM-2 rR spectrum at 310 cm^{-1}, and its assignment was based on comparisons to rR studies of other cysteine(thiolate)-ligated hemoproteins, such as $P450_{CAM}$, hCBS and the H25C variant of HO-1 (*43-45*). This putative, broad $\nu_{Fe\text{-}S}$ band is also observed in C127S *Bx*RcoM-2 at 308 cm^{-1} (Figure 2.6c) and in C130S *Bx*RcoM-2 at 309 cm^{-1} (Figure 2.6b). Thus, the rR spectra of Fe(III) C127S and Fe(III) C130S *Bx*RcoM-2 are consistent with a low-spin, six-coordinate Fe(III) heme that is ligated by a cysteine(thiolate) ligand.

Electron paramagnetic resonance (EPR) spectroscopy is also indicative of a low-spin, six-coordinate Fe(III) ($S = ½$) heme with a cysteine(thiolate) *trans* to a second, neutral ligand in both C127S and C130S *Bx*RcoM-2. The EPR spectrum of Fe(III) C127S *Bx*RcoM-2 (Figure 2.7c) displays a characteristic rhombic signal with *g* values of 1.91, 2.27, and 2.44 corresponding to g_x, g_y and g_z, respectively. Similarly, the rhombic EPR signal of Fe(III) C130S *Bx*RcoM-2 (Figure 2.7b) exhibits *g* values of 1.88, 2.27, and 2.50. For each variant, the *g* values are comparable to those obtained for WT Fe(III)*Bx*RcoM-2 (Table 2.2). Differences in

the observed *g* values among the variants and WT *Bx*RcoM-2 may be attributed to the slightly more basic pH and altered buffer conditions originally used in handling the WT protein. A second minor EPR signal with an axial *g* anisotropy ($g_{\perp}^{eff} = 5.8$) is also observed for the variants C127S and C130S (both as isolated and reoxidized). This signal is due to a small amount of high-spin Fe(III) heme present, which is consistent with rR analyses that show a small five-coordinate high-spin band at approximately 1490 cm^{-1} (ν_3) for both variants (Figure 2.5). Taken together, the aforementioned electronic absorption, rR and EPR data for the Fe(III) C127S and Fe(III) C130S *Bx*RcoM-2 variants affirm that the native His/Cys(thiolate) ligation motif is maintained.

Characterization of C94S Bx*RcoM-2*. Electronic absorption spectroscopy of purified C94S *Bx*RcoM-2 is strongly suggestive that Cys^{94} is the Fe(III) heme ligand in WT *Bx*RcoM-2. Unlike the C127S or C130S variants, electronic absorption spectra of C94S *Bx*RcoM-2 are most similar to those of Fe(III) hemes that lack a cysteine(thiolate) ligand (Figures 2.1d and 2.1e; Table 2.1). As isolated, the C94S Soret band at 418 nm is less sharp than that of WT *Bx*RcoM-2, and the α/β bands at 561 and 532 nm, respectively, are more well-defined than those expected for a six-coordinate, low-spin Fe(III) heme with Cys/His axial ligands. The pronounced δ band characteristic of thiolate ligation is absent; in its place is a broad, weak Soret shoulder near 360 nm. Only one LMCT band at 640 nm is observed, again suggesting that thiolate ligation is absent. Like the C130S variant, rR analyses initially indicated that C94S was purified as an ad-mixture of the Fe(II) and Fe(III) oxidation states; in contrast to the C130S variant, however, only a weak EPR signal was initially detected (*vide infra*). Unlike the C130S variant, oxidation of the C94S variant protein upon addition of potassium ferricyanide resulted

in a 3-nm blue-shift of the Soret band to 415 nm, a slight decrease in the intensity of the δ band shoulder, and slight shifts in the α/β band positions to 562 and 530 nm, respectively. Additionally, a band at 632 nm appeared that was suggestive of the formation of a high-spin Fe(III) heme (*46*). These observed spectral features are most similar to proteins that have an admixture of high- and low-spin Fe(III) hemes that lack a cysteine(thiolate) ligand, such as metMb, *Ax*PDEA1H and *Mt*DosH (*46, 47*). Electronic absorption spectra of Fe(II) and Fe(II)CO C94S are virtually identical to WT (Figures 2.2 and 2.3; Table 2.1), suggesting that the reduction and $CO_{(g)}$ binding behaviors of the C94S variant are unperturbed.

Resonance Raman data collected for the C94S variant supports the conclusion that Cys^{94} is indeed the distal Fe(III) heme axial ligand. The rR spectrum for as-isolated C94S *Bx*RcoM-2 (Figure 2.4d) displays a mixture of oxidation and spin-state marker bands similar to that of the C130S variant. Addition of potassium ferricyanide to as-isolated C94S results in a sharpening of the oxidation state marker band with one major frequency exhibited at 1371 cm^{-1} (Figure 2.5d), indicative of Fe(III) as the majority heme iron oxidation state. A small ν_3 shoulder, likely due to residual Fe(II), persisted in all of the studied samples. The high-frequency region that contains the spin and coordination-state marker bands (ν_3 and ν_2) displays broadened bands at 1493 and 1503 cm^{-1} (ν_3) and 1562 and 1577 cm^{-1} (ν_2). These band positions are indicative of an admixture of low-spin and high-spin Fe(III) hemes, which is most similar to what is observed in the met forms of Fe(III)*Ax*PDEA1H and Fe(III)*Mt*DosH (*47*). In addition, the spin-state marker band ν_{10} is not observed in the rR spectrum of C94S, unlike the ν_{10} band of the Fe(III) forms of WT, C130S and C127S *Bx*RcoM-2. Presumably, ν_{10} in C94S is shifted to lower energy and is hidden due to overlap with the strong, Gaussian-shaped $\nu_{c=c}$ band at 1622 cm^{-1}.

Distinct differences in the low frequency region of the resonance Raman spectrum of C94S support the conclusion that Cys^{94} is the native Cys ligand. In the region where the putative $\nu_{Fe\text{-}S}$ marker band is typically seen, there is a resonance at 304 cm^{-1} that is sharpened and downshifted compared to that of WT *Bx*RcoM-2 (Figure 2.6). This lower frequency mode might plausibly be attributed to the presence of a ligated thioether ($H_3C\text{-}S\text{-}CH_2\text{-}R$), which is the moiety known to be the distal Fe(II) heme ligand. However, Gaussian deconvolutions of the broad $\nu_{Fe\text{-}S}$ resonances of Fe(III) WT, C130S, and C127S *Bx*RcoM-2 (Figure 2.6) are most consistent with the presence of three overlapping bands present in the broad $\nu_{Fe\text{-}S}$ resonance in Fe(III) WT, C130S and C127S *Bx*RcoM-2. In the C94S spectrum, the sharper resonance at 304 cm^{-1} was fit with a single Gaussian, and because this peak persists in the low energy rR region of WT *Bx*RcoM-2 and all variants, we assign this resonance to a porphyrin mode. The two higher-energy modes (313 cm^{-1} and 321 cm^{-1}) are attributed to the $\nu_{Fe\text{-}S}$ resonance that likely overlaps with this porphyrin mode centered at 304 cm^{-1}, an observation that has also been noted for Cys-ligated NPAS2 (*48*). Additionally, the rR spectrum of C94S reacted with potassium ferricyanide exhibits an added resonance of strong intensity at 226 cm^{-1}. The proximal ligand for *Bx*RcoM-2 is His^{74} (*vide supra*); five- and six-coordinate ferric and ferrous hemoproteins that contain His as an axial ligand, such as met and oxyMb, oxy and deoxyHb, microperoxidase, *Bj*FixLH, and *Mt*DosH, show a large enhancement in band intensity in the 220-270 cm^{-1} region due to a strong, Raman-active $\nu_{Fe\text{-}His}$ stretch that is highly dependent on the hydrogen-bonding environment around the His imidazole ring (*47, 49-52*). Considering the similarity of the 226 cm^{-1} band to that of MetMb, we tentatively assign this resonance as the $\nu_{Fe\text{-}His}$ stretch.

EPR characterization of C94S *Bx*RcoM-2 provides confirmation that Cys^{94} is the sixth ligand to the Fe(III) heme in WT *Bx*RcoM-2. Data collected for the as-isolated C94S *Bx*RcoM-2 revealed no distinct set of rhombic signals between 2400 – 3800 G; however, a low intensity axial signal at $g_{\perp}^{eff} = 5.8$ was observed, consistent with a high-spin Fe(III) heme. Addition of ferricyanide to the as-isolated form of C94S resulted in an increase in intensity (Figure 2.7d), revealing signals with $g_{\perp}^{eff} = 5.82$ and $g_{||}^{eff} = 2.00$. This axial spectrum is typical of high-spin hemoproteins such as aquo metmyolgobin and high-spin cytochrome *c* oxidase (*53, 54*). Figure 2.7d also shows a small rhombic signal (marked with *) that may be due to the presence of some low-spin Fe(III), of unknown origin. That the EPR spectrum of C94S is high spin and not low-spin like that of WT RcoM-2, suggests that a strongly-donating ligand (such as Cys) has been lost. Taken all together, our spectral data strongly suggest that Cys^{94} as the distal Fe(III) heme ligand in *Bx*RcoM-2.

Discussion

Numerous heme proteins are implicated in sensing and transport of small molecules (*1, 4, 6*); discrimination among the gaseous small molecule signal transducers O_2, NO, and CO requires a recognition mechanism that is not based on charge, shape, or size because these gases cannot be readily differentiated by these methods. Instead, heme proteins must modify their affinity for small molecules by altering the iron redox potential, oxidation state, spin state, distal or proximal ligands, or interactions of the gas molecule with residues in the heme-binding pocket (*2*). Functional activity of gas-sensing heme proteins is frequently linked to the nature of the heme-binding pocket environment. One element of control utilized to poise the heme for gas binding is a redox-mediated ligand switch; however, the discriminatory binding of gas molecules is modulated by a combination of factors that a redox-mediated ligand switch alone cannot confer. In many cases, a series of events occurs in which the heme iron atom changes oxidation and ligation states preceding gas binding; the final step of regulation is commonly achieved upon stabilization of the correct effector molecule in the heme-binding pocket.

In the O_2 sensor *Ec*DOS, binding of O_2 to heme regulates phosphodiesterase activity (*3, 55*). The *Ec*DOS Fe(III) heme, bound within a PAS domain, is coordinated by a histidine residue (His^{77}) and an exogenous water molecule (*56*). Reduction of the heme to Fe(II) results in replacement of the coordinated water by a methionine (Met^{95}) as the distal heme ligand (*56, 57*). O_2 binding to Fe(II)*Ec*DOS proceeds via replacement of the weakly-bound Met^{95} thioether group. Structural and spectroscopic studies have revealed that charge build-up on the coordinated O_2, which does not happen upon CO or NO binding, is neutralized via the guanidinium group of Arg^{97} (*56, 58*). The environment of the heme-binding pocket in *Ec*DOS

enables the protein to enhance selectivity for O_2 over CO or NO as well as prevent autoxidation of the heme iron upon O_2 binding (*3, 58, 59*).

The heme-regulated eIF2α (HRI) kinase, which regulates globin synthesis in reticulocytes in response to available heme levels, is a multidomain heme protein with two distinct heme-binding sites, one of which is a low-spin, six-coordinate heme-thiolate center that functions as a NO sensor (*60, 61*). Cys^{409} of the kinase domain and a histidine (His^{119} or His^{120}) of the N-terminal domain serve as ligands to this NO-binding heme. Characteristics of cysteine(thiolate) coordination are lost following reduction, suggesting that either a ligand switch or protonation to a cysteine(thiol) occurs to stabilize the more electron-rich Fe(II) heme (*62, 63*). HRI kinase activity is specifically upregulated by forming a five-coordinate NO adduct, which is formed due to the strong *trans* influence of NO and the weakly-coordinating nature of the His ligand. CO binding opposite the anchoring histidine, forming a six-coordinate species, suppresses activity in HRI, and reaction with O_2 results in autoxidation (*61*). It is postulated that NO binding releases inhibition by the HRI heme domain, while binding of other gas signaling molecules does not (*64*).

The CO sensor *Rr*CooA utilizes a similar method of heme-dependent control to regulate expression of genes encoding CO-metabolizing enzymes. Fe(III) and Fe(II) *Rr*CooA are inactive; only the CO adduct binds to DNA (*20*). Reduction of the heme iron results in replacement of the cysteine(thiolate) ligand (Cys^{75}) with histidine (His^{77}) (*25, 26*). *Rr*CooA is unusual in that the weakly coordinated N-terminal proline (Pro^2) is retained during the redox exchange and thereafter is replaced by the exogenous CO molecule (*24, 30*). Binding of CO and replacement of the Pro ligand influences the correct formation of the active DNA-binding conformation (*30*). Addition of O_2 to Fe(II)*Rr*CooA results in autoxidation, which reverts the

protein to the Cys-His axial coordination characteristic of the Fe(III) heme (*20*). NO reacts with either Fe(III) or Fe(II) *Rr*CooA to form a five-coordinate Fe(II)-NO heme, which is inactive toward DNA binding (*65*). Thus, *Rr*CooA is also able to discriminate between O_2, CO, and NO, and regulate the biological response of *R. rubrum* to its environment.

In a manner similar to *Rr*CooA, the isolated PAS-A domain of the mammalian CO sensor NPAS2 bears an Fe(III) heme that is low-spin and is ligated by a His/Cys(thiolate) motif. Upon reduction of the Fe(III) heme, the cysteine(thiolate) ligand (Cys^{170}) is replaced with a strong donor, postulated to be the deprotonated side chain of His^{171} (*48*). Release of one of the two histidine side chains occurs in the presence of CO: whether this ligand is His^{119} or His^{171} is not clear. CO-dependent signaling is transduced through the PAS-A domain via disruption of a hydrogen-bonding network, which ultimately causes dissociation of NPAS2 from its heterodimeric partner BMAL1. Dissociation of the DNA-binding NPAS2-BMAL1 complex prevents transcription of *per* and *cry* genes, both of which are involved in regulation of the circadian clock (*18, 48, 66*). NPAS2 is reported neither to bind O_2 reversibly nor to interact with NO (*18*). The structural basis for this discrimination is unknown, but it is hypothesized that secondary interactions in the heme-binding pocket contribute.

Recent spectroscopic studies and *in vivo* functional assays have linked the heme-containing *Bx*RcoM proteins to aerobic CO sensing (*31, 35*). Similar to other small-molecule sensor proteins that respond to O_2, CO, and NO binding, *Bx*RcoM function is modulated by the oxidation state of the heme iron and by the ligand environment of the heme cofactor. Our prior studies demonstrated that *Bx*RcoM-2 is a cysteine-ligated heme protein that undergoes a redox-mediated ligand switch (*35*). In the Fe(III) state, the proximal ligand is inferred to be His^{74} based on sequence similarity to and site-directed mutagenesis studies of the homologous

*Bx*RcoM-1 protein (*vide supra*) (*31*). The *Bx*RcoM-1 and -2 proteins contain three cysteine residues as the potential distal ligand to the Fe(III) heme: Cys^{94}, Cys^{127} and Cys^{130}. Given the involvement of cysteine(thiolate) residues in redox-mediated ligand switches, which appear to prime gas-regulated hemoproteins for effector-mediated response, we set out to identify the Fe(III) *Bx*RcoM cysteine(thiolate) ligand.

Herein, Cys^{94} was identified as the distal Fe(III) heme ligand in *Bx*RcoM-2. Three cysteine-to-serine variants were generated; unlike the other studied variants, spectral data strongly suggest that C94S does not possess the native low-spin, Fe(III) heme with His/Cys(thiolate) coordination. The EPR spectrum of C94S was dominated by an axial signal characteristic of high-spin heme, providing the strongest evidence that the strongly donating thiolate axial ligand was absent. The electronic absorption spectrum of C94S lacked the well-resolved δ band and the two weak LMCT bands in the visible region characteristic of a low-spin thiolate-ligated heme. Furthermore, rR data suggested that the Fe-S stretch was absent, and a new resonance at 226 cm^{-1} was tentatively assigned as a $\nu_{Fe\text{-}His}$ mode of a high-spin heme. Our assignment of Cys^{94} as the Fe(III) distal heme ligand is further supported by evidence for two putative RcoM proteins from the organism *B. cepacia*. Sequence alignments of *Bx*RcoM-1 and -2 with those of the two postulated RcoM proteins from *B. cepacia* strains CH1-1 and BH160 show 88% and 85% amino acid identity conservation, respectively (Figure 2.8). Two of the three cysteine amino acids are conserved among all four proteins: Cys^{94} and Cys^{130}; in the place of Cys^{127} is Ser^{127} in the *B. cepacia* BH160 sequence. This finding supports the conclusion that Cys^{127} is not the distal Fe(III) heme ligand in the *Bx*RcoM proteins due to its lack of conservation. Furthermore, support for the role of Cys^{94} as the distal Fe(III) heme ligand and for Cys^{130} as a putative structural element is garnered from its conservation.

In combination with our past results on the *Bx*RcoM proteins, these data illustrate a mechanism by which the *Bx*RcoM proteins utilize changes in oxidation and ligation states at the heme cofactor to poise the protein to respond to CO (Scheme 2.1). *Bx*RcoM proteins are members of a family of cysteine(thiolate)-coordinated heme proteins that undergo redox-mediated ligand exchange and selective ligand replacement as components of the machinery to affect protein function. As shown in Scheme 2.1, reduction of the low-spin, six-coordinate Fe(III) heme center in *Bx*RcoM results in the loss of the cysteine(thiolate) distal ligand; this ligand is now known to be Cys^{94}. Loss of a cysteine(thiolate) ligand from a low-spin six-coordinate heme serves as a priming reaction that prepares *Bx*RcoM to respond to its effector molecule, similar to what is observed in *Rr*CooA and NPAS2. *Bx*RcoM Cys^{94} is replaced by a neutral, weakly-bound ligand, presumably Met^{104}; Met^{104} is then replaced by CO. Met^{104} serves an analogous function to Met^{95} in the heme-PAS O_2-sensor *Ec*DOS (*56, 67*), as the more weakly bound, more readily replaced ligand in a low-spin six-coordinate heme complex. Thus, the *Bx*RcoM proteins utilize a hybrid of the strategies seen in *Rr*CooA, NPAS2, and *Ec*DOS to ready themselves for CO-dependent transcriptional activation. Ultimately, the redox-mediated ligand switch from Cys^{94} [Fe(III)] to Met^{104} [Fe(II)] is crucial to maintaining the sensitivity of the *Bx*RcoM proteins to CO; however, the exact discriminatory nature of the RcoM proteins for CO over O_2 and NO, as well as the mode of propagation of this signal to the LytTR DNA-binding domain is still unknown.

Conclusion

Cys^{94} is the distal ligand to the Fe(III) heme in RcoM-2 and, by analogy, RcoM-1, the $CO_{(g)}$-responsive transcriptional regulators from *B. xenovorans*. In this study we altered all three cysteines, generating cysteine-to-serine variants (C94S, C127S and C130S). The electronic absorption, rR and EPR spectra of C127S and C130S variants are similar to those of WT *Bx*RcoM-2, consistent with retention of a Cys(thiolate) ligand to the Fe(III) heme. By contrast, the spectral features of the C94S variant spectral features are inconsistent with Cys(thiolate) ligation at the Fe(III) heme. In combination with our previous results, these data reveal a complete picture of the redox-mediated ligand switch that occurs at the heme cofactor in the RcoM proteins; however the mechanism by which $CO_{(g)}$ binding is transmitted to the LytTR DNA-binding domain to regulate function is yet to be elucidated.

References

1. Uchida, T., and Kitagawa, T. (2005) Mechanism for Transduction of the Ligand-Binding Signal in Heme-Based Gas Sensory Proteins Revealed by Resonance Raman Spectroscopy, *Acc. Chem. Res. 38*, 662-670.
2. Jain, R., and Chan, M. K. (2003) Mechanisms of ligand discrimination by heme proteins, *J. Biol. Inorg. Chem. 8*, 1-11.
3. Sasakura, Y., Suzuki-Yoshimura, T., Kurokawa, H., and Shimizu, T. (2006) Structure-Function Relationships of *Ec*DOS, a Heme-regulated Phosphodiesterase from *Escherichia coli*, *Acc. Chem. Res. 39*, 37-43.
4. Aono, S. (2008) Metal-containing sensor proteins sensing diatomic gas molecules, *Dalton Trans. 24*, 3137-3146.
5. Spiro, S. (2008) Metalloregulatory proteins and nitric oxide signalling in bacteria, *Biochem. Soc. Trans. 36*, 1160-1164.
6. Gilles-Gonzalez, M.-A., and Gonzalez, G. (2005) Heme-based sensors: defining characterstics, recent developments, and regulatory hypotheses, *J. Inorg. Biochem. 99*, 1-22.
7. Gilles-Gonzalez, M. A., Ditta, G. S., and Helinski, D. R. (1991) A haemoprotein with kinase activity encoded by the oxygen sensor of *Rhizobium meliloti*, *Nature 350*, 170–172.
8. Hou, S., Larsen, R. W., Boudko, D., Riley, C. W., Karatan, E., Zimmer, M., Ordal, G. W., and Alam, M. (2000) Myoglobin-like aerotaxis transducers in archaea and bacteria, *Nature 403*, 540-544.

9. Delgado-Nixon, V. M., Gonzalez, G., and Gilles-Gonzalez, M.-A. (2000) Dos, a Heme-Binding PAS Protein from *Escherichia coli*, Is a Direct Oxygen Sensor, *Biochemistry 39*, 2685-2691.

10. Ignarro, L. J. (1999) Nitric Oxide: A Unique Endogenous Signaling Molecule in Vascular Biology, *Angew. Chem. Int. Ed. 38*, 1882-1892.

11. Karow, D. S., Pan, D., Tran, R., Pellicena, P., Presley, A., Mathies, R. A., and Marletta, M. A. (2004) Spectroscopic characterization of the soluble guanylate cyclase-like heme domains from *Vibrio cholerae* and *Thermoanaerobacter tengcongensis*, *Biochemistry 43*, 10203-10211.

12. Ignarro, L. J., Degnan, J. N., Baricos, W. H., Kadowitz, P. J., and Wolin, M. S. (1982) Activation of purified guanylate cyclase by nitric oxide requires heme: Comparison of the heme-deficient, heme-reconstituted and heme-containing forms of soluble enzyme from bovine lung, *Biochim. Biophys. Acta 718*, 49-59.

13. Igarashi, J., Sato, A., Kitagawa, T., Yoshimura, T., Yamauchi, S., Sagami, I., and Shimizu, T. (2004) Activation of Heme-regulation Eukaryotic Initiation Factor 2α Kinase by Nitric Oxide Is Induced by the Formation of a Five-coordinate NO-heme Complex. Optical Absorption, Electronic Spin Resonance, and Resonance Raman Spectral Studies, *J. Biol. Chem. 279*, 15752-15762.

14. de Rosny, E., de Groot, A., Jullian-Binard, C., Borel, F., Suarez, C., Le Pape, L., Fontecilla-Camps, J. C., and Jouve, H. M. (2008) DHR51, the *Drosophila melanogaster* Homologue of the Human Photoreceptor Cell-Specific Nuclear Receptor, Is a Thiolate Heme-Binding Protein, *Biochemistry 47*, 13252-13260.

15. Reinking, J., Lam, M. M. S., Pardee, K., Sampson, H. M., Liu, S., Yang, P., Williams, S., White, W., Lajoie, G., Edwards, A., and Krause, H. M. (2005) The *Drosophila* Nuclear Receptor E75 Contains Heme and Is Gas Responsive, *Cell 122*, 195-207.

16. Giardina, G., Rinaldo, S., Johnson, K. A., Di Matteo, A., Brunori, M., and Cutrozzolà, F. (2008) NO sensing in *Pseudomonas aeruginosa*: Structure of the Transcriptional Regulator DNR, *J. Mol. Biol. 378*, 1002-1015.

17. Verma, A., Hirsch, D. J., Glatt, C. E., Ronnet, G. V., and Snyder, S. H. (1993) Carbon monoxide: a putative neural messenger, *Science 259*, 381-384.

18. Dioum, E. M., Rutter, J., Tuckerman, J. R., Gonzalez, G., Gilles-Gonzalez, M.-A., and McKnight, S. L. (2002) NPAS2: A gas-responsive transcription factor, *Science 298*, 2385-2387.

19. Aono, S., Nakajima, H., Saito, K., and Okada, M. (1996) A novel heme protein that acts as a carbon monoxide-dependent transcriptional activator in *Rhodospirillium rubrum*, *Biochem. Biophys. Res. Commun. 228*, 752-756.

20. Shelver, D., Kerby, R. L., He, Y., and Roberts, G. P. (1997) CooA, a CO-sensing transcription factor from *Rhodospirillum rubrum*, is a CO-binding heme protein, *Proc. Natl. Acad. Sci. U.S.A. 94*, 11216-11220.

21. Roberts, G. P., Kerby, R. L., Youn, H., and Conrad, M. (2005) CooA, a paradigm for gas sensing regulatory proteins, *J. Inorg. Biochem. 99*, 280-292.

22. Kerby, R. L., Ludden, P. W., and Roberts, G. P. (1995) Carbon monoxide-dependent growth of *Rhodospirillum rubrum*, *J. Bacteriol. 177*, 2241-2244.

23. Reynolds, M. F., Shelver, D., Kerby, R. L., Parks, R. B., Roberts, G. P., and Burstyn, J. N. (1998) EPR and Electronic Absorption Spectroscopies of the CO-Sensing CooA

Protein Reveal a Cysteine-Ligated Low-Spin Ferric Heme, *J. Am. Chem. Soc. 120*, 9080-9081.

24. Lanzilotta, W. N., Schuller, D. J., Thorsteinsson, M. V., Kerby, R. L., Roberts, G. P., and Poulos, T. L. (2000) Structure of the CO sensing transcription activator CooA, *Nat. Struct. Biol. 7*, 876-880.

25. Shelver, D., Thorsteinsson, M. V., Kerby, R. L., Chung, S.-Y., Roberts, G. P., Reynolds, M. F., Parks, R. B., and Burstyn, J. N. (1999) Identification of two important heme site residues (Cysteine 75 and Histidine 77) in CooA, the CO-sensing transcription factor of *Rhodospirillum rubrum*, *Biochemistry 38*, 2669-2678.

26. Aono, S., Ohkubo, K., Matsuo, T., and Nakajima, H. (1998) Redox-controlled ligand exchange of the heme in the CO-sensing transcriptional activator CooA, *J. Biol. Chem. 273*, 25757-25764.

27. Kerby, R. L., Youn, H., Thorsteinsson, M. V., and Roberts, G. P. (2003) Repositioning about the Dimer Interface of the Transcription Regulator CooA: A Major Signal Transduction Pathway between the Effector and DNA binding Domains, *J. Mol. Biol. 325*, 809-823.

28. Youn, H., Kerby, R. L., and Roberts, G. P. (2003) The Role of the Hydrophobic Distal Heme Pocket of CooA in Ligand Sensing Response, *J. Biol. Chem. 278*, 2333-2340.

29. Yamamoto, K., Ishikawa, H., Takahashi, S., Ishimori, K., Morishima, I., Nakajima, H., and Aono, S. (2001) Binding of CO at the Pro^2 side is crucial for the activation of CO-sensing transcriptional activator CooA. ^{1}H NMR spectroscopic studies., *J. Biol. Chem. 276*, 11473-11476.

30. Clark, R. W., Youn, H., Parks, R. B., Cherney, M. M., Roberts, G. P., and Burstyn, J. N. (2004) Investigation of the role of the N-terminal proline, the distal ligand in the CO sensor CooA, *Biochemistry 43*, 14149-14160.

31. Kerby, R. L., Youn, H., and Roberts, G. P. (2008) RcoM: A New Single-Component Transcriptional Regulator of CO Metabolism in Bacteria, *J. Bacteriol. 190*, 3336-3343.

32. Chain, P. S. G., Denef, V. J., Konstantinidis, K. T., Vergez, L. M., Agulló, L., Reyes, V. L., Hauser, L., Córdova, M., Gómez, L., González, M., Land, M., Lao, V., Larimer, F., LiPuma, J. J., Mahenthiralingam, E., Malfatti, S. A., Marx, C. J., Parnell, J. J., Ramette, A., Richardson, P., Seeger, M., Smith, D., Spilker, T., Sul, W. J., Tsoi, T. V., Ulrich, L. E., Zhulin, I. B., and Tiedje, J. M. (2006) *Burkholderia xenovorans* LB400 harbors a multi-replicon, 9.73-Mbp genome shaped for versatility, *Proc. Nat. Acad. Sci. USA 103*, 15280-15287.

33. Gu, Y.-Z., Hogenesch, J. B., and Bradfield, C. A. (2000) The PAS Superfamily: Sensors of Environmental and Developmental Signals, *Annu. Rev. Physiol. 40*, 519-561.

34. Nikolskaya, A. N., and Galperin, M. Y. (2002) A novel type of conserved DNA-binding domain in the transcriptional regulators of the AlgR/AgrA/LytR family, *Nucl. Acids Res. 30*, 2453-2459.

35. Marvin, K. A., Kerby, R. L., Youn, H., Roberts, G. P., and Burstyn, J. N. (2008) The Transcription Regulator RcoM-2 from Burkholderia xenovorans Is a Cysteine-Ligated Hemoprotein That Undergoes a Redox-Mediated Ligand Switch, *Biochemistry 47*, 9016-9028.

36. Park, H., Suquet, C., Satterlee, J. D., and Kang, C. (2004) Insights into Signal Transduction Involving PAS Domain Oxygen-Sensing Heme Proteins from the X-ray

Crystal Structure of *Escherichia Coli* Dos Heme Domain (*Ec* DosH), *Biochemistry 43*, 2738-2746.

37. Antonini, E., and Brunori, M. (1971) *Hemoglobin and Myoglobin in Their Reactions with Ligands*, Vol. 21, North-Holland Publishing Co., Amsterdam.

38. Abe, M., Kitagawa, T., and Kyogoku, Y. (1978) Resonance Raman spectra of octaethylporphyinato-Ni(II) and *meso*-deuterated and ^{15}N substituted derivatives. II. A normal coordinate analysis, *J. Chem. Phys. 69*, 4526-4532.

39. Woodruff, W. H., Adams, D. H., Spiro, T. G., and Yonetani, T. (1975) Resonance Raman spectra of cobalt myoglobins and cobalt porphyrins. Evaluation of protein effects on porphyrin structure., *J. Am. Chem. Soc. 97*, 1695-1698.

40. Spiro, T. G. (1975) Resonance Raman spectroscopic studies of heme proteins, *Biochim. Biophys. Acta 416*, 169-189.

41. Spiro, T. G., and Strekas, T. C. (1974) Resonance Raman spectra of heme proteins. Effects of oxidation and spin state., *J. Am. Chem. Soc. 96*, 338-345.

42. Kitagawa, T., Kyogoku, Y., Iizuka, T., Ikeda-Saito, M., and Yamanaka, T. (1975) Resonance Raman Scattering from Hemoproteins, *J. Biochem. 78*, 719-728.

43. Champion, P. M., Stallard, B. R., Wagner, G. C., and Gunsalus, I. C. (1982) Resonance Raman detection of an Fe-S bond in cytochrome $P450_{CAM}$, *J. Am. Chem. Soc. 104*, 5469-5472.

44. Green, E. L., Taoka, S., Banerjee, R., and Loehr, T. M. (2000) Resonance Raman Characterization of the Heme Cofactor in Cystathionine β-Synthase. Identification of the Fe-S(Cys) Vibration in the Six-Coordinate Low-Spin Heme, *Biochemistry 40*, 459-463.

45. Liu, Y., Loccoz-Moënne, P., Hildebrand, D. P., Wilks, A., Loehr, T. M., Mauk, A. G., and de Montellano, P. R. O. (1999) Replacement of the Proximal Histidine Iron Ligand by a Cysteine or Tyrosine Converts Heme Oxygenase to an Oxidase, *Biochemistry 38*, 3733-3743.

46. Falk, J. E. (1964) *Porphyrins and Metalloporphyrins: Their General, Physical, and Coordination Chemistry, and Laboratory Methods*, Elsevier, Amsterdam.

47. Tomita, T., Gonzalez, G., Chang, A. L., Ikeda-Saito, M., and Gilles-Gonzalex, M.-A. (2002) A Comparative Resonance Raman Analysis of Heme-Binding PAS Domains: Heme Iron Coordination Structures of the *Bj*FixL, *Ax*PDEA1, *Ec*Dos, and *Mt*Dos Proteins, *Biochemistry 41*, 4819-4826.

48. Uchida, T., Sato, E., Sato, A., Sagami, I., Shimizu, T., and Kitagawa, T. (2005) CO-dependent Activity-controlling Mechanism of Heme-containing CO-sensor Protein, Neuronal PAS Domain Protein 2, *J. Biol. Chem. 280*, 21358-21368.

49. Hirota, S., Mizoguchi, Y., Yamauchi, O., and Kitagawa, T. (2002) Observation of an isotope-sensitive low-frequency Raman band specific to metmyoglobin, *J. Biol. Inorg. Chem. 7*, 217-221.

50. Kerr, E. A., Yu, N.-T., Gersonde, K., Parish, D. W., and Smith, K. M. (1985) Iron-Histidine Stretching Vibration in the Deoxy State of Insect Hemoglobins with Different O_2 Affinities and Bohr Effects, *J. Biol. Chem. 260*, 12665-12669.

51. Walters, M. A., and Spiro, T. G. (1982) Resonance Raman Spectroscopic Studies of Axial Ligation in Oxyhemoglobin, Oxymyoglobin, and Nitrosylmyoglobin, *Biochemistry 21*, 6989-6995.

52. Othman, S., Lirzin, A. L., and Desbois, A. (1994) Resonance Raman Investigation of Imidazole and Imidazolate Complexes of Microperoxidase: Characterization of the Bis(histidine) Axial Ligation in *c*-Type Cytochromes, *Biochemistry 33*, 15437-15448.

53. Peisach, J., Blumberg, W. E., Ogawa, S., Rachmilewitz, E. A., and Oltzik, R. (1971) The Effects of Protein Conformation on the Heme Symmetry in High Spin Ferric Heme Proteins as Studied by Electron Paramagnetic Resonance, *J. Biol. Chem. 246*, 3342-3355.

54. Beinert, H., and Shaw, R. T. (1977) On the Identity of the High Spin Heme Components of Cytochrome *c* Oxidase, *Biochim. Biophys. Acta 462*, 121-130.

55. Tuckerman, J. R., Gonzalez, G., Sousa, E. H. S., Wan, X., Saito, J. A., Alam, M., and Gilles-Gonzalez, M.-A. (2009) An Oxygen-Sensing Diguanylate Cyclase and Phosphodiesterase Couple for c-di-GMP Control, *Biochemistry 48*, 9764-9774.

56. Kurokawa, H., Lee, D. S., Watanabe, M., Sagami, I., Mikami, B., Raman, C. S., and Shimizu, T. (2004) A redox-controlled molecular switch revealed by the crystal structure of a bacterial heme PAS sensor, *J. Biol. Chem. 279*, 20186-20193.

57. Hirata, S., Matsui, T., Sasakura, Y., Sugiyama, S., Yoshimura, T., Sagami, I., and Shimizu, T. (2003) Characterization of Met^{95} mutants of a heme-regulated phosphodiesterase from *Escherichia coli*. Optical absorption, magnetic circular dichroism, circular dichroism, and redox potentials, *Eur. J. Biochem. 270*, 4771-4779.

58. Gonzalez, G., Dioum, E. M., Bertolucci, C. M., Tomita, T., Ikeda-Saito, M., Cheesman, M. R., Watmough, N. J., and Gillez-Gonzalez, M.-A. (2002) Nature of the displaceable heme-axial residue in the *Ec*Dos protein, a heme-based sensor from *Escherichia coli*, *Biochemistry 41*, 8414-8421.

59. Ishitsuka, Y., Araki, Y., Tanaka, A., Igarashi, J., Ito, O., and Shimizu, T. (2008) Arg97 at the Heme-Distal Side of the Isolated Heme-Bound PAS Domain of a Heme-Based Oxygen Sensor from *Escherichia coli* (*Ec* DOS) Plays Critical Roles in Autoxidation and Binding to Gases, Particularly O_2, *Biochemistry 47*, 8874-8884.

60. Chen, J.-J., and London, I. M. (1995) Regulation of protein synthesis by heme-regulated eIF-2[alpha] kinase, *Trends Biochem. Sci 20*, 105-108.

61. Ishikawa, H., Yun, B.-G., Takahashi, S., Hori, H., Matts, R. L., Ishimori, K., and Morishima, I. (2002) NO-Induced Activation Mechanism of the Heme-Regulated eIF2α Kinase, *J. Am. Chem. Soc. 124*, 13696-13697.

62. Igarashi, J., Murase, M., Iizuka, A., Pichierri, F., Martinkova, M., and Shimizu, T. (2008) Elucidation of the Heme Binding Site of Heme-regulated Eukaryotic Initiation Factor 2α Kinase and the Role of the Regulatory Motif in Heme Sensing by Spectroscopic and Catalytic Studies of Mutant Proteins, *J. Biol. Chem. 283*, 18782-18791.

63. Hirai, K., Martinkova, M., Igarashi, J., Saiful, I., Yamauchi, S., El-Mashtoly, S., Kitagawa, T., and Shimizu, T. (2007) Identification of Cys385 in the isolated kinase insertion domain of heme-regulated eIF2[alpha] kinase (HRI) as the heme axial ligand by site-directed mutagenesis and spectral characterization, *J. Inorg. Biochem. 101*, 1172-1179.

64. Uma, S., Yun, B.-G., and Matts, R. L. (2001) The Heme-regulated Eukaryotic Initiation Factor 2α Kinase: A Potential Regulatory Target For Control of Protein Synthesis by Diffusible Gases, *J. Biol. Chem. 276*, 14875-14883.

65. Reynolds, M. F., Parks, R. B., Burstyn, J. N., Shelver, D., Thorsteinsson, M. V., Kerby, R. L., Roberts, G. P., Vogel, K. M., and Spiro, T. G. (2000) Electronic absorption, EPR, and resonance Raman spectroscopy of CooA, a CO-sensing transcription activator from R. rubrum, reveals a five-coordinate NO-heme, *Biochemistry 39*, 388-396.

66. Kitanishi, K., Igarashi, J., Hayasaka, K., Hikage, N., Saiful, I., Yamauchi, S., Uchida, T., Ishimori, K., and Shimizu, T. (2008) Heme-Binding Characteristics of the Isolated PAS-A Domain of Mouse Per2, a Transcriptional Regulatory Factor Associated with Circadian Rhythms, *Biochemistry 47*, 6157-6168.

67. Tanaka, A., Takahashi, H., and Shimizu, T. (2007) Critical role of the heme axial ligand, Met^{95}, in locking catalysis of the phosphodiesterase from *Escherichia coli* (*Ec*DOS) toward cyclic diGMP, *J. Biol. Chem. 282*, 21301-21307.

Table 2.1. Comparison of electronic absorption peak positions (nm) for the CxxS *Bx*RcoM-2 variants with WT *Bx*RcoM-2 in the Fe(III), Fe(II) and Fe(II)CO states.

Electronic Absorption							
Fe(III)	**Ligands**	**δ**	**Soret**	**β**	**α**	**LMCT**	**Ref.**
WT *Bx*RcoM-2	Cys/His	354	423	541	565	640, 730	(*35*)
C130S[b]		356	422	539	561	640, 720	a
C127S[b]		354	422	537	562	648, 728	a
C94S[b]		sh[c]	418	532	561	640	a
C94S + ferricyanide		sh[c]	415	530	562	632	a
Fe(II)							
WT *Bx*RcoM-2	Met/His		425	532	562		(*35*)
C130S			425	532	562		a
C127S			424	532	562		a
C94S			425	532	562		a
C94S + ferricyanide			426	531	562		a
Fe(II)CO							
WT *Bx*RcoM-2	His/CO		423	540	570		(*35*)
C130S			423	540	569		a
C127S			423	539	568		a
C94S			423	540	570		a
C94S + ferricyanide			423	540	570		a

[a]This work. [b]This data is provided for the protein *as isolated*; the sample may contain a fraction of the Fe(II) form. [c]Shoulder.

Table 2.2. Comparison of EPR *g* values for the CxxS *Bx*RcoM-2 variants with WT *Bx*RcoM-2.

EPR						
Protein	Ligands	g_z	g_y	g_x		Ref.
WT *Bx*RcoM-2	His/Cys	2.52	2.28	1.88	pH 8.0	(*35*)
C130S[b] *Bx*RcoM-2		2.50	2.28	1.87	pH 7.4	a
C127S *Bx*RcoM-2		2.44	2.27	1.91	pH 7.4	a
		$g_{\perp}^{eff}$		$g_{\parallel}^{eff}$		
C94S[b] *Bx*RcoM-2		5.82		2.00	pH 7.4	a

[a]This work. [b]The spectrum was obtained after reaction of the as-isolated protein with ferricyanide.

Figure 2.1. Electronic absorption spectra of purified a) WT *Bx*RcoM-2, b) C130S *Bx*RcoM-2, c) C127S *Bx*RcoM-2, d) C94S *Bx*RcoM-2 and e) C94S *Bx*RcoM-2 reacted with potassium ferricyanide. Spectra of samples a-d were taken of the protein as isolated; the spectrum of sample e was taken after oxidation of the protein with potassium ferricyanide and removal of excess oxidant via a spin concentrator. The samples contained 8-10 μM heme in 25 mM MOPS with 500 mM KCl, pH 7.4, at 25 °C.

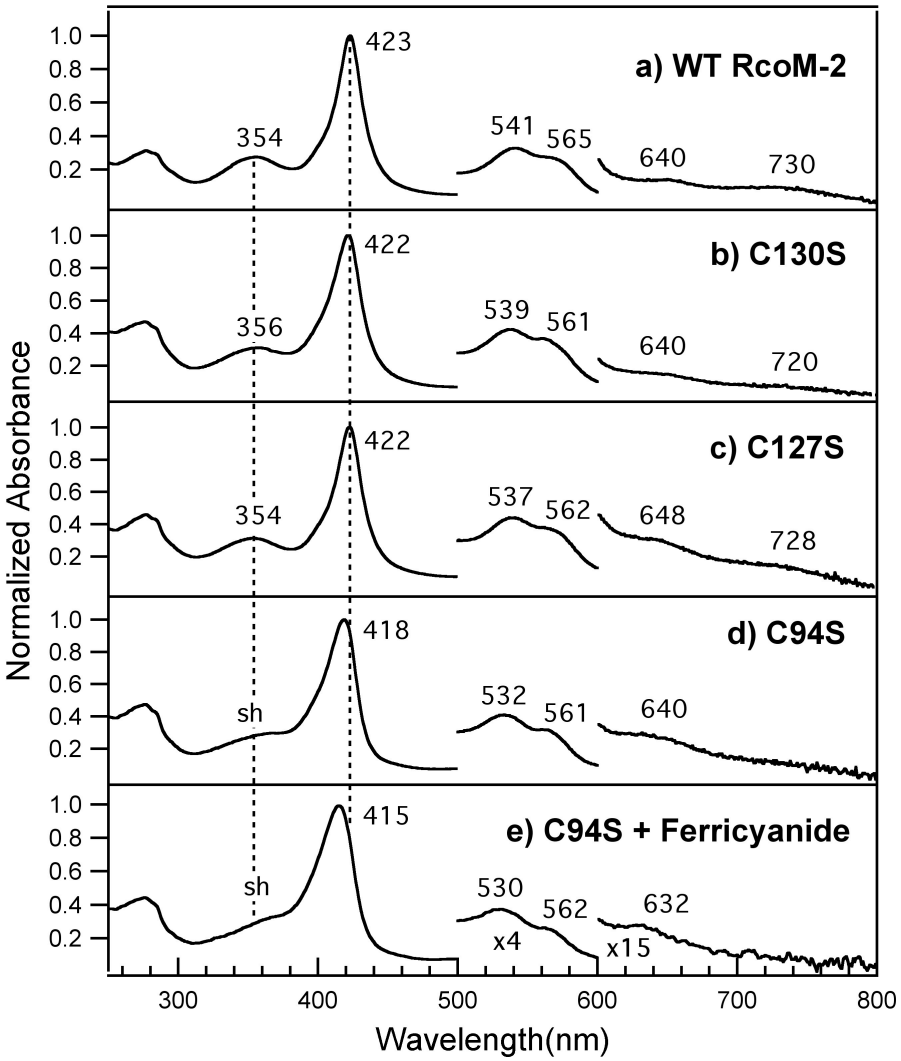

Figure 2.2. Electronic absorption spectra of a) Fe(II) WT *Bx*RcoM-2, b) Fe(II) C130S *Bx*RcoM-2, c) Fe(II) C127S *Bx*RcoM-2 and d) Fe(II) C94S *Bx*RcoM-2 as isolated. The samples contained 8-10 μM heme in 25 mM MOPS with 500 mM KCl, pH 7.4, at 25 °C.

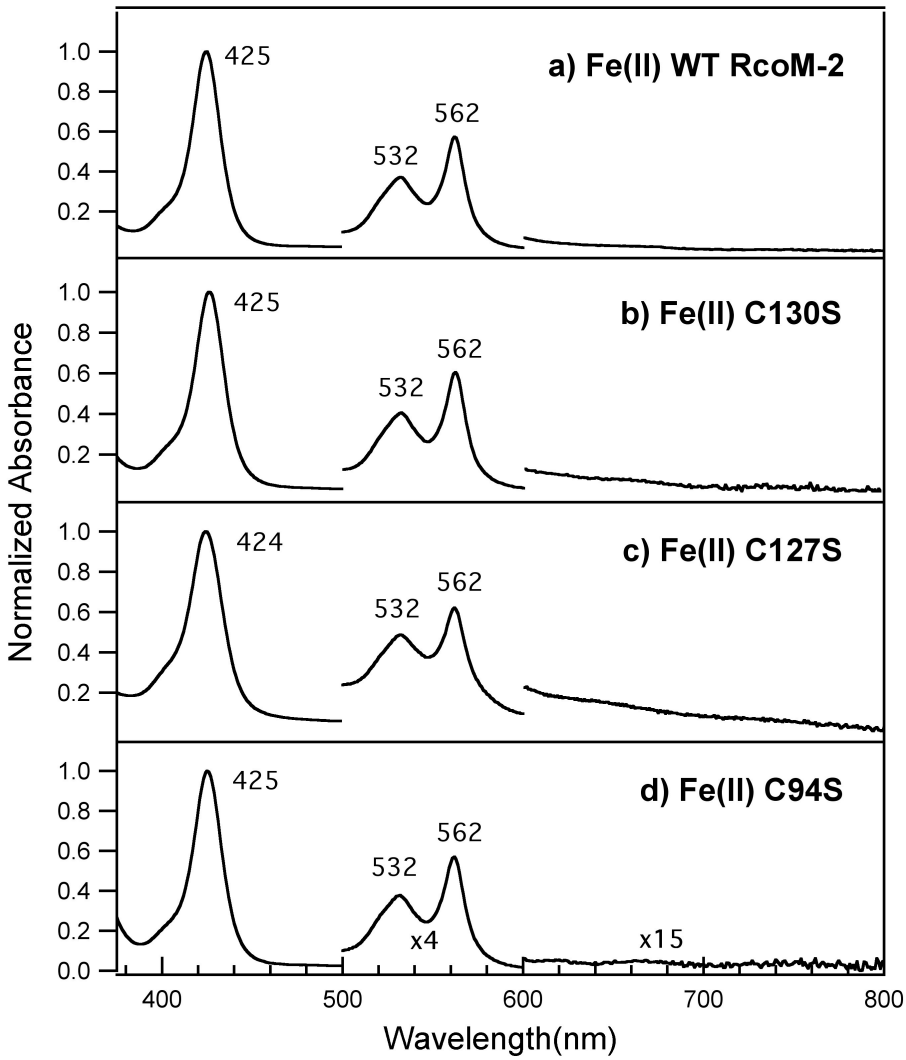

Figure 2.3. Electronic absorption spectra of a) Fe(II)-CO WT *Bx*RcoM-2, b) Fe(II)-CO C130S *Bx*RcoM-2, c) Fe(II)-CO C127S *Bx*RcoM-2 and d) Fe(II)-CO C94S *Bx*RcoM-2 as isolated. The samples contained 8-10 μM heme in 25 mM MOPS with 500 mM KCl, pH 7.4 at 25 °C.

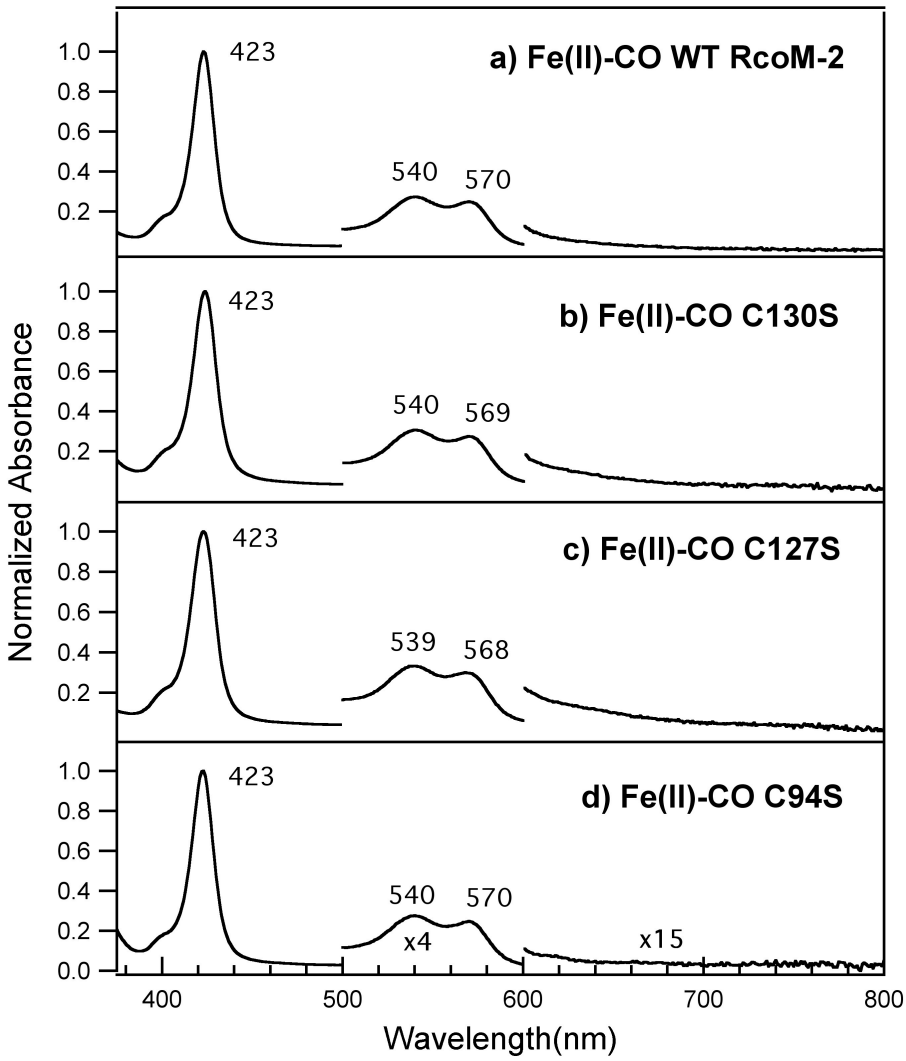

Figure 2.4. Resonance Raman spectra of a) WT Fe(III) *Bx*RcoM-2 compared to b) C130S *Bx*RcoM-2, c) C127S *Bx*RcoM-2 and d) C94S *Bx*RcoM-2 as isolated. Samples contained 80-170 μM heme in 25 mM MOPS with 500 mM KCl, pH 7.4. Spectra were acquired with 8-15 mW of power at the frozen (77 K) sample using the 413.1 nm Kr^+ laser line. Key porphyrin stretching modes are noted, including major oxidation and spin state marker bands (ν_2, ν_3, ν_4 and ν_{10}) and the putative Fe-S stretch band ($\nu_{Fe\text{-}S}$).

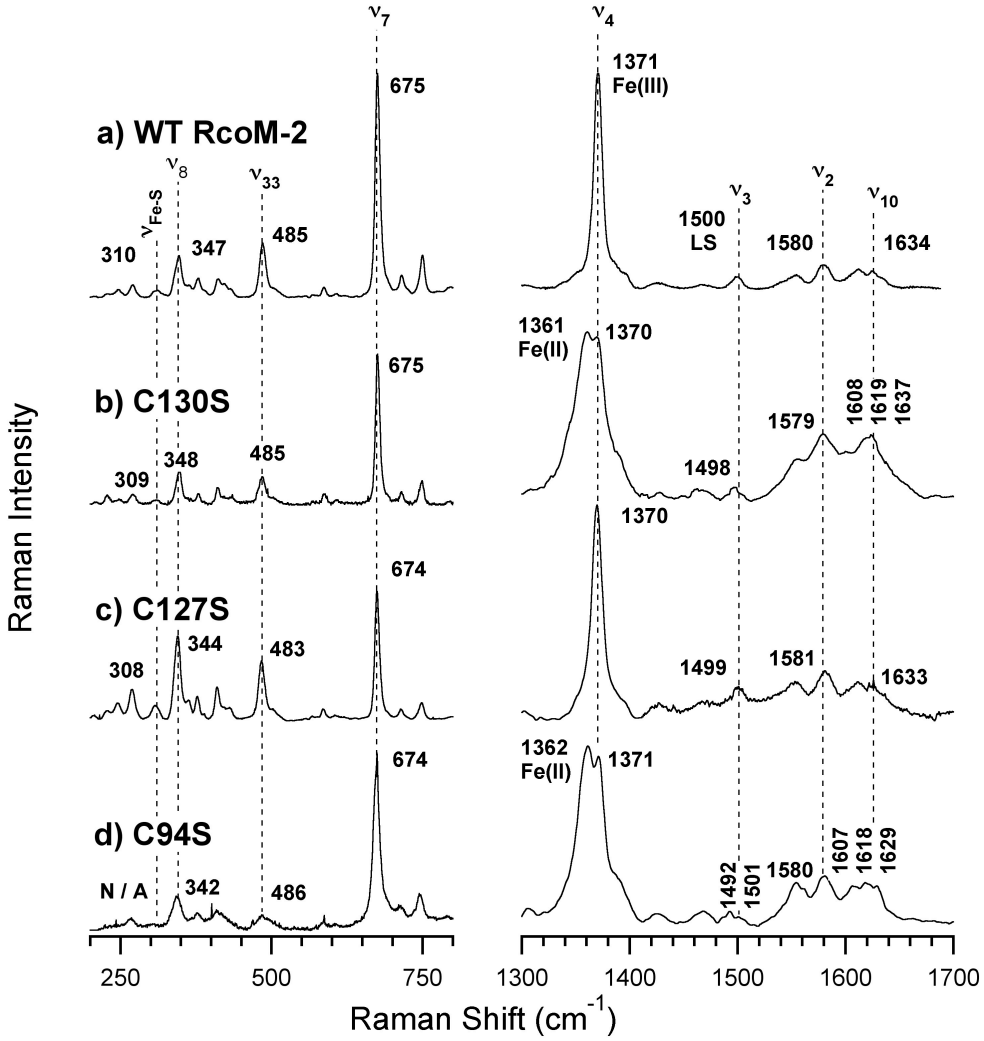

Figure 2.5. Resonance Raman spectra of a) WT Fe(III)*Bx*RcoM-2 compared to b) C130S *Bx*RcoM-2 reacted with potassium ferricyanide, c) C127S *Bx*RcoM-2 and d) C94S *Bx*RcoM-2 reacted with potassium ferricyanide. Samples contained 80-170 μM heme in 25 mM MOPS with 500 mM KCl, pH 7.4. Spectra were acquired with 8-15 mW of power at the frozen (77 K) sample using the 413.1 nm Kr^+ laser line. Key porphyrin stretching modes are noted, including major oxidation and spin state marker bands (ν_2, ν_3, ν_4 and ν_{10}) and the putative Fe-S stretch band ($\nu_{Fe\text{-}S}$).

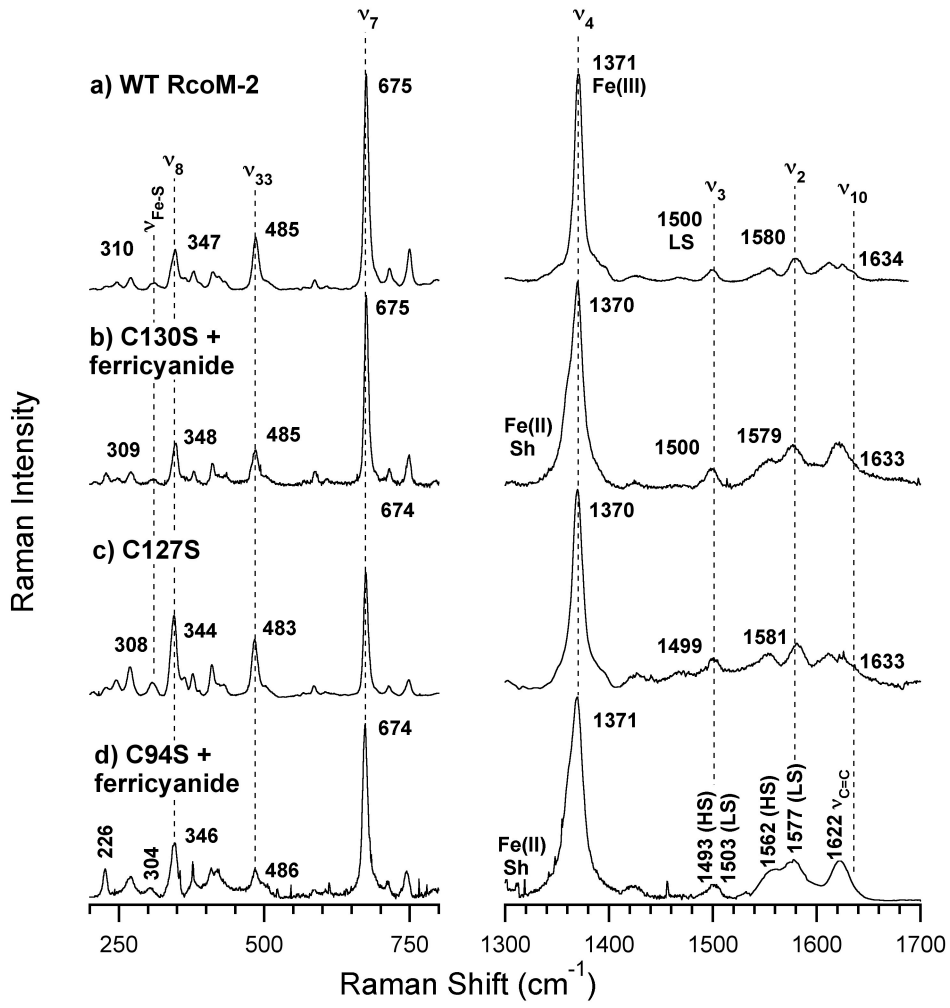

Figure 2.6. Low frequency resonance Raman spectra of a) WT Fe(III)*Bx*RcoM-2 compared to b) C130S *Bx*RcoM-2 reacted with potassium ferricyanide, c) C127S *Bx*RcoM-2 and d) C94S *Bx*RcoM-2 reacted with potassium ferricyanide. Samples contained 80-170 μM heme in 25 mM MOPS with 500 mM KCl, pH 7.4. Spectra were acquired with 8-15 mW of power at the frozen (77 K) sample using the 413.1 nm Kr^+ laser line. Key stretching modes are noted, including the Gaussian deconvolution of the putative Fe-S stretch band, $\nu_{Fe\text{-}S}$, the overlapping porphyrin mode, ν_{Por}, and the putative $\nu_{Fe\text{-}His}$ stretch. Peak positions are indicated for the putative porphyrin stretching mode ν_{Por} that overlaps with $\nu_{Fe\text{-}S}$.

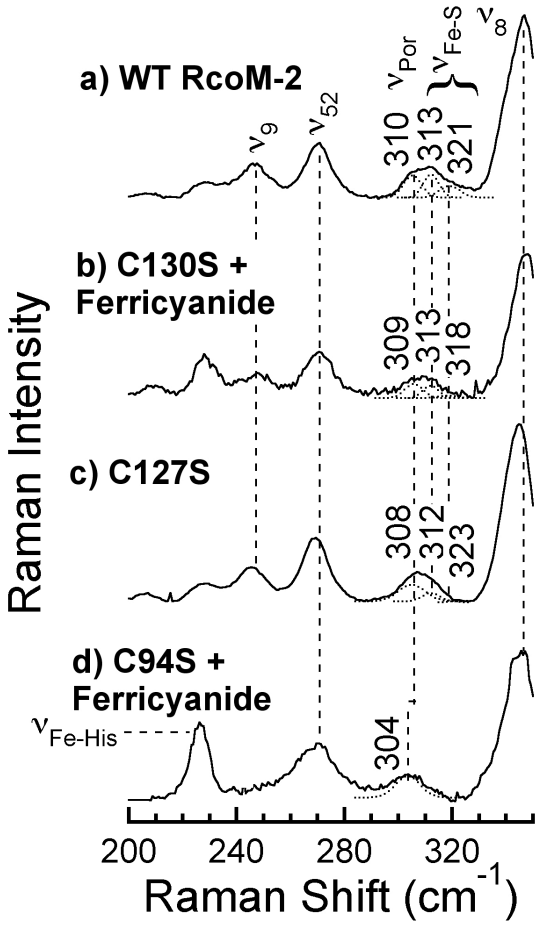

Figure 2.7. X-band EPR spectra of a) WT Fe(III)*Bx*RcoM-2 compared to b) C130S *Bx*RcoM-2 reacted with ferricyanide, c) C127S *Bx*RcoM-2 and d) C94S *Bx*RcoM-2 reacted with ferricyanide. Sample concentrations were 80-250 μM heme in 25 mM MOPS with 500 mM KCl, pH 7.4, except for WT Fe(III)*Bx*RcoM-2, which was originally recorded at pH 8.0 (*35*). The spectra were recorded at 10 K, 9.38 GHz microwave frequency, < 5 mW microwave power, 65 dB receiver gain, 8.00 G modulation amplitude, 100 kHz modulation frequency, 81.92 ms time constant and used 20 added scans, each containing 2048 data points, except for: a) 9.36 GHz microwave frequency, 8.31 G modulation amplitude, 163.84 ms time constant; c) 9.36 GHz microwave frequency, 8.31 G modulation amplitude, 10 averaged scans; d) 10.02 mW microwave power. A minor rhombic EPR signal of unknown origin is indicated with (*).

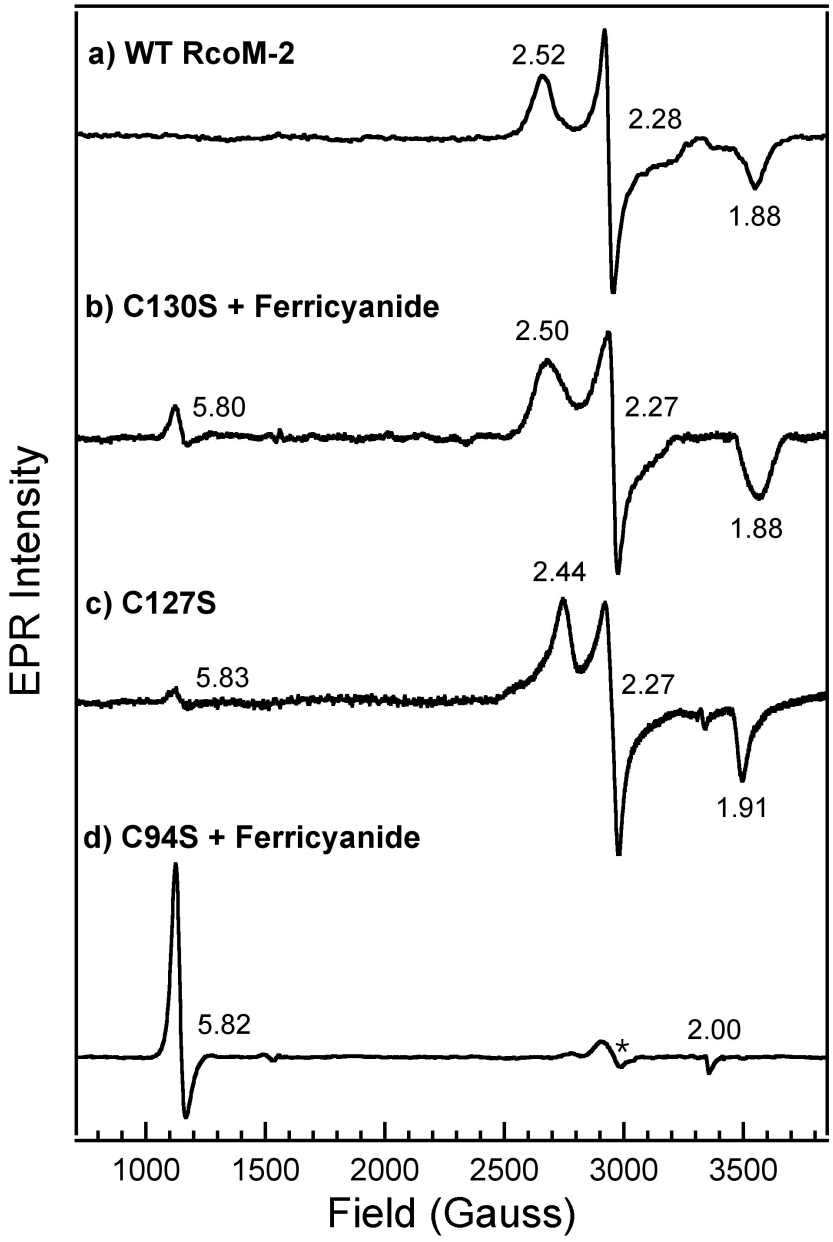
a) WT RcoM-2
2.52
2.28
1.88
b) C130S + Ferricyanide
2.50
5.80
2.27
1.88
c) C127S
2.44
5.83
2.27
1.91
d) C94S + Ferricyanide
5.82
2.00
*
EPR Intensity
1000
1500
2000
2500
3000
3500
Field (Gauss)

Figure 2.8. Sequence alignments of *B. xenovorans* RcoM-1 (UniProt accession no. Q13YL3; NCBI gi:123168453) and -2 (UniProt accession no. Q13IY4; NCBI gi:122969446) with two putative RcoM proteins from *B. cepacia* H160 (UniProt accession no. B5WBI7) and *B. cepacia* CH1-1 (UniProt accession no. D5NG05). All Cys residues are boxed in black; the appropriate numbering is indicated above an inverted arrow (⮟). The alignments show high amino-acid identity conservation among all sequences, including complete conservation of Cys^{94} and Cys^{130}, but not Cys^{127}.

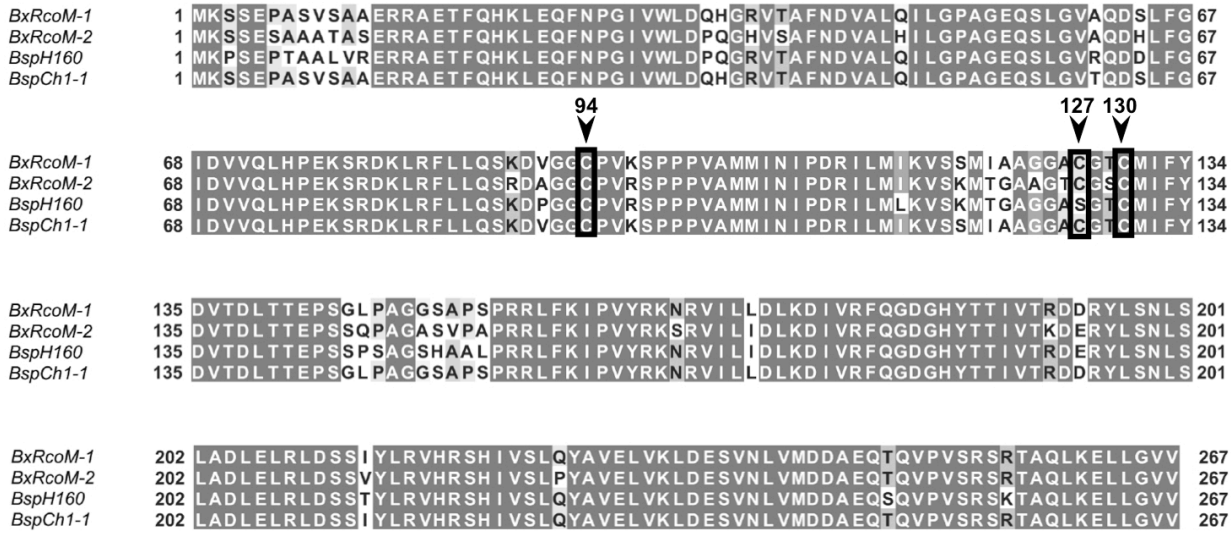

Scheme 2.1. Pictorial depiction of the varying heme coordination environments in *Bx*RcoM. Reduction of the Fe(III) heme to Fe(II) results in loss of the cysteine(thiolate) ligand (Cys^{94}) which is replaced by a nearby methionine (Met^{104}). Introduction of CO results in replacement of the weakly-bound Fe(II) distal Met^{104} ligand to form a carbon-monoxy adduct. In all states, the proximal ligand is a histidine (His^{74}) that is retained.

Burkholderia xenovorans RcoM

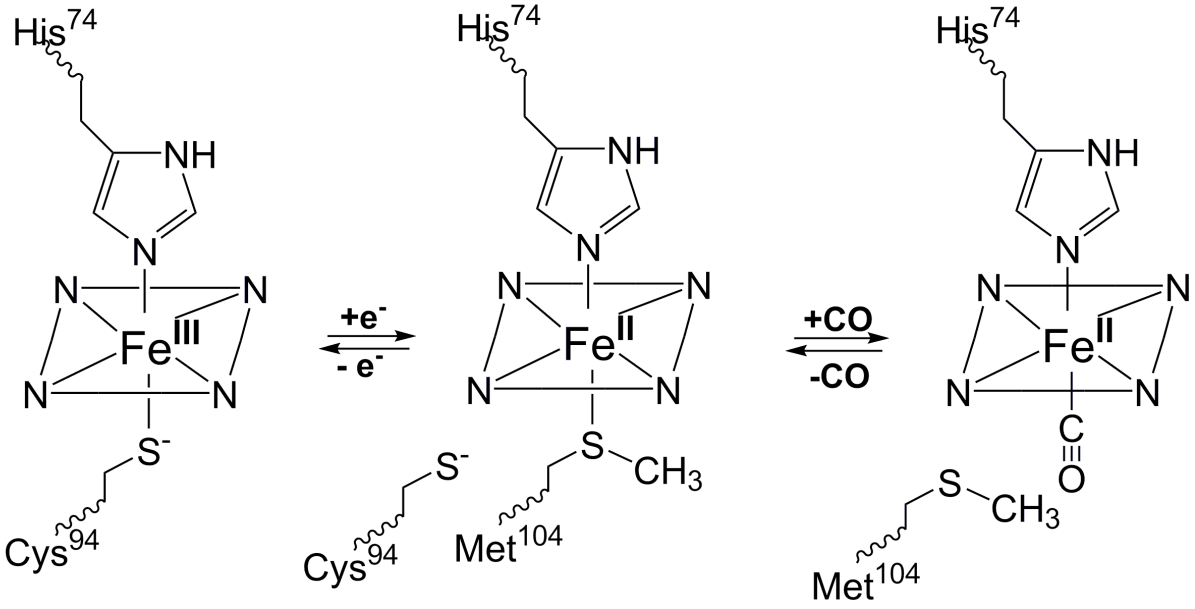

Chapter Three

Characterization of the DiGeorge Critical Region 8 Heme-Protein Interaction

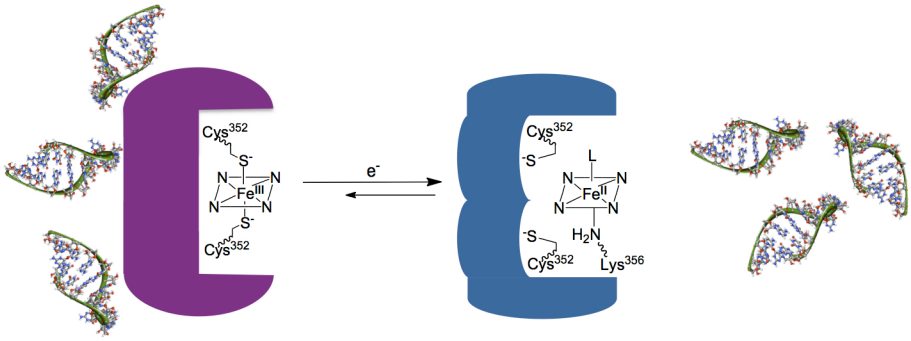

Versions of this chapter were published as:

Barr, I.; Smith, A. T.; Senturia, R.; Chen, Y.; Scheidemantle, B. D.; Burstyn, J. N.; Guo, F. *J. Biol. Chem.* **2011**, *286*, 16716-16725.

Barr, I.; Smith, A. T.; Chen, Y.; Senturia, R.; Burstyn, J. N.; Guo, F. *Proc. Natl. Acad. Sci. USA* **2012**, *109*, 1919-1924.

All DGCR8 expression, purification, and miRNA processing activity assays were performed by Ian Barr in the laboratory of Professor Feng Guo at the University of California at Los Angeles.

Introduction

MicroRNAs (miRNAs) are a type of small, noncoding RNA (approximately 20-22 nucleotides long) that function as gene regulators (*1*). They are evolutionarily widespread and are utilized in systems as complex and multicellular as humans (*1, 2*) as well as those as simple as viruses (*3*). miRNAs specifically function by targeting messenger RNAs (mRNAs) of many protein-encoding genes and may repress protein translation by binding directly to the 3' untranslated region (UTR) of a target mRNA (*4*). Alternatively, miRNAs may interfere elsewhere on the mRNA and trigger RNA degradation (*4*). Anywhere from 10-50% of all protein-encoding genes are estimated to be regulated by miRNAs (*1, 5*); these estimates reveal the importance of miRNAs in gene regulation.

miRNAs are produced from long RNA transcripts through a process that requires multiple enzyme complexes and multiple steps, both in the nucleus and the cytoplasm (Scheme 3.1). The first step requires the generation of the primary miRNA transcript (pri-miRNA) via RNA polymerase in the nucleus; these pri-miRNAs, which can be up to thousands of nucleotides long, form stem-loop structures of double-stranded pri-miRNAs (*6*). The pri-miRNA stem-loop structure is recognized by the RNase enzyme Drosha and the double-stranded RNA-binding protein Di George Critical Region 8 (DGCR8, also know as Pasha in flies and worms). Collectively, this association of proteins is called the Microprocessor complex and is responsible for cleaving the pri-miRNAs into approximately 65 nucleotides long hairpin-like intermediates known as precursor miRNAs (pre-miRNAs) (*6-8*). These pre-miRNAs are then recognized by the GTP-dependent transporter exportin-5 (Expt5) and exported into the cytoplasm (*9-11*) where they encounter the protein multicomplex consisting of the RNase Dicer, the TAR RNA-binding protein (TRBP) and the protein activator of the

interferon-induced protein kinase (PACT) (*4, 12, 13*). Once processed into mature miRNAs, they can then be incorporated into the RNA-induced silencing complex (RISC) to block protein translation (*4, 14, 15*).

Recent studies have indicated that at least one protein involved in miRNA processing, the nuclear double-stranded RNA-binding (dsRB) protein DGCR8, associates with heme (*16*). In humans, DGCR8 is a large, multi-domain protein that consists of 773 amino acids (Figure 3.1). These domains include: an N-terminal domain responsible for nuclear localization, a dimerization domain that contains a unique W-W motif, a heme-binding domain (HBD) and two C-terminal dsRB domains (*16*). A crystal structure of the dimerization domain, including a portion of the apo HBD, exists and reveals the use of a novel W-W interaction to promote oligomerization; furthermore, the structure reveals an open pocket in which heme likely binds, a requirement for the presence of Trp^{329} for successful heme binding, and an unusual set of two Cys residues (Cys^{352} from each monomer) conspicuously placed with their sidechains near one another in the apo HBD (*17*). C352A and C352H variants have successfully established the requirement for Cys^{352} as an essential residue for heme binding (*16*). Additionally, the presence of Cys^{352} and heme appear to be necessary for controlling the oligomeric status of DGCR8 as well as for upregulating pri-miRNA processing via the DGCR8-Drosha complex (*16, 18*).

In this report, we spectroscopically characterize the heme-protein interaction of DGCR8. We show that DGCR8 natively binds a low-spin, six-coordinate Fe(III) heme *b* molecule using a heretofore unseen bis(Cys) ligation motif, which is characterized by a unique hyperporphyrin electronic absorption spectrum and a high kinetic stability. We show that reduction of Fe(III) DGCR8 to Fe(II) DGCR8 is accompanied by ligand switching and results in loss of each Cys ligand bound to the heme iron atom. The Fe(II) DGCR8 is an ad-mixture of

both five- and six-coordinate high- and low-spin heme, respectively, relatively labile, and highly pH-sensitive. Importantly, Fe(III), not Fe(II), heme activates the DGCR8-Drosha complex for pri-miRNA processing, revealing the importance of the ferric heme-DGCR8 interaction in the regulation of miRNA processing. Furthermore, we show that both $CO_{(g)}$ and $NO_{(g)}$ are able to bind to Fe(II) DGCR8 and form six- and five-coordinate gas adducts, respectively, neither of which retains Cys(thiolate) coordination to the heme. We speculate that both the $CO_{(g)}$- and $NO_{(g)}$-bound forms of the Fe(II) DGCR8-Drosha complex are likely inactive in pri-miRNA processing due to ligand switching at the DGCR8 heme, which may initiate large protein conformational changes.

Materials and Methods

Materials. Materials used in buffer preparation and glycerol were purchased from Sigma-Aldrich and used as received. Sodium dithionite ($Na_2S_2O_4$) was purchased from Fluka and stored under $Ar_{(g)}$ at -20 °C until used. $HgCl_2$ solutions were made fresh for each experiment from solid $HgCl_2$ (J.T. Baker, Inc.). $CO_{(g)}$ was obtained from AGA and used as received. $NO_{(g)}$ was generated *in situ* by mixing $NaNO_2$ (Sigma-Aldrich), $CuCl_2$ (MCB Chemicals), and *L*-ascorbic acid (99+%, Sigma-Aldrich) with a previously prepared buffer solution.

Protein Isolation and Purification. The frog DGCR8 HBD-His_6 (AAs 278-498) was expressed as purified as previously described (*19, 20*). Briefly, the *Escherichia coli* cells from strain BL21(DE3) CodonPlus (Stratagene) bearing a kanamycin-resistant pET 24a(+) plasmid were cultured 6-8 hours until the small scale expression reached an OD_{500} ~ 0.5 in the presence of 50 μg/mL kanamycin. New medium was inoculated with this small-scale expression culture, and protein expression was induced by addition of stock isopropyl β-D-1-thiogalactopyranoside (IPTG) to 1 mM (final concentration) in the presence of 1 mM (final concentration) δ-aminolevulinic acid (ALA). Cells were harvested after overnight growth and lysed by sonication. The separated cell supernatant was purified using Ni-affinity chromatography followed by size-exclusion chromatography. The purified DGCR8 HBD was exchanged into the desired buffers, as indicated in the figure legends, using centrifugal concentrators with a 30 kDa molecular-weight cutoff (MWCO). Globally SeMet-labeled frog DGCR8 HBD-His_6 was expressed using the same vector as described in (*21*). Briefly, *E. coli* were cultured in M9 minimal medium lacking Met. Six other AAs that inhibit Met biosynthesis were added to the cell culture approximately 15 min prior to induction. Additionally, 40 μM $FeCl_3$ and 1 mM

ALA were added to the medium to increase heme biosynthesis. SeMet-labeled DGCR8 HBD-His_6 was expressed at 25°C overnight; it was subsequently purified using the same procedure as the native protein. SeMet incorporation was analyzed by comparison to native DGCR8 HBD-His_6 using MALDI-TOF mass spectrometry.

Reconstituted pri-miRNA Processing Assays. The pri-miRNA assays were performed as previously described (*19, 20*) and adapted for anaerobic conditions. Briefly, reaction solutions containing recombinant Drosha-His_6 (AAs 390-1374) and the appropriate DGCR8 constructs, as indicated in the figure legends, were prepared in an anaerobic chamber under $N_{2(g)}$. Either oxidized or prereduced heme was added to the appropriate protein solutions and mixed. Samples were transferred anaerobically from the chamber, and the ^{32}P-labeled pri-miRNA was injected anaerobically using a gas-tight syringe. These reactions were incubated at 37°C for 45 min; 2x RNA loading dye containing 1x TBE (a solution of 89 mM Tris, 89 mM boric acid, 2 mM EDTA, pH 8.3), 10 M urea, 10 mM EDTA, and 0.0002% (v:v) xylene cyanol was added to stop the reaction. The samples were then analyzed using radiography of 15% polyacrylamide gels, which contained 7 M urea.

Electronic Absorption Spectroscopy. Electronic absorption spectra were recorded on a double-beam Varian Cary 4 Bio spectrophotometer with a temperature controller, set to a spectral bandwidth of 0.5 nm. Spectra were obtained at varying temperatures (20 to 37 °C) and varying pHs (6.0 to 11.0), as indicated, in 50 mM buffer with an additional 400 mM NaCl. Reduction of Fe(III) protein samples was accomplished by adding an anaerobically prepared stock solution of sodium dithionite, to achieve a final sample concentration of reductant of 1-5 mM. Samples

(with and without 10% (v:v) glycerol) were purged of oxygen by flowing $Ar_{(g)}$ through the headspace of a septum-sealed cuvette for ~10 min. The solutions of dithionite and Fe(III) protein were allowed to equilibrate at the indicated sample temperature before anaerobic addition of stock reductant (~30 mM, 10 μL) to the Fe(III) protein. Reduction of Fe(III) to Fe(II) was monitored over ~1 h or until no further spectral changes were observed. Fe(II) titration curves were generated by plotting the apparent molar absorptivity at 424 nm (ε_{424}) versus pH. Data were fit to a modified version of the Henderson-Hasselbalch equation:

$$\varepsilon_{424} = \frac{\varepsilon_{7.4} + \varepsilon_{11.0} \times 10^{pH - pKa}}{1 + 10^{pH - pKa}} \quad (1)$$

where $\varepsilon_{7.4}$ represents the apparent molar absorptivity at the lowest pH unit (7.4) and where $\varepsilon_{11.0}$ represents the apparent molar absorptivity at the highest pH unit (11.0). The apparent value of the pK_a was fit to the above equation using a non-linear least-squares analysis with a goodness-of-fit value > 0.99. Reaction of Fe(III) protein with $HgCl_2$ was accomplished by addition of a stock solution of ~ 1 mM Hg^{2+} to give 1- or 2-eqs (Hg^{2+}:heme) in a final sample volume of 300 μL; the new solution was then mixed thoroughly by vortexing before the spectrum was recorded. Fe(II)-CO adducts were made by direct anaerobic addition of $CO_{(g)}$ to pre-reduced Fe(II) protein samples followed by gentle mixing until no more spectral changes were observed. NO adducts were prepared by injecting three 100 μL samples of $NO_{(g)}$ (generated by mixing $NaNO_2$, $CuCl_2$, *L*-ascorbic acid, and 1 mL of EPPS stock buffer solution) to the headspace of a septum-sealed vial containing the pre-reduced Fe(II) form of the protein. The sample solution was subject to gentle mixing, and the reaction was followed spectrophotometrically at room temperature until no further changes were observed.

MCD Spectroscopy. Magnetic circular dichroism (MCD) spectra were recorded on a Jasco J-715 CD spectropolarimeter with the sample compartment modified to accommodate an SM-4000-8T magnetocryostat (Oxford Instruments). The buffer used for the MCD samples was 50 mM EPPS, 400 mM NaCl, pH 8.0, with approximately 60% (v/v) glycerol present in the final sample. Glycerol was introduced to the Fe(III) form of the protein and stirred with a syringe until the solution was homogeneous. Fe(II) and Fe(II)-CO samples were prepared from glycerol-containing Fe(III) protein solutions, with monitoring of the visible spectral changes at 37 °C after anaerobic addition of a solution of sodium dithionite or sodium dithionite and $CO_{(g)}$, respectively. The final concentrations were typically: dithionite, ~7 mM; protein, ~29 μM in a total volume of 150 μL. Glycerol had no effect on the peak maxima of the electronic absorption spectra at room or liquid-helium temperatures unless otherwise noted. Samples were transferred via gastight syringe into cells purged with $Ar_{(g)}$, flash-frozen and stored in $N_{2(l)}$. MCD spectra were taken over a temperature range from 2.5 to 100 K. The MCD signal at each temperature was recorded at ±7 T. Negative polarity data were subtracted from positive polarity data to remove CD contributions and the resulting spectrum was divided by 2.

EPR Spectroscopy. X-band electron paramagnetic resonance (EPR) spectra were collected on a Bruker ELEXSYS E500 equipped with an Oxford ESR 900 continuous flow liquid helium cryostat and an Oxford ITC4 temperature controller. The microwave frequency was monitored using an EIP model 625A CW microwave frequency counter. Protein samples were prepared as indicated in the figure legends. Samples were transferred to a quartz EPR tube via small-bore tubing (connected to a gas-tight syringe) and frozen in $N_{2(l)}$. Samples of 150 μL had a final

concentration of ~ 100-150 μM, as noted. For all samples, scans of 0 - 10,000 Gauss revealed no signals other than those reported.

Resonance Raman Spectroscopy. Resonance Raman (rR) spectra were obtained with an excitation wavelength of either 413.1 nm from a Coherent I-302C Kr^+ laser or 457.9 nm from a Coherent I-305 Ar^+ laser in a backscattering 135° sample geometry. An Acton Research triple monochromator was used with a gratings of 2400 grooves/mm. Low incident laser powers of ≤ 20 mW were focused with a cylindrical lens onto the sample. A Princeton Instruments Spex 1877 triple spectrograph outfitted with a cooled, intensified diode array detector was operated under computer control using Spectrasense software. Samples were prepared in 50 mM EPPS buffer at 8.0 with an additional 400 mM NaCl and 10% (v:v) glycerol. Reduction of Fe(III) to Fe(II) was monitored spectrophotometrically (*vide supra*) after addition of a stock solution of sodium dithionite in an $Ar_{(g)}$-purged cuvette. Samples were transferred anaerobically in an $Ar_{(g)}$-purged chamber to a quartz EPR tube via small-bore tubing (connected to a gas-tight syringe), capped and stored on ice. Samples of ~ 150 μL had a final concentration range of ~ 130 – 150 μM. Samples were placed in a quartz Dewar filled with ice water to reduce local heating. Peak positions were calibrated relative to a Na_2SO_4 peak at 981 cm^{-1}. IGOR Pro software (Wavemetrics, Inc.; Lake Oswego, OR) was used to import and process all spectral data. Major vibrational modes are assigned based on comparison with those of other heme proteins and the work of Spiro and Kitagawa (*22-24*).

Results

The Electronic Absorption Spectrum of Fe(III) DGCR8 Displays Unique Spectral Characteristics.

The electronic absorption spectrum of DGCR8 displays a unique hyperporphyrin spectrum unprecedented for native heme proteins. As isolated, the electronic absorption spectrum of DGCR8 has two Soret (γ) $\pi \rightarrow \pi^*$ transitions of nearly equivalent intensity, one blue-shifted (366 nm) and one red-shifted (451 nm), a broad α/β region at 557 nm, and a weak LMCT transition region at 660 nm (Figure 3.2A). The nearly equivalent intensity and strongly split nature of the two Soret bands constitutes a hyperporphyrin spectrum (*25*); this unusual optical spectrum arises from either the presence of two strongly-donating Lewis bases, such as Cys (mercaptide), Met (thioether) or phosphine, bound axially to an Fe(III) heme, or the presence of one strongly-donating Lewis base, most commonly Cys, bound axially *trans* to $CO_{(g)}$ ligated to an Fe(II) heme. That the α/β region of the DGCR8 electronic absorption spectrum is asymmetric and broad suggests that the oxidation state of the heme present is low-spin Fe(III) and not Fe(II) or Fe(II)-$CO_{(g)}$ bound (*26*). Comparison of the Fe(III) DGCR8 absorption spectrum to that of ligand-bound chloroperoxidase and cytochrome $P450_{CAM}$, which each bear a Cys(thiolate)-ligated heme *b*, to which exogenous thiols, thioethers, and phosphines have been added (Table 3.1), readily reveals a similarity. In fact, the electronic absorption spectrum of Fe(III) DGCR8 is most similar to the electronic absorption spectrum of Fe(III) chloroperoxidase to which exogenous phosphines or free thiols have been added. While the reductant dithiothreitol (DTT) is used in the purification of DGCR8, it is important to note that the unusual hyperporphyrin spectrum of Fe(III) DGCR8 is still present when DGCR8 is isolated and purified in the absence of DTT, indicating that exogenous thiols do *not* interact

with DGCR8 (data not shown). Taken together, these comparisons suggests that DGCR8 binds an Fe(III) heme ligated endogenously by two sulfur-containing amino acids, such as Cys or Met.

DGCR8 Binds an Fe(III) Heme Using Two Endogenous Cys Ligands.

Magnetic circular dichroism (MCD) spectroscopy confirms that DGCR8 binds a six-coordinate, low-spin Fe(III) heme, and suggests that the two ligands to the heme are each Cys residues. The 4 K MCD spectrum of DGCR8 is shown in Figure 3.2B and is dominated by an intense, temperature-dependent *C* term corresponding to the transitions that underlie the red-shifted Soret at 451 nm with peak-crossover-trough positions of 433-438-448 nm, respectively. The second most-intense MCD feature is that of the *C* term corresponding to the transitions that underlie the blue-shifted Soret at 367 nm with peak-crossover-trough positions of 347-371-391 nm, respectively. The temperature- and field-dependence of the most intense MCD feature at 448 nm was monitored (Figure 3.2B, inset) and showed an overlapping, curved nature characteristic of a low-spin Fe(III) ion coupled with the porphyrin $\pi \rightarrow \pi^*$ transitions; the intense MCD features at 347 nm and 474 nm were also monitored for their temperature- and field-dependence and displayed overlapping, curved natures, indicative that the MCD features arise from a homogenous sample (data not shown). The peak-crossover-trough positions of the Soret MCD features may be used as diagnostics for the ligation state of the iron atom (*27, 28*). While bis(Cys) or Cys/Met ligation has not been natively encountered, models of this ligation type have been studied with MCD spectroscopy by the binding of exogenous thiols, thioethers, and phosphines (a thioether mimic) to chloroperoxidase and $P450_{CAM}$ (*29, 30*). While similarities exist between the electronic absorption and MCD spectra of Fe(III) DGCR8 and thiol- or phosphine-bound Fe(III) $P450_{CAM}$, the greatest similarity is between the electronic

absorption spectrum of Fe(III) DGCR8 and the Fe(III) chloroperoxidase-thioacetic acid (TAA) adduct (Table 3.1). To compare the MCD signatures, we generated the TAA-adduct of Fe(III) chloroperoxidase by incubation of TAA with that of chloroperoxidase before mixing with glycerol and freezing. However, whereas DGCR8 was unaffected by the presence of glycerol, the TAA-adduct of chloroperoxidase appeared to generate two distinct species in the presence of glycerol, as evidenced by two distinct peak-crossover-trough positions 418-425-430 nm and 430-441-453 nm (data not show), indicative of two Soret bands. This observation implies that glycerol induces a change in the nature of the TAA-chloroperoxidase adduct, likely due to a change in protonation. Nevertheless, the similarity of the Fe(III) TAA-chloroperoxidase peak-crossover-trough position to that of the red-shifted Soret MCD signature of Fe(III) DGCR8 suggests a bis(Cys) heme ligation motif in the native DGCR8 protein.

Reaction of Fe(III) DGCR8 with $HgCl_2$ further supports the conclusion that the Fe(III) heme in DGCR8 is bound by two sulfur-containing residues. With its soft and polarizable nature, Hg^{2+} is known to bind tightly to sulfur-containing compounds and to disrupt metal-thiolate bonds (*31-33*). Figure 3.3 shows the electronic absorption spectrum of Fe(III) DGCR8 before and after the addition of 1 and 2 molar eqs. of $HgCl_{2(aq)}$. While the addition of 1 molar eq. of $Hg^{2+}_{(aq)}$ appears to generate a mixture of species, 2 molar eqs. convert the characteristic hyperporphyrin spectrum to a new spectrum with a broad Soret band at 383 nm, an indiscernible α/β region, and a strong LMCT transition at 625 nm, which, taken together, are indicative of high-spin Fe(III) heme (*25*). Futher reaction of Fe(III) DGCR8 $HgCl_2$ resulted in no change of the electronic absorption spectrum until millimolar concentrations of $Hg^{2+}_{(aq)}$ were reached, upon which the protein precipitated, presumably due to structural disruption. These observations suggest that reaction of Fe(III) DGCR8 with 2 molar eqs. of $Hg^{2+}_{(aq)}$ disrupts each

sulfur-containing Lewis base coordinated to the Fe(III) heme, resulting in ligand displacement with a concomitant spin-state crossover. That 2 eqs. of $Hg^{2+}_{(aq)}$ are needed for full conversion of the electronic absorption spectrum strongly implies that Fe(III) DGCR8 possesses either a bis(Cys) or a mixed Cys/Met ligation motif.

Electron paramagnetic resonance (EPR) spectroscopy further supports the oxidation- and spin-state assignments of Fe(III) DGCR8 and confirms that Cys, not Met, ligates to the Fe(III) heme in both axial positions. Scans of 0-10,000 G (data not shown) revealed only a narrow signal centered ~2900 G; shorter scans revealed a tight, rhombic signal characteristic of low-spin Fe(III) (Figure 3.4) with three *g* values: $g_z = 2.60$; $g_y = 2.27$; and $g_x = 1.84$. This observation further confirms the previous oxidation and spin-state assignments; additionally, the narrow spacing of the *g* values is characteristic of a six-coordinate, Cys(thiolate)-ligated Fe(III) heme (*34*). Comparison of the EPR *g* values of Fe(III) DGCR8 with those of Fe(III) $P450_{CAM}$ and Fe(III) chloroperoxidase ligand complexes (Table 3.2) reveals a similarity with the TAA-, β-mercaptoethanol- (BME), and bis(hydroxymethyl)methyl phosphine-adducts of chloroperoxidase, further suggesting the presence of either a bis (Cys) or mixed Cys/Met ligation motif in Fe(III) DGCR8. This observation is supported by analysis of the calculated crystal field parameters of tetragonality (Δ/λ, degree of electronic donation at the iron center) and rhombicity (*V*/Δ, degree of geometric distortion of the iron center), which places Fe(III) DGCR8 in the same region as native ferric chloroperoxidase in the Blumberg-Peisach "truth" diagrams (*35*), in closest proximity to Fe(III) chloroperoxidase thiol adducts such as TAA and BME and the Fe(III) chloroperoxidase bis(hydroxymethyl)methyl phosphine adduct (Figure 3.5) (*36, 37*), further suggesting bis(Cys) or Cys/Met ligation to the Fe(III) DGCR8 heme. Binding of Met as the sixth heme axial ligand was conclusively ruled out by SeMet

substitution. Given the large difference in spin-orbit coupling between S and Se, SeMet-ligated Fe(III) hemes are expected to show large changes in their spectral features. Analysis of a globally SeMet-substituted form of DGCR8 revealed no change in the sign or position of MCD spectral features compared to WT and identical EPR *g* values compared to WT (data not shown). That the MCD and EPR spectra of the two proteins are the same argues that Met is not the sixth ligand to the heme in DGCR8. Taken all together, these data reveal that DGCR8 is, to our knowledge, the first-known hemoprotein that ligates an Fe(III) heme *b* using two endogenous Cys ligands.

Reduction of Fe(III) DGCR8 Is Accompanied by Ligand Switching.

Upon addition of sodium dithionite to Fe(III) DGCR8, a complex and pH-dependent process takes place to form Fe(II) DGCR8. Figure 3.6A illustrates the resulting electronic absorption spectrum after addition of 10 μL of a stock solution of sodium dithionite and reaction for 60 min at pH 8.0 and 37°C. The intensity of the Fe(III) 451 nm Soret is immediately reduced with a concomitant broadening accompanied by the formation of a shoulder at 424 nm. Over time, the broad peak at 451 nm is lost and a new, sharper Soret is seen at 424 nm. This loss of the Soret at 451 nm is accompanied by a loss of the broad absorption envelope at ~ 557 nm characteristic of the ferric α/β region; two new, distinct peaks are formed at 527 nm and 558 nm, characteristic of β and α bands of an Fe(II) heme, respectively. However, this process is not isosbestic, indicating that multiple species and/or intermediates are formed during the reduction process. The apparent rate of reduction is quite slow at room temperature and may be increased upon elevation of temperature. This observation may suggest some sort of conformational change that takes place in addition to heme reduction. Additional support for a possible conformational change is garnered upon

observation that the presence of glycerol greatly reduces the apparent reduction rate. An increase in overall viscosity (as provided by glycerol), would be expected to slow a conformational rearrangement but would not be expected to slow electron transfer. That the observed spectroscopic changes are slow, temperature dependent and are non-isosbestic led us to believe multiple species and/or a conformational change may occur upon formation of Fe(II) DGCR8.

Upon complete reduction at pH 8.0, Fe(II) DGCR8 exists as a mixture of spin and coordination states. The relatively low molar absorptivity of the Fe(II) DGCR8 Soret at pH 8.0 (ε_{424}~55 $mM^{-1}cm^{-1}$) as well as the broad α/β region is uncommon for a homogeneous, low-spin Fe(II) six-coordinate heme. Consequently, we used MCD and rR spectroscopies to interrogate the nature of the ferrous heme in DGCR8. Figure 3.6B illustrates the MCD spectra (4-50 K) of the ferrous DGCR8 heme at pH 8.0. The α/β region of the Fe(II) DGCR8 MCD spectra is dominated by a derivative-shaped, temperature-independent *A*-term with a crossover position of 558 nm (α band), consistent with the presence of a six-coordinate, low-spin, Fe(II) heme. However, the Soret region of the Fe(II) DGCR8 MCD spectrum is dominated by an inverted *C*-term with trough-crossover-peak positions of 422-431-442 nm, consistent with the presence of a five-coordinate, high-spin Fe(II) heme. Additionally, the magnetic saturation behavior of the most intense peak of the *C*-term, 442 nm (Figure 3.6B, inset), taken at 2.5 K, 4.0 K, 8.0 K, 15 K and 25 K has a characteristic shape and non-overlapping nature that further confirms the presence of high-spin, S=2, Fe(II) heme. In MCD spectroscopy of heme proteins, paramagnetic ($S \neq 0$) species dominate the spectrum at low temperature (<50 K) while at high temperature (≥50 K), the paramagnetic temperature dependence is minimized. At 50 K, the MCD spectrum of Fe(II) DGCR8 shows greater intensity in the Soret *C*-term than the *A*-terms in the α/β region,

suggesting that there is a greater amount of high-spin Fe(II) heme than low-spin Fe(II) heme at pH 8.0. Furthermore, the electronic absorption and MCD peak positions and intensities of Fe(II) DGCR8 do not match those of thiolate-bound Fe(II) human cystathionine β-synthase or thiol-bound Fe(II) myoglobin H93G, suggesting that neither Cys is bound to the Fe(II) heme of DGCR8 (Table 3.3) (*38, 39*).

The observation that the Fe(II) heme in DGCR8 exists as a mixture of spin states at pH 8.0 is further confirmed by rR spectroscopy. The high-energy region of the rR spectrum of heme is dominated by porphyrin in-plane vibrations and is sensitive to oxidation, spin and ligation states of the central iron atom; of particular interest are the readily identified oxidation, spin and ligation state bands ν_2, ν_3, ν_4 and ν_{10}. Figure 3.7B compares these bands for Fe(III) (•••) and Fe(II) (—) DGCR8 at pH 8.0. The most intense band, ν_4, is the well-known oxidation state marker band and is particularly sensitive to the core size of the porphyrin; there is a dramatic down-shift in energy from 1372 cm^{-1} to 1358 cm^{-1} of this band consistent with the reduction of Fe(III) to Fe(II) heme (*22, 23*). The most prominent spin and coordination state marker band, ν_3, shifts from 1501 cm^{-1} and is split between 1470 cm^{-1} (high-spin, five-coordinate) and 1489 cm^{-1} (low-spin, six-coordinate) (*23, 40*), implicating a mixture of spin and coordination states for the Fe(II) DGCR8 heme. At higher energy, the bands ν_2 and ν_{10} overlap with other porphyrin vibrations so their assignment is less robust; however, the positions of 1579 cm^{-1} and 1615 cm^{-1} are consistent with other Fe(II) heme proteins that have mixed coordination and ligation states (*23, 40, 41*). Taken all together, these data suggest that the DGCR8 Fe(II) heme exists as a mixture of spin and coordination states at pH 8.0, and that neither Cys ligand is retained upon reduction of the heme iron.

Lys^{356} Likely Binds to the Fe(II) DGCR8 heme.

The electronic absorption, MCD and rR spectra suggest that an N-bearing amino acid (likely Lys) coordinates in at least one position to the Fe(II) DGCR8 heme. The native Fe(III) form of the DGCR8 heme is ligated by two cysteines (Cys^{352}); while the exact protonation state of each cysteine residue bound to the Fe(III) DGCR8 heme is unknown, it is clear that a cysteine(thiolate) is not bound to the Fe(II) DGCR8 heme judging by the lack of a Soret peak maximum at ~ 450 nm (*42*). Thus, we initially considered that a neutral thiol were bound to the Fe(II) DGCR8 heme. While the binding of thiols to the ferrous H93G mutant of Mb produces a mixture of spin states like that Fe(II) DGCR8, the electronic absorption and MCD peak positions and intensitites of thiol-bound Fe(II) H93G Mb did not match those of Fe(II) DGCR8, suggesting that a thiol was not bound to the ferrous DGCR8 heme (*39*). Additionally, binding of a thioether side chain from Met was ruled out as no changes in peak positions and/or intensities of the Fe(II) electronic absorption and rR specta were seen for a globally SeMet-substituted form of DGCR8 (data not shown). Thus, we considered that either an N- or O-donor may ligate in at least one position to the Fe(II) DGCR8 heme upon displacement of the endogenous Fe(III) Cys^{352} ligands.

The sensitivity of the electronic absorption spectrum of Fe(II) DGCR8 to pH suggested that a Lys may ligate to the Fe(II) heme. Upon increasing the pH of the Fe(II) DGCR8 species, it was noted that the molar absorptivities of the Soret, α and β peaks all increased (Figure 3.8). The sharpening and increase in molar absorptivities of these peaks indicated a possible spin-state crossover event (from high spin to low spin) occurring. Electronic absorption spectroscopy demonstrated that this spin-state transition occurred with an apparent pK_a of 9.1 ± 0.1 (Figure 3.8, inset). This observation was further confirmed by rR spectroscopy (Figure 3.9). At pH 7.4, the two most prominent spin and coordinate state marker bands (ν_3 and ν_2) indicated

a mixture of five-coordinate high-spin and six-coordinate low-spin Fe(II) heme; upon raising the pH to 10.0, these bands shifted from 1468 cm^{-1} to 1490 cm^{-1} and from 1560 $cm^{-1}$to 1580 cm^{-1} (ν_3 and ν_2, respectively) indicating a shift from high spin (S=2) to low spin (S=0) Fe(II) heme (Figure 3.9, Δ pH 10.0 – 7.4), and a conversion from a mixed five- and six-coordinate Fe(II) heme to complete conversion to a six-coordinate Fe(II) heme. Because of protein instability, the frog HBD of Fe(II) DGCR8 at pH < 7.2 could not be explored. Recent data on a longer DGCR8 construct called NC1 (Figure 3.1), which is most stable at pH 6.0, displayed an Fe(II) electronic absorption spectrum most similar to four-coordinate, intermediate spin heme (S=1) (Table 3.3); however, the exact nature of this DGCR8-Fe(II) heme interaction at low pH has yet to be explored (*20*). Nevertheless, while the pK_a of the R group of an amino acid may be heavily influenced by factors such as relative hydrophobicity of the region in the protein and/or ligation to a metal, this apparent pK_a of 9.1 is most likely possible for amino the acid side chains of Cys, Arg and Lys (*43*). Cys was ruled out as ligating to the Fe(II) heme, as a transition from thiol to thiolate would result in a Soret peak maximum at ~450 nm (*vide supra*). Arg also seemed unlikely do to the lack of an Arg in proximity of the ligating Fe(III) Cys^{352} residue. However, it was observed that a number of Lys residues were located in the proximity of the Fe(III) Cys ligand (Figure 3.10B), making Lys an excellent candidate for ligation to the Fe(II) DGCR8 heme. In fact, the sequence of amino acids LHYKKM to the C-terminus of Cys^{352} was predicted to have alpha helical secondary structure (Figure 3.10B). While no crystal structure of the complete DGCR8 HBD exists, the predicted alpha helical nature of this region would place a Lys residue (Lys^{356}) on the same side of the alpha helix as that of the endogenous Fe(III) Cys^{352} ligand. Additionally, a weak rR band was seen upon increasing pH (Figure 3.9, panel A, inset) in the low energy region of the Fe(II) DGCR8 rR spectrum at ~ 272 cm^{-1}. This

region is particularly sensitive to metal-ligand vibrations that are coupled into porphyrin vibrational modes. Typical Fe(II) ν(Fe-His) vibrations range from ~ 200-230 cm^{-1} and increase in intensity upon formation of a higher percentage of five-coordinate species (*44-47*). Here the trend appears to be the opposite (i.e. increase in the presence of this mode upon greater formation of the six-coordinate species); moreover, the much higher frequency of vibration (272 cm^{-1}) would be expected for an amine bound to a methylene group (such as Lys) rather than the more rigid and heavier imidazole side chain of His.

That Lys may ligate to the Fe(II) DGCR8 heme is further supported by comparison to other characterized Fe(II) heme proteins. A ferrous bis(methylamine) adduct of H93G Mb was generated that illustrated very similar Soret, α and β peak positions as that of Fe(II) DGCR8 (424 nm, 527 nm and 559 nm vs. 424 nm, 527 nm and 558 nm, H93G and DGCR8, respectively) (Table 3.3) (*48*). While these peak positions are also similar to bis(His)-ligated ferrous cytochrome b_5, the position of the *C*-term of Fe(II) DGCR8 is more similar to that of the position of the *C*-term of bis(methylamine) ligated ferrous H93G Mb than ferrous cyt. b_5 (*48*). Additional pH-dependent behavior similar to Fe(II) DGCR8 is seen in both ferrocytochrome *f* (N-terminal amino/His ligation) and a M100K variant of ferrocytochrome *c*-550 (Lys/His ligation) (*49, 50*). rR spectra of Fe(II) cyt. *f* and M100K cyt. *c*-550 correlated the position of a particular porphyrin vibrational band, ν_{11}, to the degree of σ donation of the Fe(II) axial ligand(s). Whereas His/His and His/Met ligated ferrocytochromes display ν_{11} frequencies ~ 1540-1547 cm^{-1}, N-term and/or Lys ligation downshifts this frequency to ~1532-1540 cm^{-1} (*51*). In Fe(II) DGCR8, this mode is slightly obscured by ν_{38} at pH 8.0; however, it becomes more resolved at pH 10.0 at 1539 cm^{-1}, within the range for possible Lys ligation, implicating Lys or a terminal amine as a ligand to the Fe(II) DGCR8 heme. EXAFS data on thermally-

treated Fe(II) cystathionine β-synthase (CBS-424), which also bears a mixture of high-spin and low-spin Fe(II) heme, implicated N/N or N/O ligation to the Fe(II) heme, with at least one of the units being best modeled as a rigid His unit, with the other unit hypothesized to be solvent, Arg (having both an amine and an imine moiety) or an amide backbone (*52*). Coincidentally, Fe(II) CBS-424 also displays electronic absorption and MCD peak positions almost identical to that of Fe(II) DGCR8, implicating a similar ligation motif (*53*). Finally, a variant of the $CO_{(g)}$ sensor CooA, L116K, was shown to have an Fe(II) Lys/His ligation motif with an electronic absorption spectrum similar to that of Fe(II) DGCR8 (*54*). Taken together, these results suggest that the primary amine of at least one Lys residue ligates to the Fe(II) heme of DGCR8.

Fe(III), not Fe(II), Heme Activates DGCR8 for primary microRNA Processing.

Reduction of Fe(III) DGCR8 to Fe(II) is accompanied by loss of primary microRNA (pri-miRNA) processing. Incubation of low (1-2 μM) concentrations of Fe(III) NC1, a longer DGCR8 construct capable of associating with pri-miRNAs (Figure 3.1), with sodium dithionite at pH 8.0 resulted in similar spectral changes as those that occurred with the frog HBD (data not shown), indicating that similar redox-mediated ligand switching occurred during the reduction of NC1. Due to the increased lability of the high-spin Fe(II) heme in NC1, we were able to remove the heme of NC1 after incubation of Fe(II) NC1 with that of apoMb and subjecting the mixture to anaerobic size-exclusion chromatography (SEC); this method generated ~90% apoNC1, as evidenced by the increase of the A_{280}/A_{450} ratio of 2.8 to 27 (*20*). Pri-miRNA processing activity assays of apoNC1 incubated with the nuclease Drosha and either ^{32}P-labeled pri-miRNA 30a or 21 (Figure 3.10) clearly indicate that pri-miRNA processing is abrogated in the presence of apoNC1. The residual processing activity evidenced is likely due to the small fraction (<10%) of holoNC1 still present after reduction, incubation

with apoMb, and SEC. Importantly, reconstitution of apoNC1 with Fe(III) heme restores both the characteristic hyperporphyrin spectrum associated with the bis(Cys) ligation of the Fe(III) DGCR8 heme (data not shown), and the pri-miRNA processing activity; however, reconstitution of apoNC1 with Fe(II) heme, while it restores the characteristic reduced Soret at 424 nm, does not rescue pri-miRNA processing activity (Figure 3.10). These results indicate that ferric, not ferrous, heme activates DGCR8 for pri-miRNA processing.

Fe(II) DGCR8 is Capable of Binding $CO_{(g)}$ and $NO_{(g)}$.

Reaction of Fe(II) DGCR8 HBD with $CO_{(g)}$ results in a six-coordinate, low-spin Fe(II) $CO_{(g)}$-ligated heme. Addition of $CO_{(g)}$ to a pre-reduced sample of Fe(II) DGCR8 results in a sharpened Soret band at 420 nm and a symmetric set of β and α bands at 539 nm and 567 nm, respectively (Figure 3.11). The positions of these bands are similar to other low-spin, six-coordinate Fe(II) hemoproteins that bind $CO_{(g)}$ trans to a neutral, nitrogenous Lewis bases, such as His or Lys (Table 3.4). This observation is further supported by the temperature-independent MCD spectrum of Fe(II)-$CO_{(g)}$ DGCR8, which is dominated by two *A* terms with crossovers at 419 nm (Soret) and 567 nm (α band), similar to other previously-characterized Fe(II)-$CO_{(g)}$ hemoproteins (*55-57*). The lack of a characteristic Soret band at ~450 nm upon $CO_{(g)}$ binding reinforces the hypothesis that reduction of the DGCR8 heme is accompanied by loss of both Cys residues (*30, 58*). Furthermore, the lack of spectral perturbation of the Fe(II)-$CO_{(g)}$ adduct of the globally SeMet-substituted form of DGCR8 (data not shown) suggests that Met does not bind *trans* to $CO_{(g)}$. That the electronic absorption spectrum of Fe(II)-$CO_{(g)}$ DGCR8 is so similar to other His-ligated Fe(II)-$CO_{(g)}$ hemoproteins may suggest that Lys^{356} binds *trans* to $CO_{(g)}$ in DGCR8.

Reaction of Fe(II) DGCR8 HBD with $NO_{(g)}$ results in a five-coordinate, low-spin Fe(II)-$NO_{(g)}$ heme, whereas reaction of Fe(III) DGCR8 HBD with $NO_{(g)}$ results in no changes (data not shown). Addition of $NO_{(g)}$ to a pre-reduced sample of Fe(II) DGCR8 results in a broadened Soret band at 390 nm and broad α/β region with a maximum at 539 nm (Figure 3.12). The positions of the Soret and α/β regions are strongly suggestive of the formation of a five-coordinate Fe(II)-$NO_{(g)}$ heme (Table 3.5). This suggestion was confirmed by analysis of the nitrosylated species by EPR spectroscopy, which showed a characteristic three-lined signal centered around $g = 2.05$ (Figure 3.13). While a small amount of oxidized Fe(III) DGCR8 was present, as evidenced by a weak rhombic signal centered $g = 2.27$, there was virtually no overlap with the signal of the NO adduct. The five-coordinate Fe(II) $NO_{(g)}$-ligated species has a distinct three-lined spectrum due to the coupling of the unpaired electron with that of the single $I = 1$ ^{14}N nucleus that derives from the $NO_{(g)}$ molecule (*34*). While the apparent symmetry of the spectrum appears to be axially, best agreement of simulation and experiment is arrived upon by use of three distinct g values; these simulated values for DGCR8 are $g_1 = 2.010$, $g_2 = 2.053$, and $g_3 = 2.087$ with a hyperfine coupling constant $A_3 = 16.2$ G. These simulated values are in excellent agreement with other five-coordinate Fe(II)-$NO_{(g)}$ hemoproteins (Table 3.6). Interestingly, alterations in pH of the Fe(II) $NO_{(g)}$-ligated species resulted in no evidence for the formation of a six-coordinate NO adduct, suggesting that changes in the donor strength of the Fe(II) heme ligand Lys^{356} cannot overcome the strong *trans* influence of the $NO_{(g)}$ molecule. Experiments utilizing rR are currently underway to determine the local environment of the CO- and NO-adducts of Fe(II) DGCR8. Furthermore, pri-miRNA processing activities are being designed to assess the effects of $CO_{(g)}$ and $NO_{(g)}$ on the ability of DGCR8 to interact with Drosha and/or attenuate miRNA processing.

Discussion

The interaction with and influence of heme and RNA, either directly or indirectly, has been shown for a number of systems. Heme has been known to affect its own biosynthesis in plants, bacteria, and archae by indirect interaction with transfer RNA (tRNA) (*59*). For example, heme functions as part of a negative feedback loop to control the synthesis of the heme precursor δ-aminolevulinic acid (ALA), the first committed step in heme biosynthesis, either through interaction with the glutamic acid tRNA-charging enzyme glutamyl-tRNA synthetase (GluTS) (*59-61*) or the Glu-$tRNA^{Glu}$ reducing enzyme glutamyl tRNA reductase (GluRS) (*61-63*). The binding of heme to either of these two enzymes appears to cause conformational changes that suppress their activity (*61, 62*); in at least one case, this conformational change appears to make the enzyme more susceptible to degradation via proteolysis (*64*). Thus heme is able to regulate its own production. In a similar manner, heme has been implicated in interactions with at least two other tRNA synthetases, Trp-tRNA synthetase (*65*) and Arg-tRNA synthetase (*66*), although the functional implications are not currently known. Heme has also been discovered to interact directly with RNA through hydrophobic and π-stacking type interactions. Strands of RNA that are guanine (G) rich form self-assemblies called quadruplexes. These assemblies provide hydrophobic and π-rich systems that provide "landing pads" onto which heme may associate (*67*). These heme-RNA complexes (as well as heme-DNA complexes) have been shown to function as effective 1- and 2-electron oxidation catalysts *in vitro* (*68-70*). While the *in vivo* function of these complexes is still debatable, it is speculated that these direct RNA-heme interactions may represent sources of oxidative damage in cells during times of high oxidative stress, thus contributing to disease (*67*).

The discovery that heme is involved in miRNA processing further expanded the list of indirect interactions that heme has with RNA. Heme has been shown to interact with the dsRNA-binding protein DGCR8 (*16*). Together with its RNase partner Drosha, DGCR8 is part of the Microprocessor complex that recognizes and processes pri-miRNAs as one of the preliminary steps in miRNA biogenesis (Scheme 3.1) (*7, 8*). Studies have shown that the binding of heme to DGCR8 increases the cooperativity with which DGCR8 binds to dsRNA, although it is unknown if heme-binding initiates a conformational change in DGCR8 (*18*). Nevertheless, this increase in cooperativity is thought to be one of the modes by which heme-loaded DGCR8 upregulates the processing of pri-miRNAs (*18*).

In this study, we have characterized the heme-protein interaction of DGCR8, and how changes in this interaction influence the ability of DGCR8 to upregulate pri-miRNA processing, the results of which are summarized in Scheme 3.2. Previous reports implicated Cys^{352} as an important residue for heme binding (*16, 17*). We have shown that, as isolated, the electronic absorption, MCD and EPR spectral signatures are associated with a unique ligation motif that is consistent with a bis(Cys) ligation in the axial positions of a six-coordinate Fe(III) heme *b* in homodimeric DGCR8. We surmise that both of these ligands are Cys^{352}, each of which is supplied from one of the DGCR8 monomers. Previous reports have also demonstrated that this heme-protein complex is extremely kinetically stable, with a $t_{½} > 4$ days (*19*). We have shown the reduction of the DGCR8 heme, from Fe(III) to Fe(II), decreases this stability by generating a labile complex, which is a mixture of five-coordinate, high-spin and six-coordinate, low-spin Fe(II) heme. This oxidation state change is accompanied by heme ligand-switching, which presumably contributes to the lowered heme-protein affinity. Importantly, reduction of the heme iron is also accompanied with loss of the ability of DGCR8 to upregulate

pri-miRNA processing. We speculate that the lengthy time of heme reduction is accompanied by conformational changes in the DGCR8 polypeptide, which ligand-switching may initiate. This speculation is partially supported by the observation that Fe(II) DGCR8 appears to bind pri-miRNAs with reduced cooperative. Furthermore, a conformational change may contribute to the decreased stability of the Fe(II) heme-DGCR8 complex. We also show that Fe(II) DGCR8 can interact with $CO_{(g)}$ and $NO_{(g)}$ to form six-coordinate and five-coordinate species, respectively; however, the impact of these biologically important gases on pri-miRNA processing is currently unknown.

The unique heme-protein interaction of DGCR8 has implications for the function of heme in miRNA processing. First, the unusual bis(Cys) Fe(III) ligation motif, with its high kinetic stability, is likely a specific rather than adventitious interaction. While the value for K_D, a measure of the thermodynamic stability, is unknown for this complex, it has been estimated to be $< \sim 1x10^{-15}$ M, since there is no observed heme transfer to ApoMb (*19*). Further support for this specificity argument is garnered from: 1) the observation that reconstitution of ApoDGCR8 with heme consistently regenerates the same hyperporphyrin optical spectrum associated with bis(Cys) ligation, suggesting that heme rebinds in the HBD; and 2) the observance of upregulation of pri-miRNA processing in the presence of reconstituted DGCR8. Second, the strongly electron-donating bis(Cys) ligation motif likely drives the heme reduction potential highly negative, making the Fe(III)|Fe(II) reduction process unfavorable. While there are no known reduction potentials for any bis(Cys)-ligated heme *b* model complexes, reduction potentials are known for the six-coordinate Cys/His and Cys/Pro ligated heme *b* proteins cystathionine β-synthase and CooA. These proteins have Fe(III)|Fe(II) potentials of -350 mV and -320 mV, respectively (*52, 71*). The substitution of the nitrogenous ligand (His or Pro) for

a second Cys (a more strongly-donating ligand, especially in its anionic thiolate form), would be expected to drive the reduction potential further negative, likely bringing the reduction potential closer to the -550 mV reduction potential of the Tyr/His ligated heme *b* scavenger HasA, which has the lowest reported heme *b* Fe(III)|Fe(II) potential (*72*). This comparison suggests that the Fe(III) form of DGCR8 is likely the physiologically-relevant oxidation state *in vivo*. Thus, there is a third implication that, while the Fe(II) oxidation state is accessible in the presence of sodium dithionite ($\mathcal{E}^\circ$ = -660 mV) (*73*), if the physiologically relevant oxidation state is likely Fe(III), the heme in DGCR8 does not function as a gas sensor. The binding of $CO_{(g)}$ to heme occurs obligatorily in the Fe(II) oxidation state, although autoreduction of Fe(III) hemoproteins in the presence of high concentrations of $CO_{(g)}$ has been observed (*74*); the binding of $NO_{(g)}$ to heme may occur in the Fe(III) or Fe(II) oxidation states (*75*), but it is clear that $NO_{(g)}$ only binds to the DGCR8 heme in the Fe(II) form (*vide supra*). Therefore, the DGCR8 does not appear to be a target for redox or gas regulation.

We currently favor the theory that DGCR8 may function as a heme sensor *in vivo*. The specific delivery of Fe(III) heme to DGCR8 may function as a metabolic signal for upregulation of miRNA processing. The observation that there is only weak pri-miRNA processing in the absence of heme or in the presence of Fe(II) heme supports this model. How this interaction may be regulated, however, is unknown. The increase in RNA-binding cooperativity in the presence of Fe(III) heme may suggest a conformational change of the DGCR8 polypeptide takes place upon heme binding (*18*). This conformational change may make DGCR8 more susceptible to proteolysis, similar to the mode of heme-based regulation in Glu-$tRNA^{Glu}$ reductase (*64*). Interestingly, a recent study has shown that DGCR8 is susceptible to cleavage by the apoptosis-related protease caspase. One mapped cleavage site is located near

an important loop in the HBD; proteolysis results in loss of heme binding, dissociation of the dimer interface, and a loss of pri-miRNA binding cooperativity (*76*). Perhaps heme binding to DGCR8 causes a burst of miRNA upregulation before DGCR8 is subject to degradation. Further investigation will be needed to explain the exact mode of heme-based regulation in miRNA processing.

Conclusion

In this study, we have demonstrated that the heme-protein interaction in DGCR8 is unique. We have used electronic absorption, MCD and EPR spectroscopies to show that, as-isolated, DGCR8 binds an Fe(III) heme *b* molecule using a novel bis(Cys) ligation motif. This unusual binding mode contributes to the specificity and kinetic stability of the Fe(III) heme-DGCR8 interaction. Based on electronic absorption, MCD and rR studies, we demonstrate that reduction of the heme iron is accompanied by ligand switching in which both Cys^{352} ligands are lost and replaced by two new, neutral ligands, one of which is presumed to be Lys^{356}. Importantly, we show that Fe(II) DGCR8 binds pri-miRNAs with reduced cooperativity, causing pri-miRNA processing to be abrogated. Furthermore, we find that Fe(II) DGCR8 binds $CO_{(g)}$ and $NO_{(g)}$ to form six-coordinate and five-coordinate species, respectively, neither of which maintain Cys ligation; based on these findings, we speculate that the gas-bound forms of DGCR8 are also incapable of upregulating pri-miRNA processing. Taken together, these results suggest that DGCR8 may function as a ferric heme sensor *in vivo*.

References

1. Krol, J., Loedige, I., and Filipowicz, W. (2010) The widespread regulation of microRNA biogenesis, function and decay, *Nat. Rev. Genet. 11*, 597-610.

2. Altuvia, Y., Landgraf, P., Lithwick, G., Elefant, N., Pfeffer, S., Aravin, A., Brownstein, M. J., Tuschl, T., and Margalit, H. (2005) Clustering and conservation patterns of human microRNAs, *Nucleic Acids Res. 33*, 2697-2706.

3. Pfeffer, S., Sewer, A., Lagos-Quintana, M., Sheridan, R., Sander, C., Grässer, F. A., van Dyk, L. F., Ho, C. K., Shuman, S., Chien, M., Russo, J. J., Ju, J., Randall, G., Lindenbach, B. D., Rice, C. M., Simon, V., Ho, D. D., Zavolan, M., and Tuschl, T. (2005) Identification of microRNAs of the herpesvirus family, *Nat. Methods 2*, 269-276.

4. Rana, T. M. (2007) Illuminating the silence: understanding the structure and function of small RNAs, *Nat. Rev. Mol. Cel. Bio. 8*, 23-36.

5. Lewis, B. P., Burge, C. B., and Bartel, D. P. (2005) Conserved Seed Pairing, Often Flanked by Adenosines, Indicates that Thousands of Human Genes are MicroRNA Targets, *Cell 120*, 15-20.

6. Kim, V. N., Han, J., and Siomi, M. C. (2009) Biogenesis of small RNAs in animals, *Nat. Rev. Mol. Cel. Bio. 10*, 126-139.

7. Denli, A. M., Tops, B. B. J., Plasterk, R. H. A., Ketting, R. F., and Hannon, G. J. (2004) Processing of primary microRNAs by the Microprocessor complex, *Nature 432*, 231-235.

8. Gregory, R. I., Yan, K.-p., Amuthan, G., Chendrimada, T., Doratotaj, B., Cooch, N., and Shiekhattar, R. (2004) The Microprocessor complex mediates the genesis of microRNAs, *Nature 432*, 235-240.

9. Yi, R., Qin, Y., Macara, I. G., and Cullen, B. R. (2003) Exportin-5 mediates the nuclear export of pre-microRNAs and short hairpin RNAs, *Gene Dev. 17*, 3011-3016.

10. Lund, E., Güttinger, S., Calado, A., Dahlberg, J. E., and Kutay, U. (2004) Nuclear Export of MicroRNA Precursors, *Science 303*, 95-98.

11. Bohnsack, M. T., Czaplinski, K., and Görlich, D. (2005) Exportin 5 is a RanGTP-dependent dsRNA-binding protein that mediates nuclear export of pre-miRNAs, *RNA 10*, 185-191.

12. Haase, A. D., Jaskiewicz, L., Zhang, H., Lainé, S., Sack, R., Gatignol, A., and Filipowicz, W. (2006) TRBP, a regulator of cellular PKR and HIV-1 virus expression, interacts with Dicer and functions in RNA silencing, *EMBO Reports 6*, 961-967.

13. Lee, Y., Hur, I., Park, S.-Y., Kim, Y.-K., Suh, M. R., and Kim, V. N. (2006) The role of PACT in the RNA silencing pathway, *EMBO J. 25*, 522-532.

14. Gregory, R. I., Chedrimada, T. P., Cooch, N., and Shiekhattar, R. (2005) Human RISC Couples MicroRNA Biogenesis and Posttranscriptional Gene Silencing, *Cell 123*, 631-640.

15. Chendrimada, T. P., Gregory, R. I., Kumaraswamy, E., Norman, J., Cooch, N., Nishikura, K., and Shiekhattar, R. (2005) TRBP recruits the Dicer complex to Ago2 for microRNA processing and gene silencing, *Nature 436*, 740-744.

16. Faller, M., Matsunaga, M., Yin, S., Loo, J. A., and Guo, F. (2007) Heme is involved in microRNA processing, *Nat. Struct. Mol. Biol. 14*, 23-29.

17. Senturia, R., Faller, M., Yin, S., Loo, J. A., Cascio, D., Sawaya, M. R., Hwang, D., Clubb, R. T., and Guo, F. (2010) Structure of the dimerization domain of DiGeorge Critical Region 8, *Protein Sci. 19*, 1354-1365.

18. Faller, M., Toso, D., Matsunaga, M., Atanasov, I., Senturia, R., Chen, Y., Zhou, H., and Guo, F. (2010) DGCR8 recognizes primary transcripts of microRNAs through highly cooperative binding and formation of higher-order structures, *RNA 16*, 1570-1583.

19. Barr, I., Smith, A. T., Senturia, R., Chen, Y., Scheidemantle, B. D., Burstyn, J. N., and Guo, F. (2011) DiGeorge Critical Region 8 (DGCR8) Is a Double-cysteine-ligated Heme Protein, *J. Biol. Chem. 286*, 16716-16725.

20. Barr, I., Smith, A. T., Chen, Y., Senturia, R., Burstyn, J. N., and Guo, F. (2012) Ferric, not ferrous, heme activates RNA-binding protein DGCR8 for primary microRNA processing, *Proc. Natl. Acad. Sci. U.S.A. 109*, 1919-1924.

21. Van Duyne, G. D., Standaert, R. F., Karplus, P. A., Schreiber, S. L., and Clardy, J. (1993) Atomic Structures of the Human Immunophilin FKBP-12 Complexes with FK506 and Rapamycin, *J. Mol. Biol. 229*, 105-124.

22. Spiro, T. G., and Strekas, T. C. (1974) Resonance Raman spectra of heme proteins. Effects of oxidation and spin state., *J. Am. Chem. Soc. 96*, 338-345.

23. Hu, S., Smith, K. M., and Spiro, T. G. (1996) Assignment of Protoheme Resonance Raman Spectrum by Heme Labeling in Myoglobin, *J. Am. Chem. Soc. 118*, 12638-12646.

24. Kitagawa, T., Kyogoku, Y., Iizuka, T., Ikeda-Saito, M., and Yamanaka, T. (1975) Resonance Raman Scattering from Hemoproteins, *J. Biochem. 78*, 719-728.

25. Adar, F. (1978) Electronic Absorption Spectra of Hemes and Hemoproteins, in *The Porphyrins* (Dolphin, D., Ed.), pp 167-209, Academic Press, New York.

26. Falk, J. E. (1964) *Porphyrins and Metalloporphyrins: Their General, Physical, and Coordination Chemistry, and Laboratory Methods*, Elsevier, Amsterdam.

27. Gale, R., McCaffery, A. J., and Rowe, M. D. (1972) Magnetic Circular Dichroism and Absorption Spectra of the Porphyrins. Part 1, *J. Chem. Soc. Dalton*, 596-604.

28. Walker, F. A. (1999) Magnetic spectroscopic (EPR, ESEEM, Mössbauer, MCD and NMR) studies of low-spin ferriheme centers and their corresponding heme proteins, *Coord. Chem. Rev. 185-186*, 471-534.

29. Sono, M., Andersson, L. A., and Dawson, J. H. (1982) Sulfur Donor Ligand Binding to Ferric Cytochrome P-450-CAM and Myoglobin, *J. Biol. Chem. 257*, 8308-8320.

30. Dawson, J. H., and Sono, M. (1987) Cytochrome P-450 and Chloroperoxidase: Thiolate-Ligated Heme Enzymes. Spectroscopic Determination of Their Active Site Structures and Mechanistic Implications of Thiolate Ligation, *Chem. Rev. 87*, 1255-1276.

31. Taoka, S., Green, E. L., Loehr, T. M., and Banerjee, R. (2001) Mercuric chloride-induced spin or ligation state changes in ferric or ferrous human cystathionine β-synthase inhibit enzyme activity, *J. Inorg. Biochem. 87*, 253-259.

32. Kitanishi, K., Igarashi, J., Hayasaka, K., Hikage, N., Saiful, I., Yamauchi, S., Uchida, T., Ishimori, K., and Shimizu, T. (2008) Heme-Binding Characteristics of the Isolated PAS-A Domain of Mouse Per2, a Transcriptional Regulatory Factor Associated with Circadian Rhythms, *Biochemistry 47*, 6157-6168.

33. Smith, A. T., Majtan, T., Freeman, K. M., Su, Y., Kraus, J. P., and Burstyn, J. N. (2011) Cobalt Cystathionine ß-Synthase: A Cobalt-Substituted Heme Protein with a Unique Thiolate Ligation Motif, *Inorg. Chem. 50*, 4417-4427.

34. Palmer, G. (1983) Electron Paramagnetic Resonance of Hemoproteins, in *Iron Porphyrins, Part II* (Lever, A. B. P., and Gray, H. B., Eds.), pp 45-88, VCH Publishers, New York.

35. Blumberg, W. E., and Peisach, J. (1971) Low-spin compounds of heme proteins, *Adv. Chem. Ser. 100*, 271-291.

36. Sono, M., Dawson, J. H., and Hager, L. P. (1985) Phosphine Binding as a Structural Probe of the Chloroperoxidase Active Site: Spectroscopic Evidene for Endogenous Thiolate Ligation to the Heme Iron, *Inorg. Chem. 24*, 4339-4343.

37. Sono, M., Hager, L. P., and Dawson, J. H. (1991) Electron paramagnetic resonance investigations of exogenous ligand complexes of low-spin ferric chloroperoxidase: further support for endogenous thiolate ligation to the heme iron, *Biochim. Biophys. Acta 1078*, 351-359.

38. Pazicni, S., Lukat-Rodgers, G. S., Oliveriusová, J., Rees, K. A., Parks, R. B., Clark, R. W., Kraus, J. P., Rodgers, K. R., and Burstyn, J. N. (2004) The redox behavior of the heme in cystathionine β-synthase is sensitive to pH, *Biochemistry 43*, 14684-14695.

39. Perera, R., Sono, M., Sigman, J. A., Pfister, T. D., Lu, Y., and Dawson, J. H. (2003) Neutral thiol as a proximal ligand to ferrous heme iron: Implications for heme proteins that lose cysteine thiolate ligation on reduction, *Proc. Natl. Acad. Sci. U.S.A. 100*, 3641-3646.

40. Tomita, T., Gonzalez, G., Chang, A. L., Ikeda-Saito, M., and Gilles-Gonzalex, M.-A. (2002) A Comparative Resonance Raman Analysis of Heme-Binding PAS Domains: Heme Iron Coordination Structures of the *Bj*FixL, *Ax*PDEA1, *Ec*Dos, and *Mt*Dos Proteins, *Biochemistry 41*, 4819-4826.

41. Spiro, T. G. (1975) Resonance Raman spectroscopic studies of heme proteins, *Biochim. Biophys. Acta 416*, 169-189.

42. Dawson, J. H., Andersson, L. A., and Sono, M. (1983) The Diverse Spectroscopic Properties of Ferrous Cytochrome P-450-CAM Ligand Complexes, *J. Biol. Chem. 258*, 13637-13645.

43. Nelson, D. L., and Cox, M. M. (2008) *Lehninger Principles of Biochemistry*, 5th ed., W. H. Freeman and Company, New York.

44. Hirota, S., Mizoguchi, Y., Yamauchi, O., and Kitagawa, T. (2002) Observation of an isotope-sensitive low-frequency Raman band specific to metmyoglobin, *J. Biol. Inorg. Chem. 7*, 217-221.

45. Walters, M. A., and Spiro, T. G. (1982) Resonance Raman Spectroscopic Studies of Axial Ligation in Oxyhemoglobin, Oxymyoglobin, and Nitrosylmyoglobin, *Biochemistry 21*, 6989-6995.

46. Kerr, E. A., Yu, N.-T., Gersonde, K., Parish, D. W., and Smith, K. M. (1985) Iron-Histidine Stretching Vibration in the Deoxy State of Insect Hemoglobins with Different O2 Affinities and Bohr Effects, *J. Biol. Chem. 260*, 12665-12669.

47. Andrew, C. R., Kemper, L. J., Busche, T. L., Tiwari, A. M., Kecskes, M. C., Stafford, J. M., Croft, L. C., Lu, S., Moënne-Loccoz, P., Huston, W., Moir, J. W. B., and Eady, R. R. (2005) Accessibility of the Distal Heme Face, Rather than Fe-His Bond Strength,

Determines the Heme-Nitrosyl Coordination Number of Cytochromes *c*': Evidence from Spectroscopic Studies, *Biochemistry 44*, 8664-8672.

48. Du, J., Perera, R., and Dawson, J. H. (2011) Alkylamine-Ligated H93G Myoglobin Cavity Mutant: A Model System for Endogenous Lysine and Terminal Amine Ligation in Heme Proteins such as Nitrite Reductase and Cytochrome *f*, *Inorg. Chem. 50*, 1242-1249.

49. Martinez, S. E., Huang, D., Szczepaniak, A., Cramer, W. A., and Smith, J. L. (1994) Crystal structure of chloroplast cytochrome *f* reveals a novel cytochrome fold and unexpected heme ligation, *Structure 2*, 95-105.

50. Varhač, R., Antalík, M., and Bánó, M. (2004) Effect of temperature and guanidine hydrochloride on ferrocytochrome *c* at neutral pH, *J. Biol. Inorg. Chem. 9*, 12-22.

51. Desbois, A. (1994) Resonance Raman spectroscopy of *c*-type cytochromes, *Biochimie 76*, 693-707.

52. Singh, S., Madzelan, P., Stasser, J., Weeks, C. L., Becker, D., Spiro, T. G., Penner-Hahn, J., and Banerjee, R. (2009) Modulation of the heme electronic structure and cystathionine β-synthase activity by second coordination sphere ligands: The role of heme ligand switching in redox regulation, *J. Inorg. Biochem. 103*, 689-697.

53. Pazicni, S., Cherney, M. M., Lukat-Rogers, G. S., Oliveriusová, J., Rodgers, K. R., Kraus, J. P., and Burstyn, J. N. (2005) The Heme of Cystathionine β-synthase Likely Undergoes a Thermally Induced Redox-Mediated Ligand Switch, *Biochemistry 44*, 16785-16795.

54. Youn, H., Kerby, R. L., Thorsteinsson, M. V., Clark, R. W., Burstyn, J. N., and Roberts, G. P. (2002) Analysis of the L116K Variant of CooA, the Heme-containing CO Sensor,

Suggests the Presence of an Unusual Heme Ligand Resulting in Novel Activity, *J. Biol. Chem. 277*, 33616-33623.

55. Marvin, K. A., Kerby, R. L., Youn, H., Roberts, G. P., and Burstyn, J. N. (2008) The Transcription Regulator RcoM-2 from Burkholderia xenovorans Is a Cysteine-Ligated Hemoprotein That Undergoes a Redox-Mediated Ligand Switch, *Biochemistry 47*, 9016-9028.

56. Marvin, K. A., Reinking, J. L., Lee, A. J., Pardee, K., Krause, H. M., and Burstyn, J. N. (2009) Nuclear Receptors Homo sapiens Rev-erbβ and Drosophila melanogaster E75 Are Thiolate-Ligated Heme Proteins Which Undergo Redox-Mediated Ligand Switching and Bind CO and NO, *Biochemistry 48*, 7056-7071.

57. Dhawan, I. K., Shelver, D., Thorsteinsson, M. V., Roberts, G. P., and Johnson, M. K. (1999) Probing the heme axial ligation in the CO-sensing CooA protein with magnetic circular dichroism spectroscopy, *Biochemistry 38*, 12805-12813.

58. Jung, C., and Ristau, O. (1977) Quantum-Chemical Interpretation of the Unusual Absorption Spectrum of the Cytochrome P-450--CO Complex, *Chem. Phys. Lett. 49*, 103-108.

59. Heinemann, I. U., Jahn, M., and Jahn, D. (2008) The biochemistry of heme biosynthesis, *Arch. Biochem. Biophys. 474*, 238-251.

60. Levicán, G., Katz, A., de Armas, M., Núñez, H., and Orellana, O. (2007) Regulation of a glutamyl-tRNA synthetase by the heme status, *Proc. Natl. Acad. Sci. U.S.A. 104*, 3135-3140.

61. Katz, A., Banerjee, R., de Armas, M., Ibba, M., and Orellana, O. (2010) Redox status affects the catalytic activity of glutamyl-tRNA synthetase, *Biochem. Biophys. Res. Commun. 398*, 51-55.

62. de Armas-Ricard, M., Levicán, G., Katz, A., Moser, J., Jahn, D., and Orellana, O. (2011) Cellular levels of heme affect the activity of dimeric glutamyl-tRNA reductase, *Biochem. Biophys. Res. Commun. 405*, 134-139.

63. Wang, L. Y., Brown, L., Elliott, M., and Elliott, T. (1997) Regulation of Heme Biosynthesis in *Salmonella typhimurium*: Activity of Glutamyl-tRNA Reductase (HemA) Is Greatly Elevated during Heme Limitation by a Mechanism Which Increases Abundance of the Protein, *J. Bacteriol. 179*, 2907-2914.

64. Jones, A. M., and Elliott, T. (2010) A purified mutant HemA protein from *Salmonella enterica* serovar Typhimurium lacks bound heme and is defective for heme-mediated regulation *in vivo*, *FEMS Microbiol. Lett. 307*, 41-47.

65. Wakasugi, K. (2007) Human Tryptophanyl-tRNA Synthetase Binds with Heme To Enhance Its Aminoacylation Activity, *Biochemistry 46*, 11291-11298.

66. Yang, F., Xia, X., Lei, H.-Y., and Wang, E.-D. (2010) Hemin Binds to Human Cytoplasmic Arginyl-tRNA Synthetase and Inhibits Its Catalytic Activity, *J. Biol. Chem. 285*, 39437-39446.

67. Sen, D., and Poon, L. C. H. (2011) RNA and DNA complexes with hemin [Fe(III) heme] are efficient peroxidases and peroxygenases: how do they do it and what does it mean?, *Crit. Rev. Biochem. Mol. Biol. 46*, 478-492.

68. Travascio, P., Bennet, A. J., Wang, D. Y., and Sen, D. (1999) A ribozyme and a catalytic DNA with peroxidase activity: active sites versus cofactor-binding sites, *Chem. Biol. 6*, 779-787.

69. Travascio, P., Witting, P. K., Mauk, A. G., and Sen, D. (2001) The Peroxidase Activity of Hemin-DNA Oligonucleotide Complex: Free Radical Damage to Specific Guanine Bases of the DNA, *J. Am. Chem. Soc. 123*, 1337-1348.

70. Poon, L. C. H., Methot, S. P., Morabi-Pazooki, W., Pio, F., Bennet, A. J., and Sen, D. (2011) Guanine-Rich RNAs and DNAs That Bind Heme Robustly Catalyze Oxygen Transfer Reactions, *J. Am. Chem. Soc. 133*, 1877-1884.

71. Nakajima, H., Honma, Y., Tawara, T., Kato, T., Park, S.-Y., Miyatake, H., Shiro, Y., and Aono, S. (2001) Redox Properties and Coordination Structure of the Heme in the CO-sensing Transcriptional Activator CooA, *J. Biol. Chem. 276*, 7055-7061.

72. Izadi, N., Henry, Y., Haladjian, J., Goldberg, M. E., Wandersman, C., Delepierre, M., and Lecroisey, A. (1997) Purification and Characterization of an Extracellular Heme-Binding Protein, HasA, Involved in Heme Iron Acquisition, *Biochemistry 36*, 7050-7057.

73. Mayhew, S. G. (1978) The Redox Potential of Dithionite and SO2- from Equilibrium Reactions with Flavodoxins, Methyl Viologen and Hydrogen plus Hydrogenase, *Eur. J. Biochem. 85*, 535-547.

74. Bickar, D., Bonaventura, C., and Bonaventura, J. (1984) Carbon Monoxide-driven Reduction of Ferric Heme and Heme Proteins, *J. Biol. Chem. 259*, 10777-10783.

75. Enemark, J. H., and Feltham, R. D. (1974) Principles of Structure, Bonding, and Reactivity For Metal Nitrosyl Complexes, *Coord. Chem. Rev. 13*, 339-406.

76. Gong, M., Chen, Y., Senturia, R., Ulgherait, M., Faller, M., and Guo, F. (2012) Caspases cleave and inhibit the microRNA processing protein DiGeorge Critical Region 8, *Protein Sci. doi: 10.1002/pro.2062*.

77. Sono, M., Dawson, J. H., and Hager, L. P. (1984) The Generation of a Hyperporphyrin Spectrum upon Thiol Binding to Ferric Chloroperoxidase, *J. Biol. Chem. 259*, 13209-13216.

78. Barker, P. D., Nerou, E. P., Cheesman, M. R., Thomson, A. J., de Oliveria, P., and Hill, H. A. O. (1996) Bis-Methionine Ligation to Heme Iron in Mutants of Cytochrome *b562*. 1. Spectroscopic and Electrochemical Characterization of the Electronic Properties, *Biochemistry 35*, 13618-13626.

79. Margoliash, E., and Frohwirt, N. (1959) Spectrum of horse-heart cytochrome *c*, *Biochem. J. 71*, 570-572.

80. Delgado-Nixon, V. M., Gonzalez, G., and Gilles-Gonzalez, M.-A. (2000) Dos, a Heme-Binding PAS Protein from *Escherichia coli*, Is a Direct Oxygen Sensor, *Biochemistry 39*, 2685-2691.

81. Reynolds, M. F., Parks, R. B., Burstyn, J. N., Shelver, D., Thorsteinsson, M. V., Kerby, R. L., Roberts, G. P., Vogel, K. M., and Spiro, T. G. (2000) Electronic absorption, EPR, and resonance Raman spectroscopy of CooA, a CO-sensing transcription activator from *R. rubrum*, reveals a five-coordinate NO-heme, *Biochemistry 39*, 388-396.

82. Vickery, L., Nozawa, T., and Sauer, K. (1976) Magnetic circular dichroism studies of low-spin cytochromes. Temperature dependence and effects of axial coordination of the spectra of cytochrome *c* and cytochrome b_5, *J. Am. Chem. Soc. 98*, 351-357.

83. Dewilde, S., Kiger, L., Burmester, T., Hankeln, T., Baudin-Creuza, V., Aerts, T., Marden, M. C., Caubergs, R., and Moens, L. (2001) Biochemical characterization and ligand binding properties of neuroglobin, a novel member of the globin family, *J. Biol. Chem. 276*, 38949-38955.

84. Egawa, T., Hishiki, T., Ichikawa, Y., Kanamori, Y., Schimada, H., Takahashi, S., Kitagawa, T., and Ishimura, Y. (2004) Refolding Processes of Cytochrome P450cam from Ferric and Ferrous Acid Forms to the Native Conformation, *J. Biol. Chem. 279*, 32008-32017.

85. Antonini, E., and Brunori, M. (1971) *Hemoglobin and Myoglobin in Their Reactions with Ligands*, Vol. 21, North-Holland Publishing Co., Amsterdam.

86. Sun, L., Zhonghua, W., Jiang, H., Tan, X., and Huang, Z. (2010) Novel Conformation Transitions of Human Cytochrome P450 2C8 during Thermal and Acid-induced Unfolding, *Chin. J. Chem . 28*, 1491-1502.

87. Egawa, T., Lee, H. J., Ji, H., Gennis, R. B., Yeh, S.-R., and Rousseau, D. L. (2009) Identification of heme propionate vibrational modes in the resonance Raman spectra of cytochrome *c* oxidase, *Anal. Biochem. 394*, 141-143.

88. Puranik, M., Weeks, C. L., Lahaye, D., Kabil, Ö., Shinichi, T., Nielsen, S. B., Groves, J. T., Banerjee, R., and Spiro, T. G. (2006) Dynamics of Carbon Monoxide Binding to Cystathionine β-Synthase, *J. Biol. Chem. 281*, 13433-13438.

89. Hildebrand, D. P., Ferrer, J. C., Tang, H.-L., Smith, M., and Mauk, A. G. (1995) Trans effects on cysteine ligation in the proximal His93Cys variant of horse heart myoglobin, *Biochemistry 41*, 11598-11605.

90. Stone, J. R., and Marletta, M. A. (1994) Soluble guanylate cyclase from bovine long: activation with nitric oxide and carbon monoxide and spectral characterization of the ferrous and ferric states, *Biochemistry 33*, 5636-5640.

91. Reynolds, M. F., and Burstyn, J. N. (2000) Mechanisms of activation of soluble guanylyl cyclase by NO: Allosteric regulation through changes in heme geometry, *Nitric Oxide*, 381-399.

92. Taoka, S., and Banerjee, R. (2001) Characterization of NO binding to human cystathionine β-synthase: Possible implications of the efects of CO and NO binding to the human enzyme, *J. Inorg. Biochem. 87*, 245-251.

93. Decatur, S. M., Franzen, S., DePillis, G. D., Dyer, R. B., Woodruff, W. H., and Boxer, S. G. (1996) *Trans* Effects in Nitric Oxide Binding to Myoglobin Cavity Mutant H93G, *Biochemistry 35*, 4939-4944.

94. Clark, R. W., Lanz, N. D., Lee, A. J., Kerby, R. L., Roberts, G. P., and Burstyn, J. N. (2006) Unexpected NO-dependent DNA binding by the CooA homolog from *Carboxythermus hydrogenoformans*, *Proc. Natl. Acad. Sci. U.S.A. 103*, 891-896.

95. Van Doorslaer, S., Dewilde, S., Kiger, L., Nistor, S. V., Goovaerts, E., Marden, M. C., and Moens, L. (2003) Nitric Oxide Binding Properties of Neuroglobin. A Characterization by EPR and Flash Photolysis, *J. Biol. Chem. 278*, 4919-4925.

96. Tomita, T., Hirota, S., Ogura, T., Olson, J. S., and Kitagawa, T. (1999) Resonance Raman investigation of Fe-N-O structure of nitrosylheme in myoglobin and its mutants, *J. Phys. Chem. B 103*, 7044-7054.

97. Sono, M., Eble, K. S., Dawson, J. H., and Hager, L. P. (1985) Preparation and Properties of Ferrous Chloroperoxidase Complexes with Dioxygen, Nitric Oxide, and an Alkyl Isocyanide, *J. Biol. Chem. 260*, 15530-15535.

98. Hu, S., and Kincaid, J. R. (1991) Resonance Raman Spectra of the Nitric Oxide Adducts of Ferrous Cytochrome P450cam in the Presence of Various Substrates, *J. Am. Chem. Soc. 113*, 9760-9766.

99. Stone, J. R., Sands, R. H., Dunham, W. R., and Marletta, M. A. (1995) Electron Paramagnetic Resonance Spectral Evidence For the Formation of a Pentacoordinate Nitrosyl-Heme Complex On Soluble Guanylate Cyclase, *Biochem. Biophys. Res. Commun. 207*, 572-577.

100. Hille, R., Olson, J. S., and Palmer, G. (1979) Spectral Transitions of Nitrosyl Hemes During Ligand Binding to Hemoglobin, *J. Biol. Chem. 254*, 12110-12120.

101. Yoshimura, T., Suzuki, S., Nakahara, A., Iwasaki, H., Masuko, M., and Matsubara, T. (1986) Spectral Properties of Nitric Oxide Complexes of Cytochrome *c′* from *Alcaligenes* sp. NCIB 11015, *Biochemistry 25*, 2436-2442.

102. Soifer, H. S., Rossi, J. J., and Sætrom, P. (2007) MicroRNAs in Disease and Potential Therapeutic Applications, *Mol. Ther. 15*, 2070-2079.

Table 3.1. Selected electronic absorption data (nm) for Fe(III) DGCR8 NC1 and HBD proteins, Fe(III) Chloroperoxidase and ligand complexes, and Fe(III) Cytochrome $P450_{CAM}$ and ligand complexes.

Fe(III) Protein	pH	Soret (γ)		α/β	Spin state	Ref
		Hyper blue	Hyper red			
Human DGCR8 NC1	**8.0**	**366**	**450**	**556**	**LS**[a]	This work
Frog DGCR8 HBD	**8.0**	**366**	**451**	**557**	**LS**	This work
Chloroperoxidase (native)	3-7	399		514/542	LS	(*77*)
+ H_2S	6-7	369	449	NR[b]	LS	(*77*)
+ H_3CSH	6.0	372	455	NR	LS	(*77*)
+ $HO(CH_2)_2SH$	6.0	380	455	NR	HS/LS[c]	(*77*)
+ $H_3CH_2COC(O)CH_2SH$	6.0	371	454	556	LS	(*77*)
+ $(HOCH_2)_2PCH_3$	6.0, 6.5	376	450	553	LS	(*36*)
+ H_3CSCH_3	3-6	417[d]		NR	HS/LS	(*77*)
+ H_3CSSCH_3	3-6	417		NR	HS/LS	(*77*)
Cytochrome $P450_{CAM}$ (native)	7.0	417		536/569	LS	(*29*)
+ H_2S	7.0	390	467	564	LS	(*29*)
+ $H_3C(CH_2)_2SH$	9.1	377	466		LS	(*29*)
+ $HO(CH_2)_2SH$	8.2	376	464	558	LS	(*29*)
+ $ClC(CH)_4CSH$	7.0	381	463	560	LS	(*29*)
+ $(HOCH_2)_2PCH_3$	7.3	375	446	553	LS	(*36*)
+ H_3CSCH_3	7.0	424		538/570	LS	(*29*)
+ H_3CSSCH_3	7.0	418		536/568	LS	(*29*)

[a] LS: low-spin; HS: high-spin. [b] NR: not reported. [c] HS/LS indicates that the protein exists as an admixture of high- and low-spin states. [d] One value for hyper blue and hyper red indicates the lack of a hyperporphyrin spectrum.

Table 3.2. Selected EPR *g* values for the Fe(III) DGCR8 HBD protein, Fe(III) Chloroperoxidase and ligand complexes, and Fe(III) Cytochrome $P450_{CAM}$ and ligand complexes.

Fe(III) protein	pH	g_z	g_y	g_x	Ref
Frog DGCR8 HBD Native	**8.0**	**2.60**	**2.27**	**1.84**	This work
Chloroperoxidase (native)	6.0	2.62	2.26	1.83	(*37*)
	9.5	2.54	2.28	1.85	(*37*)
$+H_3CSH$	3.0	2.45	2.27	1.91	(*37*)
$+H_3CH_2COC(O)H_2CSH$	6.0	2.37	2.25	1.94	(*37*)
		[*2.43*[a]	*2.26*[a]	*1.91*[a]]	(*37*)
$+H_3CC(O)SH$	3.0	2.66	2.26	1.82	(*37*)
		[*2.44*		*1.91*]	(*37*)
$+HO(CH_2)_2SH$	6.0	2.61	2.26	1.84	(*37*)
		[*2.44*		*1.91*]	(*37*)
$+(HOCH_2)_2PCH_3$	7.0	2.59	2.28	1.82	(*36*)
$+H_3CSCH_3$	NR[b]	2.62	2.26	1.83	(*30*)
$+H_3CSSCH_3$	NR	2.62	2.26	1.83	(*30*)
Cytochrome $P450_{CAM}$ (native)	5.5-9	2.44	2.25	1.91	(*29*)
$+H_3C(CH_2)_2SH$	7.0	2.41	2.24	1.92	(*29*)
		[*2.34*		*1.94*]	(*29*)
$+HO(CH_2)_2SH$	7.0	2.42	2.27	1.92	(*29*)
		[*2.38*	*2.27*	*1.93*]	(*29*)
		[*2.52*	*2.27*	*1.90*]	(*29*)
$+(C_6H_5)CH_2SH$	6-9.5	2.39	2.25	1.94	(*29*)
		[*2.44*	*2.25*	*1.92*]	(*29*)
$+(HOCH_2)_2PCH_3$	7.0	2.51	2.28	1.86	(*36*)
$+H_3CSCH_3$	7.0	2.50	2.27	1.89	(*29*)
$+H_3CSSCH_3$	7.0	2.42	2.25	1.92	(*29*)

[a] Values in brackets represent minor signals present. In most cases, the relationship of the major signal to the minor signal was not explored. [b] NR: not reported.

Table 3.3. Selected electronic absorption data (nm) for Fe(II) DGCR8 NC1 and HBD proteins, and selected electronic absorption data for various 6-, 5-, and 4-coordinate Fe(II) heme proteins.

Fe(II) Protein		Ligands	Spin State	Soret (γ)	β	α	Ref
Frog DGCR8 HBD (pH 8.0)		**?**	**HS[a]/LS[b]**	**424**	**527**	**558**	This work
Human DGCR8 NC1 (pH 6.0)		**?**	**?**	**390**	**556**	**580**	This work
6-coordinate	$P450_{CAM}$ + OSH[c]	R-S(H)/Cys^-	LS	445	538	557	(*42*)
	$P450_{CAM}$ + DMS[d]	R-S-R/Cys^-	LS	446	541	568	(*42*)
	H93G Mb + CPSH[e]	R-SH/R-SH	LS	427	528	558	(*39*)
	H93G Mb + THT[f]	R-S-R/R-S-R	LS	427	528	558	(*39*)
	Cyt b_{562} H102M	Met/Met	LS	430	530	561.5	(*78*)
	hCBS (pH 9.0)	His/Cys^-	LS	448	540	570	(*38*)
	Cyt *c*	His/Met	LS	413	521	550	(*79*)
	*Ec*DOS	His/Met	LS	427	532	563	(*80*)
	*Rr*CooA	His/Pro	HS/LS	425	529	559	(*81*)
	hCBS-424 (pH 9.0)	His/N,O Donor[g]	HS/LS	424	530	560	(*52, 53*)
	*Rr*CooA L116K	His/Lys	LS	425	530[h]	560[h]	(*54*)
	Cyt b_5	His/His	LS	423	526	556	(*82*)
	Neuroglobin	His/His	LS	426	530	560	(*83*)
	H93G Mb + TMA[l]	NR_3/NR_3	LS	424	527	559	(*48*)
5-coordinate	$P450_{CAM}$	Cys^-	HS	409	544[k]		(*84*)
	H93G Mb + CPSH	R-SH	NR[i]	428	559		(*39*)
	H93G Mb + THT	R-S-R	NR[i]	426	530	560	(*39*)
	Deoxy Mb	His	HS	434	556		(*85*)
4-coordinate	$P450_{CAM}$ Acid Form (pH 2.0)	None	IS[j]	385	545	573	(*84, 86*)
	Deoxy-Mb Acid Form	None	IS	383	NR		(*87*)

[a]High spin. [b]Low spin. [c]Octanethiol. [d]Dimethylsulfide. [e]Cyclopentanethiol. [f]Tetrahydrothiophene. [g]The exact nature of the sixth ligand is unknown. [h]Determined by examination of the data. [i]Not reported, but appear to be high spin from examination of the data. [j]Intermediate spin. [k]One value indicates no discernible peak maxima for both α and β. [l]Trimethylamine.

Table 3.4. Selected electronic absorption data (nm) for the Fe(II)-CO DGCR8 HBD protein, and selected electronic absorption data for various 6-coordinate Fe(II)-CO heme proteins.

Fe(II)-CO Protein	Ligands	δ	Soret (γ)	β	α	Ref.
DGCR8 HBD	**?/CO**		**420**	**539**	**567**	This work
*Rr*CooA	His/CO		422	540	569	(*57*)
*Ec*DOS	His/CO		423	540	570	(*80*)
*Bx*RcoM-2	His/CO		423	540	570	(*55*)
hCBS	His/CO		419	540[a]	570[a]	(*88*)
Neuroglobin	His/CO		420	537	568	(*83*)
Myoglobin	His/CO	346	423	540	579	(*89*)
$P450_{CAM}$	Cys/CO	366	446	551	NR[b]	(*30*)

[a]Not reported, but determined from examination of the data. [b]Not reported.

Table 3.5. Selected electronic absorption data (nm) for the Fe(II)-NO DGCR8 HBD protein, and selected electronic absorption data for various 6- and 5-coordinate Fe(II)-NO heme proteins.

	Fe(II)-NO Protein	Ligands	Soret (γ)	β	α	Ref.
	DGCR8 HBD	**NO**	**390**	**539**		This work
5-Coordinate	sGC	NO	398	537	572	(*90*)
	*Rr*CooA	NO	399	544	572	(*91*)
	hCBS	NO	390	538	572[a]	(*92*)
	H93G Mb	NO	400	NR	NR	(*93*)
6-Coordinate	*Ec*DOS	His/NO	419	537	563	
	*Bx*RcoM-2	His/NO	422	544	577	(*55*)
	*Ch*CooA	His/NO	417	541	571	(*94*)
	Neuroglobin	His/NO	421	542	572	(*95*)
	Mb	His/NO	420	548	580	(*96*)
	CPO	Cys/NO	440	560	585	(*97*)
	$P450_{CAM}$	Cys/NO	439	556		(*98*)

[a] Shoulder. [b] Not reported

Table 3.6. Selected EPR *g* values for the Fe(II)-NO DGCR8 HBD protein, and selected electronic absorption data for various 5-coordinate Fe(II)-NO heme proteins.

Fe(II)-NO Protein	Ligands	g_1	g_2	g^3	A_3[a] (Gauss)	Ref.
DGCR8 HBD	**NO**	**2.087**	**2.053**	**2.010**	**16.2**	This work
sGC_2	NO	2.076	2.029	2.005	16.0	(*99*)
*Rr*CooA	^{14}NO[b]	2.106	2.050	2.015	16.0	(*81*)
hCBS	NO	2.076	2.008	1.970	16.6	(*92*)
Hb	NO	2.070	2.040	2.008	16.5	(*100*)
Cyt c'	NO	2.106	2.058	2.010	16.0	(*101*)
Mb H93G	NO	NR[c]	NR	~2.01	~17	(*93*)

[a] A_3 is the hyperfine coupling constant arising from NO (^{14}N, $I = 1$). [b] Data taken from an isotopically pure ^{14}NO sample. [c] Not reported.

Figure 3.1. Domain structure of human DGCR8. The double-stranded RNA-binding domains (dsRBD) and C-terminal tail (CTT) are required and sufficient for cooperative association with pri-miRNAs and for triggering cleavage by the Drosha nuclease. The human NC1, HBD-His_6 and frog HBD-His_6 protein constructs used in this study are represented by the brackets. Adapted from Ref (*19*).

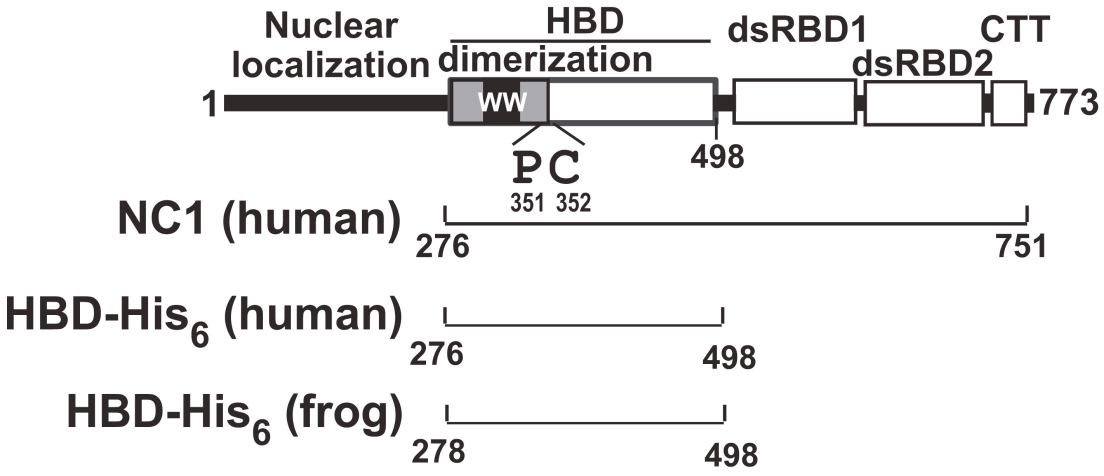

Figure 3.2. (A) Electronic absorption spectrum of Fe(III) DGCR8 HBD-His_6. Fe(III) DGCR8 HBD (12.2 μM) was in 50 mM EPPS buffer and 400 mM NaCl, pH 8.0 at room temperature. (B) MCD spectrum of Fe(III) DGCR8 HBD-His_6. Fe(III) DGCR8 HBD (24.5 μM) was in 22.5 mM EPPS buffer, 180 mM NaCl and 55% glycerol (v/v) at 4.0 K and 7 T. Inset: the field dependence of the MCD intensity at 448 nm was recorded at 2.5, 4.0, 8.0, 15 and 25 K. The curves were normalized to the most intense data point (2.5 K, 7 T).

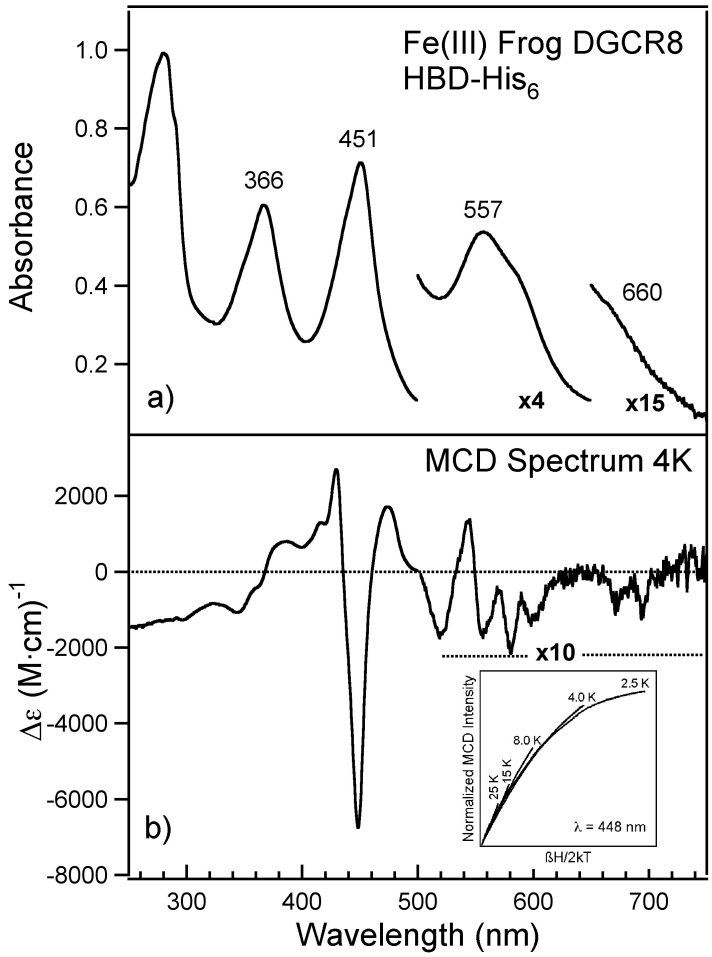

Figure 3.3. Electronic absorption spectra showing the effect of Hg^{2+} on Fe(III) DGCR8 HBD-His_6. Fe(III) DGCR8 HBD (6.5 μM, •••) was in 50 mM EPS buffer, pH 8.0 and room temperature. Spectra were recorded after equilibration of protein with 1 mol eq. (•-•) or 2 mol eq. (—) of $Hg^{2+}_{(aq)}$. Reduction in the intensity of A_{280} is a product of dilution.

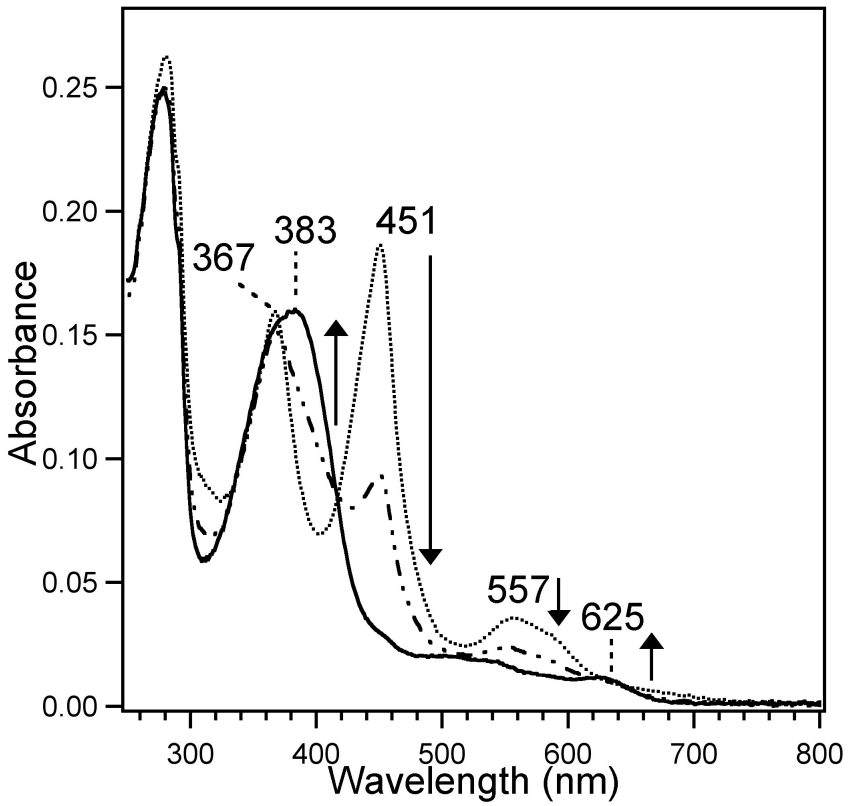

Figure 3.4. X-band EPR spectrum of the Fe(III) heme-bound frog DGCR8 HBD-His_6 protein. Fe(III) DGCR8 HBD (153 μM) was in 50 mM EPPS (pH 8.0) and 400 mM NaCl. The spectrum represents an average of 10 scans taken at 10 K, with 9.383 GHz microwave frequency, 8.000 G modulation amplitude, 100 kHz modulation frequency, 60 dB receiver gain, 163.84 ms time constant, and a power of 1.002 mW. The asterisk (*) represents a signal present in the cavity.

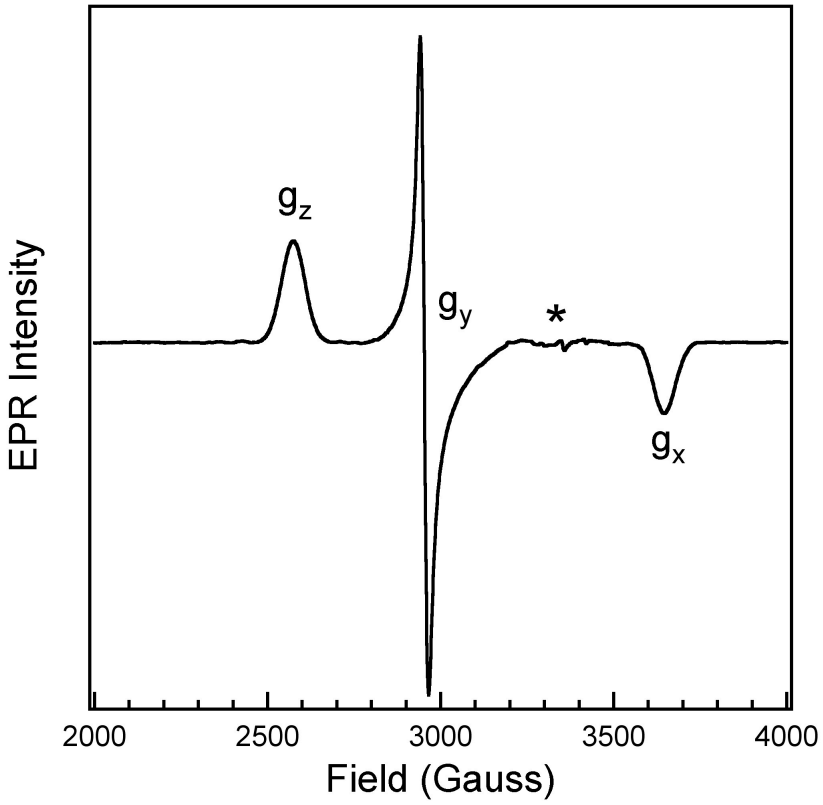

Figure 3.5. Blumberg-Peisach correlation diagram showing the position of Fe(III) DGCR8 HBD-His_6 among other sulfur- and phosphorus-donor complexes of Fe(III) chloroperoxidase and cytochrome $P450_{CAM}$. The plotted values of rhombicity ($|v/\Delta|$) versus tetragonality ($|\Delta/\lambda|$) show that the environment of the Fe(III) heme in DGCR8 HBD is most similar to that of native chloroperoxidase to which exogenous thiols or phosphines have been added. $|V/\Delta|$ and $|\Delta/\lambda|$ were calculated directly from the EPR *g* values presented in reference (*37*). The following improper axis system was used, as outlined in reference (*34*): $g_x = -g_y$; $g_y = g_z$; and $g_z = -g_x$. Rhombicity and tetragonality values were each calculated as outlined in (*34*) after the improper axis transformation was applied: $V/\lambda = (g_x/(g_z + g_y)) + (g_y/(g_z - g_x))$; $\Delta/\lambda = |(g_x/2(g_z + g_y)) + (g_z/(g_y - g_x)) - (g_y/2(g_z - g_x))|$; $V/\Delta = (V/\lambda) / (\Delta/\lambda)$. The following abbreviations are used: CPO: chloroperoxidase; $P450_{CAM}$: cytochrome $P450_{CAM}$; TAA: thioacetic acid; BME: β-mercaptoethanol; ImH: imidazole; MeSH: methanethiol; PR_3: bis(hydroxymethyl)-methyphosphine. "(a)" and "(b)" in the diagram refer to different sets of multiple, overlapping rhombic signals that are observed for a single sample. Inset: zoomed-out Blumberg-Peisach diagram illustrating the position of Fe(III) DGCR8 HBD-His_6 among the five common clusters (C, B, H, O and P) of low-spin, 6-coordinate Fe(III) heme proteins; adapted from references (*35*) and (*34*).

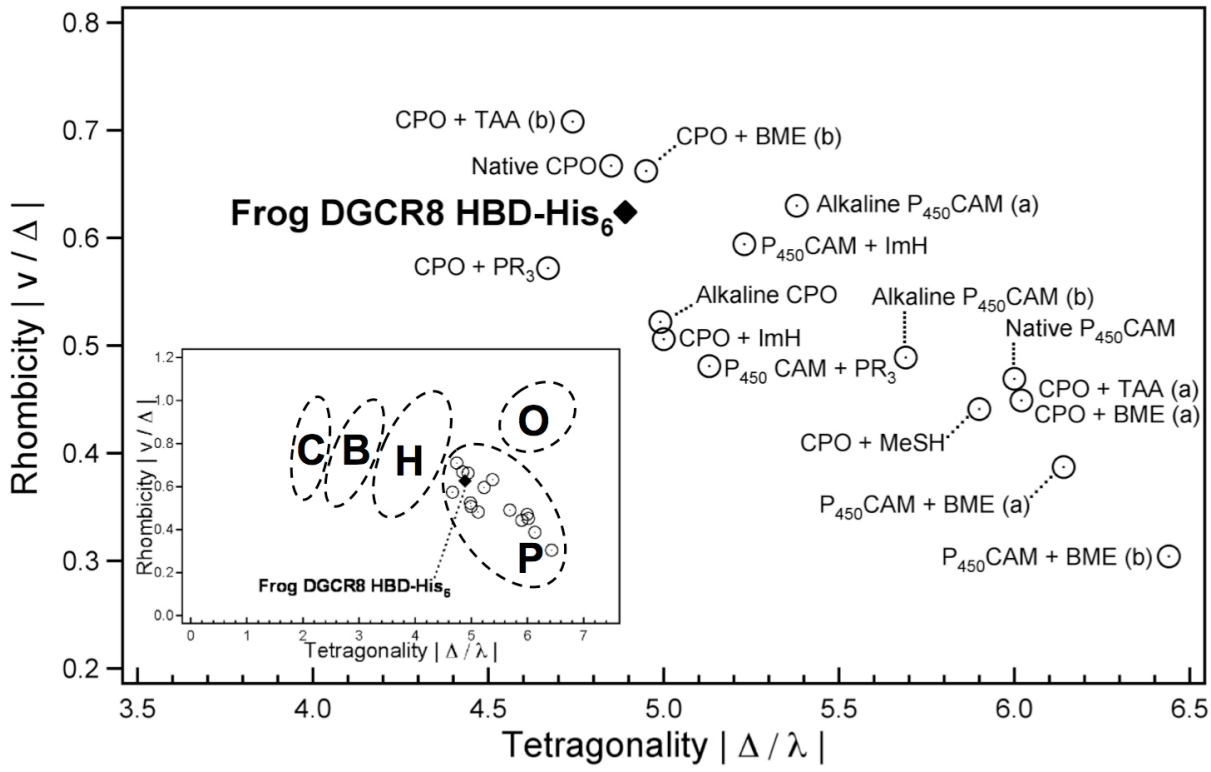
Rhombicity | v / Δ |
Tetragonality | Δ / λ |
Frog DGCR8 HBD-His6◆
CPO + TAA (b)
CPO + BME (b)
Native CPO
CPO + PR3
Alkaline P450CAM (a)
P450CAM + ImH
Alkaline CPO
Alkaline P450CAM (b)
CPO + ImH
P450 CAM + PR3
Native P450CAM
CPO + TAA (a)
CPO + BME (a)
CPO + MeSH
P450CAM + BME (a)
P450CAM + BME (b)
C
B
H
O
P
Frog DGCR8 HBD-His6

Figure 3.6. (A) Electronic absorption spectrum of Fe(II) DGCR8 HBD-His_6. Fe(II) DGCR8 HBD (11.7 μM) was in 50 mM EPPS buffer and 400 mM NaCl, pH 8.0, with 1 mM sodium dithionite at 37°C. (B) MCD spectrum of Fe(II) DGCR8 HBD-His_6. Fe(II) DGCR8 HBD (29.4 μM) was in 20.0 mM EPPS buffer, 160 mM NaCl, 60% glycerol (v/v) and 7 mM sodium dithionite at 4.0, 8.0, 15, 25 and 50 K and 7 T. Inset: the field dependence of the MCD intensity at 442 nm was recorded at 2.5, 4.0, 8.0, 15 and 25 K. The curves were normalized to the most intense data point (2.5 K, 7 T).

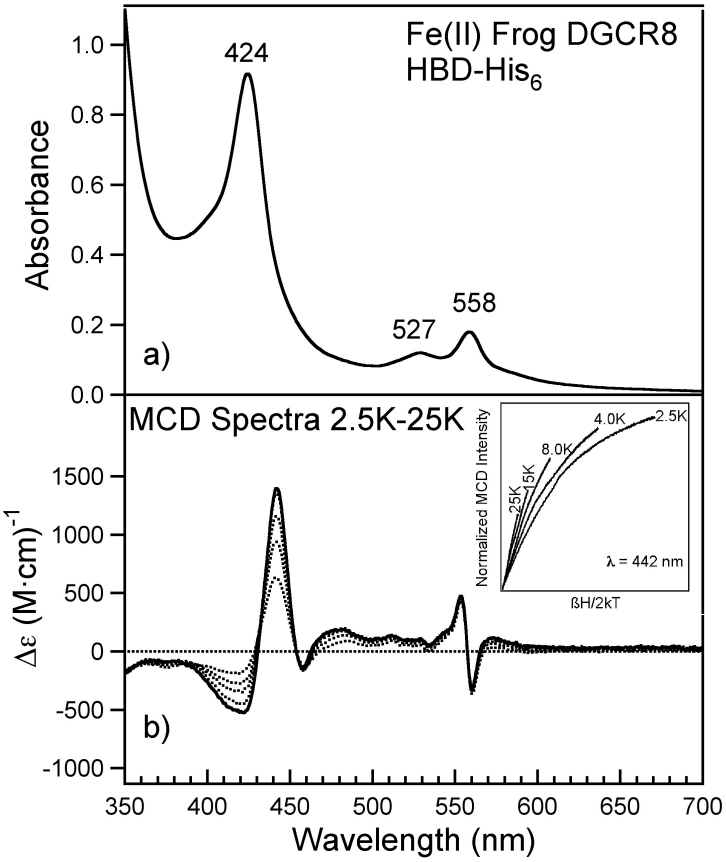

Figure 3.7. Resonance Raman spectra are shown for Fe(III) (•••) and Fe(II) (—) DGCR8 HBD-His_6 for low energy (A) and high energy (B) regions. Fe(III) DGCR8 HBD (153 μM) and Fe(II) DGCR8 HBD (136 μM) samples were in 45 mM EPPS (pH 8.0), 360 mM NaCl, and 10% (v:v) glycerol; Fe(II) HBD also contained 7 mM sodium dithionite. For the Fe(III) protein, spectra were acquired by excitation with a 457.9 nm line with 20 mW of power at the sample; for the Fe(II) protein, spectra were acquired by excitation with a 413.1 nm line with 14 mW of power at the sample.

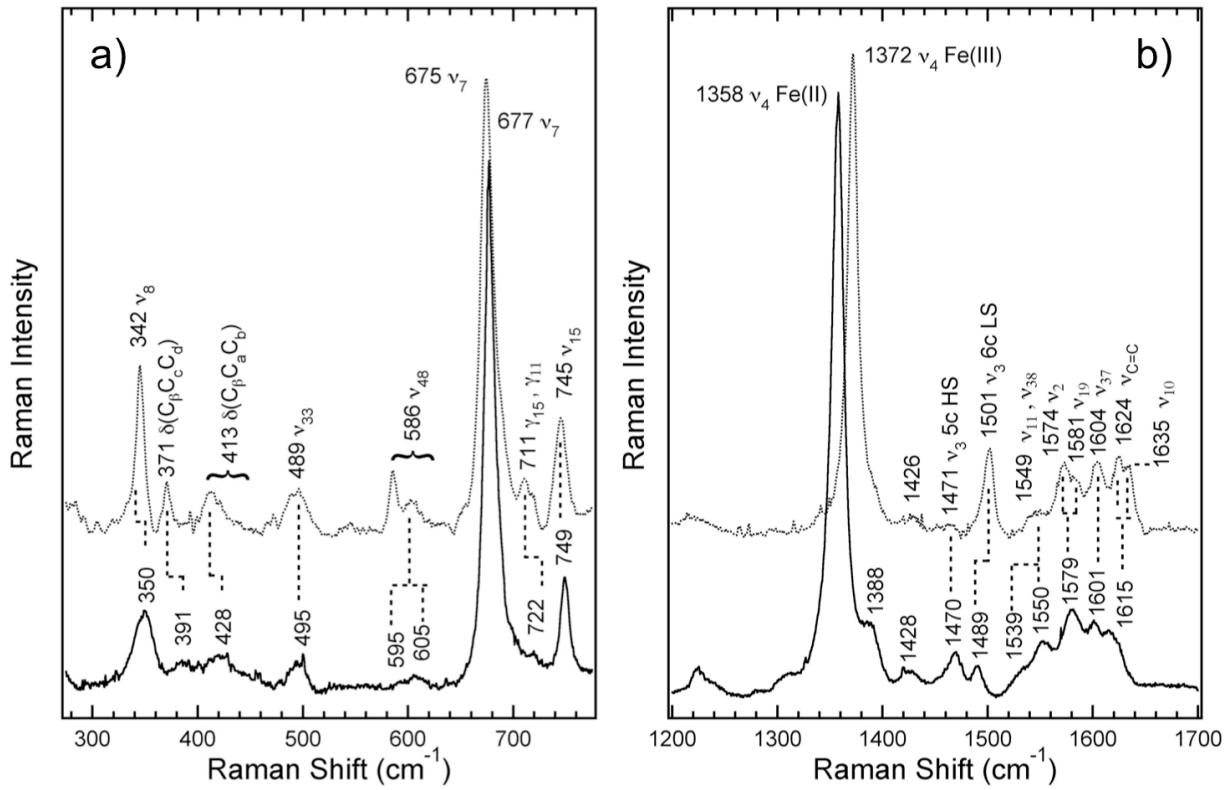

Figure 3.8. Ferrous frog DGCR8 HBD-His_6 undergoes a spin-state crossover with an apparent pK_a of 9.1 ± 0.1. The relative absorbance of Fe(III) frog DGCR8 HBD-His_6 (Soret 451 nm) is plotted and compared to Fe(II) (Soret 424 nm) frog DGCR8 HBD-His_6 as a function of pH. Representative Fe(II) spectra are shown at pHs 7.4 (HEPES), 8.0 (EPPS), 8.6 (CHES) and 10.0 (CAPS) in 50 mM buffer, 400 mM NaCl. Inset: Fe(II) apparent molar extinction coefficient at 424 nm (ε 424 nm, ♦) as a function of pH and its best-fit curve (•••).

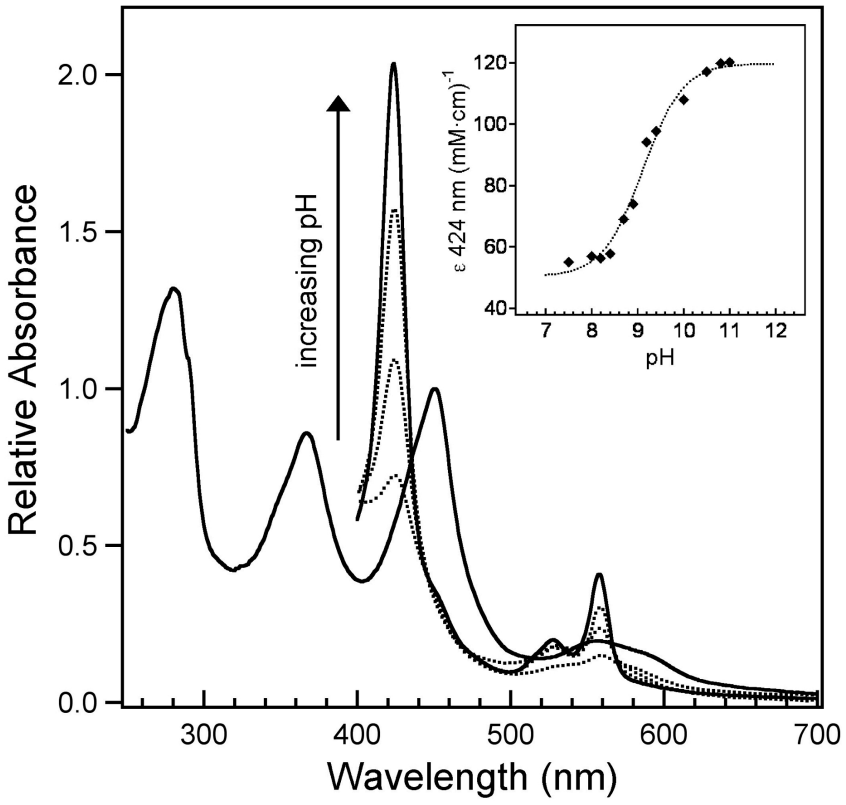

Figure 3.9. Ferrous frog DGCR8 HBD-His_6 changes from 5-coordinate high spin to 6-coordinate low spin heme as a function of pH. The low (A) and high (B) energy regions of the Fe(II) frog DGCR8 HBD-His_6 resonance Raman spectrum are shown at pHs 7.4, 8.0 and 10.0. Samples ranged from 30-136 μM in heme and were in 50 mM buffer (HEPES, EPPS and CHES for pH 7.4, 8.0 and 10.0, respectively), 400 mM NaCl and ~ 7 mM sodium dithionite. Spectra were acquired by excitation with a 413.1 nm line provided by a Kr^+ laser with ~14-15 mW of power at the sample that was capped and sealed under $Ar_{(g)}$ and immersed in a bath of ice water. The change in the positions of ν_3 and ν_2 is illustrated as the difference spectrum of the region from 1400 cm^{-1} to 1700 cm^{-1} (Δ pH 10–7.4, •••) with the appropriate modes annotated. Inset (A): a close-up of the 250-650 cm^{-1} region with the putative $\nu_{Fe\text{-}Lys}$ indicated.

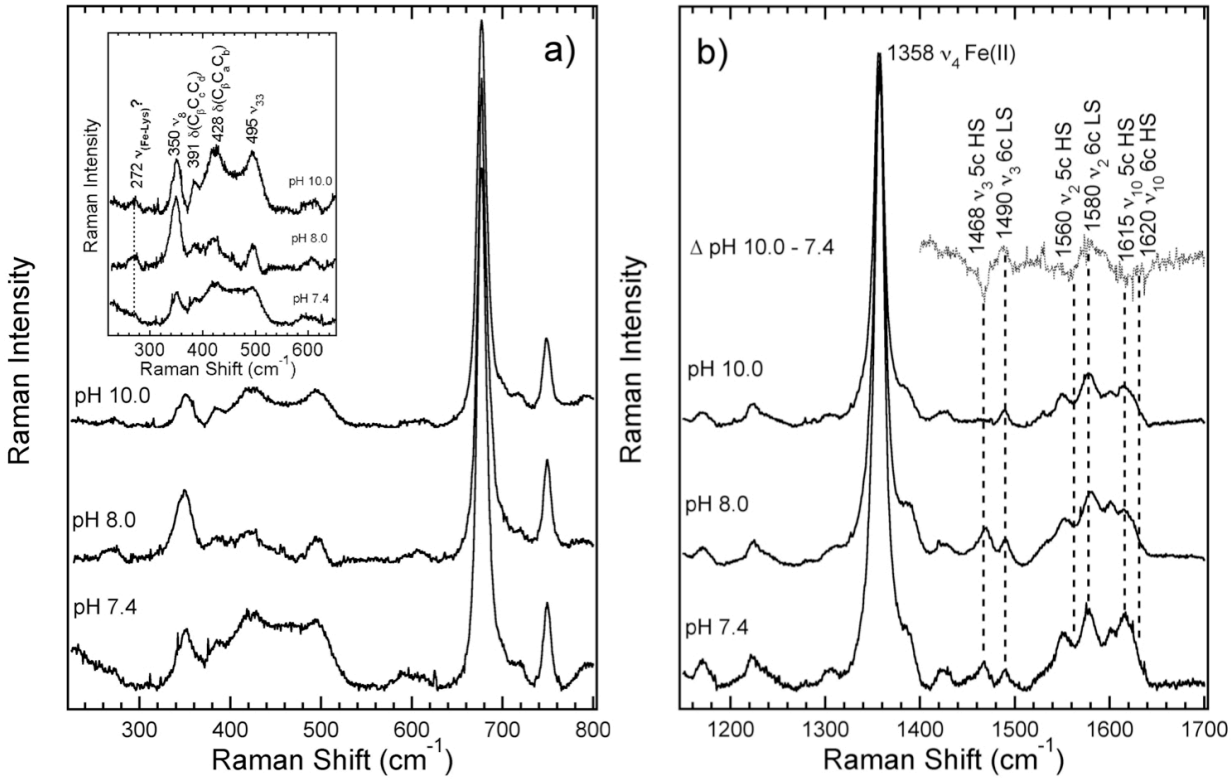

Figure 3.10. (A) PAGE demonstrating primary microRNA (pri-miRNA) processing activities. Reconstituted ^{32}P-labeled pri-miR-30a and pri-miR-21 processing assays were performed at 37 °C for 45 min using recombinant His$_6$-Drosha$^{390–1374}$ and various forms of DGCR8 as indicated. The Fe(III) and Fe(II) NC1 dimers were present at 25 nM concentrations, 89 mM Tris buffer, pH 8.6. The relationship between the low molecular weight marker (LMWM) and the Decade RNA ladder was inferred from a comparison on a similar gel. Adapted from Ref (*20*). (B) Predicted 2° structure of the DGCR8 residues in the vicinity of the Fe(III) heme ligand, Cys^{352}. The location of Cys^{352} is boxed and indicated by an inverted arrow (▼). Helical content is predicted for the residues spanning Cys^{352} to Met^{358} (sequence: CLHYKKM).

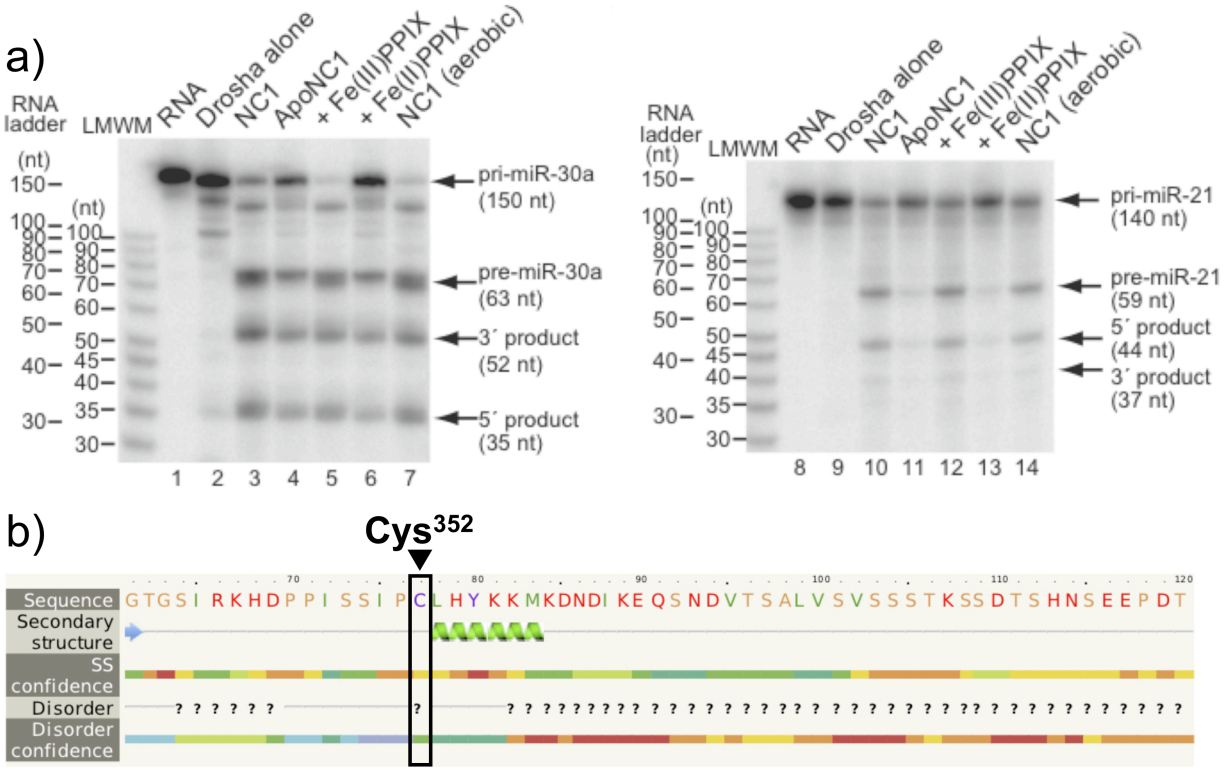

Figure 3.11. Fe(II)CO bound DGCR8 is low-spin and 6-coordinate. The electronic absorption spectrum (A) was taken at 37°C using the Fe(II)-CO DGCR8 HBD-His_6 (7.4 μM) in 50 mM EPPS (pH 8.0), 400 mM NaCl, after reaction at 37°C for 60 min with a solution of ~1 mM sodium dithionite and subsequent addition of a 300 μL bolus of $CO_{(g)}$. The MCD spectrum (B) was recorded at 50 K using the Fe(II)-CO DGCR8 HBD-His_6 (29.4 μM) in 20 mM EPPS (pH 8.0), 160 mM NaCl, and 60% (v/v) glycerol after reaction at 37°C for 2 hr with a solution of ~7 mM sodium dithionite and addition of three 300 μL boluses of $CO_{(g)}$.

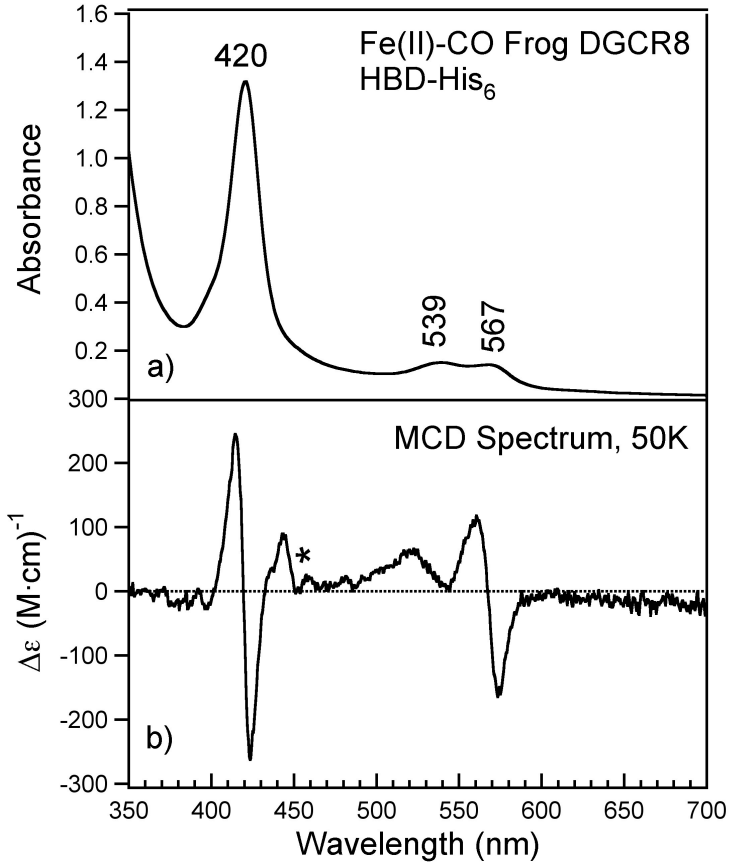

Figure 3.12. Comparison of the electronic absorption spectra of Fe(II) (•••) and Fe(II)-NO (—) DGCR8. Fe(II)-NO DGCR8 HBD-His_6 (3.7 μM) was in 50 mM EPPS, pH 8.0, 400 mM NaCl. The Fe(II) form was generated by anaerobic addition of a solution of sodium dithionite (final concentration ~1 mM) and then subsequent reaction at 37°C for ~ 60 min. The Fe(II)-NO form was generated by anaerobic addition of a 300 μL bolus of $NO_{(g)}$ to the pre-reduced protein.

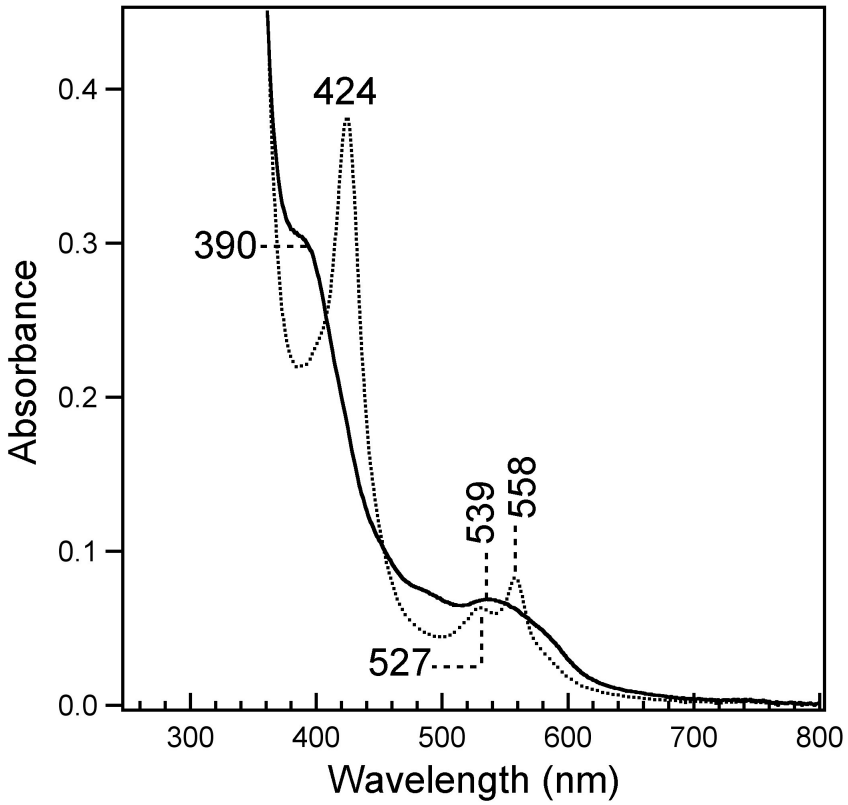

Figure 3.13. X-band EPR spectrum of the Fe(II)-NO heme-bound frog DGCR8 HBD-His_6 protein. Fe(II)-NO DGCR8 HBD (136 μM, ⎯) was in 50 mM EPPS (pH 8.0) and 400 mM NaCl. The spectrum represents an average of 10 scans taken at 25 K, with 9.385 GHz microwave frequency, 4.000 G modulation amplitude, 100 kHz modulation frequency, 60 dB receiver gain, 81.92 ms time constant, and a power of 10.02 mW. Dotted line (•••) represents the best-fit simulation.

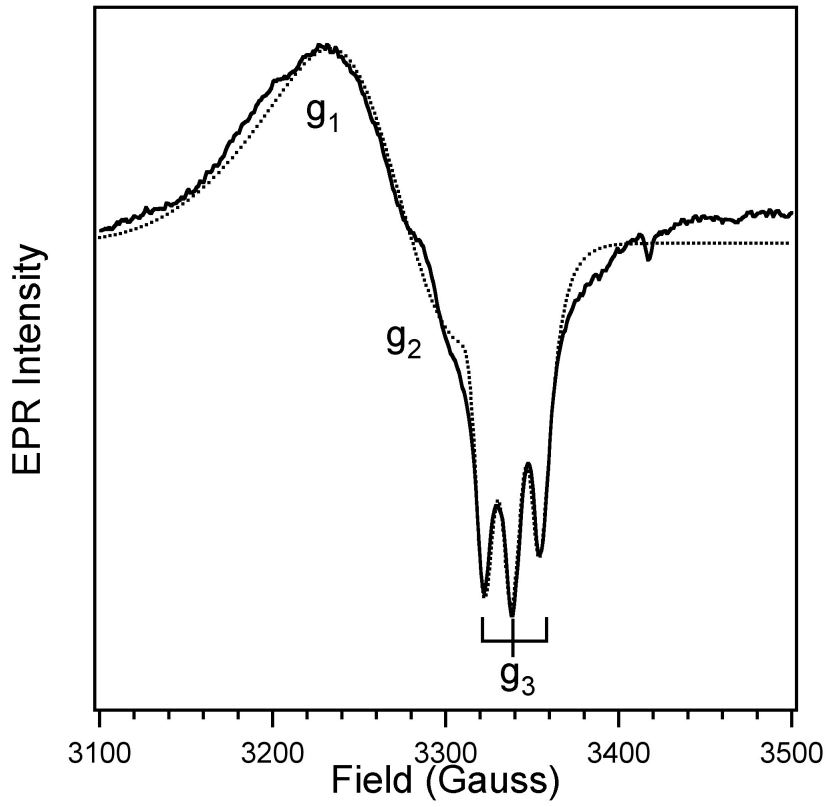

Scheme 3.1. Cartoon depiction of microRNA biogenesis. Adapted from reference (*102*).

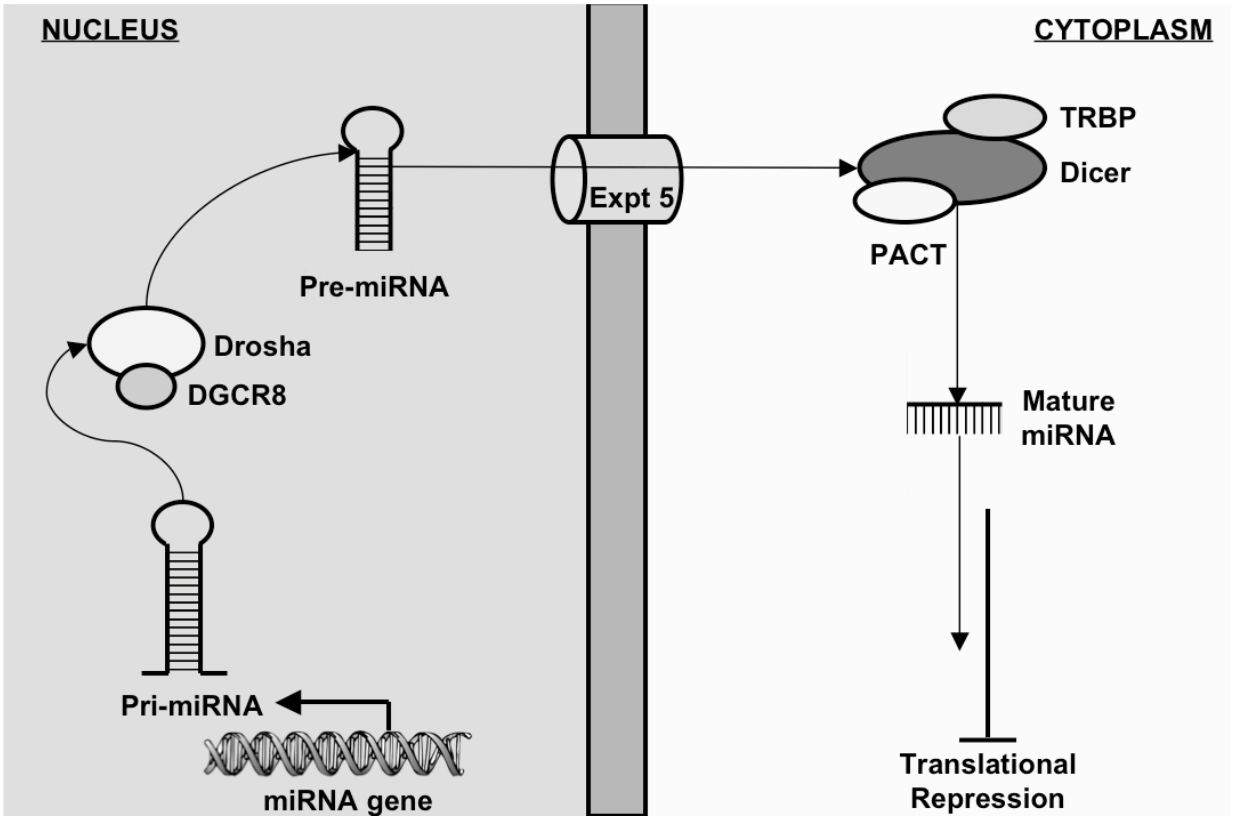

Scheme 3.2. Schematic depiction of the varying oxidation, ligation, and gas-bound states of the heme in DGCR8. Fe(III) DGCR8 is capable of processing primary microRNAs, whereas Fe(II) DGCR8 is not. The ability of the gas-bound forms (Fe(II)-CO and Fe(II)-NO) of DGCR8 to process primary microRNAs is currently unknown.

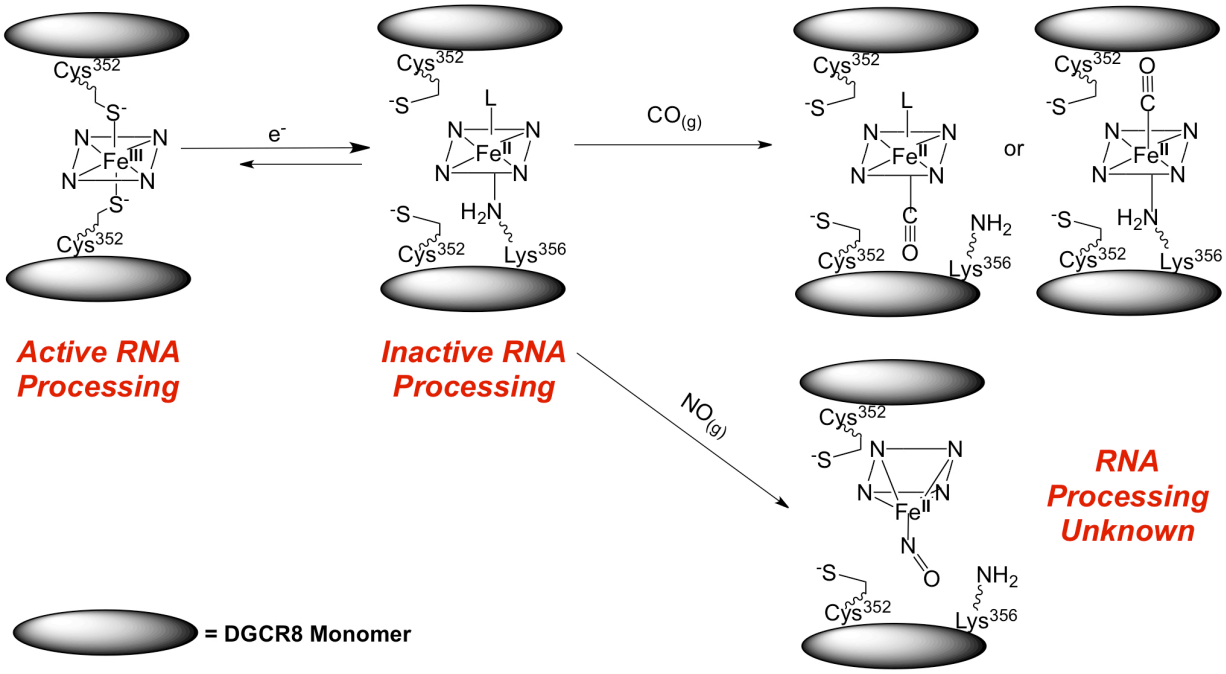

Chapter Four

Cobalt Cystathionine β-Synthase: A Cobalt-Substituted Heme Protein with a Unique Thiolate Ligation Motif

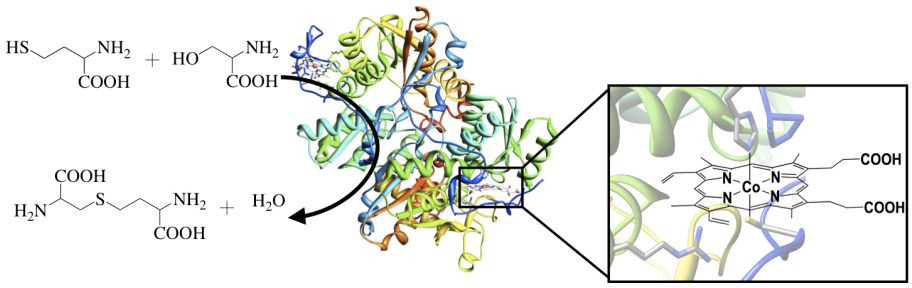

A version of this chapter was published as:

Smith, A. T.; Majtan, T.; Freeman, K. M.; Su, Y.; Kraus, J. P.; Burstyn, J. N. *Inorg. Chem.* **2011**, *50*, 4417-4427.

All cobalt CBS expression and purification was performed by Dr. Tomas Majtan in the laboratory of Professor Jan P. Kraus at the University of Colorado, Denver. Canonical and alternative CBS assays were performed by Tomas Majtan and Yang Su. Metal analyses were performed by Katherine Freeman.

Introduction

Cystathionine β-synthase (CBS) is a pyridoxal-5′-phosphate (PLP)-dependent enzyme that lies at a critical branch point in the methionine metabolic cycle. CBS is chiefly responsible for the condensation of homocysteine, a toxic metabolite and by-product of sulfur metabolism, with serine to form cystathionine (*1*). Mutations in the gene that codes for human CBS allow for accumulation of plasma homocysteine resulting in a condition called CBS-deficient homocystinuria (CBSDH). This conditions is manifested physiologically by a variety of symptoms, ranging from vascular occlusions to dislocated ocular lenses, skeletal problems, and mental retardation as well as increased risk of Alzheimer's and Parkinson's diseases (*2-5*).

Mammalian CBS is unique in that it is the only known PLP-dependent enzyme to also contain a heme *b* cofactor, and since the heme is proposed to function as a regulatory site, the relationship between these cofactors is of interest. CBS exists as an α_4 homotetramer of 63-kDa subunits. Each enzyme subunit contains three domains: N-terminal, central catalytic, and C-terminal; these domains bind heme, PLP, and S-adenosyl-methionine (AdoMet), respectively (*6, 7*). Binding of AdoMet to the C-terminal domain functions in allosteric regulation by increasing enzyme activity approximately four-fold (*8*). Removal of the C-terminal domain results in a truncated, 45-kDa form of CBS (CBS-45) in which the oligomeric status of the enzyme has changed from a tetramer to a dimer. Truncation is accompanied by loss of responsiveness to AdoMet and an approximate three-fold increase in activity. CBS-45 has been successfully crystallized and used to elucidate the tertiary structure of the enzyme and the ligands to the heme cofactor. The heme is located in proximity to the PLP active site, with the closest edge of the heme macrocycle positioned approximately 14 Å from the PLP phosphate (*9-11*).

The heme of CBS is axially coordinated via an uncommon Cys/His motif that involves the thiolate of Cys^{52} trans to the $N_{\varepsilon 2}$ atom of His^{65} with the amino acid ligands both provided by the N-terminal tail of the polypeptide (*10, 12*). While the catalytic condensation reaction of homocysteine and serine can be fully explained by reaction at the PLP cofactor, heme is necessary for optimal activity (*6, 13-16*). CBS from lower organisms such as *Saccharomyces cerevisae* and *Trypanosoma cruzi* lack either the N-terminal motif or the C- and N-terminal motifs, respectively, that bind AdoMet and heme, making them unresponsive to the allosteric regulator and exogenous forms of the cofactor; these observations suggest that AdoMet and heme are recent evolutionary acquisitions (*17-19*). The heme of CBS was initially postulated to function as a redox sensor, based on decreased enzymatic activity in the ferrous form. The logic of such redox regulation would be to control the flux between the trans-sulfuration (utilizing CBS) and transmethylation (utilizing methionine synthase) pathways (*11, 20, 21*). Yet, it has been shown that activity of the ferrous and ferric forms of CBS are identical when Cys^{52} is retained, and that the decrease in activity upon reduction is likely due to an irreversible ligand switch at the heme (*22-24*). In all cases studied to date where the heme Fe- Cys^{52} bond was disrupted or modified, including reactions with NO, CO, $HgCl_2$, and peroxynitrite, enzyme activity was lost (*22, 25-28*). The link between this loss of activity *in vitro* and CBS heme function *in vivo* is uncertain; consequently, the role of the heme in CBS is still unknown.

We report herein characterization of a cobalt-substituted variant of human CBS (Co hCBS). Recently, we described the expression of Co hCBS in *Escherichia coli* and its purification to homogeneity (*29, 30*). In this study, we demonstrate that the as-isolated form of Co hCBS is in the Co(III) oxidation state, is active in both the canonical assay and an alternative CBS reaction assay, and bears a Cys/His Co(III) porphyrin ligation motif similar to

that of WT Fe(III) hCBS but unprecedented in cobalt porphyrin-substituted proteins. We show that cysteine ligation to the Co(III) porphyrin may be disrupted upon reaction of the enzyme with $HgCl_2$, and that this metal-thiolate bond disruption occurs with a concomitant reduction in enzyme activity. We also demonstrate that the Co-substituted enzyme can access the Co(II) oxidation state, likely forming a 5-coordinate, His-ligated Co(II) porphyrin, which will bind $NO_{(g)}$ but not $CO_{(g)}$. Formation of the 5-coordinate Co(II) porphyrin with concomitant loss of the cysteine(thiolate) ligand correlates with a significant loss in enzymatic activity. Based on these findings, we postulate that the Co porphyrin binds to hCBS similarly to heme in the WT enzyme, and that the enzyme is unable to distinguish between heme (FePPIX) and CoPPIX. These data are consistent with a structural role for the CBS heme, where this structural component modulates enzyme activity.

Materials and Methods

Materials. Materials used in buffer preparation were purchased from Sigma-Aldrich and used as received. $NO_{(g)}$ was generated *in situ* by mixing $NaNO_2$ (Sigma-Aldrich), $CuCl_2$ (MCB Chemicals), and *L*-ascorbic acid (99+%, Sigma-Aldrich) with a previously prepared buffer solution. Appropriate imidazole solutions were made with 1-methylimidazole (99%, redistilled) or 4-methylimidazole (99%) both from Sigma-Aldrich. Co(III)PPIX-Cl was purchased from Frontier Scientific, Inc. and stored in a desiccator until used. $HgCl_2$ solutions were made fresh for each experiment from solid $HgCl_2$ (J.T. Baker, Inc.). Ninhydrin was purchased from Fluka; ninhydrin reagent was prepared by dissolving 0.25 g ninhydrin (as received) in a mixture of 4 mL concentrated HCl and 6 mL concentrated acetic acid.

Isolation and Purification of Co hCBS. The expression and purification of human CBS containing CoPPIX was performed as described in our previous work (*24, 29, 30*). Briefly, *E. coli* Rosetta2 (DE3) cells carrying the expression plasmid for WT human CBS (pGEX-6P1-hCBS WT) were grown overnight 12-times in M9 minimal medium supplemented with $CoCl_2$ (~150 μM final concentration). The last culture served as an inoculum for large-scale expression and purification. Purification of Co hCBS essentially continued as described for WT hCBS (*24, 31*) with the modifications described by Majtan *et al.* (*29*). Briefly, the CBS-GST fusion protein was isolated on GSH-Sepharose, and the GST fusion partner was cleaved with PreScission protease (*24*). CBS was separated from GST by DEAE Sepharose chromatography (*29*). The cobalt content in the final, purified Co hCBS was >90% (*29*).

Electronic Absorption Spectroscopy. Electronic absorption spectra were recorded on a double-beam Varian Cary 4 Bio spectrophotometer with a temperature controller, set to a spectral bandwidth of 0.5 nm. Spectra were obtained at varying temperatures from 4 to 37°C for samples of protein in 500 mM CHES with 100 mM NaCl, pH 9.0, as indicated; this non-physiological pH was chosen because WT Fe hCBS is maximally active between pH 8.5 and 9.0, and natively-coordinated (His^{65}/Cys^{52}) Fe(II)CBS is most stable at this pH (*20, 32*). Samples were purged of oxygen by flowing $Ar_{(g)}$ through the headspace of a septum-sealed cuvette for ~ 10 min. Reduction of Co(III) protein samples was accomplished by adding an anaerobically prepared stock solution of sodium dithionite or dithiothreitol (DTT), to achieve a final sample concentration of 1-5 mM. The solutions of dithionite or DTT and Co(III) protein were allowed to equilibrate at 4°C before anaerobic addition of stock reductant (~ 30 mM, 10 μL) to the Co(III) protein. The temperature controller of the spectrophotometer was slowly raised to 37°C and the reduction of Co(III) to Co(II) was monitored over ~1 hr or until no further spectral changes were observed. Fresh stock $HgCl_2$ solutions were prepared for each experiment; the stock solution (~ 60 mM, 10 μL) was administered at room temperature to achieve a final $HgCl_2$ concentration of 1-2 mM, and spectra were collected for ~2 hr or until no more spectral changes were observed. Spectra of reduced Co(II) hCBS are reported for reduction with DTT. Analysis by MCD and EPR spectroscopies indicated formation of a diamagnetic Co(II) species upon dithionite reduction, possibly suggesting formation of a $SO_2^{-\bullet}$-Co(II) adduct. NO adducts were prepared by injecting three 100 μL samples of $NO_{(g)}$ (generated by mixing $NaNO_2$, $CuCl_2$, *L*-ascorbic acid, and 1 mL of CHES stock buffer solution) to the headspace of a septum-sealed vial containing the Co(III) form of the protein. Reduction and binding of $NO_{(g)}$ were subsequently induced by anaerobic addition of a stock

solution of DTT (~ 30 mM, 10 μL), and the reaction was followed spectrophotometrically at 37°C until no further changes were observed. Reoxidation of the Co(II) form of the protein was followed spectrophotometrically over the course of 2 days by introducing ambient air to the septum-sealed cuvette containing the DTT-reduced protein. Co(III)PPIX-Cl standards were made by dissolving the solid in either CH_2Cl_2 or 1:100 (v/v) DMSO:H_2O, with ~ 0.5 mL 6*M* NaOH per every 100 mL. Porphyrin concentrations were determined using ICP-OES, to give the metal concentration, and Beer's law using the appropriate ε value. Imidazole solutions (4-MeImH or 1-MeIm) were prepared in either CH_2Cl_2 or 1:100 (v/v) DMSO:H_2O, and 1 or 2 equivalents were added to the Co(III) porphyrin solution in septum-sealed cuvettes. Ligand binding was monitored spectrophotometrically.

MCD Spectroscopy. Magnetic circular dichroism (MCD) spectra were recorded on a Jasco J-715 CD spectropolarimeter with the sample compartment modified to accommodate an SM-4000-8T magnetocryostat (Oxford Instruments). The buffer used for the MCD samples was 500 mM CHES, 100 mM NaCl, pH 9.0, with approximately 55% (v/v) glycerol present in the final sample. Glycerol was introduced to the Co(III) form of the protein and stirred with a syringe until the solution was homogenous. Co(II) samples were prepared from glycerol-containing Co(III) protein solutions, with monitoring of the visible spectral changes at 37°C. The final concentrations were: DTT, ~5 mM; protein, ~30 μM; in a total volume of 125 μL. Glycerol had no effect on the electronic absorption spectra at room or liquid-helium temperatures, for either Co(II)- or Co(III) hCBS. Samples were transferred via gastight syringe into cells purged with $Ar_{(g)}$, flash-frozen, and stored in $N_{2(l)}$. MCD spectra were taken over a temperature range from 4 to 200 K. The MCD signal at each temperature was recorded at ±7 T. Negative polarity data

were subtracted from positive polarity data to remove CD contributions, and the resulting spectrum was divided by 2. For the spectra of Co(III) and Co(II) hCBS at 4 K, MCD contributions from the native Fe-containing enzyme (< 8%) were subtracted from the Co hCBS signal. The resulting difference spectrum was compared to the high-temperature spectrum (50 K), in which the paramagnetic signals were minimized. These spectra were virtually indistinguishable.

EPR Spectroscopy. X-band electron paramagnetic resonance (EPR) spectra were collected on a Bruker ESP 300E equipped with an Oxford ESR 900 continuous flow cryostat connected to an Oxford ITC4 temperature controller. The microwave frequency was monitored using an EIP model 625A CW microwave frequency counter. Field calibration was achieved using a Varian ER 035M gaussmeter. Spectra of Co(II) hCBS and of Co(II)PPIX model complexes were recorded in 500 mM CHES buffer, 100 mM NaCl, pH 9.0. Co(II) protein samples were prepared from Co(III) protein solutions in buffer, with monitoring of the visible spectral changes at 37°C. The final concentrations were: DTT, ~16 mM; protein, ~150 μM; in a total volume of 200 μL. Co(II)PPIX model complex solutions were prepared from Co(III)PPIX model complex solutions in glycerol and buffer, with monitoring of the visible spectral changes at 37°C. The final concentrations were: DTT, ~20 mM; Co(II)PPIX complex, ~200-400 μM; in a total volume of 1000 μL and 55% glycerol (v/v). Each sample was transferred via a gastight syringe into an $Ar_{(g)}$-filled quartz EPR tube and frozen in $N_{2(l)}$. For all samples, scans of 0—10000 G revealed no signals other than those reported. EPR data were simulated using the WEPR program written by F. Neese (*33*).

Computations. All calculations were performed on a Dell Vostro desktop PC. Initial geometric models for Co(III)(porphine)(4-MeImH)thiophenolate [Co(P)(4-MeImH)(SPh)] and Co(III)(porphine)(4-MeImH)methanethiolate [Co(P)(4-MeImH)(SMe)] were based on the optimized coordinates of computational models of analogous iron(III) five-coordinate, high-spin, thiolate-bound heme systems to which 4-methylimidazole was added as a sixth ligand (*34, 35*). Spin-restricted ($S = 0$) geometry optimizations of each cobalt model were performed using ORCA 2.6.35 software developed by Dr. Frank Neese (MPI Mülheim, Mülheim, Germany) implementing the B3LYP correlation functional (*36, 37*). A triple-ζ Slater-type orbital (STO) basis set, with the Ahlrichs polarized split valence basis SV(P) and SV/C auxiliary basis sets, was chosen for all atoms except Co and S, to which an additional polarization function (TZVP) was applied. Core orbitals were frozen through 1s for C and N and through 2p for Co and S. Time-dependent density-functional theory (TD-DFT) calculations were performed similarly using ORCA 2.6.35 and the same basis sets and functionals. A total of 40 excited states were calculated within a range of ± 3 hartree from highest occupied molecular to lowest unoccupied molecular orbital gap. Isosurface plots of relevant molecular orbitals and electron density difference maps were generated with Laaksonen's gOpenMol program, v. 3.00 (*38, 39*).

CBS Activity Assays. The activities of Co(III) hCBS, Hg-reacted Co(III) hCBS and Co(II) hCBS were measured in the canonical cystathionine synthesis reaction (*29*) and one alternative cysteine synthesis reaction. To monitor cysteine synthesis, the reaction mixture (600 μL) contained: 0.5 mg/mL BSA, 10 mM DTT, 0.5 mM PLP, 0.36 mM AdoMet, 0.015 mg/mL enzyme, 24 mM L-serine and 25.5 mM Na_2S in 200 mM Tris buffer (pH 8.6). The reaction temperature was maintained at 37°C; the total incubation time was 12 min, with measurements

at 4, 6, 8, 10 and 12 min. The cysteine concentration at each of the five time points was measured by a colorimetric method (*40*). A sample (100 μL) of the reaction mixture was taken and mixed with 50%(w/v) trichloroacetic acid (20 μL). The precipitated protein was removed by centrifugation. The supernatant (100 μL) was combined with acetic acid (100 μL) and ninhydrin reagent (100 μL); the mixture was heated in a boiling water bath for 3 min and immediately cooled in ice water. The absorbance at 560 nm was measured to determine the amount of cysteine produced. A standard curve was generated by the same method using cysteine solutions of known concentration and containing all other reagents except enzyme. To prepare Hg-reacted Fe(III) hCBS or Co(III) hCBS for assay, $HgCl_2$ was added as described (*vide supra*) and allowed to react for 2 hr. The protein solution, containing excess $HgCl_2$, was loaded onto a YM-30 Amicon Ultra spin concentrator (Millipore) and washed 3 times by concentration and dilution into fresh Tris buffer (200 mM, 100 mM NaCl, pH 8.6) using a table-top centrifuge (RCF 15,000 x *g*). Hg-treated Fe(III) hCBS or Co(III) hCBS was diluted in the final step to achieve a protein concentration of ~ 0.7 mg/mL. To prepare Co(II) hCBS for assay, Co(III)hCBS was pre-incubated with 10 mM DTT, 0.5 mg/mL BSA, 0.5 mM PLP at 37°C for 3 hours. For enzymatic reactions catalyzed by Fe(III)- and Co(III) hCBS, Hg-reacted or not, the reaction was initiated by adding the enzyme. For reactions catalyzed by Co(II)hCBS, the reaction was initiated by adding the substrates.

Results

Co(III) hCBS displays unique spectral properties.

The electronic absorption features of Co(III) hCBS are unique among the family of Co-substituted heme proteins. The band shapes and positions of this spectrum, shown in Figure 4.1A, are characteristic of the Co(III) oxidation state (*41, 42*). Notable are the distinct α and β bands (588 and 553 nm, respectively) and a sharp Soret peak (442 nm); identical spectra were observed for Co(III) hCBS at pH 7.4 (500 mM HEPES, 100 mM NaCl) and at pH 6.0 (500 mM MES, 100 mM NaCl) (data not shown). A comparison of Co(III) hCBS to other Co-substituted proteins (Table 4.1) reveals that the electronic absorption spectrum of Co(III) hCBS is distinct. All three absorption bands of Co(III) hCBS are red shifted relative to those of Co(III)- Hb, Mb, HRP and Cyt *c*, which are 6-coordinate with neutral or weakly donating anionic ligands. These red-shifts suggest that at least one strongly electron-donating ligand is bound to the Co(III) center; however, the red-shifts of the Co(III) hCBS spectrum are not as pronounced as those of the dithiolate-coordinated Co(III) $P450_{cam}$(DTT) (*43*). Furthermore, Co(III) hCBS exhibits distinct α and β bands, in contrast to the poorly resolved absorption envelope of Co(III) $P450_{cam}$(DTT). These observations suggest that the axial ligands surrounding the cobalt center in Co(III) hCBS are different from those of other previously observed cobalt-substituted heme proteins.

Co(III) porphyrin model compounds provide insight into the nature of the unusual coordination environment in Co(III) hCBS. The Co(III) hCBS spectrum is different from those of 6-coordinate Co(III) PPIX complexes with bis-imidazole or bis-thiolate; however, there is a reasonably close match between the Co(III) hCBS spectrum and those of Co(III) PPIX complexes with one imidazole and one thiolate ligand (Table 4.1). These imidazole-thiolate-

bound model compounds exhibit red shifted peak maxima, with distinct α and β bands, albeit at slightly higher energy than those of Co(III) hCBS. A further important similarity is the presence of a relatively intense δ band, which is characteristic of thiolate-to-metal charge transfer transition mixing with the porphyrin $\pi \rightarrow \pi^*$ transition. Overall, there exists a distinct correlation between the red shifts of the electronic absorption spectrum and the number of thiolate ligands bound to the Co(III) center. These comparisons suggest that the coordination environment in Co(III) hCBS is like that of Fe(III) hCBS, with one thiolate and one histidine as the axial ligands.

Co(III) hCBS was further characterized by MCD spectroscopy (Figure 4.1B) to isolate the Co(III) porphyrin spectral contributions from that of the native Fe(III) heme, and to confirm that the Co coordination environment is distinct from those of previously studied Co-substituted heme proteins. Co(III) hCBS was previously shown to contain a majority Co (92%) and a residual amount of Fe (~8%) (*29*). Co(III) porphyrins are consistently low-spin (*42, 43*); because of this property, the MCD signature of a Co(III) porphyrin-containing protein should show no temperature dependence, indicative of the cobalt's d^6, $S = 0$ ground state (*44*). At 4 K, Co(III) hCBS exhibits signals that reflect contribution from both Co(III) and Fe(III), consistent with metal analyses that show ~8% Fe in the Co hCBS protein (*29*). Paramagnetic low-spin Fe(III) gives temperature dependent MCD spectra; at 50 K the Fe(III) contribution to the MCD spectrum is minimized, and the signature of diamagnetic low-spin Co(III) hCBS dominates. Figure 4.1B shows the 4 K MCD spectrum of Co(III) hCBS from which the contribution of the Fe(III) was removed by subtraction. This spectrum is virtually identical to that obtained at 50 K. No temperature dependence of the Co(III) signal is observed, consistent with the predicted spin state. The isolated spectral MCD signatures of Co(III) hCBS are shown in Table 4.2 and

compared with that of the native Fe(III) hCBS. As is typical with many diamagnetic d^6 metal porphyrins, the temperature-independent, derivative-type *A* terms in the α-β region of the spectrum dominate in intensity when compared to the *A* term in the Soret region (*45, 46*). In the MCD spectrum of the Co(III) protein, the shape of the term resulting from the $\pi \rightarrow \pi^*$ transition of the Soret region is similar to that of other Co(III) porphyrins (*47*). The α-β MCD transitions lie on the red-edge of the absorption maxima and the *A* terms display moderate asymmetry with multiple crossover peaks; these observations implicate charge-transfer bands that overlap in this region (*47*). These characteristics are not observed in the MCD spectrum of a model compound Co(III)PPIX(1-MeIm)$_2$ (Figure 4.2), implying that the coordination environment of Co(III) hCBS does not contain two neutral donor ligands.

Co(III) hCBS has one axial thiolate ligand.

The reactivity of Co(III) hCBS confirms the presence of a thiolate ligand. $HgCl_2$, a known metal-thiolate bond disrupter (*27, 48, 49*), reacts with Co(III) hCBS, as shown in Figure 4.3. Immediately upon addition of $HgCl_2$, changes were evident in the electronic absorption spectrum. The Soret and α-β bands immediately broadened and blue-shifted; the δ band, normally intense in thiolate-ligated metalloporphyrins due to orbital mixing between the sulfur and the metal, became nondescript and indistinct. After 2 h, the spectrum had settled into a new position with peak maxima at 427 nm (Soret), 538 nm (β), and 573 nm (α). These spectral changes are evidence that $HgCl_2$ disrupted a Co(III)-thiolate bond. The final spectrum was consistent with that of a Co(III) porphyrin bearing two neutral donor ligands, as revealed by the comparison of peak positions for the Hg-disrupted Co(III) hCBS protein with those of other Co-substituted proteins and model compounds (Table 4.1). This comparison clearly shows that when the thiolate ligand is lost, the Co(III) hCBS protein compensates by providing an

alternate neutral ligand. Addition of β-mercaptoethanol to the Hg-disrupted Co(III) hCBS protein did not result in further spectral changes (data not shown). Thus, β-mercaptoethanol was unable to reverse the Hg-induced ligand switch, in contrast to some other heme-thiolate proteins (*48*). The lengthy time for full conversion from thiolate-ligated Co(III) hCBS to the final Hg-disrupted form, and the fact that this process does not proceed with isosbestic spectral conversion, suggests that Co-thiolate bond disruption occurs faster than replacement with the alternate neutral donor ligand. However, no discrete spectrum for a 5-coordinate intermediate was observed.

Time-dependent density-functional theory (TD-DFT) calculations support the presence of a thiolate ligand bound to Co(III) hCBS. Calculations were carried out on two closed shell *S*=0 cobalt model compounds (Figure 4.4): Co(III)(porphine)(4-MeImH)thiophenolate [Co(P)(4-MeImH)(SPh)] and Co(III)(porphine)(4-MeImH)methanethiolate [Co(P)(4-MeImH)(SMe)]. Geometry-optimized structures were calculated, and these structures served as the input for time-dependent calculation of electronic absorption spectra. The predicted absorption spectra exhibit two dominant transitions (γ, δ) of comparable intensity, with the lower energy transition (γ) arising from pure porphyrin $\pi \rightarrow \pi^*$ transfer transitions, and the higher energy transition (δ) arising from mixing of porphyrin $\pi \rightarrow \pi^*$ and ligand-to-metal charge transfer (LMCT) ($S(p) \rightarrow Co(d_\sigma)$) transitions. Figure 4.4C illustrates the select charge-transfer transition that mixes with the porphyrin $\pi \rightarrow \pi^*$ transfer transitions (not shown) and gives rise to the intense δ band. The dark blue color on the sulfur(thiolate) p orbital represents loss of electron density; the light green color on the cobalt d orbital represents a gain of electron density. Thus, the presence of an intense δ band arises from the unique donor character of a single thiolate ligand. Additional charge transfer bands are predicted to occur at

wavelengths beyond the α-β region; however, the predicted intensity of these transitions is extremely weak. The prediction of a prominent δ band by calculation correlates well with the observation of such a δ band in the electronic absorption spectrum of Co(III) hCBS, corroborating the presence of a thiolate ligand bound to the Co(III) center.

Co(II) hCBS is similar to other known Co-substituted heme proteins.

Two redox states of Co hCBS, Co(III) and Co(II), are accessible, as is typical of other Co porphyrin-substituted heme proteins (*41, 50-53*). Figure 4.5 depicts the conversion from Co(III) hCBS to Co(II) hCBS, induced by addition of a DTT solution at pH 9.0. Reduction is slow, requiring approximately 3.5 hours to complete the reaction at 37°C (Figure 4.5, inset). Interestingly, this reduction is strongly pH dependent, proceeding slowly at pH 9.0 and pH 6.0 at 37°C, and exceedingly slowly at pH 7.4 at 37°C. Under these physiological conditions, reduction was not complete after 8 hr. A pH dependence on the rate of reduction of Co porphyrin-substituted heme proteins has been observed previously (*41*). The reduction rate of Co(III) hCBS was also temperature dependent. At <4°C, no discernible reduction takes place; at >4°C, Co hCBS exists as a mixture of oxidation states until fully reduced at high temperature (37^{o}C) and high pH (9.0). Once fully reduced, cooling the protein does not reverse the reduction process.

Co(II) hCBS (Figure 4.6A) appears to be 5-coordinate, most plausibly retaining a single histidine ligand. Table 4.3 compares the electronic absorption spectrum of Co(II) hCBS to those of other Co-substituted proteins. This comparison reveals that Co(II) hCBS resembles other 5-coordinate Co(II) proteins. When 6-coordinate Co porphyrin-substituted heme proteins are reduced, loss of one axial ligand is observed. The ligand that is retained is typically histidine, which may be identified in EPR spectra by the presence of superhyperfine coupling

between the unpaired electron ($S = ½$) and the imidazole nitrogen ($I = 1$) superimposed on the hyperfine coupling with the Co nucleus ($I = {}^{7}/_{2}$) (*50-53*). An exception is Co(II)-substituted $P450_{cam}$, in which the thiolate ligand is retained (*43*). Co(III) hCBS bears both a histidine and a thiolate, and either is a candidate to be lost upon reduction. The similarity of the Co(II) hCBS electronic absorption spectrum to that of 5-coordinate histidine ligated Co-proteins suggests that the thiolate is the ligand that is lost. Further support for this conclusion is drawn from the fact that addition of $HgCl_2$ to the fully reduced Co(II) hCBS enzyme has no effect on the absorption spectrum (data not shown).

MCD spectroscopy further supports the conclusion that the metal ion is fully reduced, and that the spectral signatures of Co(II) hCBS arise from the Co center. The MCD signature of Co(II) hCBS (Figure 4.6B, Table 4.4) is similar to those of other reported Co(II) porphyrin complexes (*45, 47*). The intensity of the asymmetric *C* term (crossover at 554 nm) that corresponds to the α-β region of the electronic absorption spectrum is smaller than that of the *C* term that corresponds to the Soret region of the electronic absorption spectrum (crossover at 387 nm). This intensity difference is indicative of the Co(II) oxidation state (*47*). Additionally, a temperature dependence was observed in the MCD spectrum of Co(II) hCBS over the range 4-25 K. A low-spin Co(II) porphyrin ($S = ½$) would be expected to show a temperature-dependent MCD signature. Magnetic saturation curves, which are sensitive to the spin state on the metal, reveal that the *C* term that dominates the MCD spectrum of Co(II) hCBS is an admixture of low-spin, Co(II) ($S = ½$) and low-spin, Co (III) ($S = 0$) after subtraction of the native, Fe(III) signal (data not shown). When the MCD spectrum of Co(II)PPIX(1-MeIm) was recorded over a range of temperatures (4-25 K, Figure 4.7), a similar temperature dependence for the dominant *C* term is observed, consistent with an $S = ½$ spin state on the Co(II) center.

The spin-state and geometry of Co(II) hCBS and of the Co(II)PPIX(1-MeIm) model complex are confirmed by EPR spectroscopy. The low-temperature (4.5K) X-band EPR spectrum of Co(II)PPIX(1-MeIm) displays axial symmetry with $g_{\perp} = 2.30$ and $g_{\parallel} = 2.03$ (Figure 4.8). This observation further confirms the oxidation state; additionally, the presence and values of the both hyperfine coupling ($A_{\parallel}^{Co} \sim 77G$) and superhyperfine coupling ($A_{\parallel}^{N} \sim 17G$) are further evidence for the presence of a nitrogenous Lewis base ligated to a 5-coordinate, square-pyramidal Co(II) center with one unpaired electron in the $3d_z^2$ orbital. These coupling constants fall squarely in range of commonly accepted coupling constants for Co(II) porphyrin-containing models and proteins bearing one nitrogenous Lewis base in the axial position (*43, 51*). Co(II) hCBS displays a similar axially-symmetric EPR signal with $g_{\perp} = 2.30$ (Figure 4.9); however, due to problems with protein aggregation at the concentrations necessary for EPR spectroscopy, no hyperfine or superhyperfine coupling could be distinguished to discern any fine structure information. Taken all together, the similarity of the band shapes and positions of the Co(II)PPIX(1-MeIm) spectra to the Co(II) hCBS spectra corroborate the assignment that Co(II) hCBS is five-coordinate and most plausibly retains a single histidine ligand.

Co(II) hCBS binds NO but not CO.

Like other Co(II)-substituted heme proteins, Co(II) hCBS will bind exogenous $NO_{(g)}$ (*53, 54*). When a limited amount of NO gas is added to pre-reduced Co(II) hCBS, a new species forms with characteristic absorption bands at 399 nm (Soret), 532 nm (β), 566 nm (α). The peak positions agree well with previous assignments for 5-coordinate Co-NO adducts (*53, 54*). Over time, the NO ligand is lost and the spectrum reverts to that of Co(II) hCBS. The Co-NO hCBS adduct may be stabilized by reducing Co(III) hCBS under an atmosphere (i.e. an excess) of NO. The electronic absorption spectrum of the NO-adduct thus formed is shown in

Figure 4.10. Co hCBS forms a 5-coordinate NO adduct; this behavior is similar to that of the native Fe hCBS, which forms a 5-coordinate Fe-NO adduct with loss of both protein-derived axial ligands (*25*). Neither the Co(III) nor the Co(II) forms of hCBS bind exogenous $CO_{(g)}$. This behavior is not unusual for Co porphyrin-containing proteins (*50, 52*), but it is in stark contrast to the native Fe hCBS which binds exogenous $CO_{(g)}$ in the Fe(II) form (*25, 55*).

Co(II) hCBS autoxidizes to Co(III) hCBS$_{Reox}$, a unique species without a thiolate ligand.

When Co(II) hCBS is exposed to ambient air, a slow reaction occurs to yield a new Co(III) species that does not bear a thiolate ligand. At room temperature, air was introduced into Co(II) hCBS and the sample was mixed to distribute oxygen through the solution. Over the course of 48 hr, the spectrum converted to that of a new species with peak maxima 424 nm (Soret), 538 nm (β) and 569 nm (α), as shown in Figure 4.11. The slow reaction of Co(II) hCBS to give the new species is quite similar to the autoxidation observed as Fe(II) hCBS converts to Fe(III) hCBS upon exposure to air (*35*). However, Co(II) hCBS does not reoxidize to give Co(III) hCBS. The most noticeable difference between Co(III) hCBS and Co(III) hCBS-424$_{Reox}$ is the absence of spectral signatures that are characteristic of thiolate ligation (*vide supra*, compare Figure 4.3 to Figure 4.11). Thus, the native thiolate ligation Co(III)hCBS is not restored upon air oxidation. The coordination environment of reoxidized Co(III) hCBS$_{Reox}$ is unclear; the peak positions most closely resemble either a Co(III) porphyrin with two neutral donors or a Co(III)-superoxide adduct with one neutral donor and one superoxide anion as the ligands (Table 4.1). The fact that Co(III) hCBS$_{Reox}$ does not show identical spectral positions to those of the $HgCl_2$-reacted Co(III) hCBS might plausibly suggest that Co(III) hCBS$_{Reox}$ may be a superoxide adduct; however, binding of an oxidized form of cysteine (cysteic acid) to the

reoxidized Co(III) porphyrin cannot be ruled out (*56*). A summary of the coordination states of the Co porphyrin in Co hCBS is given in Scheme 4.1.

Co hCBS is maximally active and AdoMet responsive only in the Co(III) state.

We compared the activity of Co hCBS in its various coordination and oxidation states, using both the canonical reaction and an alternative CBS reaction (Scheme 4.2). The alternative reaction tested was the condensation of hydrogen sulfide and serine to produce cysteine and water **(2)**. CBS enzymes from *T. cruzi* and *S. cerevisiae* are known to catalyze this cysteine synthesis reaction (*19, 57, 58*). Three states of Co hCBS were tested in each reaction: Co(III) hCBS, Hg-reacted Co(III) hCBS, and Co(II) hCBS; the results are summarized in Table 4.5. The activity of Co(III) hCBS in the canonical CBS reaction—condensation of homocysteine with serine to form cystathionine **(1)**—was essentially unchanged from that of WT Fe(III) hCBS (Table 4.5) (*29, 30*). As isolated Co(III) hCBS, with its Cys/His ligation motif, has comparable activity to WT Fe(III) hCBS in the canonical reaction **(1)** (*29, 30*) and ~76% of the activity of WT Fe(III) hCBS for the alternative reaction **(2)**. Co(III) hCBS was responsive to AdoMet stimulation in both reactions, with a comparable increase in activity to that observed for Fe(III) hCBS. Thus, the presence of cobalt in the porphyrin does not substantively affect the enzyme activity. Upon disruption of the Co(III)-Cys bond, by reaction of Co(III) hCBS with $HgCl_2$ to form a Co(III) species with two neutral donors (*i.e.* no cysteine(thiolate)), activity is diminished, but not eliminated, in each reaction. Hg-reacted Co(III) hCBS retains significant activity in the canonical reaction, but does not respond to AdoMet stimulation. This enzyme exhibits very modest activity in the alternative reaction. Comparatively, Hg-reacted WT Fe(III) hCBS (which bears a high-spin, 5-coordinate Fe(III) heme without a cysteine(thiolate)(*27*)) has minimal activity and is unresponsive to AdoMet. A similar diminution of activity with loss of

AdoMet response is seen for Co(II) hCBS, which bears a 5-coordinate Co(II) porphyrin that does not retain its cysteine(thiolate) ligand. It must be noted that some fraction of the residual activity in Co(II) hCBS is due to the small amount (~8%) of Fe(III) hCBS still present, as DTT is unable to reduce WT Fe(III) hCBS to Fe(II) hCBS. Taken together, these results suggest that the native ligation motif (Cys/His) is essential to maintain maximal activity and AdoMet responsiveness for Co hCBS, as is true for Fe hCBS.

Discussion

Replacement of heme with other metalloporphyrins has been a useful tool for studying functions and properties of proteins ranging from hemoglobin and myoglobin to cytochrome $P450_{cam}$ and soluble guanylyl cyclase (*43, 50, 51, 53*). This tool was applied to investigate the role of heme in proper folding and expression of CBS (*59*). When CBS is expressed in a heme biosynthesis-deficient yeast strain, the protein does not accumulate. CBS expression is rescued by addition of a chemical chaperone, or by protoporphyrin IX and metallated derivatives. Modest yields of active Mn hCBS and Co hCBS proteins could be isolated by expression in anaerobically grown heme deficient *E. coli* cells (*59*). Recently, we developed an aerobic expression method that enables isolation of large quantities of high purity Co hCBS sufficient for spectroscopic study (*29, 30*). This Co hCBS is of particular interest because it is virtually indistinguishable from WT Fe hCBS in terms of its native conformation, enzyme activity, AdoMet responsiveness, PLP saturation, and ability to process alternative substrates (*29, 30*). These prior expression results implicated a structural role for the CBS heme; the availability of large quantities of Co hCBS enables us to identify the similarities and differences between the Co and Fe coordination environments that may contribute to the structural significance of the heme in CBS. To date, there is still no definitive consensus on heme's function in CBS; this puzzle was the impetus for characterization of the various redox and ligation states of the Co-substituted variant of hCBS (Scheme 4.1).

To understand the spectra of Co hCBS, it is valuable to consider the unique features that characterize Fe hCBS. WT Fe(III) hCBS displays a distinct electronic absorption spectrum characteristic of a low-spin, hexacoordinate heme-thiolate protein. The spectrum is dominated by intense porphyrin ($\pi \rightarrow \pi^*$) electronic transitions (Soret, γ or B band) red-shifted with

respect to most hemoproteins. A well-resolved, intense δ (or n) band appears on the higher-energy side of the Soret and is a result of the mixing of a ligand-to-metal charge transfer (LMCT) (S(p) → Fe(d_π)) with the porphyrin ($\pi \rightarrow \pi^*$) transitions (*46, 60*). The α-β (or Q) bands are towards the low-energy side of the visible spectrum and consist of one broad envelope, typical for low-spin Fe(III) porphyrins with a neutral donor bound *trans* to a thiolate moiety from a cysteine residue (*60*). At an even lower energy *ca*. 650 nm and 750 nm lie two visible LMCT absorption bands (S(p) → Fe(III)) with low intensity (*61*). Taken together, these features distinguish the low-spin heme-thiolate environment from those of other heme proteins.

The spectral features of Co(III) hCBS suggest that the cobalt retains the same coordination environment (Cys/neutral donor, presumably His) as iron in WT Fe(III) hCBS (Cys/His) (*10*). The similarities between Co(III) hCBS and Fe(III) hCBS highlight the structural importance of the metal-cysteine(thiolate) bond in the function of the CBS heme. First, thiolate coordination to the metal center of the porphyrin in CBS is robust and not metal-specific. That is, thiolate coordination persists when cobalt is substituted in lieu of iron, and the enzyme does not distinguish between the two metals. This identical coordination environment manifests itself spectroscopically and allows for high, AdoMet responsive enzymatic activity (both canonical and alternative) even in the presence of Co(III) PPIX (Table 4.5). In contrast, Hg-reacted Fe(III), Hg-reacted Co(III)- and Co(II) hCBS, which do not bear the thiolate ligand, exhibited impaired activities and are non-responsive to AdoMet. From these data it is evident that a metal-thiolate bond is essential for normal CBS function, but the metal does not have to be iron. Furthermore, the slow rate and the odd pH dependence of Co(III) reduction to form Co(II) hCBS suggest a complex process that ultimately results in loss of the cysteine(thiolate) ligand. Previously, heme in CBS was postulated to function as a redox regulator (*62*); however,

the behavior of Fe(II) hCBS is incompatible with a redox regulatory process (*23*). Fe(II) hCBS is unstable and undergoes slow loss of activity due to replacement of the cysteine(thiolate) ligand by an unidentified neutral donor ligand (*23*). The behavior of Co hCBS, with its very slow reduction, concomitant loss of the thiolate ligand and minimal activity in the Co(II) state is similarly incompatible with redox regulation.

A second implication is that substitution of Co for Fe likely does not disturb the secondary coordination sphere of the porphyrin in CBS. Earlier work has shown that electrostatic interaction of Arg^{266} with the axial ligand Cys^{52} in the WT Fe(III) hCBS is integral to maintaining maximal activity (*49*). The proposal was made that changes in the heme coordination environment, in particular at Cys^{52}, may be transmitted through the enzyme to the active site PLP cofactor ~ 20 Å away. The fact that Co(III) hCBS is fully active suggests that this essential secondary coordination sphere is intact. Without this essential electrostatic interaction, the activity of Hg-reacted Co(III) and Co(II) hCBS is substantially altered. Furthermore, the identical coordination environment and unaffected activity of Co(III) hCBS seems incompatible with the possibilities that the Co porphyrin is bound in a different location in the polypeptide chain or that the enzyme itself is folded improperly. These results suggest that there is a specific structure required for activity, which is defined by the presence of the metalloporphyrin and the specific ligands that are bound.

That the N-terminal heme helps to define the structure of CBS is supported by a variety of evidence. An N-terminal deletion variant lacking heme exhibited low enzymatic activity (~20% of WT) (*7*); however, the origin of the low activity was not explored. The activity defect may be due to the absence of heme, misfolding, or both. The absence of heme in lower eukaryotic CBS proteins and mechanistic studies of hCBS, clearly eliminate any role for heme

in catalysis (*17-19*). Furthermore, when hCBS is expressed in heme-deficient cells, minimal activity is observed. Modest activity restoration is obtained when Fe-, Mn-, Co-, Sn- and ZnPPIX or metal free PPIX are added to the growth medium. Near complete restoration of activity is observed when the chemical chaperone, trimethylamine N-oxide, is added (*59*). These observations suggest that proper folding of the enzyme during expression is essential, but that the correctly folded structure may be obtained in a variety of ways. Once properly folded around FePPIX, subsequent disruption of the iron-cysteine(thiolate) ligand bond causes a loss of enzyme activity, which is presumed to result from a change in structure (*16, 22, 23, 25, 27*). These data, when combined with the fact that hCBS does not discriminate between Fe and Co, together support a structural role of the heme in CBS; perturbation of metal identity in the metalloporphyrin appears not to modify enzyme activity so long as the enzyme is folded correctly and/or the proper metal ligands are maintained.

Conclusion

In this study we demonstrated that cobalt-substituted cystathionine β-synthase contains a novel Cys/His cobalt(III) porphyrin coordination environment, which is unprecedented among cobalt-substituted hemeproteins. Co(III) hCBS is fully active and robustly maintains the native ligation motif that is essential for enzymatic activity. Co(III) hCBS may be reduced to Co(II) hCBS, which bears a 5-coordinate Co(II) porphyrin without the cysteine(thiolate) and shows reduced enzymatic activity. Unsurprisingly, this Co(II) state will bind $NO_{(g)}$ but not $CO_{(g)}$. Co(II) hCBS may be reoxidized to a different Co(III) form (Co(III) $hCBS_{Reox}$), in which the cysteine(thiolate) ligation is not restored. When considered in light of the functional activity of both Co hCBS and Fe hCBS, these findings are consistent with the hypothesis that the heme in cystathionine β-synthase plays a structural role.

References

1. Mudd, S. H., Levy, H. L., and Kraus, J. P., (Eds.) (2001) *Disorders of Transsulfuration*, McGraw-Hill, New York.

2. Clarke, R., Smith, A. D., Jobst, K. A., Refsum, H., Sutton, L., and Ueland, P. M. (1998) Folate, vitamin B12, and serum total homocysteine levels in confirmed Alzheimer disease, *Arch. Neurol. 55*, 1449-1455.

3. Mattson, M. P., and Shea, T. B. (2003) Folate and homocysteine metabolism in neural plasticity and neurodegenerative disorders, *Trends Neurosci. 26*, 137-146.

4. Refsum, H., Ueland, P. M., Nygard, O., and Vollset, S. E. (1998) Homocysteine and cardiovascular disease, *Annu. Rev. Med. 49*, 31-62.

5. Mills, J. L., McPartlin, J. M., Kirke, P. N., Lee, Y. J., Conley, M. R., Weir, D. G., and Scott, J. M. (1995) Homocysteine metabolism in pregnancies complicated by neural-tube defects, *Lancet 345*, 149-151.

6. Kery, V., Bukovska, G., and Kraus, J. P. (1994) Transsulfuration depends on heme in addition to pyridoxal 5'-phosphate. Cystathionine β-synthase is a heme protein, *J. Biol. Chem. 269*, 25283-25288.

7. Oliveriusová, J., Kery, V., Maclean, K. N., and Kraus, J. P. (2002) Deletion Mutagenesis of Human Cystathionine beta-synthase. Impact on Activity, Oligomeric Status, and S-Adenosylmethionine Regulation, *J. Biol. Chem. 277*, 48386-48394.

8. Janosik, M., Kery, V., Gaustadnes, M., MacLean, K. N., and Kraus, J. P. (2001) Regulation of human cystathionine β-synthase by S-adenosyl-L-methionine: Evidence for two catalytically active conformations involving an autoinhibitory domain in the C-terminal region, *Biochemistry 40*, 10625-10633.

9. Kery, V., Poneleit, L., and Kraus, J. P. (1998) Trypsin Cleavage of Human Cystathionine β-Synthase into an Evolutionarily Conserved Active Core: Structural and Functional Consequences, *Arch. Biochem. Biophys. 355*, 222-232.

10. Meier, M., Janosik, M., Kery, V., Kraus, J. P., and Burkhard, P. (2001) Structure of human cystathionine β-synthase: A unique pyridoxal 5'-phosphate dependent hemeprotein, *EMBO J. 20*, 3910-3916.

11. Taoka, S., Lepore, B. W., Kabil, O., Ojha, S., Ringe, D., and Banerjee, R. (2002) Human Cystathionine β-Synthase Is a Heme Sensor Protein. Evidence That the Redox Sensor Is Heme and Not the Vicinal Cysteines in the CXXC Motif Seen in the Crystal Structure of the Truncated Enzyme, *Biochemistry 41*, 10454-10461.

12. Ojha, S., Hwang, J., Kabil, O., Penner-Hahn, J. E., and Banerjee, R. (2000) Characterization of the Heme in Human Cystathionine β-Synthase by X-ray Absorption and Electron Paramagnetic Resonance Spectroscopies, *Biochemistry 39*, 10542-10547.

13. Kery, V., Poneleit, L., Meyer, J. D., Manning, M. C., and Kraus, J. P. (1999) Binding of Pyridoxal 5'-Phosphate to the Heme Protein Human Cystathionine β-Synthase, *Biochemistry 38*, 2716-2724.

14. Evande, R., Ojha, S., and Banerjee, R. (2004) Visualization of PLP-bound intermediates in hemeless variants of human cystathionine β-synthase: evidence that lysine 119 is a general base, *Arch. Biochem. Biophys. 427*, 188-196.

15. Bruno, S., Schiaretti, F., Burkhard, P., Kraus, J. P., Janosik, M., and Mozzarelli, A. (2001) Functional Properties of the Active Core of Human Cystathionine β -Synthase Crystals, *J. Biol. Chem. 276*, 16-19.

16. Taoka, S., West, M., and Banerjee, R. (1999) Characterization of the Heme and Pyridoxal Phosphate Cofactors of Human Cystathionine β-Synthase Reveals Nonequivalent Active Sites, *Biochemistry 38*, 2738-2744.

17. Jhee, K.-H., McPhie, P., and Miles, E. W. (2000) Yeast Cystathionine β-Synthase Is a Pyridoxal Phosphate Enzyme but, Unlike the Human Enzyme, Is Not a Heme Protein, *J. Biol. Chem. 275*, 11541-11544.

18. Maclean, K. N., Janosìk, M., Oliveriusova, J., Kery, V., and Kraus, J. P. (2000) Transsulfuration in *Saccharomyces cerevisiae* is not dependent on heme: purification and characterization of recombinant yeast cystathionine β-synthase, *J. Inorg. Biochem. 81*, 161-171.

19. Nozaki, T., Shigeta, Y., Saito-Nakano, Y., Imada, M., and Kruger, W. D. (2001) Characterization of Transsulfuration and Cysteine Biosynthetic Pathways in the Protozoan Hemoflagellate, Trypanosoma cruzi. Isolation and Molecular Characterization of Cystathionine β-Synthase and Serine Acetyltransferase from *Trypanosoma*, *J. Biol. Chem. 276*, 6516-6523.

20. Taoka, S., Ohja, S., Shan, X., Kruger, W. D., and Banerjee, R. (1998) Evidence for Heme-mediated Redox Regulation of Human Cystathionine β-Synthase Activity, *J. Biol. Chem. 273*, 25179-25184.

21. Chen, Z., Chakraborty, S., and Banerjee, R. (1995) Demonstration that mammalian methionine synthases are predominantly cobalamin-loaded, *J. Biol. Chem. 270*, 12946-12949.

22. Cherney, M. M., Pazicni, S., Frank, N., Marvin, K. A., Kraus, J. P., and Burstyn, J. N. (2007) Ferrous Human Cystathionine β-Synthase Loses Activity during Enzyme Assay Due to a Ligand Switch Process, *Biochemistry 46*, 13199-13210.

23. Pazicni, S., Cherney, M. M., Lukat-Rogers, G. S., Oliveriusová, J., Rodgers, K. R., Kraus, J. P., and Burstyn, J. N. (2005) The Heme of Cystathionine β-synthase Likely Undergoes a Thermally Induced Redox-Mediated Ligand Switch, *Biochemistry 44*, 16785-16795.

24. Frank, N., Kent, J. O., Meier, M., and Kraus, J. P. (2008) Purification and characterization of the wild type and truncated human cystathionine β-synthase enzymes expressed in *E. coli*, *Arch. Biochem. Biophys. 470*, 64-72.

25. Taoka, S., and Banerjee, R. (2001) Characterization of NO binding to human cystathionine β-synthase: Possible implications of the efects of CO and NO binding to the human enzyme, *J. Inorg. Biochem. 87*, 245-251.

26. Shintani, T., Iwabuchi, T., Soga, T., Kato, Y., Yamamoto, T., Takano, N., Hishiki, T., Ueno, Y., Ikeda, S., Sakuragawa, T., Ishikawa, K., Goda, N., Kitagawa, Y., Kajimura, M., Matsumoto, K., and Suematsu, M. (2009) Cystathionine β-synthase as a carbon monoxide-sensitive regulator of bile excretion, *Hepatology 49*, 141-150.

27. Taoka, S., Green, E. L., Loehr, T. M., and Banerjee, R. (2001) Mercuric chloride-induced spin or ligation state changes in ferric or ferrous human cystathionine β-synthase inhibit enzyme activity, *J. Inorg. Biochem. 87*, 253-259.

28. Celano, L., Gil, M., Carballal, S., Durán, R., Denicola, A., Banerjee, R., and Alvarez, B. (2009) Inactivation of cystathionine β-synthase with peroxynitrite, *Arch. Biochem. Biophys. 491*, 96-105.

29. Majtan, T., Freeman, K. M., Smith, A. T., Burstyn, J. N., and Kraus, J. P. (2011) Purification and Characterization of Cystathionine Beta-Synthase Bearing a Cobalt Protoporphyrin, *Arch. Biochem. Biophys. 508*, 25-30.

30. Majtan, T., Frerman, F. E., and Kraus, J. P. (2011) Effect of cobalt on *Escherichia coli* metabolism and metalloporphyrin formation, *BioMetals 24*, 335-347.

31. Janosik, M., Meier, M., Kery, V., Oliveriusov·, J., Burkhard, K. A., and Kraus, J. P. (2001) Crystallization and preliminary X-ray diffraction analysis of the active core of human recombinant cystathionine β-synthase: an enzyme involved in vascular disease, *Acta Crystallogr., Sect D: Biol. Crystallogr. 57*, 289-291.

32. Pazicni, S., Lukat-Rodgers, G. S., Oliveriusová, J., Rees, K. A., Parks, R. B., Clark, R. W., Kraus, J. P., Rodgers, K. R., and Burstyn, J. N. (2004) The redox behavior of the heme in cystathionine β-synthase is sensitive to pH, *Biochemistry 43*, 14684-14695.

33. Neese, F. (1997) Electronic structure and spectroscopy of novel copper chromophores in biology, University of Konstanz, Konstanz, Germany.

34. Dey, A., Okamura, T.-A., Ueyama, N., Hedman, B., Hodgson, K. O., and Solomon, E. I. (2005) Sulfur K-Edge XAS and DFT Calculations on P450 Model Complexes: Effects of Hydrogen Bonding on Electronic Structure and Redox Potentials, *J. Am. Chem. Soc. 127*, 12046-12053.

35. Pazicni, S. (2006) Towards Understanding the Role of the Heme Cofactor in Cystathionine β-Synthase, in *Department of Chemistry*, University of Wisconsin-Madison, Madison, WI.

36. Neese, F., and Olbrich, G. (2002) Efficient use of the resolution of the identity approximation in time-dependent density functional calculations with hybrid density functionals, *Chem. Phys. Lett. 362*, 170-178.

37. Lee, C., Yang, W., and Parr, R. G. (1988) Development of the Colle-Salvetti correlation-energy formula into a functional of the electron density, *Phys. Rev. B: Condens. Matter Mater. Physics. 37*, 785-789.

38. Laaksonen, L. (1992) A graphics program for the analysis and display of molecular dynamics trajectories, *J. Mol. Graph. 10*, 33-34.

39. Bergman, D. L., and Laaksonen, A. (1997) Visualization of solvation structures in liquid mixtures, *J. Mol. Graphics Modell. 15*, 301-306.

40. Gaitonde, M. K. (1967) A spectrophotometric method for the direct determination of cysteine in the presence of other naturally occuring amino acids, *Biochem. J. 104*, 627-633.

41. Dickinson, L. C., and Chien, J. C. W. (1975) Cobalt-Cytochrome *c*. I. Preparation, Properties, and Enzymic Activity, *Biochemistry 14*, 3526-3533.

42. Falk, J. E. (1964) *Porphyrins and Metalloporphyrins: Their General, Physical, and Coordination Chemistry, and Laboratory Methods*, Elsevier, Amsterdam.

43. Wagner, G. C., Gunsalus, I. C., Wang, M. Y., and Hoffman, B. M. (1981) Cobalt-substituted cytochrome P-450cam, *J. Biol. Chem. 256*, 6266-6273.

44. Johnson, M. K. (2000) CD and MCD Spectroscopy, in *Physical Methods in Bioinorganic Chemistry* (Que, L., Jr., Ed.), pp 233-285, University Science Books, Sausalito.

45. Gale, R., McCaffery, A. J., and Rowe, M. D. (1972) Magnetic Circular Dichroism and Absorption Spectra of the Porphyrins. Part 1, *J. Chem. Soc. Dalton*, 596-604.

46. Dawson, J. H., Andersson, L. A., and Sono, M. (1983) The Diverse Spectroscopic Properties of Ferrous Cytochrome P-450-CAM Ligand Complexes, *J. Biol. Chem. 258*, 13637-13645.

47. Gasyna, Z., and Stillman, M. J. (1990) Absorption and magnetic circular dichroism spectroscopy of metal- and ring-oxidized porphyrins. Spectral characteristics of the one- and two-electron oxidation products of cobalt octaethylporphyrin, *Inorg. Chem. 29*, 5101-5109.

48. Kitanishi, K., Igarashi, J., Hayasaka, K., Hikage, N., Saiful, I., Yamauchi, S., Uchida, T., Ishimori, K., and Shimizu, T. (2008) Heme-Binding Characteristics of the Isolated PAS-A Domain of Mouse Per2, a Transcriptional Regulatory Factor Associated with Circadian Rhythms, *Biochemistry 47*, 6157-6168.

49. Singh, S., Madzelan, P., Stasser, J., Weeks, C. L., Becker, D., Spiro, T. G., Penner-Hahn, J., and Banerjee, R. (2009) Modulation of the heme electronic structure and cystathionine β-synthase activity by second coordination sphere ligands: The role of heme ligand switching in redox regulation, *J. Inorg. Biochem. 103*, 689-697.

50. Yonetani, T., Yamamoto, H., and Woodrow, G. V., III. (1974) Studies on Cobalt Myoglobins and Hemoglobins. I. Preparation and Optical Properties of Myoglobins and Hemoglobins Containing Cobalt Proto-, Meso-, and Deuteroporphyrins and Thermodynamic Characterization of their Reversible Oxygenation, *J. Biol. Chem. 249*, 682-690.

51. Yonetani, T., Yamamoto, H., and Iizuka, T. (1974) Sudies on Cobalt Myoglobins and Hemoglobins III. Electron Paramagnetic Resonance Studies on Reversible Oxygenation of Cobalt Myoglobins and Hemoglobins, *J. Biol. Chem. 249*, 2168-2174.

52. Wang, M. Y., Hoffman, B. M., and Hollenberg, P. F. (1977) Cobalt-substituted horseradish peroxidase, *J. Biol. Chem. 252*, 6268-6275.

53. Dierks, E. A., Hu, S., Vogel, K. M., Yu, A. E., Spiro, T. G., and Burstyn, J. N. (1997) Demonstration of the Role of Scission of the Proximal Histidine-Iron Bond in the Activation of Soluble Guanylyl Cyclase through Metalloporphyrin Substitution Studies, *J. Am. Chem. Soc. 119*, 7316-7323.

54. Makino, R., Matsuda, H., Obayashi, E., Shiro, Y., Iizuka, T., and Hori, H. (1999) EPR Characterization of Axial Bond in Metal Center of Native and Cobalt-substituted Guanylate Cyclase, *J. Biol. Chem. 274*, 7714-7723.

55. Puranik, M., Weeks, C. L., Lahaye, D., Kabil, Ö., Shinichi, T., Nielsen, S. B., Groves, J. T., Banerjee, R., and Spiro, T. G. (2006) Dynamics of Carbon Monoxide Binding to Cystathionine β-Synthase, *J. Biol. Chem. 281*, 13433-13438.

56. Choudhury, K., Sundaramoorthy, M., Hickman, A., Yonetani, T., Woehl, E., Dunn, M. F., and Puolos, T. L. (1994) Role of the Proximal Ligand in Peroxidase Catalysis, *J. Biol. Chem. 269*, 20239-20249.

57. Braunstein, A. E., Goryachenkova, E. V., and Lac, N. D. (1969) Reactions catalysed by serine sulfhydrase from chicken liver, *Biochim. Biophys. Acta 171*, 366-368.

58. Ono, B.-I., Kijima, K., Inoue, T., Miyoshi, S.-I., Matsuda, A., and Shinoda, S. (1993) Purification of properties of *Saccaromyces cerevisiae* cystathionine β-synthase, *Yeast 10*, 333-339.

59. Majtan, T., Singh, L. R., Wang, L., Kruger, W. D., and Kraus, J. P. (2008) Active Cystathionine β-Synthase Can Be Expressed in Heme-free Systems in the Presence of Metal-substituted Porphyrins or a Chemical Chaperone, *J. Biol. Chem. 283*, 34588-34595.

60. Dawson, J. H., Andersson, L. A., and Sono, M. (1982) Spectroscopic investigations of ferric cytochrome P-450-CAM ligand complexes. Identification of the ligand trans to cysteinate in the native enzyme, *J. Biol. Chem. 257*, 3606-3617.

61. McKnight, J., Cheesman, M. R., Thomson, A. J., Miles, J. S., and Munro, A. W. (1993) Identification of charge-transfer transitions in the optical spectrum of low-spin ferric cytochrome P-450 *Bacillus megaterium*, *Eur. J. Biochem. 213*, 683-687.

62. Banerjee, R., and Zou, C.-G. (2005) Redox regulation and reaction mechanism of human cystathionine-β-synthase: a PLP-dependent hemesensor protein, *Arch. Biochem. Biophys. 433*, 144-156.

63. Dickinson, L. C., and Chien, J. C. W. (1975) Cobalt-Cytochrome C. II. Magnetic Resonance Spectra and Conformational Transitions, *Biochemistry 14*, 3534-3542.

64. Sakurai, H., Ishizu, K., Sugimoto, H., and Gunsalus, I. C. (1986) Model of the Coordination Site for Cobalt-Substituted Cytochrome P450cam, *J. Inorg. Biochem. 26*, 55-62.

Table 4.1. Comparison of Co(III) hCBS electronic absorption peak positions (nm) with those of other select Co-substituted proteins and Co(III) PPIX models. TGE = thioglycolate ethyl ester; TN = thionalide; TGB = thioglycolate *n*-butyl ester; TGEH = thioglycolate 2-ethylhexyl ester. [a] Not Reported

Co(III) Species	δ	Soret (γ)	β	α	Ligands	Spin State	Ref.
Co hCBS pH 9.0	**366**	**442**	**553**	**588**			**this work**
Co hCBS pH 9.0 + $HgCl_2$	**~ 350**	**427**	**538**	**573**			**this work**
Co $hCBS_{Reox}$	**~ 351**	**424**	**538**	**569**			**this work**
CoPPIX(4-MeImH)$_2$	352	426	542	573	4-MeImH / 4-MeImH	LS	this work
CoPPIX(1-MeIm)$_2$	354	423	535	568	1-MeIm / 1-MeIm	LS	this work
Co Hb[a]	NR[a]	433	535	568	His / His	LS	(*50, 51*)
Co Hb (O_2^-)[b]	NR[a]	428	538	571	His / O_2^-	LS	(*50, 51*)
Co Mb (O_2^-)[b]	NR[a]	426	539	577	His / O_2^-	LS	(*50, 51*)
Co HRP (pH > 9.5)	NR[a]	427	533	565	His / H_2O	LS	(*52*)
Co Cyt *c*	NR[a]	426	530	567	His / Met	LS	(*41, 63*)
CoPPIX(TGE)(ImH)	356	430	548	576	RS^- / ImH	LS	(*64*)
CoPPIX(TGE)(1-MeIm)	357	430	547	576	RS^- / 1-MeIm	LS	(*64*)
CoPPIX(TGE)(2-MeIm)	370	435	562	576	RS^- / 2-MeImH	LS	(*64*)
CoPPIX(TGE)(4-MeIm)	360	431	548	575	RS^- / 4-MeImH	LS	(*64*)
CoPPIX(TN)(ImH)	358	430	546	575	RS^- / ImH	LS	(*64*)
CoPPIX(TGE)$_2$	372	465	574		RS^- / RS^-	LS	(*64*)
CoPPIX(TGB)$_2$	373	464	574		RS^- / RS^-	LS	(*64*)
CoPPIX(TGEH)$_2$	373	463	575		RS^- / RS^-	LS	(*64*)
CoPPIX(TN)$_2$	370	463	572		RS^- / RS^-	LS	(*64*)
Co P-450$_{cam}$(DTT)	375	467	573		RS^- / RS^-	LS	(*43*)

[a]Met form; i.e. Co(III) Hb bearing two His residues. [b]Oxy form; i.e. Co(III) Hb/Mb superoxide adduct.

Table 4.2. Comparison of MCD peak, crossover, and trough positions (nm) between Co(III) hCBS and Fe(III) hCBS (*32*).

	Band	**Peak**	**Crossover**	**Trough**
Co(III) hCBS	Soret(γ)	442	446	452
	β	551	553	557
	α	577	582	587
Fe(III) hCBS	Soret(γ)	419	425	433
	α / β	545	555	567

Table 4.3. Comparison of Co(II) hCBS electronic absorption data (nm) with other select Co(II)-substituted proteins.

Co(II) Species	Soret(γ)	α / β	Ligands	Spin State	Ref.
Co hCBS pH 9.0	**401**	**560**			**this work**
Co Hb	402	552	His (5c)	LS	(*50, 51*)
Co Mb	406	558	His (5c)	LS	(*50, 51*)
Co sGC	405	560	His (5c)	LS	(*53*)
Co HRP	401	553	His (5c)	LS	(*52*)
Co P-450$_{cam}$	404	556	RS^- (5c)	LS	(*43*)

Table 4.4. Comparison of MCD peak, crossover, and trough positions (nm) between Co(II) hCBS and Fe(II) hCBS (*32*).

	Band	**Peak**	**Crossover**	**Trough**
Co(II) hCBS	Soret(γ)	373	387	400
	α / β	546	554	559
Fe(II) hCBS	Soret(γ)	445	448	452
	α / β	563	566	569

Table 4.5. Comparison of the enzyme activities of Co(III) hCBS, Fe(III) hCBS, Hg-reacted Co(III) hCBS, Hg-reacted Fe(III) hCBS, and Co(II) hCBS.

	Specific Activity (U)[a,b]	
	cystathionine synthesis (1)	**cysteine synthesis (2)**
Fe(III) hCBS	404 ± 25[c]	108 ± 1
Hg-reacted Fe(III) hCBS	19 ± 4	0.8 ± 0.20
Co(III) hCBS	372 ± 19[c]	82 ± 3
Hg-reacted Co(III) hCBS	166 ± 3	7 ± 1
Co(II) hCBS	10 ± 1	10 ± 0.1

[a]1 unit (U) = (μmol product·mg enzyme^{-1}·hr^{-1}) [b]Values are all reported in the presence of AdoMet and excess PLP. Hg-reacted Fe(III) and Co(III) hCBS as well as Co(II) hCBS were not stimulated by AdoMet. [c]From reference (*29*)

Figure 4.1. (A) Electronic absorption spectrum of Co(III) hCBS. Co(III) hCBS (3.9 μM) was in 500 mM CHES buffer, 100 mM NaCl, pH 9.0, room temperature. (B) MCD spectrum of Co(III) hCBS. Protein concentration was 31.1 μM in 225 mM CHES buffer, 45 mM NaCl, 55% glycerol (v/v), 4 K, and 7 T, with the residual Fe(III) hCBS signal subtracted. Asterisk (*) indicate the presence of a residual overlapping, paramagnetic Fe(III) signal unable to be removed without significantly altering the spectral integrity.

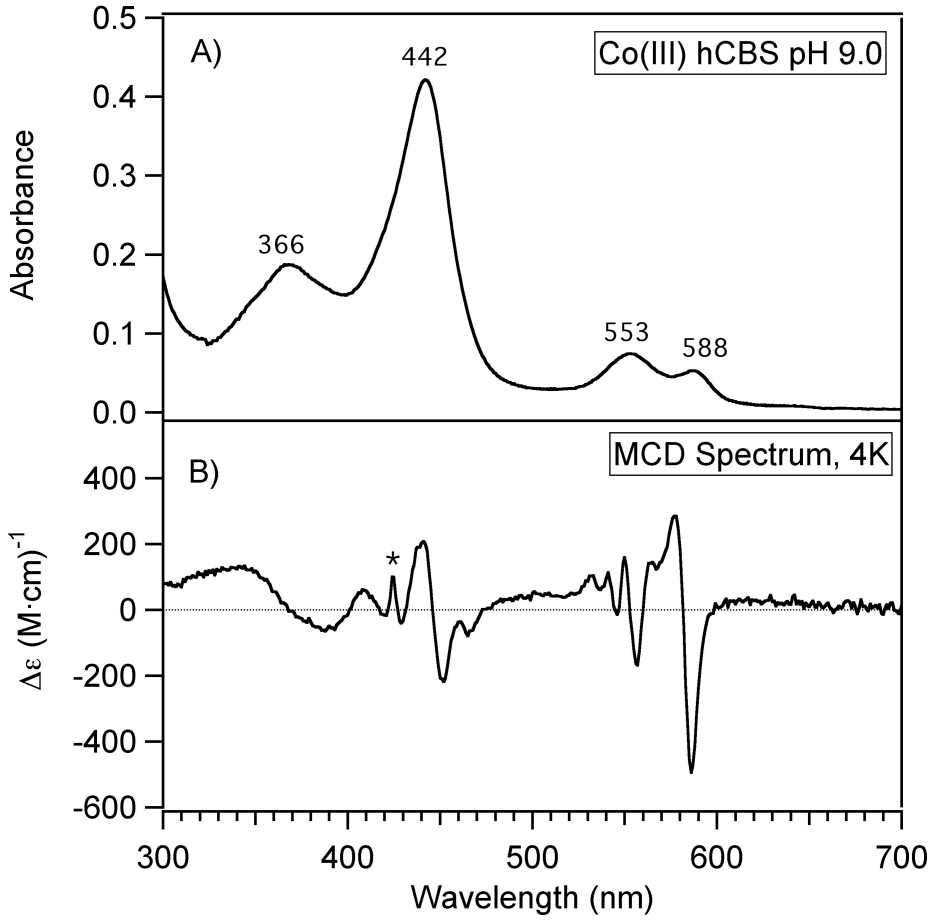

Figure 4.2. (A) Electronic absorption spectrum of Co(III)PPIX(1-MeIm)$_2$. Co(III)PPIX(1-MeIm)$_2$ (10 μM) was in 1:100 DMSO:H_2O (v/v), room temperature. (B) MCD spectrum of Co(III)PPIX(1-MeIm)$_2$. Co(III)PPIX(1-MeIm)$_2$ (19.8 μM) was in 1:100 DMSO:H_2O (v/v), 55% glycerol (v/v), 4 K, and 7 T.

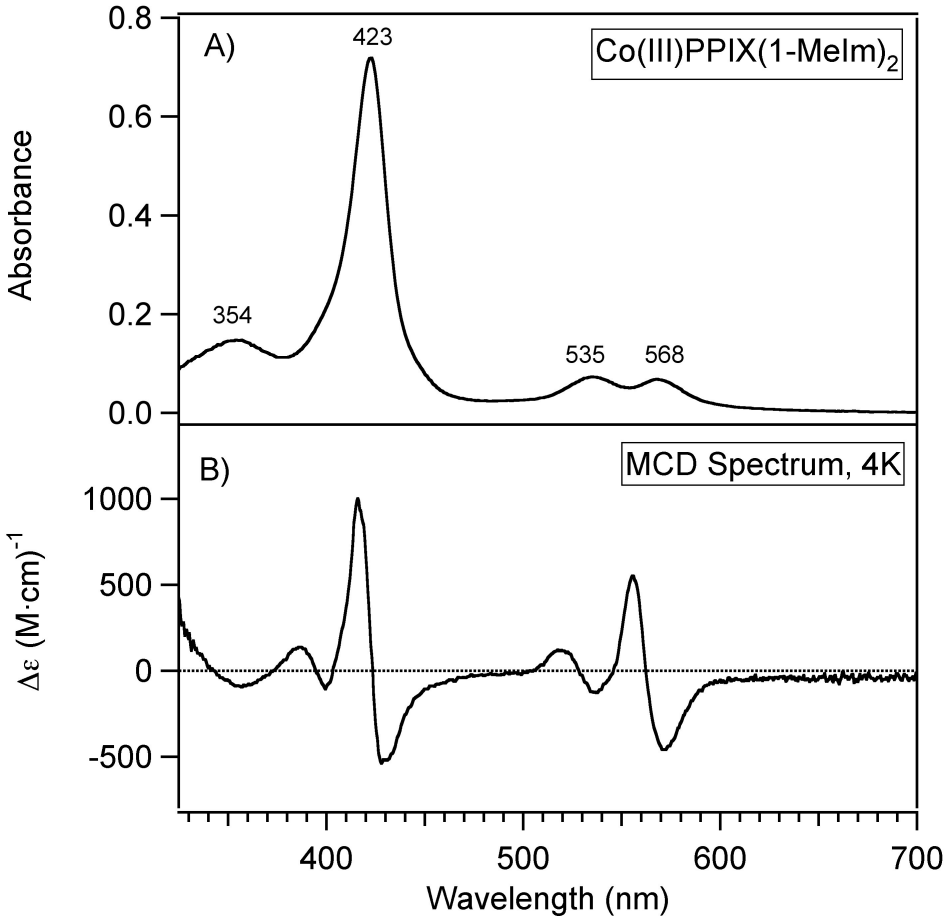

Figure 4.3. Electronic absorption spectra of Co(III) hCBS before (···) and 2 h after (—) addition of $HgCl_2$. Co(III) hCBS (3.9 μM) was in 500 mM CHES buffer, 100 mM NaCl, pH 9.0 with $HgCl_2$ added to a final concentration of 1.26 mM.

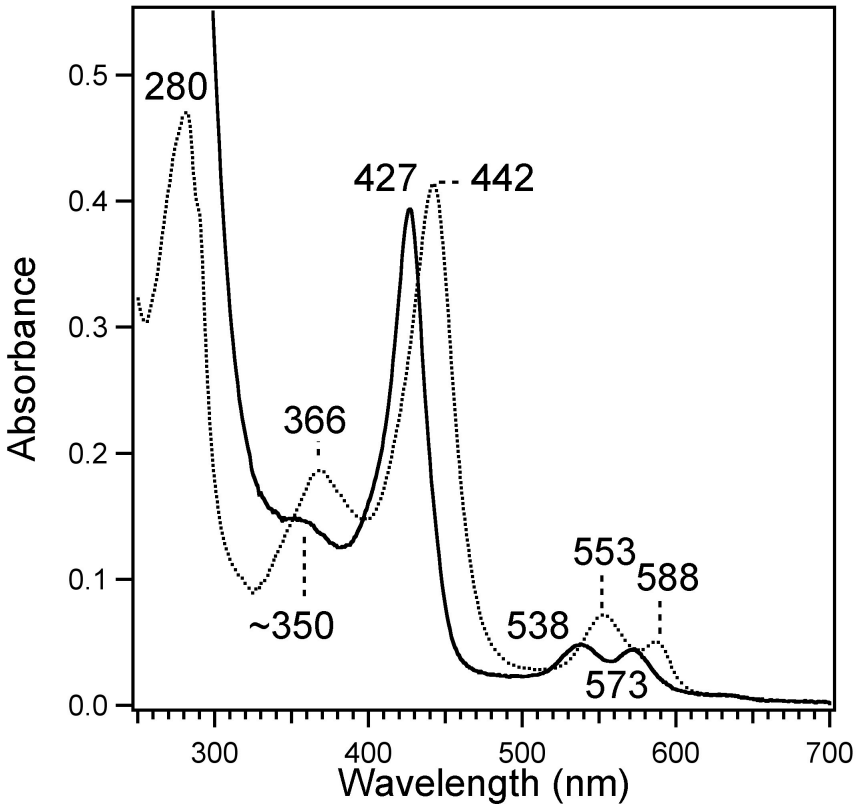

Figure 4.4. (A) Stick representation of Co(III) porphine [Co(III)P]. (B) Stick representation of Co(III)(porphine)(4-MeImH)(thiophenolate) [Co(P)(4-MeImH)(SPh)]. (C) TD-DFT computed electron density difference map (EDDM) of the selected transition that illustrates the ligand-to-metal charge transfer transition (LMCT, S(p) → Co(d_σ)) in the model [Co(P)(4-MeImH)(SPh)]. Dark blue represents the loss of electron density; light green represents the gain in electron density.

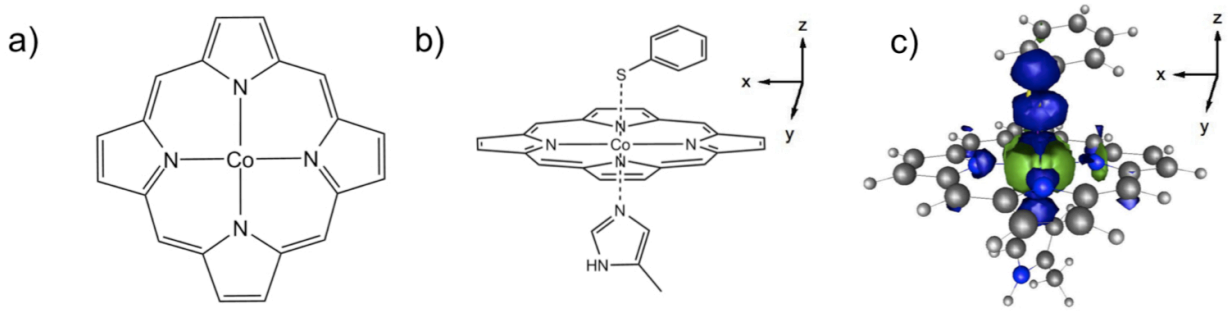

Figure 4.5. Electronic absorption spectrum of the reduction of Co(III) hCBS to Co(II) hCBS. Co(III) hCBS (3.9 μM) was in 500 mM CHES buffer, 100 mM NaCl, pH 9.0 with 5.3 mM DTT (final concentration) at 37°C. Inset: Time-dependent spectral change monitored at the noted wavelengths following the reduction of Co(III) hCBS (◆) to Co(II) hCBS (◇).

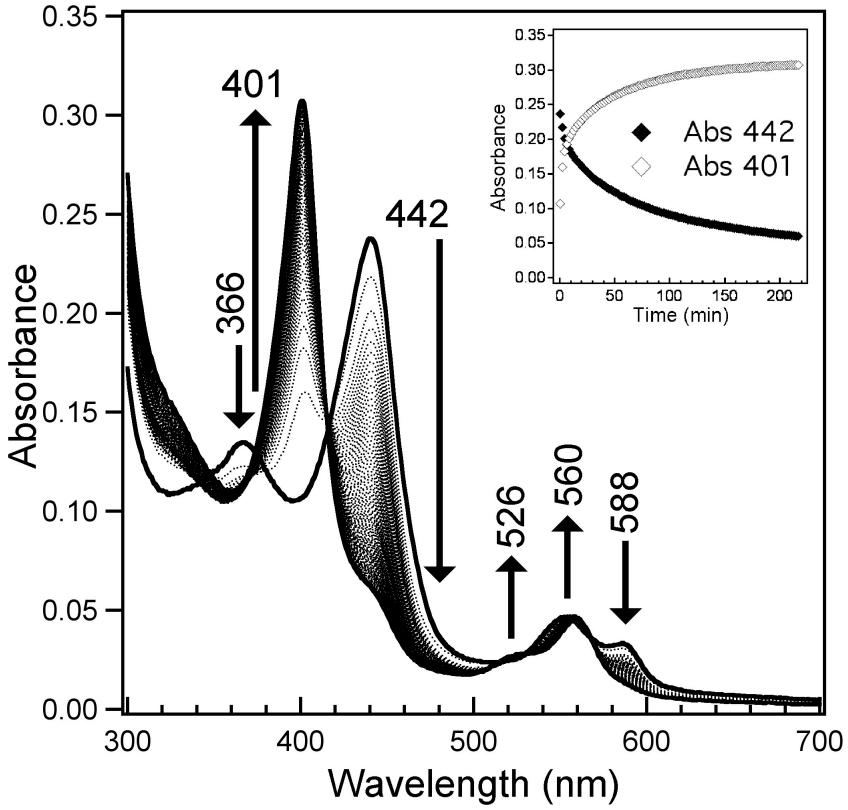

Figure 4.6. (A) Electronic absorption spectrum of Co(II) hCBS. Co(II) hCBS (3.9 μM) was in 500 mM CHES buffer, 100 mM NaCl, pH 9.0, 1.3 mM DTT (final concentration), room temperature. (B) MCD spectra of Co(II) hCBS. Co(II) hCBS (31.1 μM) was in 225 mM CHES buffer, 45 mM NaCl, 55% glycerol (v/v), 24.7 mM DTT (final concentration), 4-25 K, and 7 T. Asterisk (*) indicate the presence of an overlapping, diamagnetic Co(III) signal unable to be removed without significantly altering the spectral integrity.

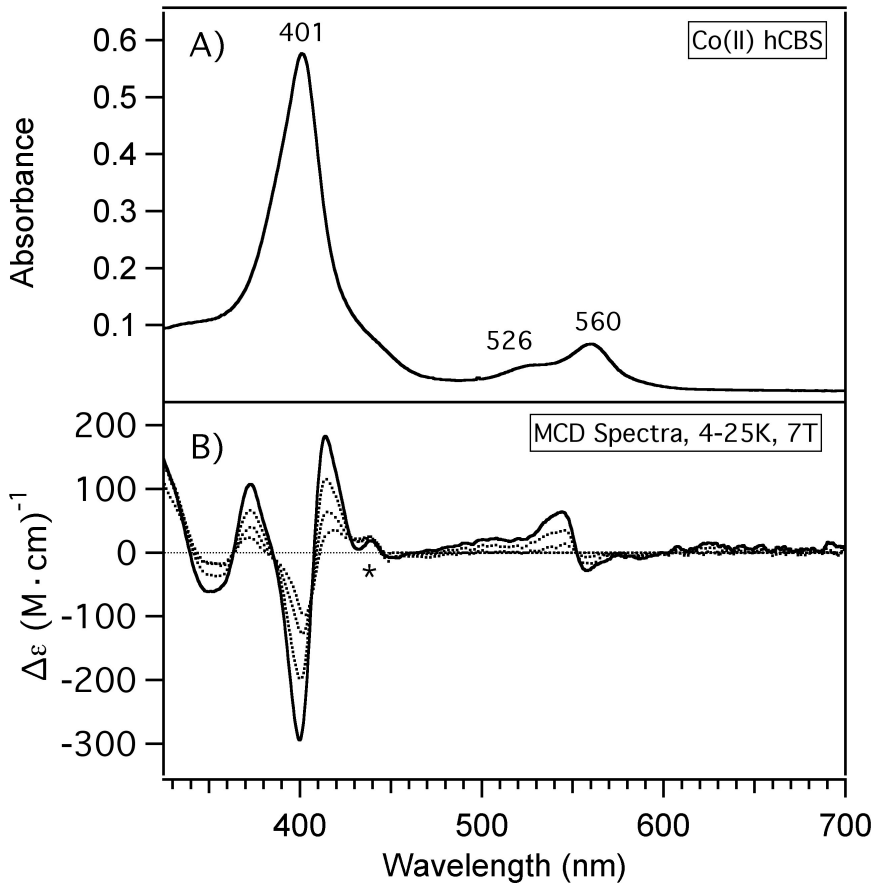

Figure 4.7. (A) Electronic absorption spectrum of Co(II)PPIX(1-MeIm). Co(II)PPIX(1-MeIm) (10 μM) was in 1:100 DMSO:H_2O (v/v), room temperature. (B) MCD spectrum of Co(II)PPIX(1-MeIm). Co(II)PPIX(1-MeIm) (30.0 μM) was in 1:100 DMSO:H_2O (v/v), 55% glycerol (v/v), 4-25 K, and 7 T. Asterisk (*) indicates the presence of an overlapping, diamagnetic Co(III) signal unable to be removed without significantly altering the spectral integrity.

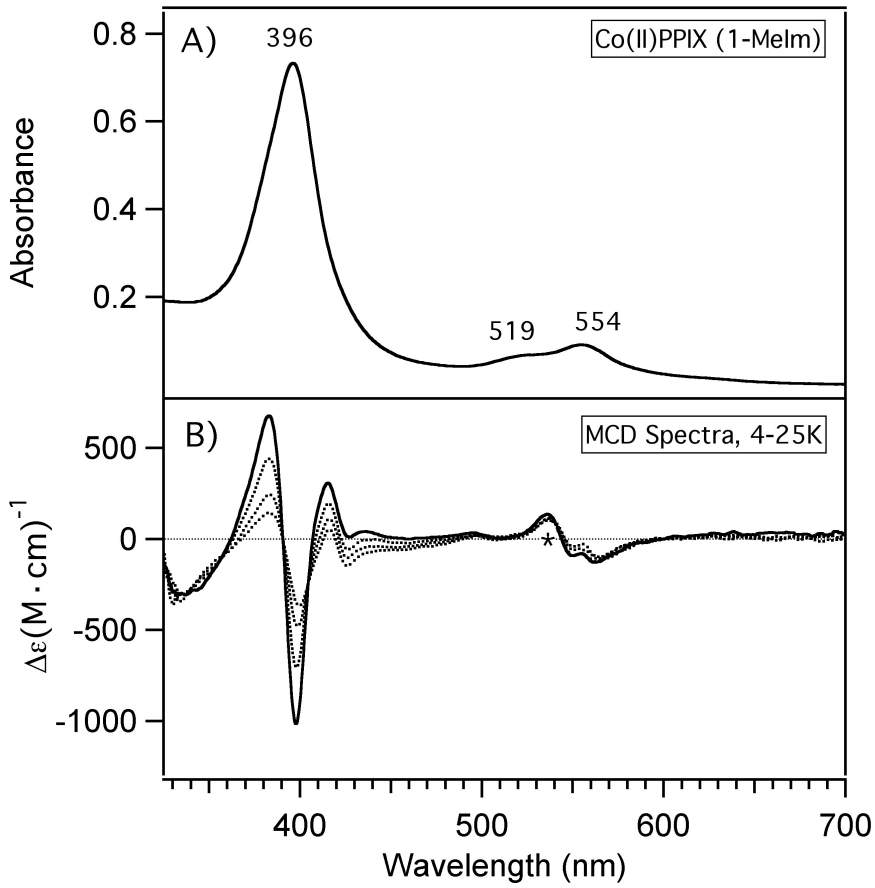

Figure 4.8. X-band EPR spectrum for Co(II)PPIX(1-MeIm) model (—) and best-fit simulation (····). Co(II)PPIX(1-MeIm) (410 μM) was in 1:100 DMSO:H_2O (v/v), and 55% glycerol (v/v). The spectrum was recorded at 4.5 K, 9.3540 GHz microwave frequency, 1.589 mW microwave power, 75 dB receiver gain, 4.00 G modulation amplitude, 100 kHz modulation frequency, 327.68 ms time constant, using 20 added scans each containing 10,000 data points. Asterisk (*) indicates the presence of a cavity signal.

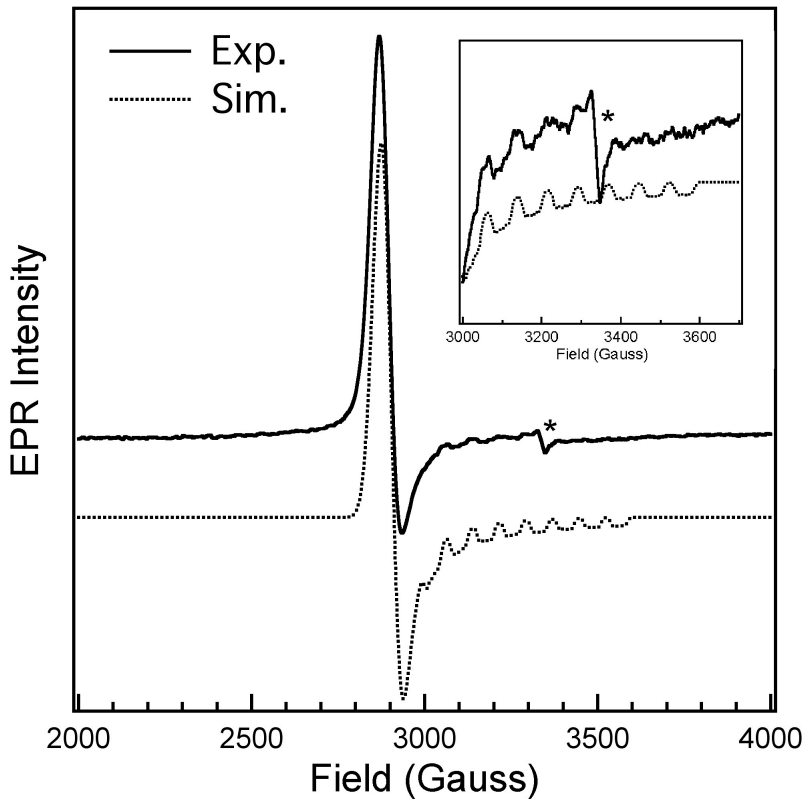

Figure 4.9. X-band EPR spectrum for Co(II) hCBS. Co(II) hCBS (150 μM) was in 500 mM CHES, 100 mM NaCl, pH 9.0. The spectrum was recorded at 25 K, 9.3790 GHz microwave frequency, 0.6325 mW microwave power, 73 dB receiver gain, 10.00 G modulation amplitude, 100 kHz modulation frequency, 163.84 ms time constant, using 20 added scans each containing 4,096 data points. Asterisk (*) indicates the presence of a cavity signal.

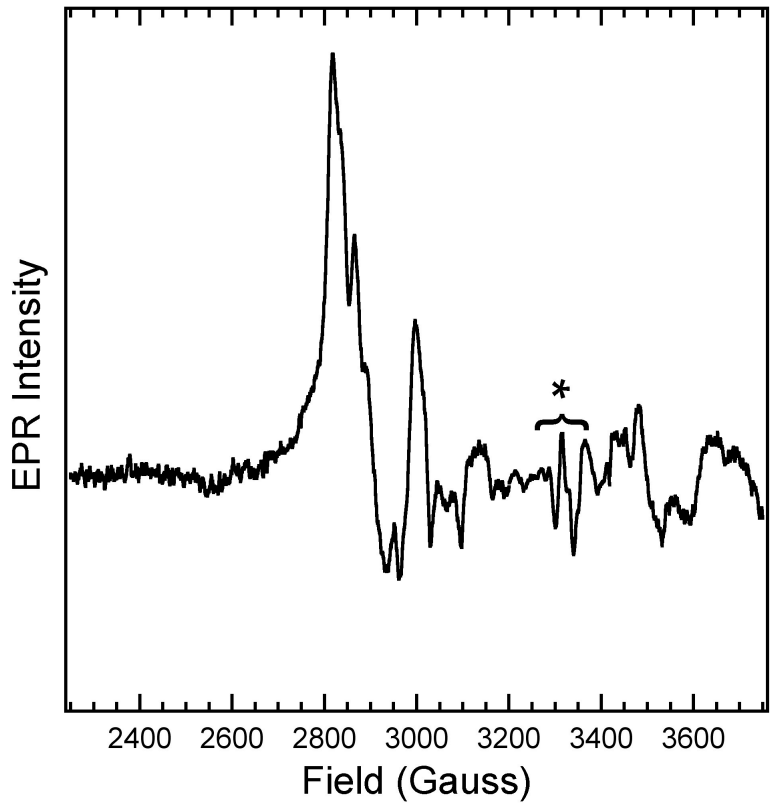

Figure 4.10. Comparison of electronic absorption spectra of Co-NO hCBS adduct (—) with Co(III) hCBS (····). Each species was 3.9 μM in concentration in 500 mM CHES buffer, 100 mM NaCl, pH 9.0, room temperature. After three additions of 100 μL samples of $NO_{(g)}$ to the cuvette headspace, reduction of Co(III) hCBS was achieved by addition of a stock solution of DTT (~ 30 mM, 10 μL) to a final concentration of ~ 1 mM.

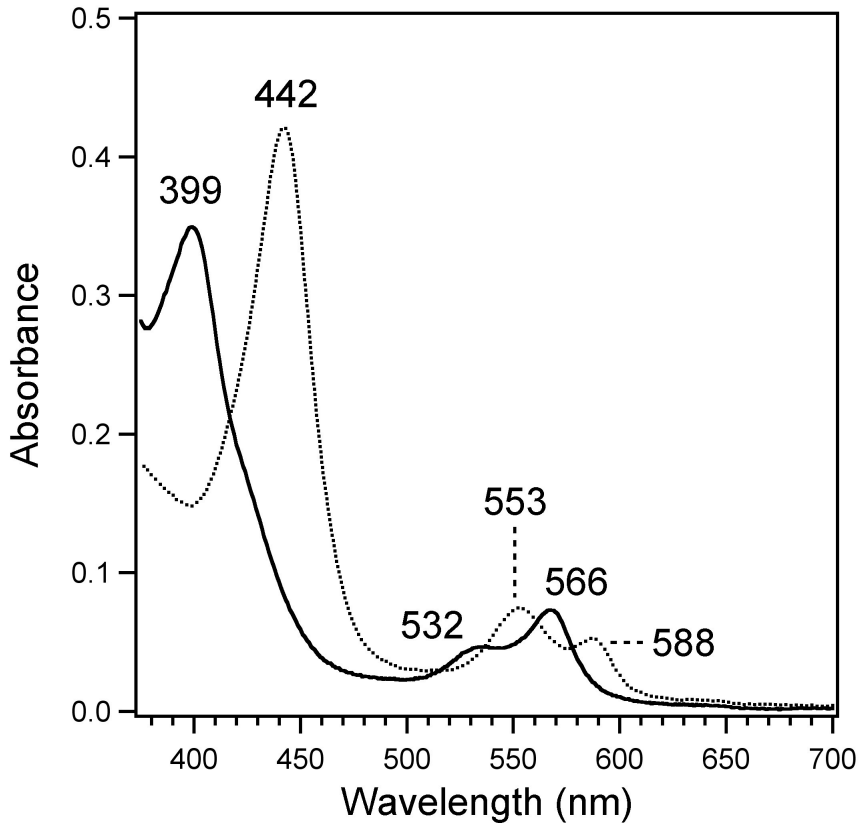

Figure 4.11. Reoxidized Co(III) hCBS electronic absorption spectrum (—), compared to as-isolated Co(III) hCBS electronic absorption spectrum(····). Each species was 3.9 μM in concentration in 500 mM CHES buffer, 100 mM NaCl, pH 9.0, room temperature.

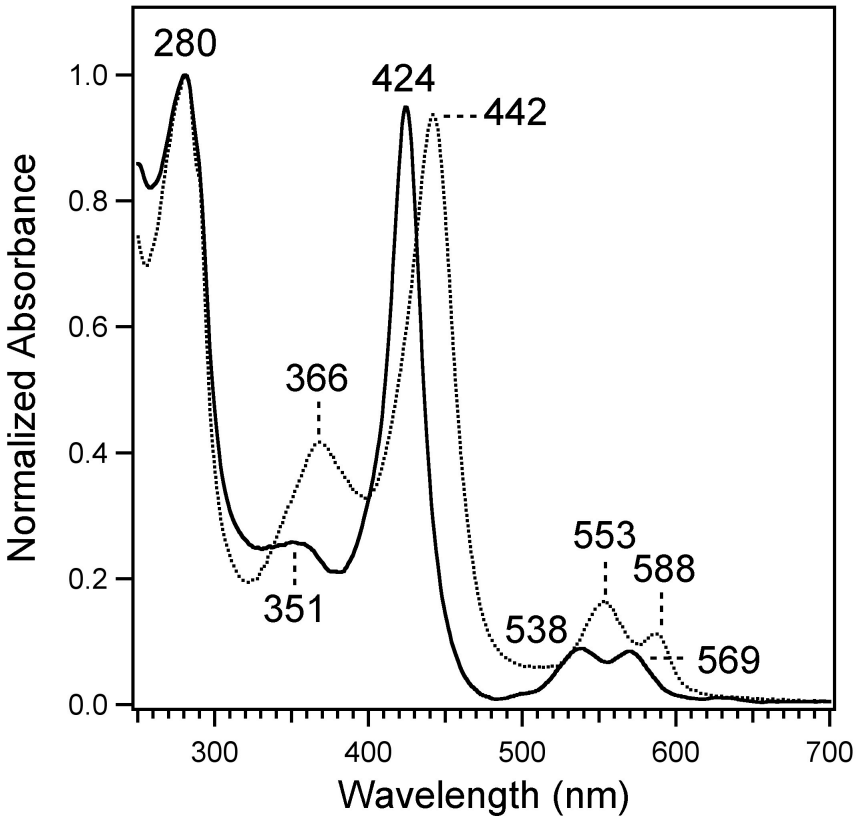

Scheme 4.1. Depiction of the coordination states of Co hCBS. L represents any generic, neutral ligand. X may represent O_2^-, RSO_x—a product of cysteine oxidation—or another generic ligand.

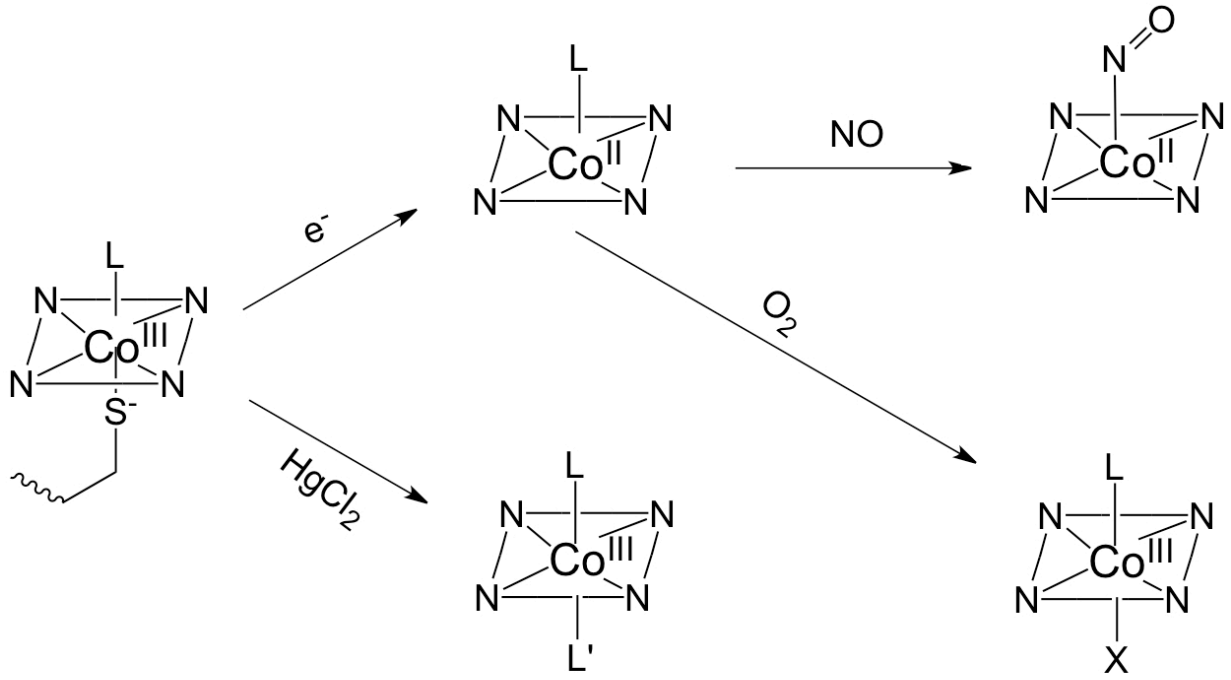

Scheme 4.2. Reactions catalyzed by CBS.

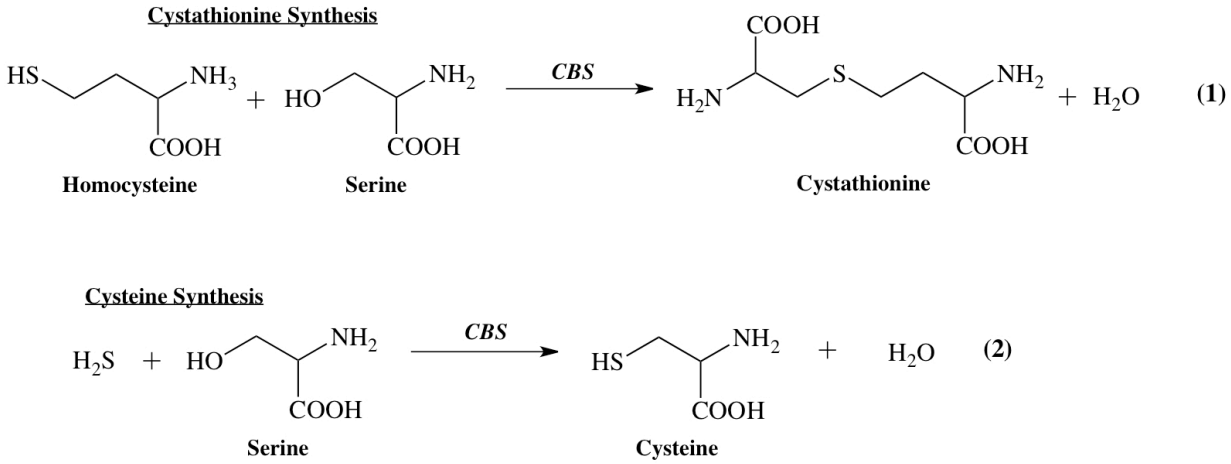

Chapter Five

The Effect of the Disease-Causing R266K Mutation on the Heme and PLP Environments of Human Cystathionine β-Synthase

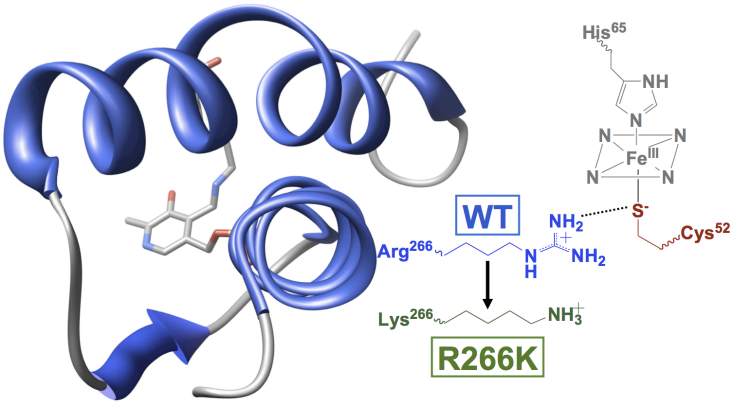

A version of this chapter has been submitted as:

Smith, A. T.; Su, Y.; Stevens, D.J.; Majtan, T.; Kraus, J.P; Burstyn, J. N. *Biochemistry* **2012**.

All CBS expression and purification was performed by Dr. Tomas Majtan in the laboratory of Professor Jan P. Kraus at the University of Colorado, Denver. Enzyme assays were performed by Yang Su. Sequence alignments were generated by Dr. Daniel J. Stevens.

Introduction

Homocysteine (Hcy) is a toxic metabolite of the methionine metabolic cycle. In addition to its role in proteins, the amino acid methionine is a fundamental building block for the biological methylating agent, *S*-adenosylmethionine (AdoMet). Homocysteine is generated from the de-adenosylation of *S*-adenosylhomocysteine (AdoHcy), the by-product of methylation reactions that use AdoMet (*1*). It has been found that Hcy in its cyclic form (Hcy thiolactone) reacts readily with proteins causing deleterious post-translational modifications, providing a possible molecular explanation for Hcy toxicity (*2, 3*). At the cellular level, increased levels of Hcy are correlated with an elevated risk of atherosclerosis (a primary cause of both cardiovascular disease and stroke) as well as thrombosis (*4*). Elevated levels of Hcy may be caused by nutritional abnormalities, such as dietary deficiencies in vitamins B_2, B_6 and B_{12}, or by genetic abnormalities, most commonly caused by mutations in the gene that encodes for the Hcy-metabolizing enzyme cystathionine β-synthase (CBS) (*4, 5*).

CBS is an essential pyridoxal-5'-dependent (PLP) enzyme that catalyzes the β-replacement reaction of serine with homocysteine to form cystathionine and water (Scheme 1). Elevated levels of Hcy due to CBS deficiency, chiefly caused by abnormalities in the CBS gene, result in a medical condition called classical homocystinuria or CBS-deficient homocystinuria (CBSDH). Increased plasma Hcy results in a variety of physiological symptoms including cardiovascular, skeletal and cognitive defects. Additionally, patients with CBSDH show increased risk of developing Alzheimer's and Parkinson's diseases (*5-9*).

CBS from higher organisms is the only known PLP-dependent enzyme to contain a heme *b* cofactor (*10*). In mammals, CBS is an α_4 homotetramer of 63-kDa subunits, each of which contains an N-terminal heme-binding domain, a central catalytic PLP-binding domain,

and a C-terminal AdoMet-binding domain (*10, 11*). Binding of AdoMet allosterically regulates the enzyme by increasing activity 3- to 5-fold (*12*). Activation of CBS may also be achieved by removal of the C-terminal AdoMet-binding domain, which causes a concomitant change in protein oligomeric status from homotetrameric to homodimeric; the 45-kDa truncated form of the enzyme is known as CBS-45 (*13*). This observation suggests that the regulatory domain is autoinhibitory, and the inhibition may be relieved by AdoMet binding, limited proteolysis, or partial thermal denaturation (*12*). Crystal structures of human CBS-45 (*14*) and the full-length *Drosophila melanogaster* CBS (*Dm*CBS) (*15*) show that the heme is unusually solvent exposed with its nearest edge located 14 Å from the anchoring phosphate moiety of the active site PLP. These structures confirmed spectroscopic results that showed that the ferric heme in CBS is ligated by an uncommon Cys/His motif that involves the thiolate of Cys^{52} trans to the $N_{\varepsilon 2}$ atom of His^{65} (human enzyme numbering, Figure 1); both ligands are provided by amino acids on the N-terminal portion of the polypeptide (*16, 17*). Additionally, the crystal structures reveal a complex hydrogen-bonding network that connects the heme macrocycle to the PLP active site. Of particular interest is the interaction of the positively charged guanidinium group of Arg^{266} with that of the negatively charged thiolate moiety of Cys^{52}; this interaction connects the heme to the active site via helix 8, which contains Arg^{266}, Thr^{257} and Thr^{260}. The hydroxyl side chains of Thr^{257} and Thr^{260} hydrogen bond directly to the PLP phosphate; thus, this H-bond network provides a direct means of communication between the heme cofactor and the enzyme active site (*14, 15*). While there is no definitive consensus on the role of heme in CBS, it is clear that heme is necessary for maximal activity of CBS from higher organisms (*10, 18-21*).

In this study, we examine the effect of the disease-associated R266K mutation on the spectroscopic and catalytic properties of full-length hCBS. We show that the R266K variant is

enzymatically competent but displays differences in reaction specificity, as well as PLP- and AdoMet-responsiveness compared to WT hCBS. We show that there are subtle differences in the electronic absorption, EPR and rR spectroscopic signatures of Fe(III) R266K hCBS, which may be attributed to geometric distortions at the heme iron atom, including a lengthening of the Fe(III)-S(Cys) bond due to a change in hydrogen bonding at Cys^{52}. We use fluorescence spectroscopy to demonstrate that these spectroscopic changes at the heme cofactor correlate with spectroscopic and enzymatic changes at the PLP active site. Additionally, we show that Fe(II) R266K undergoes a thermally-induced ligand switch that is more facile than that of WT hCBS. Taken together, these data suggest that the R266K variation destabilizes the Fe(III)-Cys^{52}(thiolate) interaction, and that this change at the heme is communicated to the enzyme active site.

Materials and Methods

Materials. Buffers and glycerol were purchased from Sigma-Aldrich and used as received. High-purity sodium dithionite was purchased from Fluka and stored under $Ar_{(g)}$ at -20°C until used.

Isolation and Purification of WT hCBS and R266K hCBS. Both the WT and variant proteins were expressed and purified to homogeneity as described previously (*22*). Briefly, *Escherichia coli* Rosetta2(DE3) cells were transformed with pET-28-C-hCBS plasmid carrying either WT or the R266K human CBS sequence with a non-removable 6xHis tag at its C-terminal end. The bacterial cells were grown at 30°C, 275 rpm in 2.8-L Fernbach flasks containing 1 L of LB medium supplemented with 0.001% thiamine-HCl, 0.0025% pyridoxine-HCl, 0.1 mM $FeCl_3$, 0.3 mM δ-aminolevulinic acid, and 30 μg/mL kanamycin (all final concentrations). The expression of hCBS was induced by adding in IPTG to a final concentration of 1 mM once the cell density reached $A_{600} \sim 0.8$; cell growth was then continued overnight. Cells were harvested and then resuspended in lysis buffer (50 mM sodium phosphate at pH 7.4, 300 mM NaCl, 0.1 mM PLP and protease inhibitor cocktail VII [A.G. Scientific]) and treated with 2 mg/mL lysozyme for 1 hr at 4°C prior to sonication. After removal of any non-soluble and particulate material, the soluble fraction was loaded on a TALON column (Contech) equilibrated in 50 mM sodium phosphate, pH 7.4, 300 mM NaCl. The resin with bound CBS was extensively washed (50 mM sodium phosphate, pH 7.4, 300 mM NaCl, 10 mM imidazole); bound protein was eluted by using 200 mM imidazole (final concentration) in the wash buffer. Eluted protein was immediately desalted on a Sephadex G-25 resin (GE Healthcare), and the buffer was exchanged with DEAE loading buffer (15 mM potassium phosphate, pH 7.2, 1 mM EDTA, 1 mM DTT, 10% ethylene glycol). The desalted sample was bound to a DEAE Sepharose resin

(GE Healthcare), washed, and hCBS protein was eluted with 300 mM potassium phosphate in the DEAE loading/wash buffer. The hCBS protein was concentrated, buffer exchanged into 20 mM HEPES, pH 7.4, 100 mM NaCl, 1 mM TCEP, and 0.01% Tween20, and stored in aliquots at -80°C. Protein was buffer exchanged into the appropriate buffer as described in the activity and spectroscopy sections (*vide infra*).

Activity Measurements. The cysteine-synthesis activity of WT and R266K Fe(III) hCBS was determined as previously described (*23*). Briefly, the reaction mixture (600 μL) contained 0.5 mg/mL BSA, 10 mM DTT, 0.5 mM PLP, 0.35 mM AdoMet, 0.020 mg/mL enzyme, 10 mM *L*-serine, and 10 mM Na_2S in 200 mM Tris buffer at pH 8.6. This solution was incubated for 12 min at 37°C, and then an aliquot of the reaction mixture (100 μL) was taken and mixed with 50% (w/v) trichloroacetic acid. Precipitated protein was removed by centrifugation, and the supernatant (100 μL) was combined with acetic acid (100 μL) and ninhydrin (100 μL), and the mixture was heated in a boiling water bath for 3 min and then immediately cooled on ice. The absorbance at 560 nm was measured to determine the amount of cysteine generated, and the value was interpolated from a standard curve generated by the same method using cysteine solutions of known concentrations that contained all other reagents except enzyme (*24*). Cystathionine-synthesis activity was determined as reported in (*22*).

Electronic Absorption Spectroscopy. Electronic absorption spectra were recorded on a double-beam Varian Cary 4 Bio spectrophotometer with a temperature controller, set to a spectral bandwidth of 0.5 nm. Spectra of protein samples were recorded in 100 mM CHES buffer, 100 mM NaCl, pH 8.6. Samples were purged of oxygen by flowing $Ar_{(g)}$ through the headspace of a septum-sealed cuvette for 20 min. Reduction of Fe(III) protein samples was accomplished by adding an anaerobically prepared stock solution of sodium dithionite to achieve a final sample

concentration of 1-5 mM. For spectral measurements, solutions of dithionite and Fe(III) protein were allowed 20 min to equilibrate at 4°C before anaerobic addition of stock dithionite (40 mM, 10 μL) to the Fe(III) protein. For kinetic measurements, solutions of dithionite and Fe(III) protein were allowed 20 min to equilibrate at 10, 20 or 30°C before anaerobic addition of the dithionite solution (40 mM, 10 μL) to the Fe(III) protein. The rate at which Fe(II) R266K hCBS (Soret 447 nm) was converted to Fe(II) R266K hCBS424 (Soret 424 nm) was fitted by a single-wavelength method utilizing the Solver function in Microsoft Excel 2004; the values for the rate constants with minimal residuals between experimental and predicted absorbance measurements are reported. Loss of the Soret at 447 nm was best fitted using a biexponential decay, as described in eq 1. The absorbance at time infinity (Abs_∞) was measured experimentally by forcing full conversion of Fe(II) R266K hCBS to Fe(II) R266K hCBS424 using thermal treatment (*25*). Briefly, Fe(III) protein was equilibrated at 4°C; a solution of sodium dithionite (40 mM, 10 μL) was added to the Fe(III) protein, and reduction was monitored spectrophotometrically until no further changes were observed at 447 nm. The temperature was then ramped to 37°C, and conversion from the 447 nm Soret to the 424 nm Soret was monitored spectrophotometrically; thermal conversion was considered complete when no further changes in the intensity of the 424 nm Soret were observed. The constants α and β represent the collection of values that include the absorbance at time zero and the extinction coefficients of each species, respectively.

$$Abs_t = Abs_\infty + \alpha \cdot e^{-k_1 t} + \beta \cdot e^{-k_2 t} \qquad (1)$$

Fluorescence Spectroscopy. Fluorescence measurements were taken on an ISS PC1 photon counting fluorometer (ISS Instruments, Inc., Champaign, IL) at room temperature. Spectra of protein samples were recorded in 100 mM CHES buffer, 100 mM NaCl, pH 8.6. Protein

samples (7-10 μM, 400 μL) were placed in a quartz cuvette with a 2 mm excitation path length and a 1 cm emission path length. Emission spectra were recorded from 425 nm to 635 nm with an excitation wavelength of 410 nm and excitation and emission slit widths of 4 mm and 2 mm, respectively. Corrections for buffer fluorescence were made by subtracting the emission spectrum of buffer from spectra of samples containing buffer and protein.

MCD Spectroscopy. Magnetic circular dichroism (MCD) spectra were recorded on a Jasco J-715 CD spectropolarimeter with the sample compartment modified to accommodate an SM-4000-8T magnetocryostat (Oxford instruments). Spectra of protein samples were recorded in 100 mM CHES buffer, 100 mM NaCl, pH 8.6. For each protein sample in buffer, approximately 55% (v/v) glycerol was present. Glycerol was introduced to the Fe(III) form of the protein and stirred with a syringe until the solution was homogeneous; the final protein concentration was 16 μM in a total volume of 150 μL. Glycerol had no effect on the electronic absorption spectra at room or liquid-helium temperatures. Samples were transferred via gastight syringe into cells, flash-frozen and stored in $N_{2(l)}$. MCD spectra were taken over a temperature range from 4 to 200K. The MCD signal at each temperature was recorded at ±7 T. Negative polarity data were subtracted from positive polarity data to remove CD contributions, and the resulting spectrum divided by 2.

EPR Spectroscopy. X-band electron paramagnetic resonance (EPR) spectra were collected on a Bruker ELEXSYS E500 equipped with an Oxford ESR 900 continuous flow cryostat connected to an Oxford ITC4 temperature controller. The microwave frequency was monitored using an EIP model 625A CW microwave frequency counter. Field calibration was achieved using a Varian ER 035 gaussmeter. Spectra of protein samples were recorded in 100 mM CHES buffer,

100 mM NaCl, pH 8.6. The final concentration of protein was 140-240 μM in a total volume of 150 μL. Each sample was transferred via a gastight syringe into a quartz EPR tube and frozen in $N_{2(l)}$. For all samples, scans of 0—10000 G revealed no signals other than those reported.

Resonance Raman Spectroscopy. Resonance Raman spectra were recorded using an excitation wavelength of 413.1 nm from a Coherent I-302C Kr^+ laser in a backscattering 135° sample geometry with an Acton Research monochromator set to a grating of 2400 groves/mm. Incident powers ranged from 10-12 mW and were focused with a cylindrical lens onto the sample. A Princeton Instruments Spex 1877 triple spectrograph outfitted with a cooled, intensified diode array detector was operated under computer control using Spectrasense software. The solution samples were prepared as described for EPR spectroscopy (*vide supra*) and were placed in a quartz dewar cooled with ice water to reduce local heating. Peak positions were calibrated relative to a K_2SO_4 resonance at 981 cm^{-1}. Assignments of key vibrational modes are noted and are based on the work of Spiro *et al.* and Green *et al.* (*26-28*).

Results

R266K hCBS Binds Heme Similarly to WT hCBS. The electronic absorption and MCD spectra of purified R266K hCBS are only subtly different from those of WT hCBS, indicating that the R266K variant binds heme in a similar manner as WT hCBS. Indeed, the electronic absorption spectrum of as-isolated R266K (Figure 5.2A), exhibits a distinct δ band at 364 nm, a sharp Soret band at 428 nm and a broad absorption envelope for the α/β region with maximal intensity at 549 nm. These peak positions are only slightly shifted from those of the WT protein (364 nm, 430 nm and 550 nm; δ, Soret and α/β, respectively), suggesting that the heme in the R266K variant is in its Fe(III) oxidation state and is bound by Cys^{52} and His^{65}, like that of the WT protein. Additionally, there are two ligand-to-metal charge-transfer transitions (Cys(thiolate)→Fe(III)) evident in the 600-750 nm region of R266K (Figure 5.2A, inset); however, these transitions are shifted to longer wavelength (lower energy) by 4 nm, suggesting the R266K Cys(thiolate)-Fe(III) heme interaction is slightly different than that of WT hCBS.

MCD spectroscopy, with its unique ability to fingerprint the spin and coordination states of heme proteins, confirms the conclusion that the heme is low-spin Fe(III) and ligated by a Cys/His motif. The MCD spectrum of R266K (Figure 5.2B) is dominated by an intense, temperature-dependent *C*-term in the Soret region with peak-crossover-trough positions of 416 nm-423 nm-432 nm, almost identical to those of WT Fe(III) hCBS (*29*), as well as other Fe(III) Cys/His or Cys/neutral donor ligated heme proteins such as P-450_{CAM} + ImH, *Bx*RcoM, hRev-Erbβ, *Dm*E75 and *Rr*CooA (*30-33*). The magnetic saturation behavior of the most intense wavelength of this dominating *C*-term (432 nm) displays an overlapping nature at different temperatures (Figure 5.2B, inset), similar to that of WT Fe(III) hCBS, indicative that the

R266K heme is in a low-spin, Fe(III) S=½ state. Taken together, these data suggest that the heme in R266K is low-spin, Fe(III) and bound by the native heme ligands, Cys^{52} and His^{65}.

EPR and rR Spectroscopies Suggest a Geometric Distortion and Lengthening of the Fe(III)-S(Cys) Bond. EPR spectroscopy suggests a perturbation in the relative energies of the *d*-orbitals of Fe(III) R266K hCBS compared to those of Fe(III) WT hCBS. The EPR spectra, which are sensitive to the environment of the paramagnetic Fe(III) center, are shown in Figure 5.3, A and B, for WT and R266K hCBS, respectively. Scans of 0-10,000 Gauss revealed only the presence of a rhombic, low-spin Fe(III) signal for both WT and R266K. The Fe(III) WT hCBS spectrum displays three major g values at 2.49, 2.31 and 1.87 (g_z, g_y and g_x, respectively), essentially identical to previous reports (*16, 29*). However, the positions of the major g values for the Fe(III) R266K hCBS variant are different; the g values g_z, g_y and g_x are 2.45, 2.29 and 1.89, respectively, with additional minor signals present (a common feature for rhombic EPR signals of low-spin heme thiolate-ligated proteins). Analysis of the g values for the Fe(III) R266K variant, using the method outlined by Palmer (*34*), yields values for rhombicity (V/Δ) and tetragonality (Δ/λ) of 0.37 and 5.50, respectively. These values place Fe(III) R266K hCBS in the "P" family of the Blumberg-Peisach diagram—the same region in which WT Fe(III) hCBS resides, as well as other ferric cysteine(thiolate)-ligated heme proteins bearing a sixth neutral donor ligand (*35*). While WT and R266K exhibit virtually the same rhombicity (0.38 and 0.37, respectively), their tetragonality values different significantly (5.08 and 5.50, respectively). These results suggest that both a rhombic distortion (V) and an axial distortion (Δ) take place in concert in the R266K variant; these geometric distortions are predicted to change 1) the effective overlap of the orbitals of the heme axial ligands as well as 2) the relative *d*-orbital energies in Fe(III) R266K with respect to Fe(III) WT hCBS.

Resonance Raman spectroscopy reveals a lowering of the vibrational energy of the Fe(III)-S(Cys) resonance of R266K hCBS, suggesting a lengthening of the Fe(III)-Cys(thiolate) bond in the R266K hCBS variant. Figure 5.5 depicts the low-energy region of the rR spectra of Fe(III) WT (A) and R266K (B) hCBS; this region typically contains low-energy metal-ligand vibrations that are enhanced due to coupling to porphyrin vibrations. The ν(Fe-S(Cys)) resonance was previously identified at 312 cm^{-1} based on global ^{34}S substitution of the C-terminal 143 amino acid-truncated version of hCBS, CBS-45 (*28*). In our hands, using the full-length 63 kDa WT hCBS bearing a C-term His_6 tag, we observe a similar broad band centered at 315 cm^{-1} for ν(Fe-S(Cys)). In the Fe(III) R266K variant, this same resonance is downshifted in energy to 307 cm^{-1}, indicative of a longer (i.e. weaker) Fe(III)-S(Cys) bond. While ν(Fe-S(Cys)) is shifted to lower energy in R266K, the relative energies and intensities of the oxidation, spin and coordination-state marker bands ν_3, ν_4, ν_2 and ν_{10} remained unchanged (Figure 5.4), consistent with electronic absorption, MCD, and EPR spectra that indicated the same oxidation, spin and coordination states for the Fe(III) R266K variant compared to Fe(III) WT hCBS. Additionally, the rR results confirm the observations made from electronic absorption and EPR spectroscopies that suggested that the nature of the Fe(III)-Cys(thiolate) interaction had changed subtly between WT and the R266K variant (*vide supra*).

R266K Is Active but Exhibits Differential Behavior Towards Cofactors. The R266K variant, expressed as a soluble and tetrameric protein, was previously tested for cystathionine-synthesis activity (Scheme 5.1) (*22*). The results demonstrated that Fe(III) R266K hCBS displays maximal AdoMet- and PLP-responsive activity approximately 76% that of Fe(III) WT hCBS (Table 5.1). Interestingly, while the presence of exogenous PLP had no effect on WT activity, exogenous PLP increased basal R266K activity 1.7-fold. Additionally, activation of

the R266K variant by the hCBS allosteric activator AdoMet was significantly decreased compared to that of WT hCBS. Upon addition of AdoMet, R266K was activated 2.3-fold without exogenous PLP and 2.0-fold with exogenous PLP. Comparatively, upon addition of AdoMet, WT was activated 3.5-fold without exogenous PLP and 3.7-fold with exogenous PLP (*22*) (Table 5.1).

We tested R266K activity in an alternative cysteine-synthesis reaction (Scheme 5.1). In contrast with the cystathionine-synthesis results, Fe(III) R266K is significantly less active in cysteine synthesis and has maximal AdoMet- and PLP-responsive cysteine-synthesis activity approximately 34% that of Fe(III) WT (Table 5.1). In a manner similar to the cystathionine-synthesis results, the addition of PLP increases basal R266K cysteine-synthesis activity 1.5-fold, whereas PLP has no effect on the cysteine-synthesis activity of WT Fe(III) hCBS. The presence of AdoMet increases cysteine-synthesis activity of R266K 2.0-fold without exogenous PLP and 2.3-fold with exogenous PLP (Table 5.1). When taken together, these results suggest that the R266K enzyme is functionally competent in the canonical and alternative reactions, but its differential behavior towards PLP and AdoMet suggests that 1) the PLP environment is disturbed by the R266K mutation; 2) the R266K enzyme may not be PLP replete; or 3) the conformation rearrangement of the R266K variant upon binding of AdoMet yields only partially activated enzyme.

Differences in the Fe(III) R266K Heme Are Transmitted to the PLP. It appears that changes in the hydrogen-bonding stabilization of the Cys(thiolate) ligand in hCBS are transmitted to the PLP active site, as evidenced by a change in the PLP emission spectrum. The electronic absorption spectrum of the PLP active site is obscured by that of the heme; however, the presence and nature of the PLP may be interrogated using fluorescence spectroscopy.

Figure 5.6 presents the fluorescence emission spectra (λ_{exc} = 410 nm) of full-length Fe(III) WT (A) and R266K (B) hCBS at room temperature and pH 8.6. The PLP emission spectrum of Fe(III) WT hCBS is relatively weak and displays a broad emission envelope with maximal intensity at 492 nm as well as a smaller emission band at 614 nm; this emission spectrum is similar to, albeit slightly red-shifted from, that described previously for the ketoenamine tautomer of the PLP-Lys^{119} internal aldimine of hCBS-45 (*36*). Interestingly, the fluorescence spectrum of Fe(III) R266K hCBS is red-shifted by comparison to Fe(III) WT hCBS, and displays a new peak maximum at 496 nm as well as loss of the minor peak at 614 nm. Comparison of the WT and R266K emission spectra suggests that the internal aldimine ketoenamine tautomer is still present in R266K, consistent with the high activity observed, but its environment is different. This observation implies that changes in the hydrogen-bonding network at the heme and/or the Cys(thiolate) axial ligand to the heme are transmitted to the PLP active site, a conclusion consistent with previous reports (*21, 23, 25, 36-40*).

Fe(II) R266K hCBS is Less Thermally Stable Than Fe(II) WT hCBS and Undergoes a More Facile Ligand-Switch Process. Low-temperature reduction of Fe(III) R266K hCBS is accompanied by retention of the native Cys(thiolate)/His ligation motif. Addition of a solution of the reducing agent sodium dithionite to the Fe(III) R266K variant, each equilibrated at 4°C, induces changes in the electronic absorption spectrum; the Soret band sharpens and is shifted to 447 nm with transformation of the broad α/β absorption envelope into two discrete bands at 539 nm and 570 nm (α and β, respectively, Figure 5.7), indicative of a six-coordinate, low-spin Fe(II) heme. This process is isosbestic and appears to follow first-order kinetics (Figure 5.7, inset); additionally, the positions of the highly red-shifted Soret (~450 nm) and α and β bands are almost identical to that of WT Fe(II) hCBS when it is initially reduced (*16, 18*), suggesting

that Fe(II) R266K hCBS retains the Cys(thiolate)/His ligation motif (like that of WT) when reduced at low temperature (*17*).

Similar to that of WT Fe(II) hCBS, this Cys(thiolate)-ligated Fe(II) R266K species is not stable to heat treatment; by contrast, however, the Cys(thiolate)-ligated Fe(II) R266K variant is significantly less thermally stable. Upon elevation of temperature, Cys(thiolate)-ligated Fe(II) R266K hCBS undergoes a thermally-induced ligand switch much more rapidly than does Cys(thiolate)-ligated WT Fe(II) hCBS. Previous reports have shown that WT Cys(thiolate)-ligated Fe(II) hCBS undergoes a slow and irreversible ligand-switch process at 37°C and pH 8.6 that is accompanied by a loss of the WT Fe(II) Soret at 449 nm and an increase of a new Soret at 424 nm (CBS424); however, this process was shown to be slow at physiological temperature and took 48 h to reach completion (*25, 39*). This Soret shift from 449 nm to 424 nm results from a loss of the Cys(thiolate) as an Fe(II) axial ligand (*25*). While the identity of the new ligand is unknown, EXAFS data have confirmed that Cys^{52} is replaced by a neutral heme ligand that is either a nitrogenous or oxygen-containing Lewis base, resulting in a Soret maximum at 424 nm (*41*). Similar to WT hCBS, thermally treated Cys(thiolate)-ligated Fe(II) R266K loses its Soret at 447 nm with concomitant formation of new Soret, β and α positions at 424 nm, 530 nm and 558 nm, respectively (Figure 5.8A). However, this ligand-switching process is much more facile in the R266K variant than WT. Ligand switching begins spontaneously at 4°C; although this process is quite slow at 4°C, the rate accelerates rapidly upon elevation of temperature (Figure 5.8B). In stark contrast with Cys(thiolate)-ligated Fe(II) WT hCBS, the R266K variant converts to CBS424 almost instantaneously upon reduction at 37°C, prohibiting the direct comparison of ligand switching rates between WT and R266K at physiological temperature (*39*). However, kinetics of this ligand-switching process were

measured at 10, 20 and 30°C (Table 5.2), and using an Arrhenius plot, the kinetic constants for the ligand-switch process were extrapolated to 37°C (Figure 5.9; Table 5.2). Unlike the WT enzyme, in which the loss of 449 nm appears to follow a three-state triexponential decay, the R266K variant exhibits different kinetics. Loss of 447 nm peak is best modeled as a biexponential decay, suggesting that the ligand-switch process may be different in the R266K compared to WT. Alternatively, the first step of the ligand-switch process may be so facile in the R266K variant that it is not measured, and thus the apparent rate of ligand-switching is biexponential. Furthermore, it was noted that the molar absorptivity of the R266K CBS424 species (ε_{424}) was approximately a third that of WT CBS424, implying that these Fe(II) CBS424 species may be distinct from one another. Taken together, these data suggest that the weaker Fe-S bond in R266K significantly destabilizes Cys(thiolate) ligation in the Fe(II) form, leading to more facile ligand switching.

Discussion

The influence and importance of the hydrogen-bonding network associated with the heme iron-Cys(thiolate) interaction has been extensively explored for cytochrome P-450 (Cyt P-450) and nitric oxide synthase (NOS). Both enzymes possess a heme cofactor ligated by a strongly-donating mercaptide Lewis base in the axial position (*42*). A hydrogen-bonding network to the Cys(thiolate) heme ligand is found in a number of Cyt P-450 active sites consisting of Leu (backbone amide), Gly (backbone amide), and Gln (sidechain amide) (*43-46*). Similarly, a number of NOS enzymes have a highly conserved Trp residue that hydrogen bonds to the Cys(thiolate) via the indole nitrogen (*47-51*). While a definitive consensus on the role of this hydrogen-bonding network has yet to be achieved, studies (both *in vitro* and *in silico*) of hydrogen-bonding variants at the Cys(thiolate) heme ligand of Cyt P-450$_{CAM}$ (*44, 52-54*) and NOS (*55-58*) have demonstrated dramatic changes in the redox potential, stability, and reactivity of these proteins relative to the WT proteins.

CBS exhibits similarities to and differences from Cyt P-450 and NOS. Whereas Cyt P-450 and NOS are monooxygenases and use heme as their active site (*42*), CBS is a PLP-dependent enzyme in which the PLP cofactor is spatially removed from the heme macrocycle, which is proposed to be a regulatory site (*14, 15, 59, 60*). The heme cofactors of Cyt P-450 and NOS are each ligated by a single Cys(thiolate) ligand with labile sixth coordination site (occupied sometimes by H_2O or substrate) (*42, 61*), whereas the CBS heme is coordinatively-saturated and is ligated by both a Cys(thiolate) and His residue (*14, 15*). Similar to Cyt P-450 and NOS, the hCBS and *Dm*CBS crystal structures reveal residues within hydrogen-bonding distance of the Cys(thiolate) ligand (Figure 5.1): the amide backbone of a Trp residue (3.59 Å distance) and the guanidinium group of an Arg side chain (3.54 Å distance) (*14, 15*).

Additionally, sequence alignments of CBS enzymes from a number of different organisms illustrate strong conservation of both the Arg and Trp residues (Figure 5.10), similar to the strong conservation of hydrogen-bonding residues in the Cyt P-450 and NOS enzymes (*vide supra*). In CBS enzymes that do not possess heme, such as those from *T. cruzi* and *S. cerevisiae*, a Lys residue is found in a position analogous to Arg^{266}, maintaining a locus of positive charge in this area. Unlike the NOS enzymes, which use the Trp indole N-H moiety to hydrogen bond directly to the Cys(thiolate), CBS enzymes use the Trp backbone amide; however, the strong conservation of this residue (Figure 5.10) suggests that the sidechain bulk and aromaticity may play an important role in the heme binding pocket. Interestingly, the Arg residue that hydrogen bonds to the Cys(thiolate) heme ligand is a relatively frequent site for human mutation, and the loss or alteration of this hydrogen-bonding residue is correlated with increased levels of Hcy in human patients (*62-64*).

CBS missense mutations represent the most common cause of CBS deficiency and hyperhomocysteinemia (*5, 62, 65*), and Arg^{266} is the location of two missense mutations, R266G and R266K, which were originally identified in Japanese and Norwegian patients, respectively (*63, 64*). Interestingly, while the patient with the R266G pathogenic mutation was unresponsive to vitamin B_6 (a PLP precursor) supplementation (*63*), the patients carrying the R266K mutation were B_6-responsive (*64*). Previous studies on the variants R266G, R266A and R266E have clearly demonstrated that these proteins are either unstable and do not accumulate (R266G) or create soluble but heme- and PLP-deplete protein (R266A/E) (*41, 66*). These results showed that mutation of Arg^{266} to either a hydrophobic or anionic residue dramatically affected the overall stability of the polypeptide. Analysis of R266M (an isosteric but not pathogenic variation) demonstrated that retention of the salt bridge between Cys^{52} and Arg^{266}

appears to be necessary for maximal AdoMet- and PLP-responsive activity. Furthermore, electronic absorption spectroscopy of the R266M variant demonstrated complete conversion to the catalytically inactive CBS-424 species upon heme reduction (*41*); fluorescence and rR data correlated the loss of the Arg-Cys salt bridge in the R266M variant with a shift to the inactive enolimine PLP tautomer (*36*). These results demonstrated that complete loss of one of the hydrogen-bonding partners to the Cys(thiolate) heme ligand disrupts CBS function.

Recently, we have shown that the position and nature of the affinity tag for expression and purification of R266K hCBS plays an important role in enabling isolation of this variant (*22*). Moreover, biochemical characterization of purified R266K suggested that this pathogenic mutation negatively impacts the enzyme's saturation with PLP, its response to AdoMet, and its thermal stability, despite having similar heme saturation as compared to that of WT hCBS (*22*). However, none of the previous studies addressed the mode in which the structurally modest and charge invariant R266K substitution elicits changes at the heme and the PLP cofactors that are associated with diminished enzyme activity.

In this work, we have used spectroscopic methods to demonstrate that R266K hCBS bears a geometric distortion at the heme iron center, resulting in a weakening and a lengthening of the Fe(III)-Cys(thiolate) bond. The longer Fe(III)-S(Cys) bond present in the R266K variant is likely due to the closer match between the free amino acid pK_a values of Cys (8.2) and Lys (10.5) versus Arg (12.5) (*67*). This closer pK_a match between Cys and Lys would be expected to form a stronger hydrogen bond and a more fully protonated thiolate residue, thus destabilizing the Coulombic attraction between the ferric and mercaptide ions and leading to a longer Fe-S(Cys) bond. Destabilization of the Fe-Cys(thiolate) interaction results in rapid displacement of Cys^{52} upon reduction of the heme iron, as evidenced by the increased rate of

ligand switching in Fe(II) R266K. A similar facile ligand switch was seen in the Fe(II) R266M variant (*41*). These *in vitro* findings suggest that the R266K hCBS heme would be unstable if reduced *in vivo*. Surprisingly, spectroelectrochemical titration showed that the redox potential of the hCBS heme (approximately –350 mV) remained virtually unchanged in the R266K variant (*41*); however, the facile ligand switching that we observed for this variant may call into question the accuracy of the prior measurement. A weaker Fe-thiolate interaction, with a more fully compensated charge neutralization through stronger hydrogen bonding to Lys, would be expected to make the reduction potential of the heme iron in R266K more thermodynamically favorable. Whether redox chemistry is relevant to CBS function is unclear; the unfavorable reduction potential may imply that ferric is the only relevant oxidation state of the CBS heme *in vivo*.

The spectral and activity data suggest that changes at the PLP active site induced by alteration of the hydrogen-bonding partner to the Cys(thiolate) heme ligand may be the source of diminished enzymatic activity in R266K hCBS. The shift in the PLP emission spectrum suggests an alteration of the PLP environment in R266K. Interestingly, this variant is more impaired in cysteine synthesis than in cystathionine synthesis. While the first substrate (Ser) is identical in each enzymatic reaction, the second substrate differs (Scheme 5.1). Sulfide (K_m= 3.1 mM, *T. cruzi* CBS; 16.8 mM *S. cerevisiae* CBS) has been shown to be a poorer second substrate than Hcy (K_m 0.9 mM, *T. cruzi* CBS; 2.25 mM *S. cerevisiae* CBS) (*68, 69*). We speculate that a looser PLP environment in R266K, coupled with the inefficiency of sulfide as a substrate, may facilitate loss of the PLP-Ser external aldimine from the enzyme during the cysteine-synthesis reaction. This speculation is supported by the observation that saturation of the enzyme's active site with Ser, followed by extensive dialysis, has been used as an effective

method to generate PLP-free, and thus inactive, hCBS (*36*). Furthermore, the greater sensitivity of R266K toward partial rescue of activity by exogenous PLP in both the cystathionine- and cysteine-synthesis reactions is consistent with a more facile loss of the PLP-Ser external aldimine.

This study directly demonstrates that even modest changes at the heme Cys(thiolate) ligand may be communicated to the PLP active site, suggesting that changes in the heme environment modulate CBS activity. Indeed, numerous examples exist in which CBS activity is abrogated upon loss of the metal-thiolate bond, strongly implying that communication exists between the heme and PLP active site (*21, 23, 25, 37-39, 60*). While a consensus on the function of heme in CBS has yet to be achieved, these data, in combination with previous results, demonstrate a clear necessity for the presence of a metal-thiolate bond and an intact hydrogen-bonding network for optimal activity in heme-containing CBS.

Conclusion

In this study, we have demonstrated that the charge invariant R266K mutation generates a CBS protein that exhibits subtle spectroscopic and enzymatic changes consistent with alteration of the environment of the ligating cysteine residue. We have used electronic absorption and EPR spectroscopies to show that a change in a hydrogen bonding residue (R→K) elicits minor geometric perturbations at the Fe(III)-Cys(thiolate) bond, as evidenced by red shifts in LMCT transitions of the visible spectrum, as well as alterations of the rhombic (V) and axial distortions (Δ) of the EPR spectrum. Using rR spectroscopy, we have demonstrated that the R266K variant exhibits a longer and weaker Fe-S(Cys) bond; upon heme reduction, this weaker interaction causes a more facile rate of ligand-switching compared to WT. Finally, we have used fluorescence spectroscopy to demonstrate that even minor changes in hydrogen bonding at the heme site may be transmitted to the PLP active site; the alteration of the PLP environment is correlated with diminished canonical and alternative activities in CBS. Taken together, these data illustrate that the heme and PLP active sites are able to communicate to one another via hydrogen bonding at the heme Cys(thiolate) axial ligand.

References

1. Trudinger, P. A., and Loughlin, R. E. (1981) Metabolism of Simple Sulphur Compounds, in *Comprehensive Biochemistry: Amino Acid Metabolism and Sulphur Metabolism* (Neuberger, A., Ed.), Elsevier, Amsterdam.

2. Jakubowski, H. (2000) Homocysteine Thiolactone: Metabolic Origin and Protein Homocysteinylation in Humans, *J. Nutr. 130*, 377S-381S.

3. Jakubowski, H. (2008) The Pathopysiological Hypothesis Of Homocysteine Thiolactone-Mediated Vascular Disease, *J. Physiol. Pharmacol. 59*, 155-167.

4. de Koning, A. B. L., Werstuck, G. H., Zhou, J., and Austin, R. C. (2003) Hyperhomocysteinemia and its role in the development of atherosclerosis, *Clin. Biochem. 36*, 431-441.

5. Mudd, S. H., Levy, H. L., and Kraus, J. P., (Eds.) (2001) *Disorders of Transsulfuration*, McGraw-Hill, New York.

6. Clarke, R., Smith, A. D., Jobst, K. A., Refsum, H., Sutton, L., and Ueland, P. M. (1998) Folate, vitamin B12, and serum total homocysteine levels in confirmed Alzheimer disease, *Arch. Neurol. 55*, 1449-1455.

7. Mattson, M. P., and Shea, T. B. (2003) Folate and homocysteine metabolism in neural plasticity and neurodegenerative disorders, *Trends Neurosci. 26*, 137-146.

8. Refsum, H., Ueland, P. M., Nygard, O., and Vollset, S. E. (1998) Homocysteine and cardiovascular disease, *Annu. Rev. Med. 49*, 31-62.

9. Mills, J. L., McPartlin, J. M., Kirke, P. N., Lee, Y. J., Conley, M. R., Weir, D. G., and Scott, J. M. (1995) Homocysteine metabolism in pregnancies complicated by neural-tube defects, *Lancet 345*, 149-151.

10. Kery, V., Poneleit, L., Meyer, J. D., Manning, M. C., and Kraus, J. P. (1999) Binding of Pyridoxal 5'-Phosphate to the Heme Protein Human Cystathionine β-Synthase, *Biochemistry 38*, 2716-2724.

11. Oliveriusová, J., Kery, V., Maclean, K. N., and Kraus, J. P. (2002) Deletion Mutagenesis of Human Cystathionine beta-synthase. Impact on Activity, Oligomeric Status, and S-Adenosylmethionine Regulation, *J. Biol. Chem. 277*, 48386-48394.

12. Janosik, M., Kery, V., Gaustadnes, M., MacLean, K. N., and Kraus, J. P. (2001) Regulation of human cystathionine β-synthase by S-adenosyl-L-methionine: Evidence for two catalytically active conformations involving an autoinhibitory domain in the C-terminal region, *Biochemistry 40*, 10625-10633.

13. Kery, V., Poneleit, L., and Kraus, J. P. (1998) Trypsin Cleavage of Human Cystathionine β-Synthase into an Evolutionarily Conserved Active Core: Structural and Functional Consequences, *Arch. Biochem. Biophys. 355*, 222-232.

14. Meier, M., Janosik, M., Kery, V., Kraus, J. P., and Burkhard, P. (2001) Structure of human cystathionine β-synthase: A unique pyridoxal 5'-phosphate dependent hemeprotein, *EMBO J. 20*, 3910-3916.

15. Koutmos, M., Kabil, O., Smith, J. L., and Banerjee, R. (2010) Structural basis for substrated activation and regulation by cystathionine beta-synthase (CBS) domains in cystathionine β-synthase, *Proc. Natl. Acad. Sci. U.S.A. 107*, 20958-20963.

16. Omura, T., Sadano, H., Hasegawa, T., Yoshida, Y., and Kominami, S. (1984) Hemoprotein H-450 Identified as a Form of Cytochrome P-450 Having an Endogenous Ligand at the 6th Coordination Position of the Heme, *J. Biochem. 96*, 1491-1500.

17. Svastits, E. W., Alberta, J. A., Kim, I.-C., and Dawson, J. H. (1989) Magnetic Circular Dichroism Studies of the Active Site Structure of Hemoprotein H-450: Comparison to Cytochrome P-450 and Sensitiviy to pH Effects, *Biochem. Biophys. Res. Commun. 165*, 1170-1176.

18. Kery, V., Bukovska, G., and Kraus, J. P. (1994) Transsulfuration depends on heme in addition to pyridoxal 5'-phosphate. Cystathionine β-synthase is a heme protein, *J. Biol. Chem. 269*, 25283-25288.

19. Evande, R., Ojha, S., and Banerjee, R. (2004) Visualization of PLP-bound intermediates in hemeless variants of human cystathionine β-synthase: evidence that lysine 119 is a general base, *Arch. Biochem. Biophys. 427*, 188-196.

20. Bruno, S., Schiaretti, F., Burkhard, P., Kraus, J. P., Janosik, M., and Mozzarelli, A. (2001) Functional Properties of the Active Core of Human Cystathionine β -Synthase Crystals, *J. Biol. Chem. 276*, 16-19.

21. Taoka, S., West, M., and Banerjee, R. (1999) Characterization of the Heme and Pyridoxal Phosphate Cofactors of Human Cystathionine β-Synthase Reveals Nonequivalent Active Sites, *Biochemistry 38*, 2738-2744.

22. Majtan, T., and Kraus, J. P. (2012) Folding and activity of mutant cystathionine β-synthase depends on the position and nature of the purification tag: Characterization of the R266K CBS mutant, *Protein Expres. Purif. 82*, 317-324.

23. Smith, A. T., Majtan, T., Freeman, K. M., Su, Y., Kraus, J. P., and Burstyn, J. N. (2011) Cobalt Cystathionine ß-Synthase: A Cobalt-Substituted Heme Protein with a Unique Thiolate Ligation Motif, *Inorg. Chem. 50*, 4417-4427.

24. Gaitonde, M. K. (1967) A spectrophotometric method for the direct determination of cysteine in the presence of other naturally occuring amino acids, *Biochem. J. 104*, 627-633.

25. Pazicni, S., Cherney, M. M., Lukat-Rogers, G. S., Oliveriusová, J., Rodgers, K. R., Kraus, J. P., and Burstyn, J. N. (2005) The Heme of Cystathionine β-synthase Likely Undergoes a Thermally Induced Redox-Mediated Ligand Switch, *Biochemistry 44*, 16785-16795.

26. Spiro, T. G. (1975) Resonance Raman spectroscopic studies of heme proteins, *Biochim. Biophys. Acta 416*, 169-189.

27. Hu, S., Smith, K. M., and Spiro, T. G. (1996) Assignment of Protoheme Resonance Raman Spectrum by Heme Labeling in Myoglobin, *J. Am. Chem. Soc. 118*, 12638-12646.

28. Green, E. L., Taoka, S., Banerjee, R., and Loehr, T. M. (2000) Resonance Raman Characterization of the Heme Cofactor in Cystathionine β-Synthase. Identification of the Fe-S(Cys) Vibration in the Six-Coordinate Low-Spin Heme, *Biochemistry 40*, 459-463.

29. Pazicni, S., Lukat-Rodgers, G. S., Oliveriusová, J., Rees, K. A., Parks, R. B., Clark, R. W., Kraus, J. P., Rodgers, K. R., and Burstyn, J. N. (2004) The redox behavior of the heme in cystathionine β-synthase is sensitive to pH, *Biochemistry 43*, 14684-14695.

30. Shimizu, T., Iizuka, T., Shimada, H., Ishimura, Y., Nozawa, T., and Hatano, M. (1981) Magnetic circular dichroism studies of P-450CAM. Characterization of axial ligands of ferric and ferrous low-spin complexes, *Biochim. Biophys. Acta 670*, 341-354.

31. Marvin, K. A., Kerby, R. L., Youn, H., Roberts, G. P., and Burstyn, J. N. (2008) The Transcription Regulator RcoM-2 from *Burkholderia xenovorans* Is a Cysteine-Ligated Hemoprotein That Undergoes a Redox-Mediated Ligand Switch, *Biochemistry 47*, 9016-9028.

32. Marvin, K. A., Reinking, J. L., Lee, A. J., Pardee, K., Krause, H. M., and Burstyn, J. N. (2009) Nuclear Receptors *Homo sapiens* Rev-erbβ and *Drosophila melanogaster* E75 Are Thiolate-Ligated Heme Proteins Which Undergo Redox-Mediated Ligand Switching and Bind CO and NO, *Biochemistry 48*, 7056-7071.

33. Dhawan, I. K., Shelver, D., Thorsteinsson, M. V., Roberts, G. P., and Johnson, M. K. (1999) Probing the heme axial ligation in the CO-sensing CooA protein with magnetic circular dichroism spectroscopy, *Biochemistry 38*, 12805-12813.

34. Palmer, G. (1983) Electron Paramagnetic Resonance of Hemoproteins, in *Iron Porphyrins, Part II* (Lever, A. B. P., and Gray, H. B., Eds.), pp 45-88, VCH Publishers, New York.

35. Blumberg, W. E., and Peisach, J. (1971) Low-spin compounds of heme proteins, *Adv. Chem. Ser. 100*, 271-291.

36. Weeks, C. L., Singh, S., Madzelan, P., Banerjee, R., and Spiro, T. G. (2009) Heme Regulation of Human Cystathionine β-Synthase Activity: Insights from Fluorescence and Raman Spectroscopy, *J. Am. Chem. Soc. 131*, 12809–12816.

37. Taoka, S., Green, E. L., Loehr, T. M., and Banerjee, R. (2001) Mercuric chloride-induced spin or ligation state changes in ferric or ferrous human cystathionine β-synthase inhibit enzyme activity, *J. Inorg. Biochem. 87*, 253-259.

38. Taoka, S., and Banerjee, R. (2001) Characterization of NO binding to human cystathionine β-synthase: Possible implications of the efects of CO and NO binding to the human enzyme, *J. Inorg. Biochem. 87*, 245-251.

39. Cherney, M. M., Pazicni, S., Frank, N., Marvin, K. A., Kraus, J. P., and Burstyn, J. N. (2007) Ferrous Human Cystathionine β-Synthase Loses Activity during Enzyme Assay Due to a Ligand Switch Process, *Biochemistry 46*, 13199-13210.

40. Puranik, M., Weeks, C. L., Lahaye, D., Kabil, Ö., Shinichi, T., Nielsen, S. B., Groves, J. T., Banerjee, R., and Spiro, T. G. (2006) Dynamics of Carbon Monoxide Binding to Cystathionine β-Synthase, *J. Biol. Chem. 281*, 13433-13438.

41. Singh, S., Madzelan, P., Stasser, J., Weeks, C. L., Becker, D., Spiro, T. G., Penner-Hahn, J., and Banerjee, R. (2009) Modulation of the heme electronic structure and cystathionine β-synthase activity by second coordination sphere ligands: The role of heme ligand switching in redox regulation, *J. Inorg. Biochem. 103*, 689-697.

42. Sono, M., Roach, M. P., Coulter, E. D., and Dawson, J. H. (1996) Heme-Containing Oxygenases, *Chem. Rev. 96*, 2841-2888.

43. Cupp-Vickery, J., and Poulos, T. L. (1995) Structure of cytochrome P450 eryF: an enzyme involved in erythromycin biosynthesis, *Nat. Struct. Biol. 2*, 144-153.

44. Galinato, M. G. I., Spolitak, T., Ballou, D. P., and Lehnert, N. (2011) Elucidating the Role of the Proximal Cysteine Hydrogen-Bonding Network in Ferric Cytochrome P450cam and Corresponding Mutants Using Magnetic Circular Dichroism Spectroscopy, *Biochemistry 50*, 1053-1069.

45. Ravichandran, K. G., Boddupalli, S. S., Hasemann, C. A., Peterson, J., and Deisenhofer, J. (1993) Crystal structure of hemoprotein domain of P450BM-3, a prototype for microsomal P450's, *Science 261*, 731-736.

46. Hasemann, C. A., Ravichandran, K. G., Boddupalli, S. S., Peterson, J., and Deisenhofer, J. (1995) Structure and function of cytochromes P450: a comparative analysis of three crystal structures, *Structure 3*, 41-62.

47. Bird, L. E., Ren, J., Zhang, J., Foxwell, N., Hawkins, A. R., Charles, I. G., and Stammers, D. K. (2002) Crystal Structure of SANOS, a Bacterial Nitric Oxide Synthase Oxygenase Protein from *Staphylococcus aureus*, *Structure 10*, 1687-1696.

48. Sughamsu, J., and Crane, B. R. (2006) Structure and Reactivity of a Thermostable Prokaryotic Nitric-oxide Synthase That Forms a Long-lived Oxy-Heme Complex, *J. Biol. Chem. 281*, 9623-9632.

49. Li, H., Igarashi, J., Jamal, J., Yang, W., and Poulos, T. L. (2006) Structural studies of constitutive nitric oxide synthases with diatomic ligands bound, *J. Biol. Inorg. Chem. 11*, 753-768.

50. Crane, B. R., Arvai, A. S., Ghosh, D. K., Wu, C., Getzoff, E. D., Stuehr, D. J., and Tainer, J. A. (1998) Structure of Nitric Oxide Synthase Oxygenase Dimer with Pterin and Substrate, *Science 279*, 2121-2126.

51. Pant, K., Bilwes, A. M., Adak, S., Stuehr, D. J., and Crane, B. R. (2002) Structure of a Nitric Oxide Synthase Heme Protein from *Bacillus subtilis*, *Biochemistry 41*, 11071-11079.

52. Yoshioka, S., Tosha, T., Takahashi, S., Ishimori, K., Hori, H., and Morishima, I. (2002) Roles of the Proximal Hydrogen Bonding Network in Cytochrome P450cam-Catalyzed Oxidation, *J. Am. Chem. Soc. 124*, 14571-14579.

53. Yoshioka, S., Takahashi, S., Ishimori, K., and Morishima, I. (2000) Roles of the axial push effect in cytochrome P450cam studied with site-directed mutagenesis at the heme proximal site, *J. Inorg. Biochem. 81*, 141-151.

54. Usharani, D., Zazza, C., Lai, W., Chourasia, M., Waskell, L., and Shaik, S. (2012) A Single-Site Mutation (F429H) Converts the Enzyme CYP 2B4 into a Heme Oxygenase: A QM/MM Study, *J. Am. Chem. Soc. dx.doi.org/10.1021/ja211905e*.

55. Lang, J., Driscoll, D., Gélinas, S., Rafferty, S. P., and Couture, M. (2009) Trp180 of endothelial NOS and Trp56 of bacterial saNOS modulate sigma bonding of the axial cysteine to the heme, *J. Inorg. Biochem. 103*, 1102-1112.

56. Brunel, A., Wilson, A., Henry, L., Dorlet, P., and Santolini, J. (2011) The Proximal Hydrogen Bond Network Modulates *Bacillus subtilis* Nitric-oxide Synthase Electronic and Structural Properties, *J. Biol. Chem. 286*, 11997-12005.

57. Couture, M., Adak, S., Stuehr, D. J., and Rousseau, D. L. (2001) Regulation of the Properties of the Heme-NO Complexes in Nitric-oxide Synthase by Hydrogen Bonding to the Proximal Cysteine, *J. Biol. Chem. 276*, 38280-38288.

58. Hannibal, L., Somasundaram, R., Tejero, J., Wilson, A., and Stuehr, D. J. (2011) Influence of Heme-Thiolate in Shaping the Catalytic Properties of a Bacterial Nitric-Oxide Synthase, *J. Biol. Chem. 286*, 39224-39235.

59. Banerjee, R., and Zou, C.-G. (2005) Redox regulation and reaction mechanism of human cystathionine-β-synthase: a PLP-dependent hemesensor protein, *Arch. Biochem. Biophys. 433*, 144-156.

60. Kabil, O., Weeks, C. L., Carballal, S., Gherasim, C., Alvarez, B., Spiro, T. G., and Banerjee, R. (2011) Reversible Heme-Dependent Regulation of Human Cystathionine β-Synthase by a Flavoprotein Oxidoreductase, *Biochemistry 50*, 8261-8263.

61. Omura, T. (2005) Heme-thiolate proteins, *Biochem. Biophys. Res. Commun. 338*, 404-409.

62. Mudd, S. H. (2011) Hypermethioninemias of Genetic and Non-Genetic Origin: A Review, *Am. J. Med. Genet. Part C Semin. Med. Genet. 157*, 3-32.

63. Katsushima, F., Oliveriusova, J., Sakamoto, O., Ohura, T., Kondo, Y., Iinuma, K., Kraus, E., Stouracova, R., and Kraus, J. P. (2006) Expression study of mutant cystathionine β-synthase found in Japanese patients with homocystinuria, *Mol. Genet. Metab. 87*, 323-328.

64. Kim, C. E., Gallagher, P. M., Guttormsen, A. B., Refsum, H., Ueland, P. M., Ose, L., Følling, I., Whitehead, A. S., Tsai, M. Y., and Kruger, W. D. (1997) Functional Modeling of Vitamin Responsiveness in Yeast: A Common Pyridoxine-Responsive Cystathionine β-Synthase Mutation in Homocystinuria, *Hum. Mol. Genet. 6*, 2213-2221.

65. Meier, M., Oliveriusova, J., Kraus, J. P., and Burkhard, P. (2003) Structural insights into mutations of cystathionine β-synthase, *Biochim. Biophys. Acta 1647*, 206-213.

66. Ozaki, S.-i., Sakaguchi, C., Nakahara, A., and Yoshiya, M. (2010) Mutagenesis Studies of Human Cystathionine β-Synthase: Residues Important for Heme Binding and Substrate Interaction, *Protein Peptide Lett. 17*, 351-355.

67. Nelson, D. L., and Cox, M. M. (2008) *Lehninger Principles of Biochemistry*, 5th ed., W. H. Freeman and Company, New York.

68. Nozaki, T., Shigeta, Y., Saito-Nakano, Y., Imada, M., and Kruger, W. D. (2001) Characterization of Transsulfuration and Cysteine Biosynthetic Pathways in the Protozoan Hemoflagellate, *Trypanosoma cruzi*, *J. Biol. Chem. 276*, 6516-6523.

69. Ono, B.-I., Kijima, K., Inoue, T., Miyoshi, S.-I., Matsuda, A., and Shinoda, S. (1994) Purification of properties of *Saccaromyces cerevisiae* cystathionine β-synthase, *Yeast 10*, 333-339.

70. Tamura, K., Peterson, D., Peterson, N., Stecher, G., Nei, M., and Kumar, S. (2011) MEGA5: Molecular Evolutionary Genetics Analysis using Maximum Likelihood, Evolutionary Distance, and Maximum Parsimony Methods, *Mol. Biol. Evol. 28*, 2731-2739.

Table 5.1. Specific activity of Fe(III) WT and R266K hCBS. WT and R266K were each assayed for cysteine-synthesis activity (i.e. condensation of serine with H_2S to form cysteine) and cystathionine-synthesis activity (i.e. condensation of serine with homocysteine to form cystathionine). Data are reported with and without the addition of exogenous PLP and AdoMet. Cystathionine-synthesis data are from reference (*22*), and are reported here for comparison.

hCBS Cysteine-Synthesis Activity (U)[a]			
PLP	**AdoMet**	**WT**	**R266K**
-	-	27.3 ± 0.1	10 ± 1
-	+	69 ± 2	20 ± 3
+	-	28 ± 1	15 ± 1
+	+	70 ± 4	23.4 ± 0.8
hCBS Cystathionine-Synthesis Activity (U)[a,b]			
PLP	**AdoMet**	**WT**	**R266K**
-	-	128 ± 6	130 ± 10
-	+	444 ± 22	299 ± 35
+	-	137 ± 5	191 ± 17
+	+	507 ± 34	386 ± 26

[a] 1 Unit (U) = μmol product·(mg enzyme)$^{-1}$·hr^{-1}
[b] Data from reference (*22*).

Table 5.2. Experimentally fit rate constants (min^{-1}) for loss of the Cys(thiolate)-ligated heme Soret of Fe(II) R266K hCBS. The loss of the Cys(thiolate)-ligated heme Soret was monitored at at 447 nm for Fe(II) R266K hCBS and was fit to a biexponential decay.

	Rate of Cys^{52} Ligand Loss (min^{-1})			
	37°C[a]	**30°C**	**20°C**	**10°C**
k_1	$(9 \pm 1.1) \times 10^{-2}$	$(5 \pm 1.4) \times 10^{-2}$	$(1.4 \pm 0.1) \times 10^{-2}$	$(9.1 \pm 0.5) \times 10^{-3}$
k_2	$(1.2 \pm 0.5) \times 10^{0}$	$(6.6 \pm 0.8) \times 10^{-1}$	$(2.5 \pm 0.3) \times 10^{-1}$	$(1.0 \pm 0.3) \times 10^{-1}$

[a]Upon equilibration at physiological temperature (37°C), Fe(II) R266K hCBS exists almost exclusively as the ligand-switched form (424 nm Soret), which prevented the measurement of k_1 and k_2 at this temperature; reported values were extrapolated from Arrhenius plots of k_1 and k_2 (Figure S3).

Figure 5.1. Location of key residues that interact with the heme and PLP in hCBS. Labeled are: the Fe(III) heme ligands Cys^{52} and His^{65}; the cysteine(thiolate) hydrogen bonding partners Arg^{266} and the amide backbone of Trp^{54}; the PLP phosphate hydrogen bonding partners Thr^{257} and Thr^{260}; and the PLP internal aldimine forming Lys^{119}. Data taken from PDB file 1JBQ (*14*).

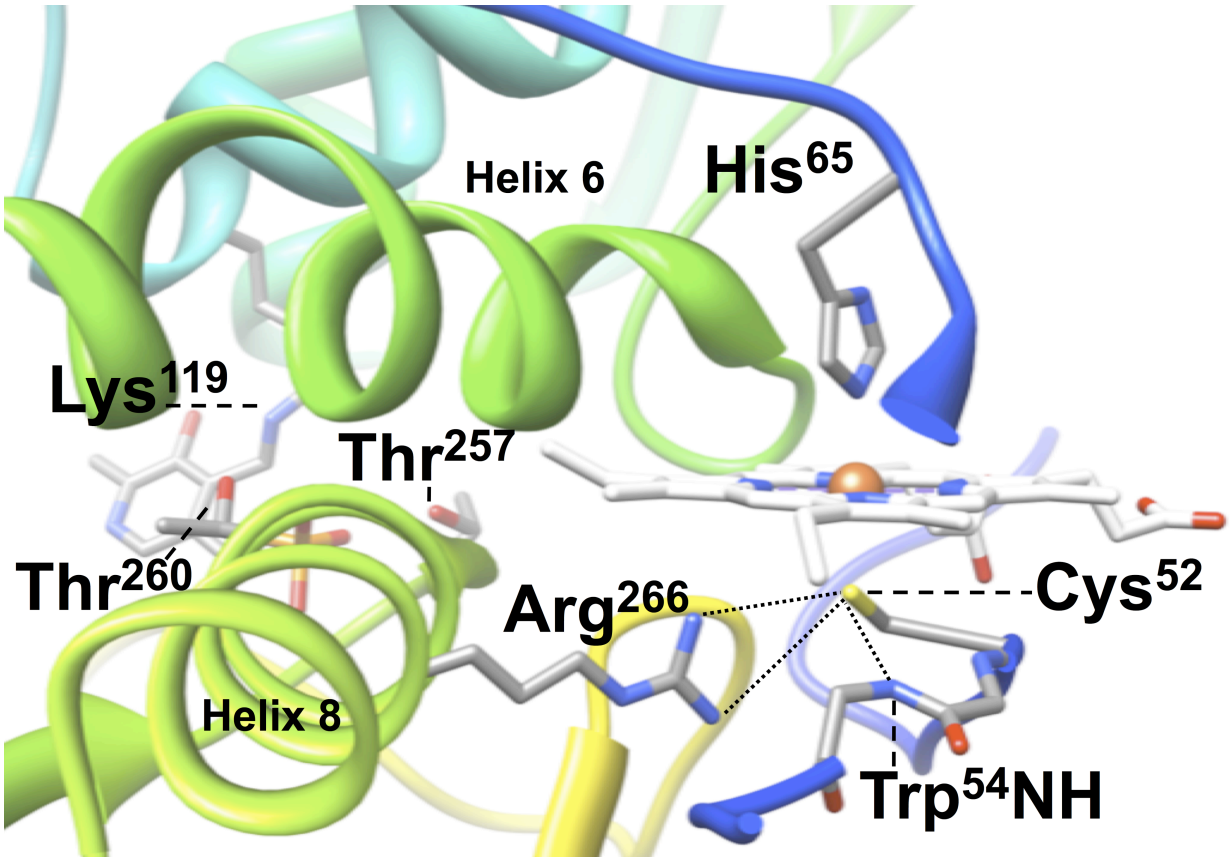

Figure 5.2. (A) Electronic absorption spectrum of Fe(III) R266K hCBS. Fe(III) R266K (7.8 μM) was in 100 mM CHES buffer and 100 mM NaCl, pH 8.6 at room temperature. Inset: close-up of the ligand-to-metal charge transfer (LMCT) transitions including the best-fit bands assuming a Gaussian peak shape (dotted). (B) MCD spectrum of Fe(III) R266K hCBS. Fe(III) R266K (15.7 μM) was in 100 mM CHES buffer, 100 mM NaCl and 55% glycerol (v/v) at 4.0 K and 7 T. Inset: the field dependence of the MCD intensity at 432 nm was recorded at 2.5, 4.0, 8.0 and 15 K. The curves were normalized to the most intense data point (2.5 K, 7 T).

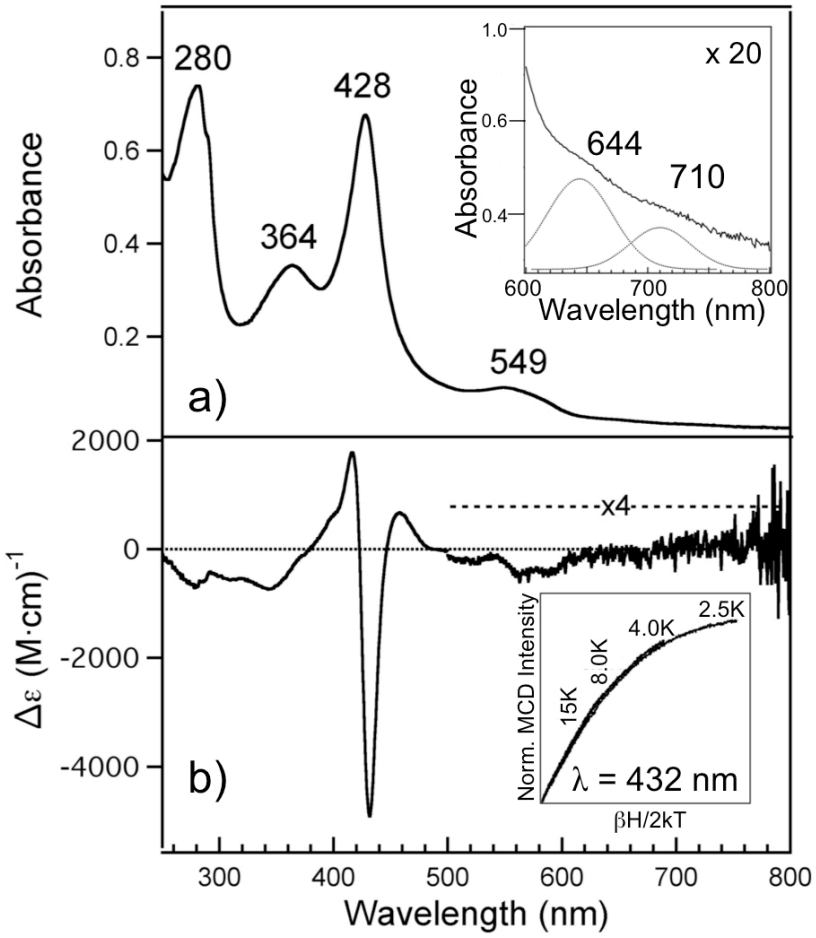

Figure 5.3. X-band EPR spectra of Fe(III) A) WT hCBS and B) R266K hCBS. Proteins (141 μM WT and 235 μM R266K) were in 100 mM CHES buffer and 100 mM NaCl, pH 8.6. Each spectrum represents an average of 10 scans taken at 10K, with 9.379 GHz microwave frequency, 8.000 G modulation amplitude, 100 kHz modulation frequency, 74 dB receiver gain, 163.84 ms time constant and a power of 1.002 mW.

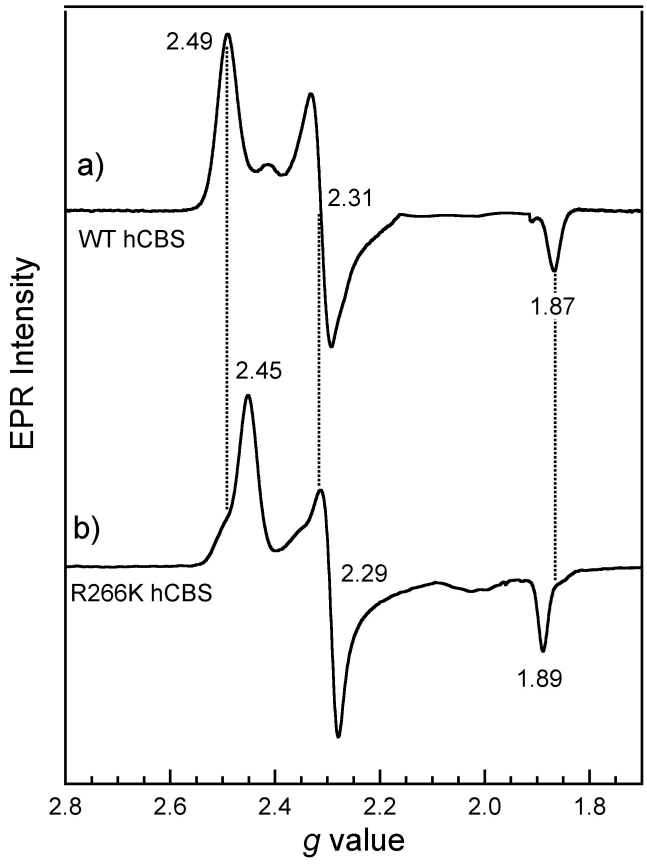

Figure 5.4. Mid-frequency resonance Raman spectra of Fe(III) (A) WT hCBS and (B) R266K hCBS. Proteins (141 μM WT and 235 μM R266K) were in 100 mM CHES buffer and 100 mM NaCl, pH 8.6. Spectra were acquired using solution samples by excitation with a 413.1 nm line provided by a Kr^+ laser with 10.5 mW of power at the sample. All measurements were carried out with the sample immersed in a bath of ice water to reduce local heating. Peak positions were calibrated against a K_2SO_4 standard.

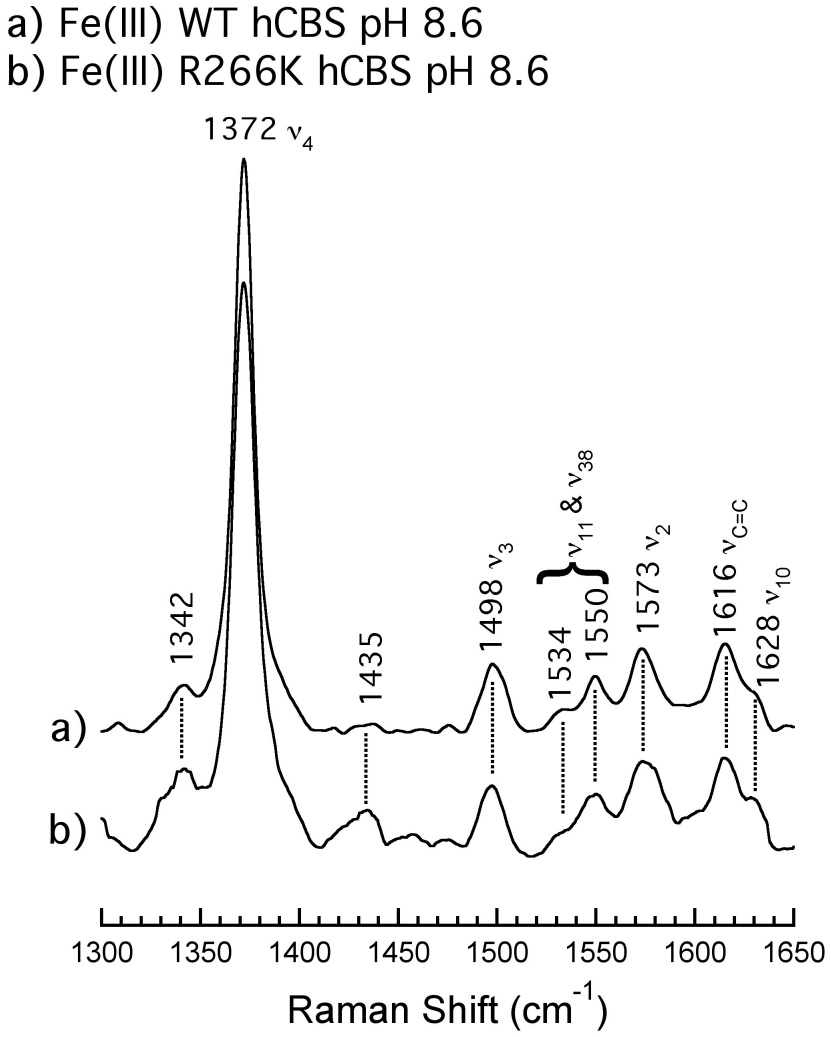

Figure 5.5. Low frequency resonance Raman spectra of Fe(III) A) WT hCBS and B) R266K hCBS. Proteins (141 μM WT and 235 μM R266K) were in 100 mM CHES buffer and 100 mM NaCl, pH 8.6. Spectra were acquired using solution samples by excitation with a 413.1 nm line of a Kr^+ laser with 10.5 mW power at the sample. All measurements were carried out with the sample immersed in a bath of ice water to reduce local heating. Peak positions were calibrated against a K_2SO_4 standard.

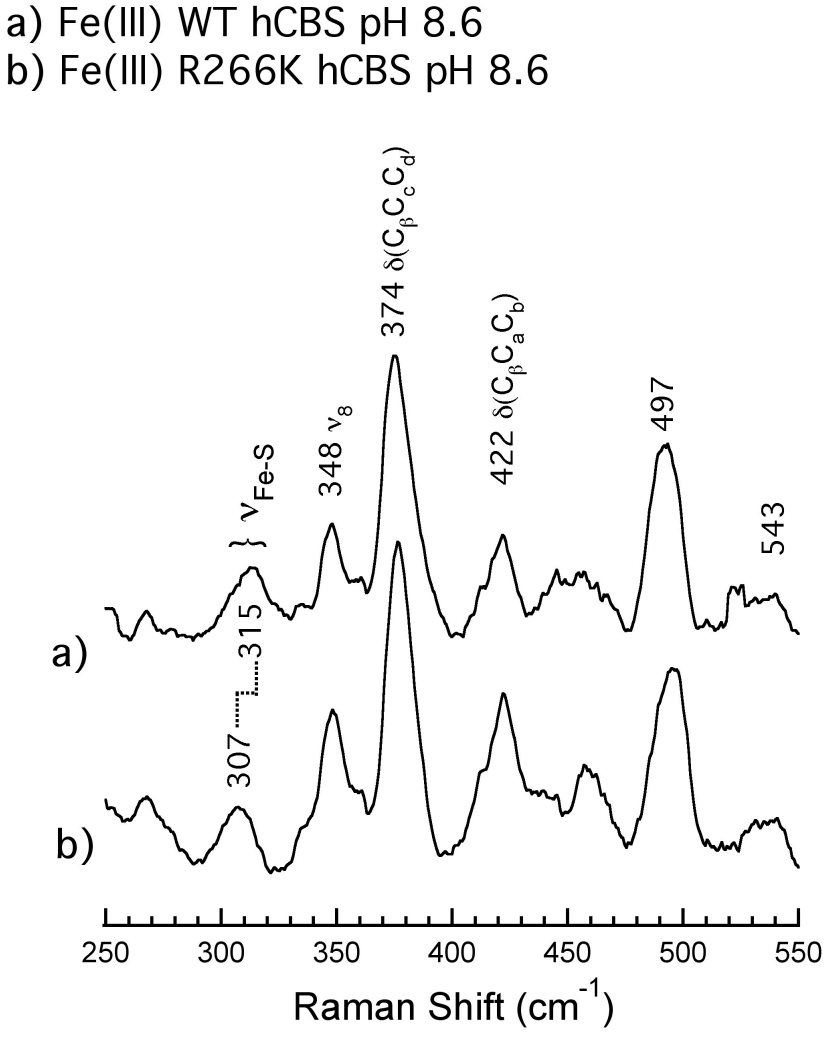

Figure 5.6. Emission spectra of Fe(III) WT (solid line) and R266K (dotted line) hCBS. Proteins (7.4 μM WT and 10.4 μM R266K) were in 100 mM CHES buffer and 100 mM NaCl, pH 8.6 at room temperature. Emission spectra were recorded as follows: excitation at 410 nm with a 4 mm excitation slit width; output recorded from 425 nm to 635 nm with a 2 mm emission slit width. Total emission counts were normalized to protein concentration for each sample.

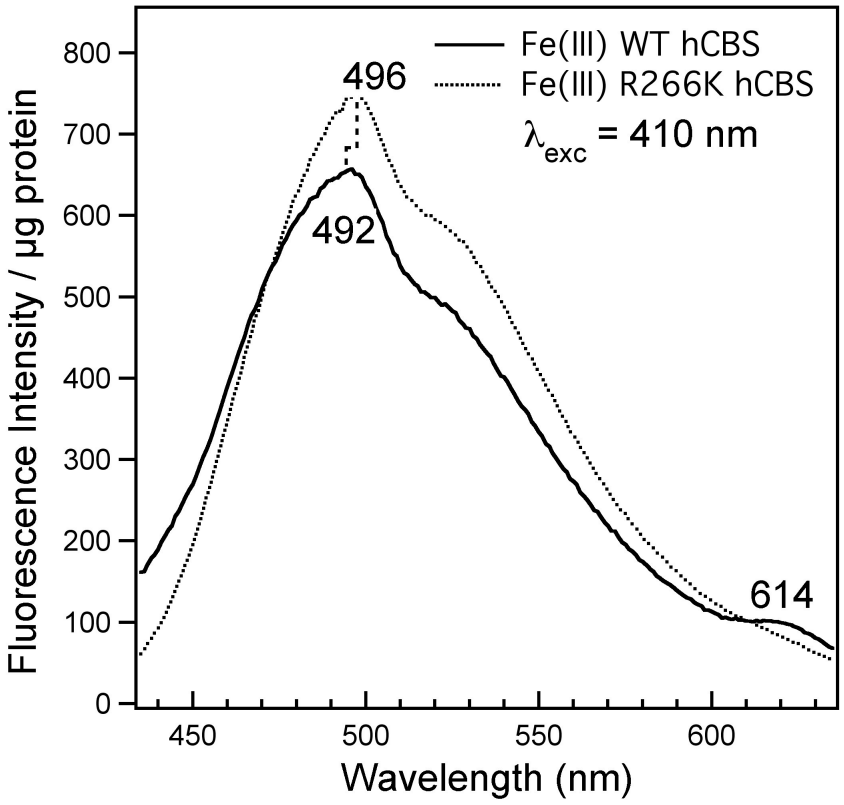

Figure 5.7. Reduction process of Fe(III) to Fe(II) R266K hCBS at 4°C. Protein (7.8 μM) was in 100 mM CHES buffer, 100 mM NaCl, pH 8.6; the reduction process was initiated by addition of a stock solution of sodium dithionite to a final concentration of 1.5 mM. Solid lines indicate the initial (428 nm Soret) and final (447 nm Soret) spectra; dotted spectra were taken at 1 min intervals after addition of reductant. Inset: time course plots showing the loss of the Fe(III) Soret (428 nm, dashed) and the growth of the Fe(II) Soret (447 nm, dashed-dot) upon introduction of sodium dithionite at 4°C.

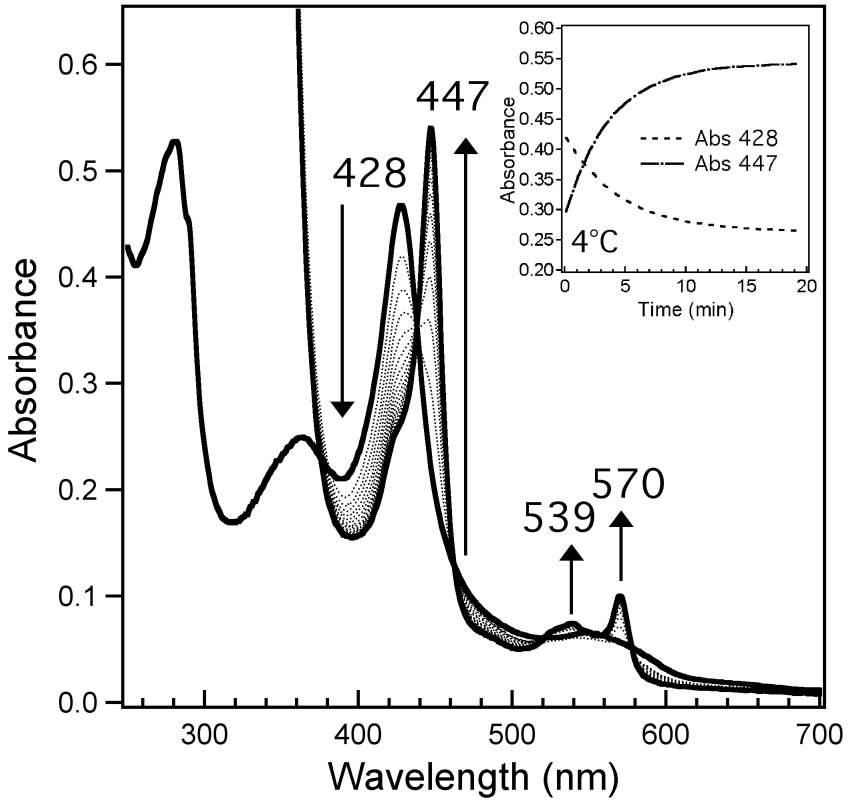

Figure 5.8. Ligand switch process of Fe(II) R266K hCBS at 30°C. Protein (3.8 μM) was in 100 mM CHES buffer, 100 mM NaCl, pH 8.6; sodium dithionite was added to a final concentration of 1.5 mM. (A) Solid lines indicate the initial (447 nm Soret) and final (424 nm Soret) spectra; dotted spectra were taken at 1 min intervals after addition of reductant. (B) Time course plots showing the loss of the Fe(II) WT hCBS Cys(thiolate)-ligated heme Soret at 449 nm (♦) and the loss of the Fe(II) R266K hCBS Cys(thiolate)-ligated heme Soret at 447 nm (◊).

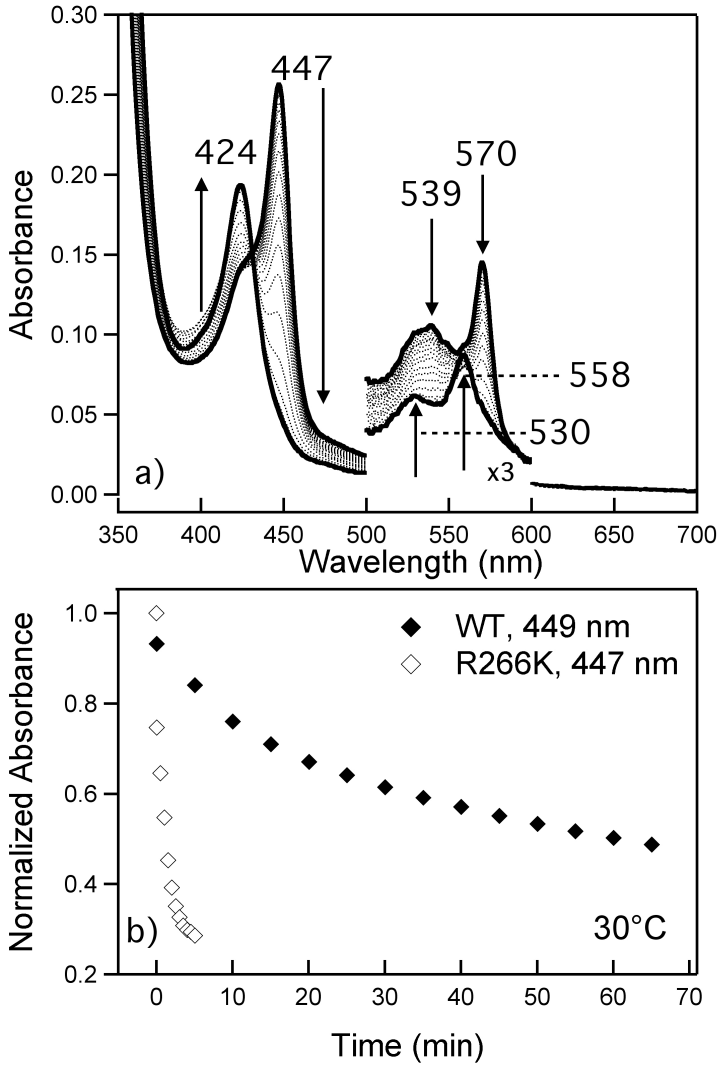

Figure 5.9. Arrhenius plots of the fit rate constants (min^{-1}) for the loss of the Cys(thiolate)-ligated heme Soret of Fe(II) R266K hCBS. Experimental values of k_1 (solid circles, ●) and k_2 (solid squares, ■) were determined for 10, 20 and 30°C (283, 293, and 303 K, respectively). Extrapolated values for k_1 (open circle, ○) and k_2 (open square, □) were determined at 37°C (310 K). Error bars represent ± one standard deviation of the fit value determined from three replicate measurements.

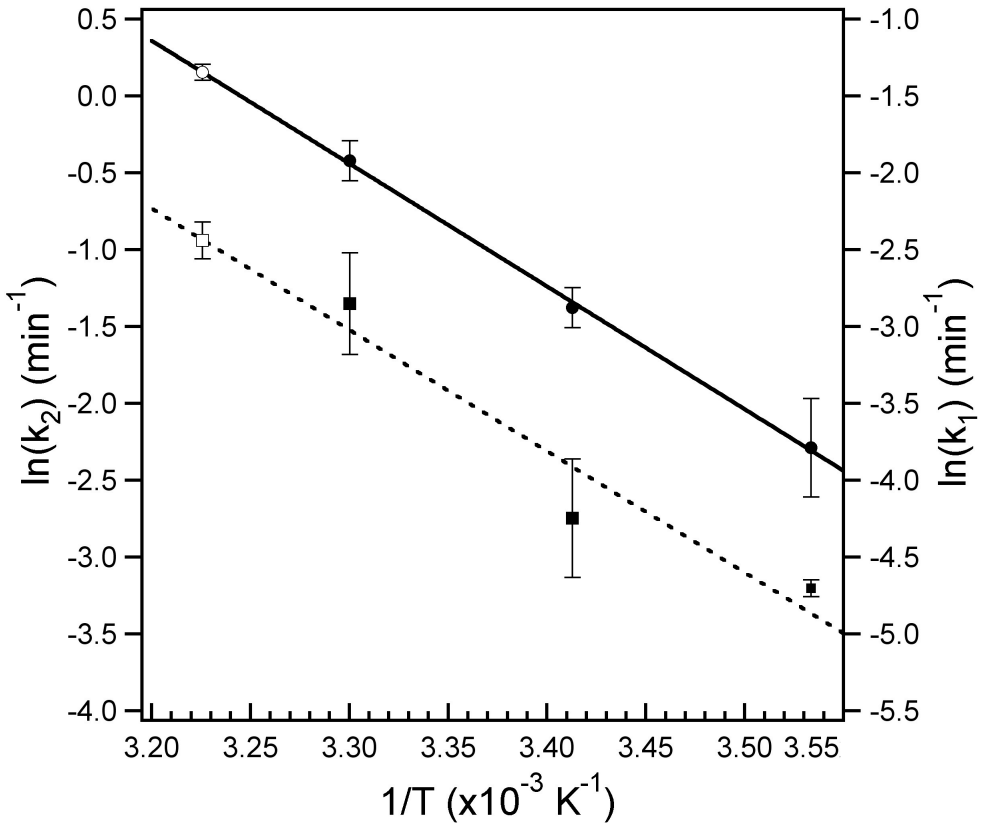

Figure 5.10. Partial sequence alignment of CBS enzymes from selected species, with human enzyme numbering. Heme ligands Cys[52] and His[65], PLP-internal-aldimine forming Lys[119], Cys[52](thiolate)-contacts Trp[54] and Arg[266], and PLP-contacts Thr[257] and Thr[260] are all labeled with an inverted arrow (▼). Human (*H. sapiens* accession no. P35520), rat (*R. norvegicus*, P32232), frog (*X. tropicalis*, Q640V0), zebrafish (*D. rerio*, B7ZV69), fruit fly (*D. melanogaster*, Q9VRD9), mosquito (*A. gambiae*, Q7QEV0) and slime mold (*D. discoideum*, P46794) sequences all contain the necessary ligands for heme binding and have Arg[266] completely conserved. Trypanosoma (*T. cruzi*, Q9BH24) and yeast (*S. cerevisiae*, P32582) CBS, which do not contain heme or its associated ligands, have a Lys residue at the position that is analogous to human Arg[266]. Sequence alignments were visualized using the MEGA5 program (*70*).

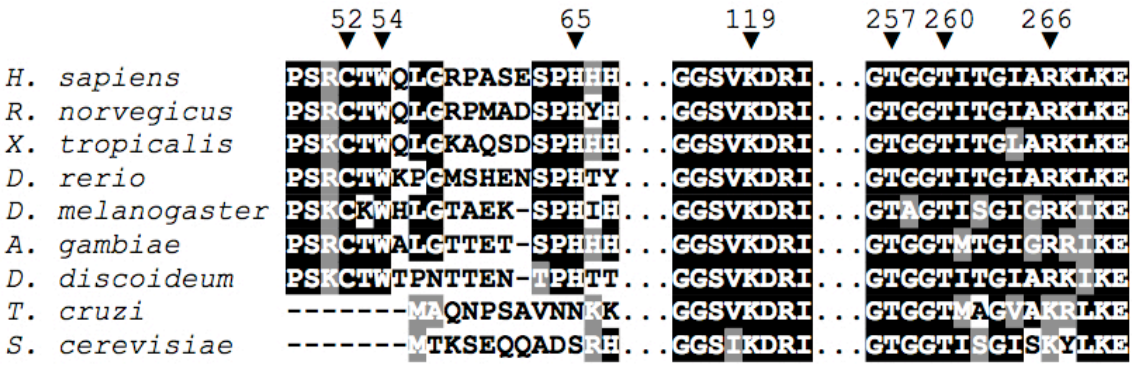

Scheme 5.1. CBS-catalyzed reactions: **(2)** condensation of serine with homocysteine to form cystathionine and **(3)** condensation of serine with hydrogen sulfide to form cysteine.

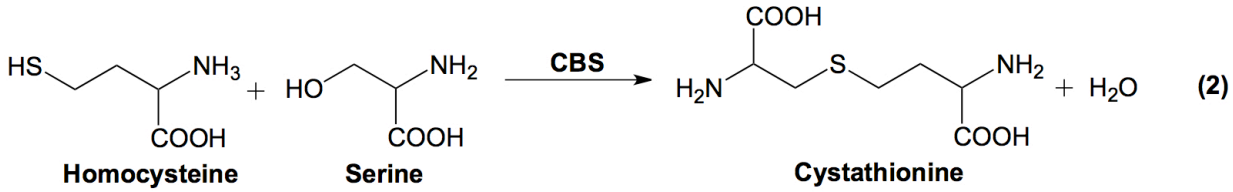

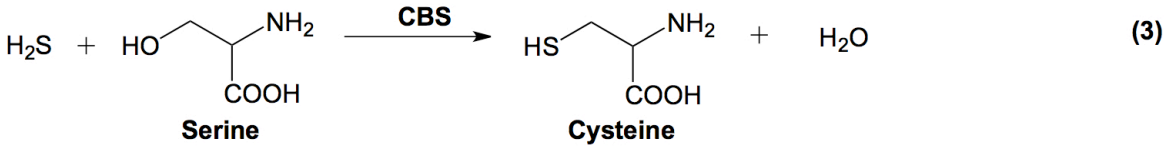

Appendix

EPR simulation parameters for Co(II)PPIX(1-MeIm)

```
#
# Co Model Complex
#
OUT    = "Co Model Complex.out";
ITOT   = 0.5e4;
# Co Model Complex
NEW_SPECIES = "Co(II)1-MeIm Model Complex" 1.00;
Freq   =  9.354000;
Hmin   =   2000.00;
Hmax   =   4000;
NDATA  = 2500;
S      =   0.5;
gx     =   2.03;
gy     =   2.300;
gz     =   2.300;
Wx     = 20.00;
Wy     = 20.00;
Wz     = 20.00;
Shape    = 2;
CutOff   = 4.464422;
WidthMode= 4.730188;
TMIN     =    0.00;
TMAX     =   360;
NT       =   360;
PMIN     =     0.00;
PMAX     =    180.00;
NP       =    180;

NUMNUCLEI =    2;

Spin[0]   =    3.5;
Num[0]    =    1;
SecondOrder[0]=    0;
ISTP[0]   =    1;
gnRatio[0]=  1.00;
Abund[0]  =  1.000;
AX[0]     =     219;
AY[0]     =     0;
AZ[0]     =     0;
```

```
C2X[0]  =  0.00; C2Y[0]  =  0.00; C2Z[0]  =  0;
EX[0]  =  0.00; EY[0]  =  0.00; EZ[0]  =  -0.00;
Spin[1]  =  1;
Num[1]  =  1;
SecondOrder[1]=  0;
ISTP[1]  =  1;
gnRatio[1]=  1.00000;
Abund[1]  =  1.00000;
AX[1]  =  48;
AY[1]  =  0.00;
AZ[1]  =  0.00;
ALPHAA[1] =  0.00;
BETAA[1]  =  0.00;
GAMMAA[1] =  0.00;
C2X[1]  =  0.00;
C2Y[1]  =  0.00;
C2Z[1]  =  0.00;
EX[1]  =  0; EY[1]  =  -0.0000; EZ[1]  =  -0.0000;

MODELPARS

gper  = 2.30;
gpar  = 2.03;
ACoper=  0;
ACopar= 219;
Wpar  = 8.690554;
Wper  = 29.091320;
ANper = 0;
ANpar = 48;
END;

MODELFCNS

gx  = "gpar";  gy  = "gper";  gz  = "gper";
Ax[0]= "ACopar"; Ay[0]= "ACoper";  Az[0]= "ACoper";
Ax[1]= "ANpar";  Ay[1]= "ANper";  Az[1]= "ANper";
Wx  = "Wpar";  Wy  = "Wper";  Wz  = "Wper";
END;
FitPars = Wpar, Wper, CutOff, WidthMode;
FitMin = 5, 30, 2, 1;
FitMax = 10, 50, 6, 6;
END;
```

EPR simulation parameters for Fe(II)-NO DGCR8

```
# DGCR8-NO Model Complex
#
OUT    = "DGCR8-NO Model Complex.out";
ITOT   = 1.40e3;
# Simulation of DGCR8-NO Spectrum
NEW_SPECIES = "DGCR8-NO" 1.00;
Freq   =  9.385000;
Hmin   =   3100;
Hmax   =   3500;
NDATA  = 410;
S      =   0.5;
gx     =   2.01;
gy     =   2.01;
gz     =   2.07;
Wx     = 10.00;
Wy     = 10.00;
Wz     = 40.00;
Shape    = 2;
CutOff   = 4;
WidthMode= 1;
TMIN     =    0.00;
TMAX     =   90.00;
NT       =   100;
PMIN     =     0.00;
PMAX     =    90.00;
NP       =    180;

NUMNUCLEI =    2;
Spin[0]   =    0;
Num[0]    =    1;
SecondOrder[0]=    0;
ISTP[0]   =    1;
gnRatio[0]=  1.00;
Abund[0]  =  1.000;
AX[0]     =     0;
AY[0]     =     0;
AZ[0]     =     0;
C2X[0]    =    0.00; C2Y[0]   =    0.00; C2Z[0]   =   0;
EX[0]     =    0.00; EY[0]    =    0.00; EZ[0]    =  -0.00;
Spin[1]   =    1;
Num[1]    =    1;
SecondOrder[1]=    0;
ISTP[1]   =    1;
```

```
gnRatio[1]=  1.00000;
Abund[1]  =  1.00000;
AX[1]    =   44.1;
AY[1]    =   0.00;
AZ[1]    =   0.00;
ALPHAA[1] =    0.00;
BETAA[1]  =    0.00;
GAMMAA[1] =    0.00;
C2X[1]   =    0.00;
C2Y[1]   =    0.00;
C2Z[1]   =    0.00;
EX[1]   =    0; EY[1]   =    -0.0000; EZ[1]   =    -0.0000;

MODELPARS
gper  = 2.010313;
gpar  = 2.063359;
AFeper=  0;
AFepar= 0;
Wpar  = 49.547257;
Wper  = 4.290358;
ANper = 45.709688;
ANpar = 0;
END;

MODELFCNS
gx   = "gper";   gy   = "gpar";    gz   = "gpar";
Ax[0]= "AFeper"; Ay[0]= "AFepar";  Az[0]= "AFepar";
Ax[1]= "ANper";  Ay[1]= "ANpar";   Az[1]= "ANpar";
Wx   = "Wper";   Wy   = "Wpar";    Wz   = "Wpar";
END;
FitPars = gper  , gpar , AFeper , ANper , Wper , Wpar;
FitMin = 1.90, 2.00, 0, 30, 0, 0;
FitMax = 2.10, 2.20, 0, 50, 10, 60;
END;
```